UNIVERSITY OF LIVERPOOL

THE USE OF ARCHAEOMAGNETISM TO ANSWER ARCHAEOLOGICAL AND GEOMAGNETIC QUESTIONS WITH PARTICULAR FOCUS ON DETERMINATION OF THE STRENGTH OF THE GEOMAGNETIC FIELD IN THE MIDDLE EAST DURING THE BRONZE AGE

Thesis submitted in accordance with the requirements of the University of Liverpool

for the degree of Doctor in Philosophy by

Megan Louise Hammond

12th December 2014

Abstract

The principles of archaeomagnetism can be applied to answer archaeological and geomagnetic questions and examples of both are presented in this thesis. Firstly, this thesis demonstrates the use of archaeomagnetism to establish the maximum palaeotemperature reached in a kiln at the Oylum Höyük archaeological site in Turkey. A maximum temperature of between 600 and 700 °C was determined confirming that the feature was more likely to have been a lime kiln than a bread oven. Archaeomagnetism was next used to determine the relative ages of different construction events on the St Jean Poutge archaeological site in Southern France. The results of archaeointensity experiments on 137 core samples taken from bricks and tiles confirmed the different relative ages of two construction events. Average intensity values determined using Thermal Thellier-Thellier methods were 56±7 and 58±8 for the 2nd Century AD and 68±6 and 68±7 for the 3rd Century AD.

There is an increasing body of evidence that the geomagnetic field in the Middle East during the Bronze Age reached exceptionally high field values extremely quickly. Both archaeomagnetic jerks (marked by sharp cusps in geomagnetic field direction coinciding with intensity maxima) and geomagnetic spikes (where the field rises and falls over a period of less than 30 years with associated virtual axial dipole moment fluctuations of at least 70 ZAm^2 /~38 μT) have been proposed to have occurred in the Middle East between 3000 BC and 0 BC. Here, Coe and IZZI method archaeointensity experiments were carried out on 154 Bronze Age pot sherds from two archaeological sites in Turkey, Tell Atchana and Kilise Tepe, and 2 archaeological sites in Cyprus, Marki *Alonia* and Bellapais *Vounous*. In addition, thermal Thellier experiments were conducted on 18 mud brick cores from Tell Atchana. The results of these experiments were corrected for cooling rate whilst experimental design mitigated the effects of anisotropy. A success rate of 56% was recorded overall. The effects of applying cooling rate corrections, anisotropy corrections and the impact of varying archaeointensity selection criteria cut-off values, on the results, are discussed in this thesis.

An average field value of 47μT was determined for Turkey over the time period ~2200-~700 BC which is indistinguishable from the current average field value. An archaeointensity

value of 84 μT (153 ZAm^2) was measured for the time period 800-600 BC. This is consistent with data from other authors who found evidence of high geomagnetic field intensity in the Middle East around 1000 BC. It is proposed here that this geomagnetic intensity high was of a longer duration and felt over a wider geographic area than has previously been suggested.

Contrary to previously published studies based in Syria, evidence is presented here of decreasing geomagnetic field intensity in Cyprus between 2400 BC and 1900 BC. The proposal that an archaeomagnetic jerk was experienced in Cyprus over this time period is therefore rejected.

Acknowledgements

I would like to thank my entire supervisory team; Mimi Hill, Andy Biggin and Alan Greaves. I count myself very lucky to have had such brilliant researchers as my supervisors, all of whom contributed something different to my PhD. Thank you for always answering my questions with a smile (even the less intelligent ones) and for all the constructive criticism and imparted knowledge.

I am grateful to Philippe Lanos of Rennes 1 University whom I consider to be a surrogate supervisor. Thank you for introducing me to field archaeomagnetism, French archaeomagnetism and how to make Plaster of Paris with the right consistency. I wish to also extend my gratitude to the rest of the Paléo-Archéomagnétisme community at Géosciences-Rennes for making me feel welcome and for making my trips to France so enjoyable. To Lucie Garnier and Philippe Dufresne, in particular, thank you for your assistance with sample preparation and for your good humour and patience when I butchered the French language.

Thanks are due to Andy Herries, Cor Langereis and Pinar Ertepinar for many fruitful and interesting discussions on all things archaeomagnetism. I owe a great debt to Aslihan Yener, Murat Akar, Mara Horowitz, Nicholas Postage, Jenny Webb and David Frankel for supplying the samples on which this thesis is based. Thank you for your generosity.

Particular thanks are due to my office mates, and fellow PhD sufferers, Laura Roberts-Artal and Emma Hodgson. Thank for both for always being ready with a sympathetic ear, helpful advice, tea and cake! You both made me look forward to coming into the office in the morning. To the Geomagnetism Laboratory at Liverpool University in general, thank you. To Elliot Hurst, Andreas Nilsson, Andy Roberts, John Shaw and John Piper, thank you for making the Geomagnetism Laboratory such a friendly and welcoming place to work. To Neil Suttie, in particular, thank you for your patience and tolerance. Thank you for taking the time to explain numerous difficult concepts in an effective way. Thank you to all my friends at Liverpool University who provided encouragement, good food and good company along the way.

I wish to express my gratitude to my family; my parents, Mervyn and Judith Thomas, my sisters; Rebecca Ainscough, Beth Thomas and Viktoria Goodwin and their partners; Philip Ainscough, Matthew Ingram and Daniel Goodwin. Thank you all for always being at the end of a phone and for your constant support throughout my life.

Finally, but by no means least, I would like to thank my husband, James Hammond. Thank you for all your support, encouragement, and patience and for generally putting up with me without complaining! I could not have done it without you.

This study was possible thanks to the financial support of a NERC studentship.

Contents

1. Introduction

The Earth's magnetic field varies on timescales from days to billions of years. These changes can be in both direction and strength. This is known as secular variation. The most dramatic changes in the geomagnetic field are magnetic reversals when the polarity of the Earth is reversed. Such events have occurred at irregular intervals, most recently, around 780,000 years ago. Here we focus on changes in the geomagnetic field on time scales of tens to 100s of years. It is important we understand these changes as they convey vital information about the processes occurring in the Earth's core where the field is generated. Such shorter timescale changes include (but are not limited to): "archaeomagnetic jerks" which have time characteristics intermediate between "geomagnetic jerks" and "magnetic excursions" and are marked by a sharp cusp in geomagnetic field direction coinciding with a maxima in geomagnetic field strength (Gallet et al., 2003) and "geomagnetic spikes" which are short episodes (less than 30 years duration) of exceptionally high field intensity in excess of 200ZAm^2 (104 μT) (Ben-Yosef et al., 2009, Shaar et al., 2011). Both features are highly controversial and poorly understood in terms of the geographic extent over which they are felt, their exact definition, the internal processes causing them and the frequency of their occurrence. Both events are proposed to have been recorded by archaeological material e.g. Gallet et al. (2006) and Ben-Yosef et al. (2009).

The geomagnetic field is a vector quantity and has both direction (defined by its declination and inclination) and strength (its intensity). Magnetic declination is the angle between magnetic north and true north whilst magnetic inclination is the angle made with the horizontal by the Earth's magnetic field lines. Direct measurements of the declination of the magnetic field did not being until the early 1500s followed shortly after by measurements of inclination in the mid 1500s. The first measurements of absolute geomagnetic field intensity were made in the 1800s. Therefore, in order to extend our knowledge of the behaviour of the field further back in time we must use archaeomagnetic and palaeomagnetic data recorded by archaeological material and rocks. For a more detailed overview of geomagnetism and palaeomagnetism, the interested reader is advised to consult Merrill et al. (1996) and Merrill and McElhinny (1983).

Archaeomagnetism is the study of changes in the Earth's magnetic field using burnt archaeological material as the recorder of these changes. Studied material can include tiles, bricks, hearths, and pottery e.g. Hill et al. (2007) and Kovacheva et al. (2004). The archaeomagnetic material records the field at the time the sample was last cooled below the Curie temperature of its component magnetic materials. At, and above, the Curie temperature the magnetic moments within the sample are free to align themselves with the field. Once the sample has cooled down below this temperature, the magnetic moments are locked in place. In addition, samples can also record later thermal and chemical overprints as well as viscous remanent magnetisation. Viscous remanent magnetisation is remanence acquired by ferromagnetic materials as a consequence of sitting in a magnetic field for some time.

If the material remains *in situ* then directional information (declination and inclination) and the strength (intensity) of the field can be extracted from the material. If the material is not *in situ* then only the intensity can be usefully determined. In certain cases where the orientation of the sample when it was fired can be inferred, for example if an intact pot is studied (typically pots are fired upright), then it is also possible to determine the inclination at the time of firing. Following the pioneering work of Thellier and Thellier (1959) who recognised the potential of archaeological material as excellent recorders of the ancient geomagnetic field, the field of archaeomagnetism has grown substantially e.g. Lanos et al. (1999). It is now possible to carry out archaeomagnetic dating by using changes in the geomagnetic field as a proxy for time. This can only be carried out in certain parts of the world over certain time periods where the changes in the direction and strength of the field are well known and a secular variation (SV) curve has been constructed e.g. France (Le Goff et al., 2002), Germany (Schnepp et al., 2003), Spain (Gomez-Paccard et al., 2006) and the UK (Zananiri et al., 2007). One of the aims of this thesis was to carry out archaeomagnetic dating of a French archaeological site in order to prove or disprove the archaeological interpretation of a relative age difference between a number of architectural features.

The attention of the archaeomagnetic community has recently turned to the Middle East where a number of papers have reported high geomagnetic field strength in the Bronze Age. These include studies in Syria (Gallet and Butterlin, 2014, Gallet and Le Goff, 2006), Turkey (Ertepinar et al., 2012), Jordan (Shaar et al., 2011) and Israel (Ben-Yosef et al., 2009). Two different names have been ascribed to these periods of high geomagnetic field strength. The first of these are archaeomagnetic jerks, defined by Gallet et al. (2003) as a

sharp cusp in geomagnetic field direction coinciding with a period of intensity maxima with time characteristics intermediate between geomagnetic jerks and magnetic excursions. In this initial paper four jerks were identified at ~ 800 BC, ~200 BC, ~750 AD and ~1400 AD based on full field vector data from France and intensity data from Syria. Additional archaeomagnetic jerks have subsequently been proposed at ~2800-2600 BC, ~2100-1900 BC, ~1750-1500 BC and ~1100-750 BC (Gallet et al., 2006). The latter of these proposed jerks (~1100-800 BC) is roughly coincident with the ~800 BC jerk proposed in Gallet et al. (2003). These second set of jerks were identified based on intensity data from the Middle East and correlated in time with directional changes observed in Swedish lake varves (Snowball and Sandgren, 2004). The time coincidence between archaeomagnetic jerks and periods of cooling in the North Atlantic, episodes of enhanced aridity in the Middle East and abrupt societal changes in the Eastern Mediterranean and Mesopotamia was also highlighted and led to much discussion over the exact links (if any) between the geomagnetic field and climate (Bard and Delaygue, 2008, Courtillot et al., 2008, Courtillot et al., 2007, Dergachev et al., 2012, Gallet et al., 2006, Gallet and Le Goff, 2006, Genevey et al., 2013, Knudsen and Riisager, 2009, Lockwood, 2012). A number of papers have proposed links between the geomagnetic field and climate e.g. Knudsen and Riisager (2009), Dergachev et al. (2012), but an exact mechanism is still highly controversial and as yet not clearly elucidated.

The second name ascribed to periods of high geomagnetic field strength is “geomagnetic spikes” which are defined as short episodes of exceptionally high field intensity in excess of 200 ZAm^2 (104.2 ± 6.3 μT) (Ben-Yosef et al., 2009, Shaar et al., 2011). The rate of change in the field strength (4-5μT/ year) and the maximum intensity values measured by these authors (114.7 μT or 250.8 ZAm^2) are exceptional and have yet to be observed elsewhere. This rate of change is 40 to 50 times greater than the current rate of change in the strength of the geomagnetic field.

A key aim of this thesis is to determine to what extent the magnetic record contained within pottery samples from Turkey and Cyprus confirms or refutes the occurrence of archaeomagnetic jerks and geomagnetic spikes. If they do record either of these features to what extent is our understanding of them increased as a consequence? In order to produce high quality archaeointensity data, the 14 GHz microwave system (MWS) at the University of Liverpool Geomagnetism Laboratory was used in many of the experiments.

The motivation for using the MWS was to reduce alteration of the magnetic mineralogy of samples during intensity determination and thus increase experimental success rates.

Archaeomagnetism can be applied in a variety of ways to answer a multitude of archaeological questions and we have only really begun to scratch the surface of the usefulness of archaeomagnetism from an archaeological perspective. A further aim of this thesis was to explore some of the ways archaeomagnetism can be used to answer archaeological questions. There are many examples of this e.g. using variations in mineral magnetic signatures to identify different fuel sources (Church et al., 2007) or investigating the spatial patterning of burning and occupation using magnetic susceptibility and other mineral magnetic parameters (Herries and Fisher, 2010). It is possible to use changes in susceptibility or magnetic mineralogy with temperature as a palaeothermometer (Hrouda et al., 2003, Henry et al., 2005). The final aim of this thesis was, therefore, to use the magnetic signature recorded in samples from an unidentified burnt feature (most likely a kiln) from the Oylum Höyük archaeological site in Turkey to determine the temperature this feature reached in antiquity and therefore establish what materials the kiln was producing. New material potentially suitable for archaeomagnetic studies is frequently being proposed, for example Carrancho et al. (2014) who explored the potential of using lithic clasts for archaeointensity analysis. One of the strengths of archaeomagnetism is its diversity and ability to be combined with other techniques to understand an archaeological site (e.g. Herries et al., 2007).

This thesis is subdivided into 3 sections. A palaeotemperature experiment on samples from a kiln at the Oylum Höyük archaeological site in Southern Turkey can be found in Chapter three. As detailed above, the aim of this work was to establish the maximum temperature reached in the kiln during antiquity. This would enable the site archaeologists to determine what product the kiln produced and enhance their understanding of the site. In order to achieve this aim, a variety of plaeotemperature experiments and demagnetisation experiments were carried out.

An example of the use of archaeomagnetism to carry out archaeomagnetic dating is demonstrated in Chapter four. The aim of this site-study was to prove or disprove a relative age difference between architectural features at the St Jean Poutge archaeological site. In order to achieve this aim, archaeointensity and demagnetisation experiments were carried out with corrections for sample anisotropy as well as corrections for cooling rate differences between the laboratory and in antiquity.

Chapters five and six describe the methods used and analysis performed on samples from Bronze Age Turkey and Cyprus with a discussion of how the findings of this work impact on our understanding of archaeomagnetic jerk and geomagnetic spike theory. The combined aim of these two chapters was to determine to what extent the magnetic record contained within pottery samples from Turkey and Cyprus confirms or refutes the occurrence of archaeomagnetic jerks and geomagnetic spikes. This was achieved by conducting archaeointensity experiments on a large number of potsherds from four archaeological sites in Turkey and Cyprus. Chapter seven discusses the impact of this thesis and potential future research avenues whilst Chapter eight summarises the main findings.

The form of the thesis evolved organically due to a number of external factors. As a consequence of the ongoing conflict in Syria, it was not safe to travel to Eastern Turkey throughout the duration of this PhD (2010-2014). Consequently, the samples studied from Tell Atchana (South Eastern Turkey) were collected by Pinar Ertepinar (Utrecht University) in 2007. Whilst the sample set from Tell Atchana is substantial, it was desirable to study samples from a number of locations in order to broaden the scope of the thesis. Samples from Kilise Tepe (Southern Turkey) were kindly donated by Nicholas Postgate of Oxford University whilst samples from two sites in Cyprus (Marki *Alonia* and Bellapais *Vounous*) were supplied by Jennifer Webb and David Frankel of La Trobe Univesity, Melbourne.

A further consequence of being unable to visit Tell Atchana was that I had not had an opportunity to carry out archaeomagnetic sampling in the field. In order to redress the gap in my skill set, we approached Philippe Lanos and I was able to join him on the St Jean Poutge archaeological site where I carried out archaeomganetic dating. I was also able to take directional samples which was not something I had previously had the opportunity to do.

The first results chapter (chapter four) came about as an interesting study into the diversity of archaeomagnetism. My supervisor, Alan Greaves had samples from a burnt depression feature. The use of this feature in antiquity was unknown and so it was hoped that if I could establish the maximum temperature reached in the feature when it was burnt in antiquity then it might be possible to determine its use. Again, this provided me with an opportunity to broaden the scope of this thesis and my own skills base.

Three of the chapters presented here, have been (or soon will be) submitted in their entirety for publication in the following peer reviewed journals:

- Chapter 4: Archaeometry,

  Paper co authors:

  - Philippe Lanos (University of Rennes 1)
  - Mimi Hill (University of Liverpool)
  - Fabian Colleoni (University of Rennes 2)

- Chapter 5: Earth and Planetary Science Letters

  Paper co authors:

  - Mimi Hill (University of Liverpool)
  - Andy Biggin (University of Liverpool)
  - Alan Greaves (University of Liverpool)
  - Cor Langereis (Utrecht University)
  - Pinar Ertepinar (Utrecht University)
  - K. Aslıhan Yener (Koç University, Istanbul)

- Chapter 6: Physics of the Earth and Planetary Interiors.

  Paper co authors:

  - Mimi Hill (University of Liverpool)
  - Andy Biggin (University of Liverpool)
  - Andy Herries (La Trobe University, Melbourne)
  - David Frankel (La Trobe University, Melbourne)
  - Jennifer Webb (La Trobe University, Melbourne)

Consequently there is a degree of repetition between these chapters. Each of these co-authors has made minor edits to earlier drafts of these chapters (in the form of papers). These edits were typically in the form of grammatical changes and/ or suggestions that sections are expanded upon in the interest of clarity. The exceptions to this are as follows: section 4.3. was written by Fabian Colleoni (note: Fabian's first language is French so this section was subsequently heavily edited by myself to improve the quality of the English), figure 4.17 was drawn by Philippe Lanos using the ChronoModel 1.1 software, section 6.3. was a collaboration between myself and Jennifer Webb and David Frankel and section 6.9.1 was written by Jennifer Webb and David Frankel.

2. Methodology

In this chapter a very brief introduction to the basic principles on which rock magnetism and archaeomagnetism are based is presented. Rock magnetism and archaeomagnetism are divisions of the field of palaeomagnetism. The primary objective of palaeomagnetic research is to determine the past configurations of the geomagnetic field. This is achieved by studying recorders of the field which can include rocks and burnt archaeological material. Archaeomagnetism is the study of the magnetic properties of archaeological materials that have been magnetically altered by human activity. In order to understand the magnetic signature recorded within a sample, it is important we understand its magnetic properties. Samples magnetic properties are investigated using "rock" magnetism principles. The term "rock" magnetism encompasses the study of the magnetic minerals within rocks, sediments, soil and archaeological material. A variety of techniques, methods and sample preparations were used throughout the studies described in this thesis in order to achieve this objective. It was clearest to include the relevant methodology with the associated experiments. Therefore, the methodology relevant to each chapter is detailed during the course of that chapter. For a more in-depth overview of palaeomagnetism the interested reader is recommended to read either Tauxe (2010) or Butler (1992).

2.1. Sampling Technique and Preparation

A variety of materials were studied during the course of this thesis. Where potsherds were studied the same sampling procedure was followed. At least three, 5 mm diameter and between 1 and 5 mm length, sister sub-samples from each potsherd were drilled perpendicular to the sherd's surface (figure 2.1). One subsample was subject to a set of standard rock magnetism experiments. The other two subsamples were used for demagnetisation and archaeointensity experiments. Some potsherds were too finely laminated to drill, therefore, small, arbitrarily orientated pieces, were cut from the potsherd using a hand held circular saw and trimmed into a cylindrical shape.

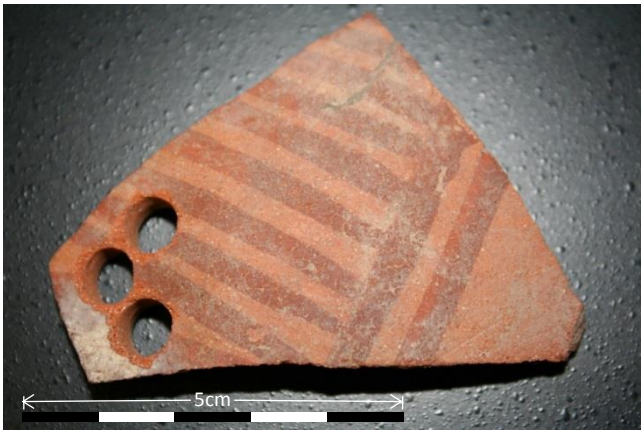

Figure 2.1: A potsherd from Level 9 of the Tell Atchana archaeological site, Turkey. Notice the three 5 mm diameter holes drilled within close proximity to each other. The rock magnetic properties of one subsample were analysed in the Variable Field Translation Balance at the University of Liverpool. A second subsample underwent a microwave demagnetisation experiment whilst the final subsample was subject to a microwave archaeointensity experiment.

2.2. Rock Magnetism

Rock magnetism is the study of the magnetic properties of rocks and minerals. Characterising samples rock magnetic properties is an integral part of every archaeo- and palaeo- magnetic investigation. In this thesis, the vast majority of rock magnetism experiments were carried out on the Vibrating Field Translation Balance (VFTB) based at the University of Liverpool Geomagnetism Laboratory. On this instrument Isothermal Remament Magnetisation experiments, Hysteresis and backfield measurements as well as Thermomagnetic measurements were carried out. In addition to this, the Kappabridge housed at the Geomagnetism Laboratory of the University of Liverpool was used to conduct Anisotropy of Magnetic Susceptibility (AMS) experiments. Whilst conducting experiments at the University of Rennes 1 (for more detail, see chapter 4), the low-field magnetic susceptibility of samples was measured using a Bartington MS2 susceptibility meter. This was to monitor mineralogical changes during the course of an archaeointensity experiment.

2.2.1. Isothermal Remanenent Magnetisation

To enable the preservation of an ancient magnetic field, the approach to equilibrium magnetization (relaxation time) within a sample must be on geological timescales (billions of years). Equilibrium magnetisation is achieved when a grain shows no preference towards one easy axis over another easy axis. Therefore the net moment at equilibrium

magnetization is zero. Relaxation time reflects the probability of magnetic moments jumping over the anisotropy energy barrier between easy axes. Factors which can influence this include anisotropy energy, thermal energy, time, coercivity and grain volume. The theoretical basis for the preservation of magnetic fields was first established by Néel (1949, 1955).

The magnetization of a grain will follow an applied field, if that field is larger than the coercivity. Exposing a particle to a large magnetic field will allow magnetic particles whose coercivity is below that field to change their magnetic moments by 180° to a direction with a more favourable angle to the applied field, resulting in a gain in magnetic remanence in that direction. This is an Isothermal Remanenent Magnetisation (IRM). The magnitude of an IRM in a sample is sensitive to the magnetic mineralogy, concentration and grain size. The maximum IRM achievable is known as the saturation IRM (sIRM), also known as saturation remanence (M_{rs}).

Using the VFTB, the acquisition of an Isothermal Remanent Magnetisation in a sample is measured by applying and then removing fields which increase incrementally from 1 to 800 mT. Samples containing low coercivity minerals such as magnetite, maghemite, titanomagnetite or titanomaghemite saturate in fields between 100 and 300 mT whilst high coercivity minerals such as haematite and goethite tend not to saturate at fields below 1T.

2.2.2. Hysteresis Experiments and Backfield Experiments

Hysteresis experiments are widely used in the rock magnetism community as they provide a number of magnetic parameters, including saturation magnetization and coercive force. The net magnetization is equal to the sum of all the individual magnetizations and is the saturation magnetization (M_s). At this stage in the experiment all the magnetizations in a sample are drawn into the field direction. The field necessary to reduce this net moment to zero is defined as the coercive field (H_c). During a hysteresis experiment a sample is exposed to increasing external fields from 0 mT to +800 mT followed by exposure to anti-parallel fields to -800 mT before finally the field is increased to +800 mT again. Throughout this experiment, the magnetisation of the sample is measured in-field. Consequently, ferro(i)magnetic fractions along with the paramagnetic phases are measured (in contrast to IRM experiments).

After saturation magnetisation following exposure to a field of +800 mT at the end of the hysteresis experiment, the sample is then subjected to increasingly large back-fields. The

back-field sufficient to remagnetise half of the moments (resulting in a net remanence of zero) is defined as the coercivity of remanence (H_{cr}).

2.2.3. Magnetic Domain State Estimation

One of the key difficulties in archaeomagnetism/palaeomagnetism is that Néel's theory is based on single-domain grains (Néel, 1949, Néel, 1955). Below a certain particle size, it is not energetically favourable to subdivide a grain into numerous domains. Instead, the grain will contain only one domain and is referred to as a Single Domain (SD) grain. The magnetic properties of SD grains are dramatically different to those of Multidomain (MD) grains. MD grains are much larger than SD grains and typically contain numerous magnetic domains within a single grain. SD grains are very efficient carriers of remanent magnetization whilst MD grains are not. MD grains are frequently quite unstable. There is a third grain type known as Pseudo-Single Domain (PSD) grains. PSD grains are too large to be truly single domain, however, they exhibit a stability unexpected for grains with domain walls. The physics of PSD grains is much more complicated than SD grains and is not fully understood, however, they can acquire a TRM stable against time decay and against demagnetization by later magnetic fields.

Estimation of a sample's bulk magnetic domain state in this thesis is through the use of Day diagrams (Day et al., 1977). A Day diagram plots M_{rs}/M_s against H_c/ H_{cr} because both ratios are sensitive to grain size variations. Areas of the diagram are designated as SD, PSD or MD and indicate regions of predominantly SD, PSD and MD behaviour. Whilst this is the most common method of grain size estimation and the Day paper has been cited nearly 1,500 times, it is noted that its value is a matter of debate. The key problem is that virtually all paleomagnetically useful specimens yield hysteresis ratios that fall within the PSD region of the Day diagram. The interested reader is directed to begin their reading of this subject with Pick and Tauxe (1994), Tauxe et al. (1996) and Dunlop (2002a,b).

2.2.4. Thermomagnetic Measurements

The final stage in the suite of VFTB experiments run was a thermomagnetic experiment during which the sample was exposed to increasing temperatures up to a maximum of 600°C or 700°C before cooling back to room temperature, at a rate of 30°C/ min. [Note: the lower temperature was applied when the water reaching the VFTB was hot, not cold (due to a technical problem) and therefore the system was not cooling as efficiently as it should have been. Using a lower maximum temperature helped reduce damage to the

equipment. This lower temperature was applied in roughly 25% of the experiments run]. The entire experiment was conducted in fields of up to 800mT. When the sample reached the Curie temperature of its component magnetic minerals, a decrease in magnetization was recorded. This was indicated by at least one change in slope on a temperature vs magnetization diagram. The exact point at which this change in slope occurs was determined using the two-tangent method developed by Grommé et al. (1969).

For more detail on rock magnetism, see Dunlop and Özdemir (1997). For flow diagrams detailing the experimental steps followed for each material studied here, see appendix 2.7.

2.3. Absolute Archaeointensity Experiments

It is possible to determine the intensity of the ancient magnetic field (H_{anc}) from archaeological samples and rocks because the mechanisms by which they gained a Natural Remanent Magnetization (a NRM) (which could be a thermal, chemical or detrital remanent magnetization) are frequently approximately linearly related to the ambient field for low fields such as the Earth. A NRM is the permanent magnetisation of a material that persists after the magnetising field is removed.

$$M_{NRM} = \propto_1 \cdot H_{anc} \tag{2.1}$$

$$M_{lab} = \propto_2 \cdot H_{lab} \tag{2.2}$$

H_{anc} describes the field strength during the acquisition of an NRM, whilst H_{lab} describes the field strength during a laboratory archaeointensity experiment. The constants of proportionality, α_1 and α_2 can be assumed to be equal if no magnetic mineralogical alteration occurs between the acquisition of the NRM and the subsequent acquisition of a TRM. Therefore equations (2.1) and (2.2) can be rearranged to give:

$$H_{anc} = H_{lab} \cdot \frac{M_{NRM}}{M_{lab}} \tag{2.3}$$

This simple equation is the basis of the field of palaeo- and archaeo- intensity. Palaeointensity and archaeointensity determinations differ only in the material being

studied. Palaeointensity studies focus on rocks and sediments whilst archaeointensity determinations are from archaeological material.

2.3.1. The Thellier-Thellier Method

The classical method of paleointensity determination for single domain grains was first developed by Thellier and Thellier (1959) using equation (2.3). The Thellier and Thellier (1959) method was the first step-wise heating method and spawned a number of variations and improvements. The step-wise heating approach is based on three laws, the first of which is the Law of Independence of partial thermal remanences (pTRMs) which assumes that pTRMs acquired by cooling in a field between any two temperature steps are independent of those acquired between any two other temperature steps. In other words, equation 2.3 is true for every temperature interval. Additionally step-wise heating methods also assume that the total TRM is the sum of all the independent pTRMs. This assumption is the second law; the Law of Additivity. The third and final law which these methods are based on is the Law of Reciprocity which states that the blocking and unblocking temperatures are the same ($T_b = T_{ub}$). This assumes that a pTRM acquired at a particular temperature step can be completely replaced by reheating to the same temperature. Blocking temperature is defined as a temperature above which a grain is superparamagnetic and in magnetic equilibrium with an applied field. Below this temperature the grain is effectively blocked and out of equilibrium with an applied field. The unblocking temperature is the temperature at which remanence is unblocked. Blocking and unblocking temperatures are only identical for single domain grains, in multidomain grains they can be dramatically different.

In a Thellier-Thellier experiment, the specimen is heated to a particular temperature and then cooled to room temperature in a laboratory field, B_{lab}. The specimen is next heated for a second time to the temperature reached in the first step before cooling back down to room temperature again, this time in the opposite field, $-B_{lab}$. Vector subtraction of these two steps allows the determination of the NRM remaining at each temperature step and the pTRM gained. The ancient field strength is proportional to the gradient of the best fit line on an Arai plot (Nagata et al., 1963) which is a plot of NRM against pTRM (figure 2.2).

Following the work of Thellier and Thellier (1959) many modifications to this method have been suggested. In this thesis, in addition to the Thellier-Thellier method, the Coe method and the IZZI method were also employed. It is acknowledged, however, that these are just

two of the more popular methods and if time had permitted more methods would have been utilized. In the Coe Method, the first in-field step of a Thellier-Thellier experiment is substituted for a zero field step (ZI) (Coe, 1967). In the Aitken (Aitken et al., 1988) method (not employed here) the first heating and cooling step is carried out in a laboratory field whilst the second step is conducted in zero field (IZ). The IZZI method (Yu et al., 2004) is a combination of the Aitken method and the Coe method.

In order to determine whether the remanence carrying capacity of the sample has changed during the course of experiment (which would therefore mean the sample failed the Law of Reciprocity) lower temperature in-field cooling steps are repeated. These so-called pTRM checks (Coe, 1967) are widely used and have been used here to monitor possible alteration. Unfortunately, a sample can fail to meet the Law of Reciprocity for reasons other than the ability to acquire a pTRM. For example, there may be an inequality of the unblocking temperature, T_{ub}, and the original blocking temperature, $T_{b,}$ as is the case for MD grains. In order to check for the presence of MD grains, pTRM-tail checks (Riisager and Riisager, 2001) were used during Coe experiments and involved an additional zero field step after the second infield step. For a pTRM-tail check to pass, the partial thermal remanence gained in the laboratory at a given temperature must be completely removed by reheating to the same temperature in zero field. The difference between the first zero field step and this additional second zero field step is a pTRM tail. The effectiveness of this check is dependent on the orientation of the applied field with respect of the NRM (Yu and Dunlop, 2003). The IZZI method is designed to check for MD behaviour by apparent zigzagging of the Arai plot, it is therefore not necessary to carry out pTRM tail checks during an IZZI experiment.

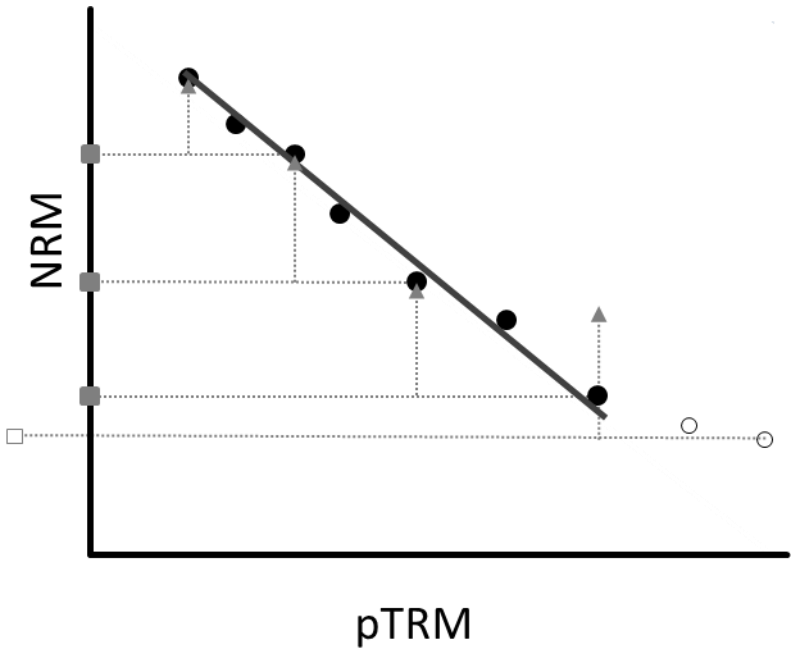

Figure 2.2: Sketch of an Arai plot. During the course of the intensity experiment the NRM is progressively removed from the sample whilst pTRM is progressively gained. The circles indicate experiment steps with full symbols indicating accepted results and open symbols indicating rejected results. The triangles indicate pTRM checks. The two final steps were rejected in this hypothetical example because the final pTRM check "failed" and did not reproduce exactly the experiment step it was reproducing. This indicates the remanence carrying capacity of the sample had changed during the course of the experiment. All of the other checks pass as they reproduce the earlier experiment steps exactly. The line is a best fit line plotted using the accepted results. The squares represent pTRM tail checks. Again an open symbol represents a failed result. Ideally a pTRM tail check will plot on the y axis unless the sample contains MD grains.

2.3.2. The Microwave System

As detailed above, one of the key assumptions of archaeointensity experiments is that the sample has undergone no mineralogical changes between the acquisition of the NRM and the acquisition of the laboratory TRM. In reality many samples fail to meet this condition because alteration has either a) occurred prior to the archaeointensity experiment or b) occurs during it. The rock magnetism experiments explained in section 2.2 demonstrate our efforts to understand the mineralogy of the sample prior to conducting archaeointensity experiments. For example, if a sample shows non-reversible behaviour of its thermomagnetic curve, it may not be suitable for an intensity experiment. In order to

minimise alteration during the experiment, a number of methods are employed throughout the field of archaeomagnetism. For example, the Triaxe method (Le Goff and Gallet, 2004) involves measuring the samples at high temperature, the multiple-specimen method (Hoffman and Biggin, 2005, Dekkers and Böhnel, 2006) minimises the number of temperature steps carried out on samples, whilst the Shaw method uses an AF demagnetiser rather than an oven to de- and re- magnetise a sample (Shaw, 1974). It is stressed at this point that these examples are just a small subset of the multitude of methods employed to reduce alteration and many of these (in particular the Shaw method) have spawned many variations. See Tauxe and Yamazaki (2007) for a review of archaeointensity experimental methods.

In this study, alteration is minimised by the use of the Microwave method to determine archaeointensity. Here, a brief overview of the microwave system will be presented, for a comprehensive description of microwave methodology and equipment please see Hill (2000) and Suttie et al. (2010).

In a conventional thermal archaeointensity experiment (e.g. Thellier and Thellier, 1959), heating of the bulk sample leads to increased vibrations of the lattice (phonons) which in turn generates electron spin waves (magnons). In contrast, during a microwave archaeointensity experiment, a sample is demagnetised through the direct excitation of the magnons in the magnetic particles without substantially heating the bulk sample. The key difference between thermal and microwave techniques is that, in microwave techniques, theoretically, only the magnetic particles within the sample are heated whilst in thermal techniques the entire sample is heated. In practise, the amount of time over which a sample is exposed to microwaves (between 3 and 30 seconds) is sufficient for some magnons to be converted to phonons which can cause some heating (Suttie et al., 2010). As the matrix of the samples is often composed of non-conducting materials, dielectric heating in the range of 150°C to 250°C can also occur (e.g. Suttie et al., 2010, Hill, 2000).

A number of comparative studies have demonstrated the equivalence of thermal and microwave techniques (e.g. Biggin, 2010, Hill et al., 2002, Poletti et al., 2013); however, the equivalence between thermal and microwave unblocking has not yet been described theoretically. In addition to the reduction in alteration, e.g. Hill et al. (2005), the microwave method has the advantage of treating samples individually, as opposed to the more usual batch heatings, meaning that experiments can be tailored to each individual sample. Discrete microwave archaeointensity experiments take considerably less time

(1.5-2 hours) than using conventional thermal methods (average 2 weeks) which take the same amount of time regardless of how many or how few samples are studied.

2.3.3. The 14 GHz Microwave System

The 14 GHz Microwave system (MWS) housed at the University of Liverpool was used to carry out all the microwave experiments recorded in this thesis. Attached to this MWS is a Tristan Technologies, Inc. DRM -300 Squid magnetometer. The sample cavity within this system is surrounded by three pairs of Helmhotlz coils in X, Y and Z directions, enabling the application of a magnetic field in any direction. The specimen is mounted on a quartz glass tube using negative pressure from a vacuum pump and then inserted vertically into the MWS. The sensitivity of the magnetometer can be adjusted according to the magnetic strength of an investigated sample. Prior to each experiment a sensitivity test is performed where an appropriate gain for the magnetometer is determined. The cavity itself is also tuned prior to each step in every experiment. This was necessary because the samples varied in size and, hence, resonant characteristics and these resonant characteristics were sometimes observed to change during the course of an experiment. In order to tune the microwave, a "wide" frequency sweep at low power (0.5W) between 14 GHz and 1.5 GHz was performed by the instrument. Having identified the area of optimal resonance frequency, a narrow sweep is then performed to identify the exact value of the resonance frequency. This is the frequency at which the reflected power is at a minimum. During a microwave experiment, the sample is demagnetised by applying microwaves of a particular energy (microwave power multiplied by exposure time). The sample is then remagnetised using the same energy. It is essential that the same energy is used for both but this is not always straight forward to achieve and may require a re-sweeping of the absorption frequency or a slight change in the amount of microwave power applied or the exposure time. This ensures that the same amount of energy is absorbed by the magnetic particles during de- and re-magnetisation (to ensure experimental procedure meets the Law of Reciprocity). If the energy difference between the two steps was greater than 10% of the total amount of energy absorbed in the demagnetisation step then the remagnetisation step was repeated.

2.4. Cooling Rate Corrections

A number of studies have demonstrated the potentially significant impact of cooling rate on the ability of a sample to acquire magnetisation (Fox and Aitken, 1980, Halgedahl et al.,

1980, Biggin et al., 2013, Genevey and Gallet, 2002). For an assemblage of single domain (SD) grains TRM increases with slower cooling e.g. Fox and Aitken (1980) Halgedahl et al. (1980) Dodson and McClellandbrown (1980) and McClellandbrown (1984). The importance of applying a cooling rate correction for samples containing pseudo single domain (PSD) and multi-domain (MD) grains is less well understood; some recent studies have suggested that in coarse grains the cooling rate effect is indistinguishable from zero (Biggin et al., 2013, Ferk et al., 2014) whilst others believe TRM decreases with slower cooling (Papusoi, 1972, Yu, 2011, McClellandbrown, 1984, Muxworthy and Heslop, 2011, Winklhofer et al., 1997).

Whilst it is less vital in studies of archaeological materials to apply a cooling rate correction than it is in studies of certain geological materials, cooling rate differences can still introduce errors of ~10% (e.g. Genevey and Gallet (2002). This is because the cooling rate for clays (about 1.5 days e.g. Chauvin et al. (2000)) is closer to the laboratory cooling rate than it is for large igneous bodies when cooling may take thousands of years (Halgedahl et al., 1980). Polleti et al. (2013) demonstrated that similar experimental behaviour is observed between microwave and thermal procedures despite the different ways in which the energy is transferred into the spin system and therefore it is necessary to apply cooling rate corrections to microwave determined archaeointensity results.

Cooling rate experiments were carried out using the in-house, thermally insulated, cooling-rate oven at the University of Liverpool. Experiments were only conducted on samples which showed no sign of alteration during the original intensity experiment (where equations 2.1 and 2.2 were still valid).

2.5. Correcting for Anisotropy of Thermal Remanent Magnetisation (ATRM)

In addition to correcting results for cooling rate effects, it is important to correct for anisotropy effects, as the anisotropy of the TRM of a sample can lead to an error in the intensity estimation of up to 40% (Rogers et al., 1979). Pottery has been shown to be strongly anisotropic (Chauvin et al., 2000) due to the preferential alignment of magnetic grains presumed to be related to the moulding of the clay. There are two key ways to correct for anisotropy. Either the effects of anisotropy on archaeointensity determination can be minimised by applying the laboratory field parallel to the NRM direction or an ATRM correction factor is applied. The ATRM tensor in a sample can be determined by successive infield experiment steps during which the pTRM is acquired and measured in six orthogonal

directions (Veitch et al., 1984). Both of these methods have been applied in this thesis to correct for/ mitigate the effects of anisotropy.

2.6. Archaeointensity Selection Criteria

A very brief introduction to archaeointensity selection criteria is presented here, for a more detailed discussion, the interested reader is recommended to begin their reading of the subject with Paterson et al. (2014), Tauxe and Staudigel (2004), Chauvin et al. (2005), Biggin et al. (2007) and Paterson et al. (2012).

Archaeointensity selection criteria are routinely applied to the results of archaeointensity experiments, with the aim of ensuring that only reliable results are accepted. However, there is very little consensus on which selection criteria are the most effective at discriminating inaccurate results from accurate results. In total, more than 40 archaeointensity statistics have been proposed and are regularly used (Paterson et al., 2014). This issue is complicated by the fact that relatively arbitrary cut off values of a criterion are used to distinguish inaccurate results from accurate results.

Most studies use unique combinations of selection criteria although there are a number of frequently used criteria sets: e.g. PICRIT03 (Kissel and Laj, 2004), SELCRIT2 (Biggin, 2010), ThellierTool A and B (Leonhardt et al., 2004). Paterson et al. (2014) evaluated these four commonly used criteria sets and found that Thellier Tool A was no more effective at eliminating inaccurate results and accepting accurate results than if the data was randomly selected. As dictated by the quality and quantity of the archaeointensity data, in this thesis, more or less lenient criteria were applied to different data sets. Less stringent criteria were only applied when doing so did not significantly affect the average intensity value determined, whilst simultaneously increasing the total number of accepted results. The ideal selection criteria should have the right balance of E_A and E_I (as defined by Paterson et al. (2014)):

$$\mathrm{E_A} = \frac{Number\ of\ accurate\ results\ accepted}{Total\ number\ of\ accurate\ results} \tag{2.4}$$

$$\mathrm{E_I}\ \frac{Number\ of\ inaccurate\ results\ rejected}{Total\ number\ of\ inaccurate\ reults} \tag{2.5}$$

In this thesis the following archaeointensity selection criteria have been used with the applied cut-off values indicated. The criteria set used is similar to that adopted by Hervé et al. (2013) and Ertepinar et al. (2012) which are a modification of Coe et al. (1978), Selkin and Tauxe (2000) and Biggin et al. (2007):

a) NRM fraction factor *f* greater than 0.35, with the minimum number of selected points defining this *f* being 5 *(Coe et al., 1978)*,
b) The upper acceptance limits for maximum angular deviation (MAD) and α are taken as 15% (Kirschvink, 1980)
c) Deviation angle (DANG) lower than 5° (Selkin and Tauxe, 2000)
d) The acceptance criterion of quality factor (q) is 1.
e) The ratio of the standard error of the slope to the absolute value of the slope (β) lower than 0.05 (Kissel and Laj, 2004)
f) pTRM checks were deemed to have been successful if the ratio of the difference between the check and the relevant TRM value to the length of the selected NRM-TRM segment (DRAT) was smaller than 7% (Selkin and Tauxe, 2000) and the cumulative DRAT (CDRAT), defined as the sum of all the DRATs, should be less than 20% (Kissel and Laj, 2004) from a minimum of 3 pTRM checks.
g) The DRATtail (Biggin et al., 2007) must be less than 10%.

Slight modifications to these overall selection criteria are made in each chapter, partly led by the archaeointensity method used and partly as a consequence of the quality of the data as the balance of E_A and E_I was dictated by the material analysed.

2.7 Appendix: Flow diagrams for experiments run on discrete sample sets.

a)

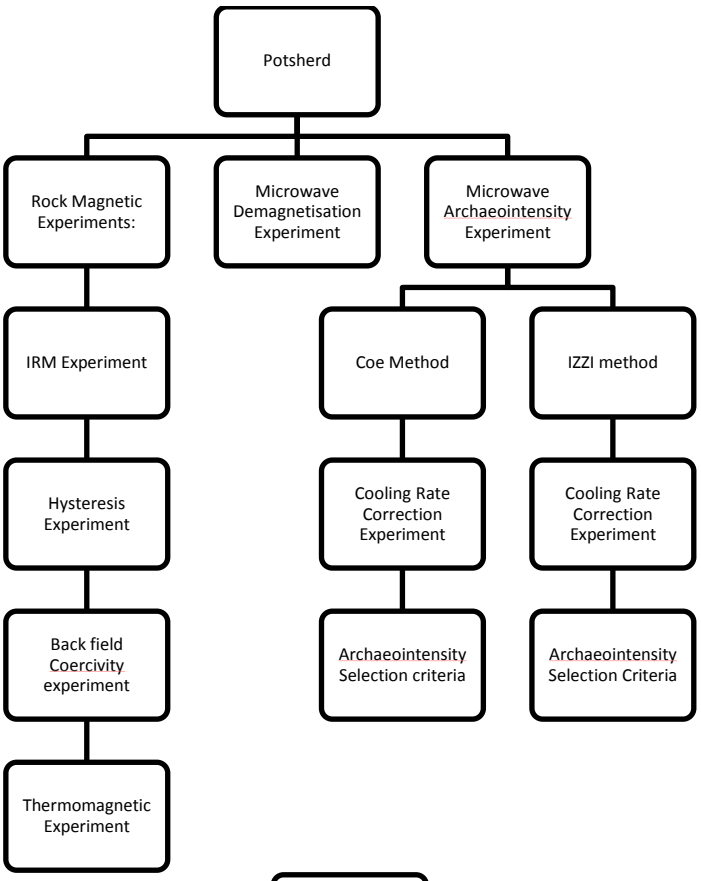

b)

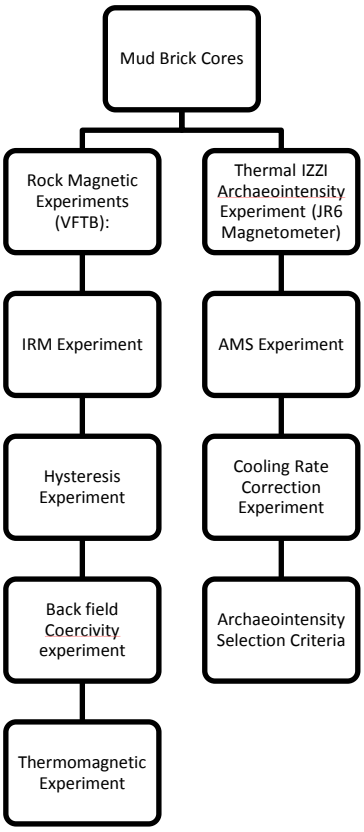

c)

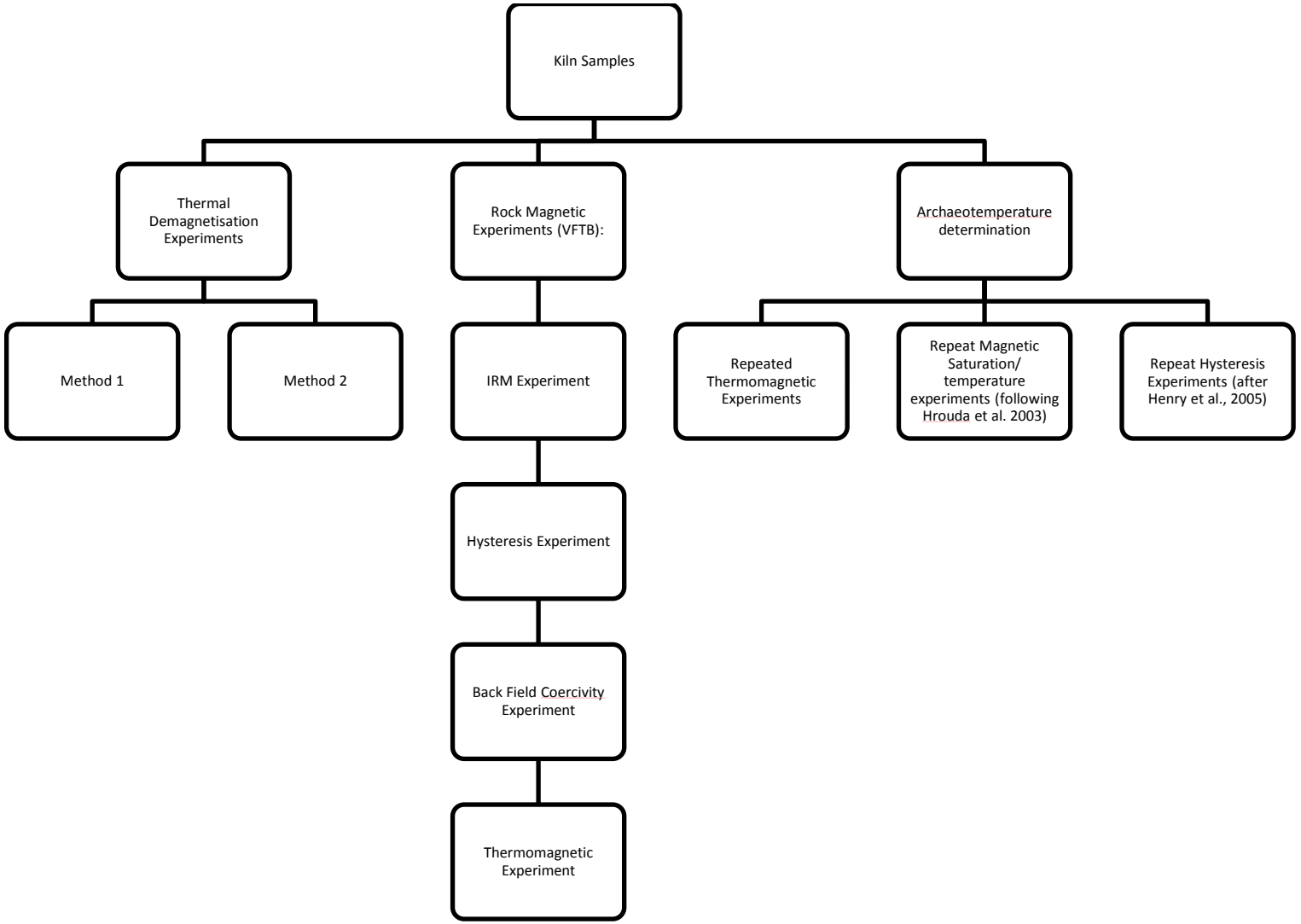
Kiln Samples
Thermal Demagnetisation Experiments
Rock Magnetic Experiments (VFTB):
Archaeotemperature determination
Method 1
Method 2
IRM Experiment
Repeated Thermomagnetic Experiments
Repeat Magnetic Saturation/ temperature experiments (following Hrouda et al. 2003)
Repeat Hysteresis Experiments (after Henry et al., 2005)
Hysteresis Experiment
Back Field Coercivity Experiment
Thermomagnetic Experiment

d)

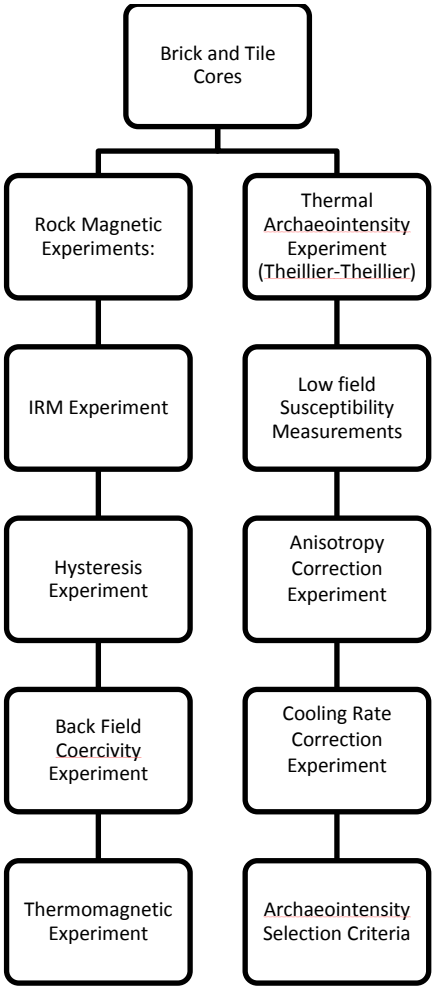

Flow diagrams indicating the order of experiments run on samples from each sample set studied in this thesis. Each flow line indicates experiments carried out on one subsample i.e. in d) a subsample of each sample was subject to a suite of rock magnetic experiments whilst another subsample from the same parent sample was subject to an archaeointensity experiment, low field susceptibility measurements and so on. The flow diagram in a) indicates the experimental procedure followed on potsherds, from a number of archaeological sites, b) the procedure followed here when studying burnt mud bricks from the Tell Atchana archaeological site, c) lists the experiments conducted on blocks of mud from Oylum Höyük where the aim was to establish the maximum temperature to which the blocks were exposed. The difference between Method 1 and Method 2 is explained in detail in chapter 3 but suffice to say they represent different sampling methods. d) is the experimental method followed during the study of sedimentary blocks, bricks and tiles taken from the St Jean Poutge archaeological site.

3. Use of Archaeomagnetism to Elucidate Kiln Type at Oylum Höyük

3.1. Abstract

Kiln identification is not straightforward when the products manufactured in a kiln are not in evidence. A number of kilns technologically resemble each other, for example, the baking oven, the lime kiln, the glass furnace and the bath furnace (praefurnium). These kilns do, however, differ in the maximum temperature reached and, therefore, archaeomagnetism can be used to distinguish between them. In this chapter thermal demagnetisation experiments and rock magnetic experiments were conducted in order to establish the maximum temperature reached in an undefined kiln found on the Oylum Höyük archaeological site in Southern Turkey. The aim was to identify what the kiln was used to produce in antiquity. The two block samples studied were very dry and poorly consolidated making subsampling exceptionally difficult. Two components of magnetisation were found in some subsamples of Block 1. The secondary component of which was removed by 350°C whilst the primary component was removed by 600°. In Block 2 only one component of magnetisation was found and the direction of this component was consistent across the block. The stability of the remanence contained within Block 2 is consistent with this sample being heated to between 600°C and 700°C. Whilst it was possible to determine a maximum temperature reached in the samples this is probably lower than the maximum temperature reached in the kiln because the surfaces of the samples were removed during sampling. The inconsistency between the two blocks and the difficulties associated with sampling make the temperature estimate a best guess at most. This study would have benefited from substantially more field sampling.

3.2. Introduction

Archaeomagnetism can be a useful tool in the study of kilns: it can date the final heating of the kiln (e.g. Ech-Chakrouni et al., 2013, Casas et al., 2013) and can determine firing temperatures and temperature profiles (e.g. Carrancho and Villalain, 2011, Spassov and Hus, 2006). Equally kilns can provide well dated archaeomagnetic information about the geomagnetic field (e.g. Gomez-Paccard et al., 2006, Schnepp et al., 2003). There are a large

variety of kiln types: bread kilns; tile kilns; pottery kilns; lime kilns; glass and metallurgical kilns, to name a few. In all previous archaeomagnetism papers mentioned here, the kiln type is known prior to experimentation. However, the baking oven, the lime kiln, the glass furnace and the bath furnace (praefurnium) all technologically resemble a ceramic kiln and/ or leave similar archaeological traces (i.e. they all have similar shapes and internal structures) (Hasaki, 2002). For example, lime is easily dissolved after it is burnt leaving little visual aid to the determination of the kiln's use (Hasaki, 2002). Without an unambiguous association with the material that was treated in the kiln it is difficult to distinguish between kilns using observations alone. However, the different kilns would have reached different maximum temperatures. A bread oven would have routinely been heated to between 300-500°C (Hasaki, 2002 and references therein) whilst a lime kiln would have been heated to 900°C (Zuideveld and van den Berg, 1971).

Two blocks of floor material were collected by Alan Greaves from the Turkish archaeological site, Oylum Höyük (figure 3.1 and 3.2) in 2004. The blocks were collected from the floor of an undefined feature which had green and black vitrified surfaces indicative of burning (figure 3.3a). The feature was an elongated depression with rounded ends and straight, brick-lined sides. It was approximately 3.5m long and 0.5m wide at its base. As the surface of the depression was vitrified the archaeological interpretation was that it was a type of oven/kiln. The aim of the archaeomagnetic investigation was to determine the temperature the feature had last been heated to. The objectives of this study are to determine the maximum temperature reached in this kiln using thermal demagnetisation experiments in association with an analysis of the samples' rock magnetic properties and the temperature at which alterations of these properties occurs. Knowing the firing temperature would enable the archaeologists to better decide what type of oven/kiln it was. The depression has been dated by radiocarbon dating of three bone samples either associated with the feature itself or from levels stratigraphically above. A further aim was to determine the declination and inclination of the geomagnetic field in Turkey around 3600 BC.

3.3. Olyum Höyük

Oylum Höyük (36°41'56"N, 37°10'42"E) is a double-summited ancient settlement mound located on the fertile terra rossa soil of the Kilis Plain in South-Eastern Turkey (see figures 3.1 and 3.2). It is on the small perennial stream, the Akpýnar Suyu. Oylum Höyük rises to a height of 38m and covers an area of 17 hectares making it the largest settlement on the

Kilise Plain and one of the largest in South-Eastern Turkey (Özgen and Helwing, 2003). The site is a multi-period settlement with evidence of occupation from the Neolithic to the Hellenistic periods (Greaves, 2002).

Figure 3.1: Map of Turkey with the approximate location of Oylum Höyük indicated by a black star.

Figure 3.2: Aerial photograph of Oylum Höyük *showing a number of buildings. The black square indicates the feature studied here. The black and white scale bar in the foreground is 1m long.*

3.3.1. Dating

Three bone samples associated with the feature were radiocarbon dated at Darden G. Hood Beta Analytic, Inc. 4985 SW 74 Court Miami, Florida 33155, USA. The first was a sample of cremated animal bone found in the archaeological feature (table 3.1, sample OYO4KN521). As the sample was burnt the carbon had to be extracted from the sample before it could be analysed using Accelerator Mass Spectrometry (AMS) dating. AMS is a very precise technique and the sample age was given to be ±30 years (compare this with more traditional radiocarbon dating which gives ages to ±200 years). In addition to this bone fragment, 2 more bone fragments, found in association with the 'red walls' (Greaves, 2002) which are stratigraphically above the feature, were also analysed (see table 3.1, samples OYO2KN151 and OYO2KN538). The date of the feature has been further constrained by stratigraphy as it is below the remains of the Achamenid House. Some have dated the Achamenid house as Hellenistic (~400BC to ~50BC) but there is some evidence to suggest that Hellenistic is in reality a minimum age (Greaves, 2002).

Theoretically this means the feature is directly dated by only one sample and given a minimum age by the samples from stratigraphically above. However, the radiocarbon date recorded by the bone sample found in the feature was 3640 to 3510 BC which is significantly older than the archaeological interpretation of the feature as being late 2nd century/ early 3rd century BC. This older age is not incompatible with the archaeological interpretation because the whole area is quite disturbed and there is a lot of evidence of redisposition. The feature itself is a negative feature as it was dug down into earlier layers so this bone is likely to be dating an earlier event. However, the radiocarbon date for the bone fragments found in the red walls is also significantly older (between 920 and 1270 BC) than the kiln is interpreted to be. It is difficult to reconcile these two very disparate dates (3640-2510 BC with late 2nd century/ early 3rd century BC). If there is sufficient previous inclination and declination data from this region, it may be possible to identify which of the two ages is more probable based on the declination and inclination recorded in the feature. In other words an additional aim of this work is to use archaeomagnetism to try and resolve whether the radiocarbon or archaeological date is more probable.

Table 3.1: Results from the carbon dating of samples associated with the feature

Sample	**Analysis**	**Material/ Pre-treatment**	**Measured age**	**13C/ 12C Ratio**	**Conventional Radiocarbon Age**	**Age Cal BC (2σ)**	**Age Cal BP (2σ)**
Beta-OYO4KN521	AMS-standard delivery	Cremated bone carbonate	4660 ±30 BP	-18.4 ‰	4770 ±30 BP	3640 to 3510	5590 to 5460
Beta-OYO2KN151	AMS-standard delivery	(residual organics in bone): collagen extraction: with alkali	2820 ±40 BP	-21.7‰	2870 ±40 BP	1190 to 1140, 1140 to 920	3140 to 3090, 3090 to 2870
Beta-OYO2KN538	AMS – Standard delivery	(charred material): acid/alkali/acid	2900 ±40 BP	-23.2‰	2930 ±40 BP	1270 to 1010	3220 to 2960

The calendar calibrated result is calculated from the Conventional Radiocarbon Age which was calculated using an assumed delta 13C.

3.4. Sampling Methods

Two brick shaped samples (10cm x 14cm x 21 cm) (figure 3.3b) were excavated from the floor of the depression (figure 3.3a). The floor samples were collected in 2004 and were very dry and prone to crumbling when touched. The two blocks were next to each other in the feature. It is emphasised that although the extracted samples are brick shaped they were not created and shaped as bricks in antiquity. The floor of the feature is not soil *sensu stricto* because Oylum Höyük is made of a sequence of occupation levels built on top of one another so it is likely the material was heavily reworked prior to being incorporated at the base of this depression. This makes it unlikely that a coherent detrital magnetic remanence would be found in the samples.

Figure 3.3: (a-d) show the sampled depression and the methods employed to accurately extract a levelled, orientated sample from this feature. The black and white scale bar in a) is 30 cm long. The tape measure in b) shows 5cm increments.

3.5. Sample Preparation

3.5.1 In the Field

Prior to the blocks being cut out by Dr Alan Greaves, they were levelled off using a spatula until the entire sample top was horizontally level as confirmed by a spirit level (figures 3.3c and d). They were orientated with a north arrow (figure 3.3b). The blocks were then cut out of the ground and placed in a plastic container (figure 3.3d). Within these rigid containers the blocks were covered with tin foil and the box filled with Plaster of Paris to restrict movement. The blocks were taken within 0.5 metres of each other and within 1.5 meters of the heat source although unfortunately their exact location within the feature and relative to each other was not recorded.

3.5.2. In the Lab

The blocks were very dry (see figures 3.4a-d) and weakly consolidated. This lack of consolidation is a consequence of their composition which is a very dry, compacted soil containing heterogeneities like rootlets. For the preliminary study (carried out by Dr Mimi Hill), no consolidator was used prior to cutting the samples out of the block. Despite efforts to cut oriented samples it was not possible to do so with such dry material so the largest fragments that were cut (but unfortunately were no longer oriented) were used. These samples were suitable because the aim of the preliminary experiment was to determine if a measurable and consistent record of the magnetic field was recorded in the blocks. It was apparent from this preliminary experiment that a consolidator was essential to the collection of orientated samples. Due to uncertainties associated with the best method of sampling, two methods were employed during the initial sampling of Block 1 with the aim of determining which would be more suitable at ensuring the material survived the measurement and experimentation process.

Method 1

The first method employed (which transpired to be the more successful of the two methods) was to pour dilute sodium silicate (“water glass”) over the entire block surface and leave it to set over night. This ensured that the surface was hardened. The sodium silicate was diluted with water. The following day, fixwool cement (which hardens as it is heated) was applied and on top of this a square plastic cap was placed (figure 3.4b) and made level using a spirit level. The north arrow was drawn on this cap. These samples were

cut out using a mini hand-held saw and trimmed to 8cm^3 cubes. The plastic caps were then pulled off and the north arrow redrawn on the cement.

Figure 3.4: Various stages in the sampling procedure denoted as Method 1. The pictures highlight the difficultly of taking consolidated, orientated samples from this very dry heterogeneous material.

Method 2

Method 2: Again dilute sodium silicate was used to ensure the surface was consolidated. A small section of this sodium silicate treated region was covered with Plaster of Paris. The samples were then cut from these levelled, Plaster of Paris sections. North arrows were drawn on the plaster surface. Unfortunately with this method, a significant amount of plaster had to be used to ensure the surface was level. This meant that the actual amount of the block in each sample was relatively small compared with method 1. The Plaster of Paris also started to crumble at the higher end of the temperatures reached during the demagnetisation experiment meaning the sample started to disintegrate which had a consequential effect on the precision of the result.

In total, six samples from Block 1 (this is in addition to three samples previously studied as part of a preliminary study) and nine samples from Block 2 were analysed. In total during the main study, two samples were sub-sampled using Method 2 and the remaining 13 samples were sub-sampled using Method 1. In the preliminary study no consolidator was

used and unorientated samples were cut using a circular saw (this information is summarised in table 3.2).

Table 3.2. List of demagnetisation samples

Block	Study	Sampling method	Sample name
1	Preliminary	Unorientated cut samples	ATOLOLYO1A
	Preliminary	Unorientated cut samples	ATOLOLYO2A
	Preliminary	Unorientated cut samples	ATOLOLYO3A
	Main	Method 1	BK1S1
	Main	Method 1	BK1S2
	Main	Method 1	BK1S3
	Main	Method 1	BK1S4
	Main	Method 2	BK1S5
	Main	Method 2	BK1S6
2	Main	Method 1	BK2S1
	Main	Method 1	BK2S2
	Main	Method 1	BK2S3
	Main	Method 1	BK2S4
	Main	Method 1	BK2S5
	Main	Method 1	BK2S6
	Main	Method 1	BK2S7
	Main	Method 1	BK2S8
	Main	Method 1	BK2S9

3.6. Experimental Method

In a preliminary study 3 unorientated subsamples taken from Block 1 were demagnetised in 50°C temperature steps up to 600°C (orthogonal vector plots for these samples are shown in figure 3.5). The subsamples were unoriented with respect to each other and with respect to the orientation markings on the block. These samples were stepwise demagnetised using a fan-cooled Magnetic Measurements Thermal Demagnetising (MMTD) Oven and measured using the Molspin spinner magnetometer at the University of Liverpool Geomagnetism Laboratory.

Following the interpretation of the results from the preliminarily study, six subsamples from Block 1 were stepwise demagnetised using a fan cooled MMTD oven and measured using the JR-6 Agico magnetometer at the University of Liverpool Geomagnetism Laboratory. These samples were heated from 100°C to 450°C at intervals of between 20°C and 100°C and their orthogonal vector plots are shown in figure 3.6. In the preliminary study an observed change in direction of the orthogonal plot (e.g. ATOLOLY02A, figure 3.5) occurred

at 350°C, therefore, the subsequent experiment on the six subsamples from Block 1 ended at 450°C as it had been established in the pilot study that the primary component demagnetised towards the origin and in the follow up experiment we were interested in isolating the secondary component (figure 3.6). For more detail, the reader is referred to the Discussion.

Nine subsamples from Block 2 underwent stepwise demagnetisation from 0°C to 580°C with experiment steps every 20°C from 200°C to 500°C (figure 3.7). The aim when analysing these samples was to isolate the temperature at which any secondary component of magnetisation was removed. As there had been no previous studies on Block 2 samples, the demagnetisation of these samples continued until less than 10% of the NRM remained (at 580°C).

The demagnetization results were interpreted via orthogonal projection diagrams (Zijderveld, 1967) and by principal component analysis (Kirschvink, 1980). Mean directions were calculated according to Fisher (1953). The accepted means for both the maximum angular deviation (MAD) of individual directions and α95 of the means was taken to be 10°.

3.7. Demagnetisation Results

3.7.1. Preliminary Study

The results of the preliminary demagnetisation experiments were mutually consistent across the three samples suggesting that there were two components of remanent magnetisation in Block 1. The secondary component of magnetisation was removed by 350°C (indicated by a change in direction on the orthogonal vector plots for the three samples, see figure 3.5). The remaining primary component then headed towards the origin and was entirely removed by 600°C. A small viscous component is removed from all samples by 150°C.

The dual aims of the follow up experiment to this initial preliminary study were to carry out orientated demagnetisation experiments on Block 1 and to more closely isolate the temperature at which the secondary component is removed. A further aim was to determine if two components of magnetisation were recorded in Block 2 as had been inferred from the preliminary study of Block 1.

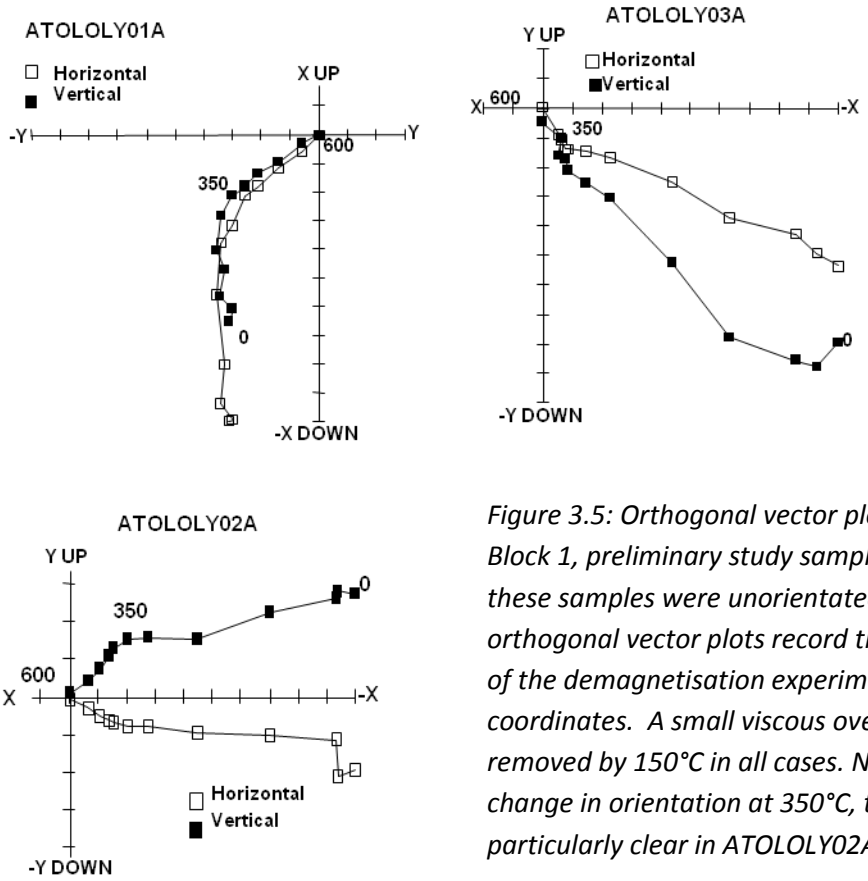

Figure 3.5: Orthogonal vector plots for Block 1, preliminary study samples. As these samples were unorientated, these orthogonal vector plots record the results of the demagnetisation experiment in core coordinates. A small viscous overprint is removed by 150°C in all cases. Note the change in orientation at 350°C, this is particularly clear in ATOLOLY02A.

3.7.2. Main Experiment Results

For all samples from Block 1 and Block 2, a small viscous component was removed at low temperatures (by 150°C) (tables 3.2 and 3.3). The experiments on the six Block 1 samples ended at 450°C because the aim was to isolate the temperature at which the secondary component was removed and the preliminary study indicated that this happened before 450°C. Above 450°C, the primary component demagnetised towards the origin. The results from this follow up study were noisy and inconsistent with the results of the preliminary study which all had a change in direction of the Arai plot at around 350°C. Only three of the six samples (BK1S3, BK1S4 and BK1S5) appeared to record two components of magnetisation. This secondary component of magnetisation was removed by 250°C, 300°C and 350°C respectively. BK1S2 does not appear to contain a stable primary component and BK1S6 is not heading towards the origin.

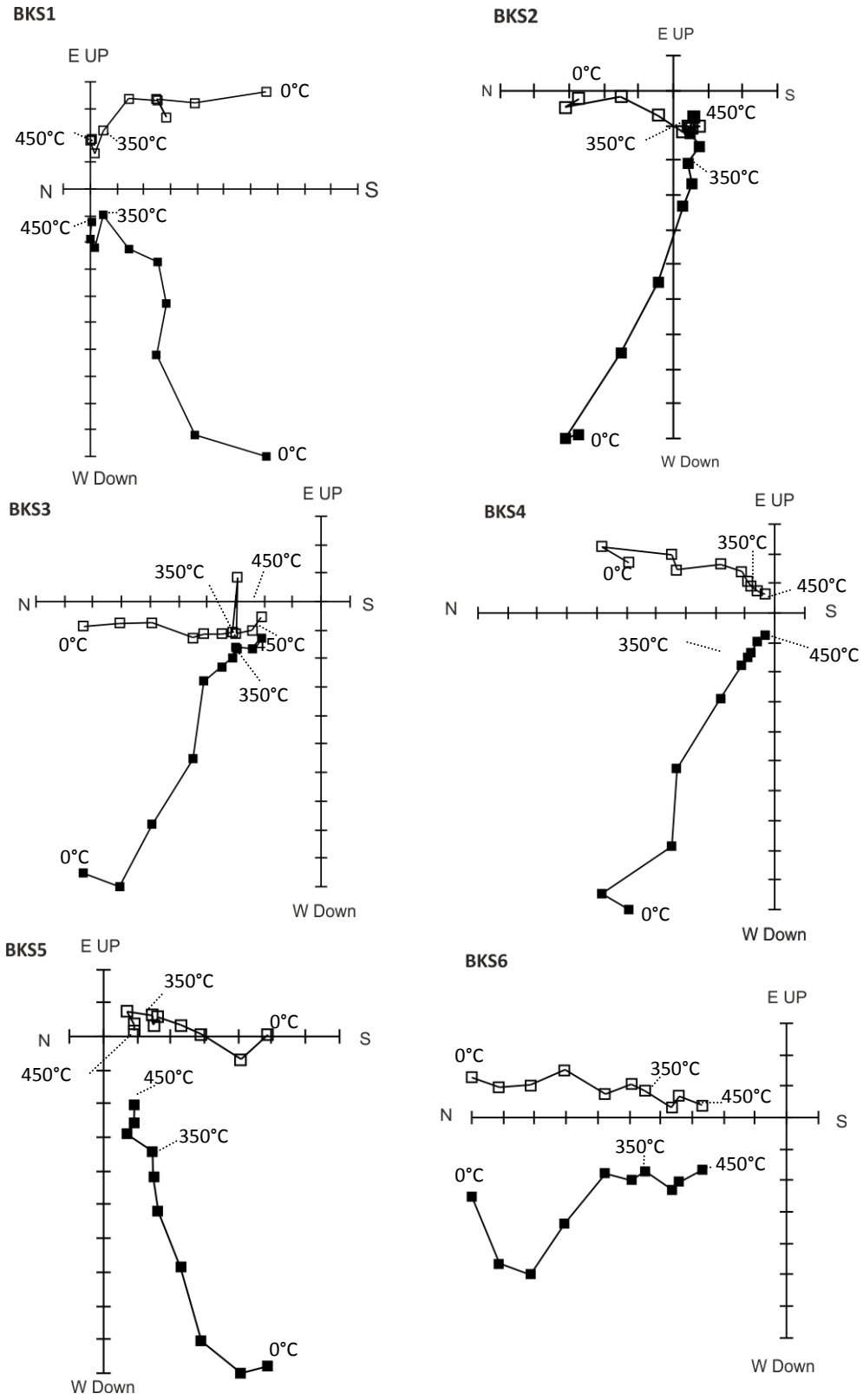

Figure 3.6: Representative Orthogonal Vector plots for orientated subsamples taken from Block 1. Notice the same viscous overprint as seen in the preliminary study samples shown in figure 3.5. Samples BKS12-4 were subsampled using method 1 and samples BK1S5 and 6 were sub-sampled using method 2 (the exact details of each are outlined in the text). The solid symbols represent the vertical component; the open symbols represent the horizontal component.

3.7.3. Block 2, Main Study Results

As the results of the follow-up experiment on Block 1 samples were inconsistent with each other and with the results of the preliminary study, the aim for the experiments on Block 2 was to establish if two components of magnetisation could be observed in this block and if so at what temperature the secondary component was removed. An additional aim was to determine the declination and inclination of the magnetic field recorded in the sample.

Figure 3.7: Block 2 orientated samples

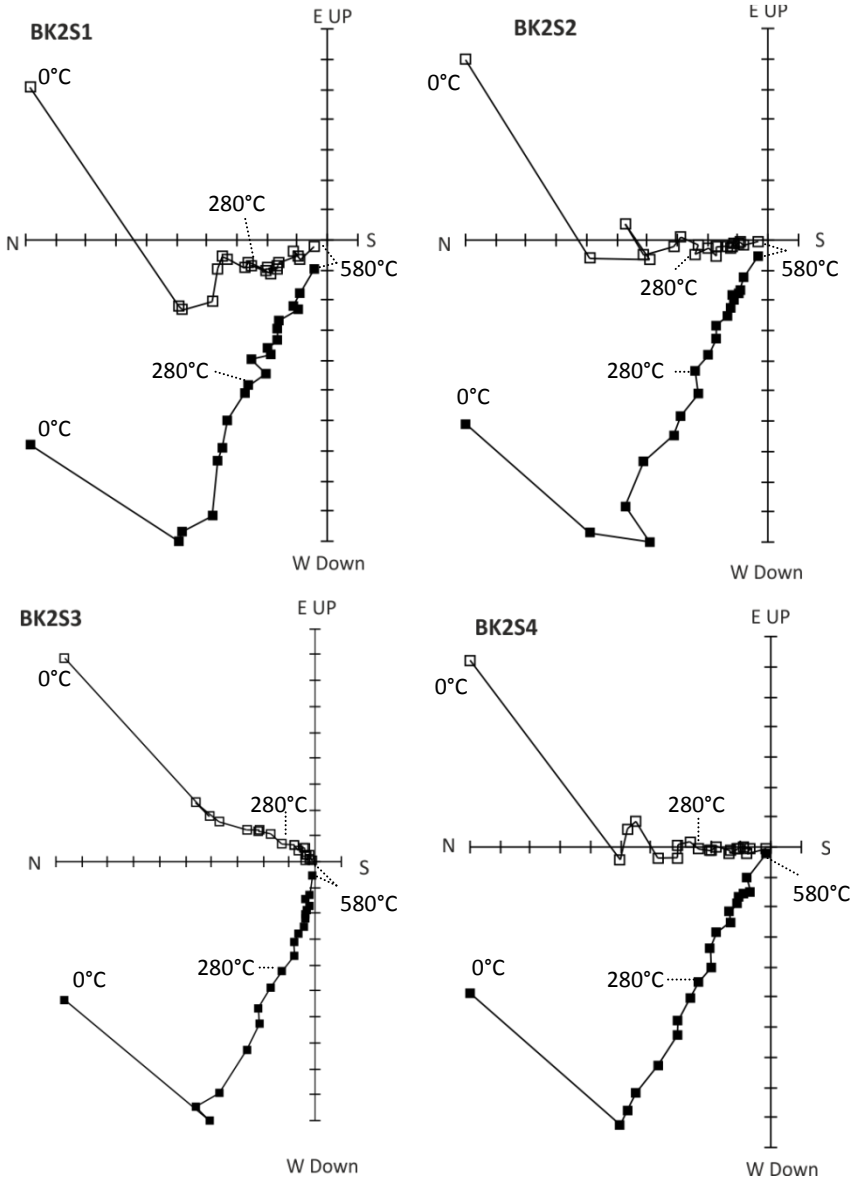

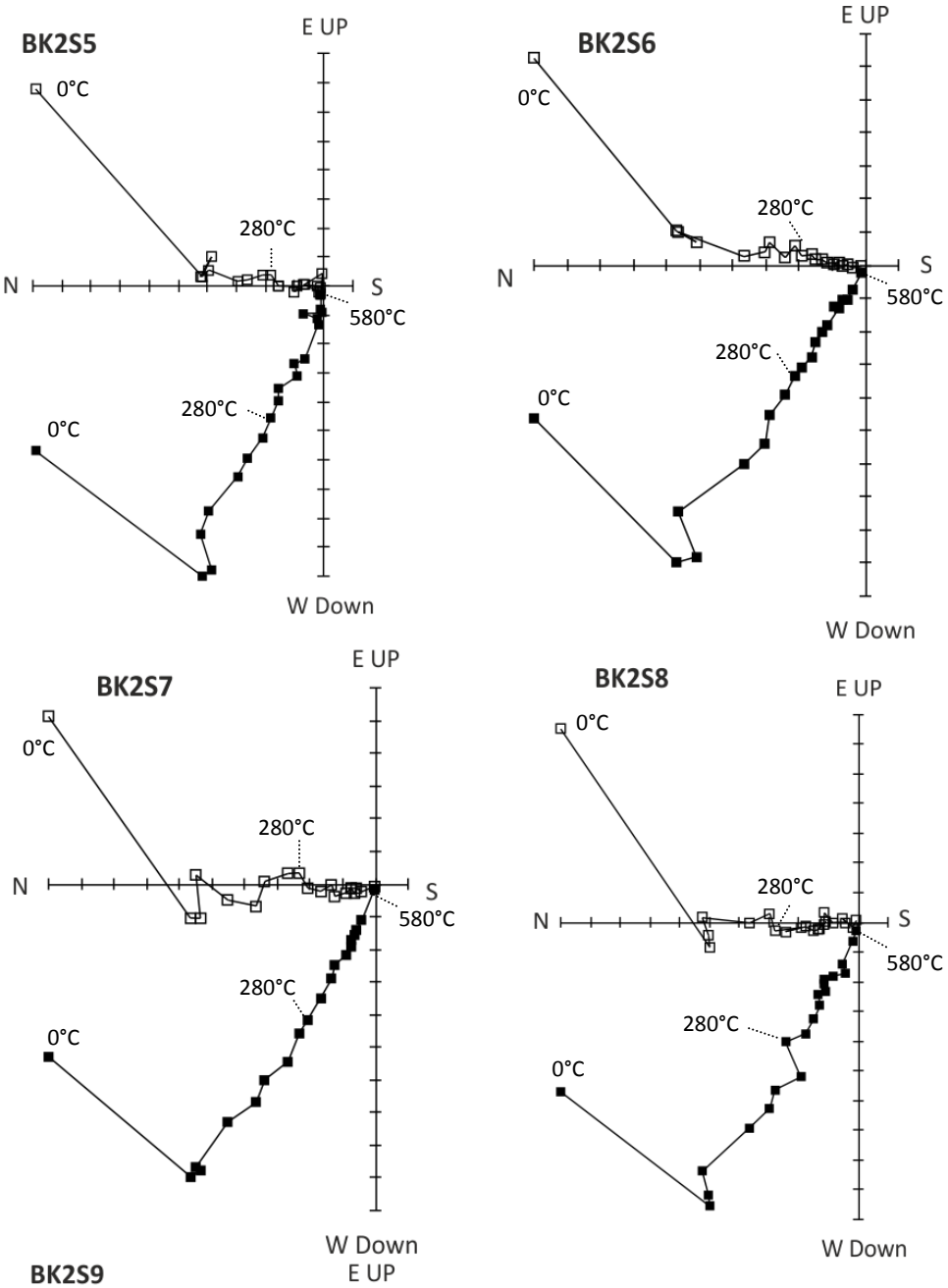

Figure 3.7: Orthogonal Vector plots for all orientated subsamples taken from the top of Block 2. All of these samples were analysed using method 1 described in the text above. It is noted that the viscous overprint observed in Block 1 is also apparent here, however, the change in direction observed in the preliminary study is not.

As can be seen from the orthogonal vector plots above and the equal area plot (figure 3.8), the results for the nine samples from Block 2 are quite uniform and less noisy than the results from Block 1. Only two samples, BK2S3 and BK2S6 appear to contain more than one component which is removed by 280°C. This secondary component is consistent between these two subsamples with an average inclination of 58° ±3 and an average declination of 15° ±8. For all Block 2 samples a viscous remanent magnetisation is removed by 50°C (with the exception of one case where it is removed by 100°C).

The results from the 9 samples from Block 2 give an alpha 95 of 5° and a k value of 105 with a mean inclination of 65°and a mean declination of 356°.

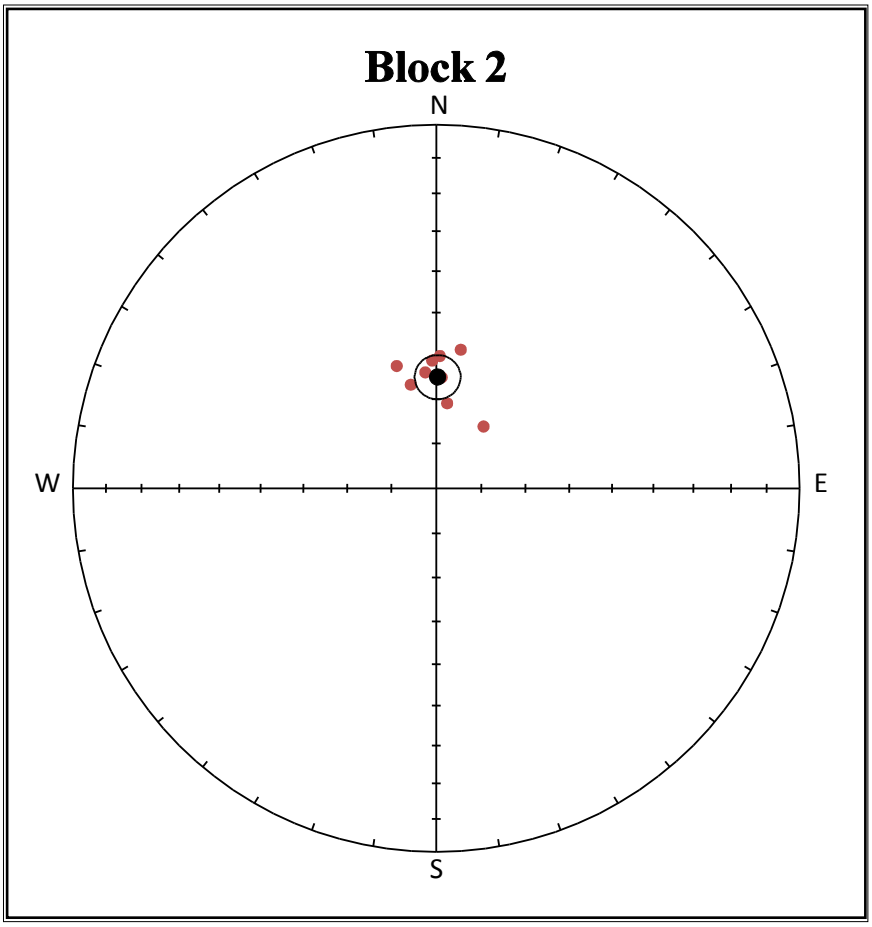

Figure 3.8: Equal area plot for each of the 9 sub- samples from Block 2. The results have been plotted as single components. Also plotted is the 95% cone of confidence. Full symbols indicate that the points are plotted in the upper hemisphere of the projection. The mean inc and dec is plotted as the black circle in the centre of the 95% cone of confidence.

Table 3.3: Directional results for Block 1

Sample	Dec	Inc	MAD	α95	No. of steps	T_1-T_2	Comments
ATOLOLY01A	219.1	25	5.6	17.2	6	350-600°C	Unoriented
ATOLOLY02A	209.1	-35.6	4	11	6	350-600°C	Unoriented
ATOLOLY03A	237.8	56.6	15.1	15.9	6	350-600°C	Unoriented
BK1S1	117.4	44.9	16.8	12.4	9	100-450°C	
BK1S2	257.1	67.3	6.4	14.3	9	100-450°C	Does not head to the origin
BK1S3	352.3	37.5	11.4	8.6	9	100-450°C	
BK1S4	48.9	51.3	6.5	6.9	9	100-450°C	
BK1S5	170.1	69.9	7.2	3.9	9	100-450°C	
BK1S6	14	26.3	13.6	3.8	9	100-450°C	Does not head to the origin

Dec, mean declination; Inc, mean inclination; MAD, Mean Angular Deviation; α95, 95% cone of confidence; No. of steps, number of temperature steps in the demagnetisation experiment from which the dec and inc has been calculated; T1-T2, the temperature of the first and last accepted steps. To correct for local declination at the time of sampling 5° has been added to all orientated declination values.

Table 3.4: Directional results for Block 2

Sample	Dec	Inc	MAD	α95	No. of steps	T_1-T_2
BK2S1	341.8	61.0	7.5	1.8	19	50-580°C
BK2S2	357.9	61.2	7.6	1.6	19	50-580°C
BK2S3	37.3	72.6	5	2.6	18	100-580°C
BK2S4	361.6	60.2	5.8	2.1	19	50-580°C
BK2S5	7.2	70.8	5.5	4.8	19	50-580°C
BK2S6	10.1	58.2	4.8	1.9	19	50-580°C
BK2S7	354.5	63.8	6.7	3.2	19	50-580°C
BK2S8	2.9	65.1	6.3	3	19	50-580°C
BK2S9	345.9	66	7.5	2.6	19	50-580°C

Dec, mean declination; Inc, mean inclination; MAD, Mean Angular Deviation; α95, 95% cone of confidence; No. of steps, number of temperature steps in the demagnetisation experiment from which the dec and inc has been calculated; T1-T2, the temperature of the first and last accepted steps. To correct for local declination at the time of sampling 5° has been added to all orientated declination values.

The average mean directional result for Block 2, corrected for local declination at the time of sampling, is relocated to Kayseri which is the approximate centre of Turkey (lat: 38.85°N, long: 35.63°E) and plotted against all the data in GEOMAGIA50v2 (Donadini et al., 2006, Korhonen et al., 2008) from within a 1500km radius of Kayseri, previously published Turkish data (Saribudak and Tarling, 1993, Ertepinar et al., 2012, Sayin and Orbay, 2003) and the global geomagnetic field models ARCH3k_cst.1 (Korte et al., 2009, Donadini et al., 2009), CALS3k.4 (Korte and Constable, 2011), CALS10k.1 (Korte et al., 2011) and pfm9k.1A (Nilsson et al., 2014) calculated for Kayseri (figure 3.9a and b). Relocating the results to Kayseri allows direct comparison with the work of Ertepinar et al. (2012). The data points with α95 > 15° or precision parameter k < 50 are rejected. The result determined here for Oylum Höyük is plotted twice, using two different dates: the black diamond is the result from

Oylum Höyük plotted using the archaeological date of late 2nd century BC/ Early 3rd Century BC (plotted at 200 BC as this is the middle value for this age range). The red diamond is plotted at the centre of the date assigned to the feature based on the radiocarbon dates. The date from the radiocarbon gave a maximum age of 3640 to 2510 BC and a minimum age of between 1270 to 920 BC. Using the minimum value for the maximum age of the feature (2510 BC - based on the cremated animal bone found in the feature) and the maximum value for the minimum age of the feature (1270 BC - based on radiocarbon samples from stratigraphically above the feature) gives an age bracket of 2240 years. The result from Block 2 was plotted in the middle of this age bracket at 2390 BC. Due to the significant age error associated with the radiocarbon dates, it is difficult to draw any definitive conclusions about the probable date of the feature. This is particularly true as the determined inclination and declination values are consistent with values across the entire age bracket plotted. Therefore, it is not possible to reject either of the proposed dates of the feature based on the record of the geomagnetic field recorded in this block based on our current limited knowledge of the field in Turkey at this time.

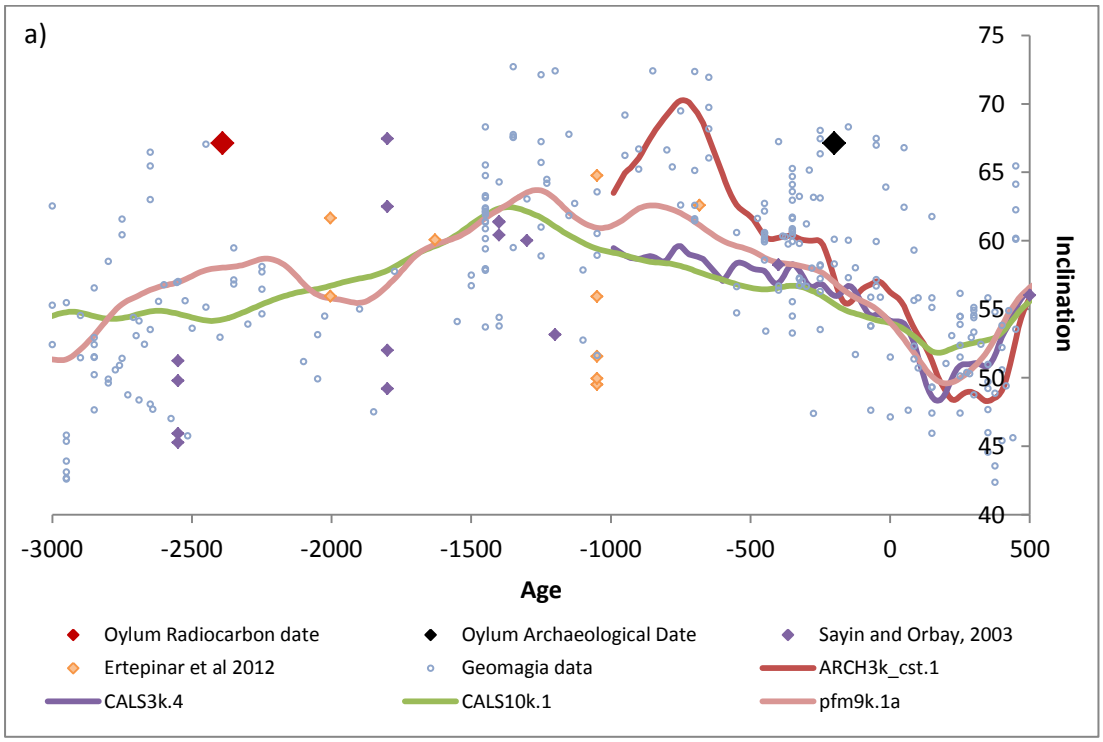

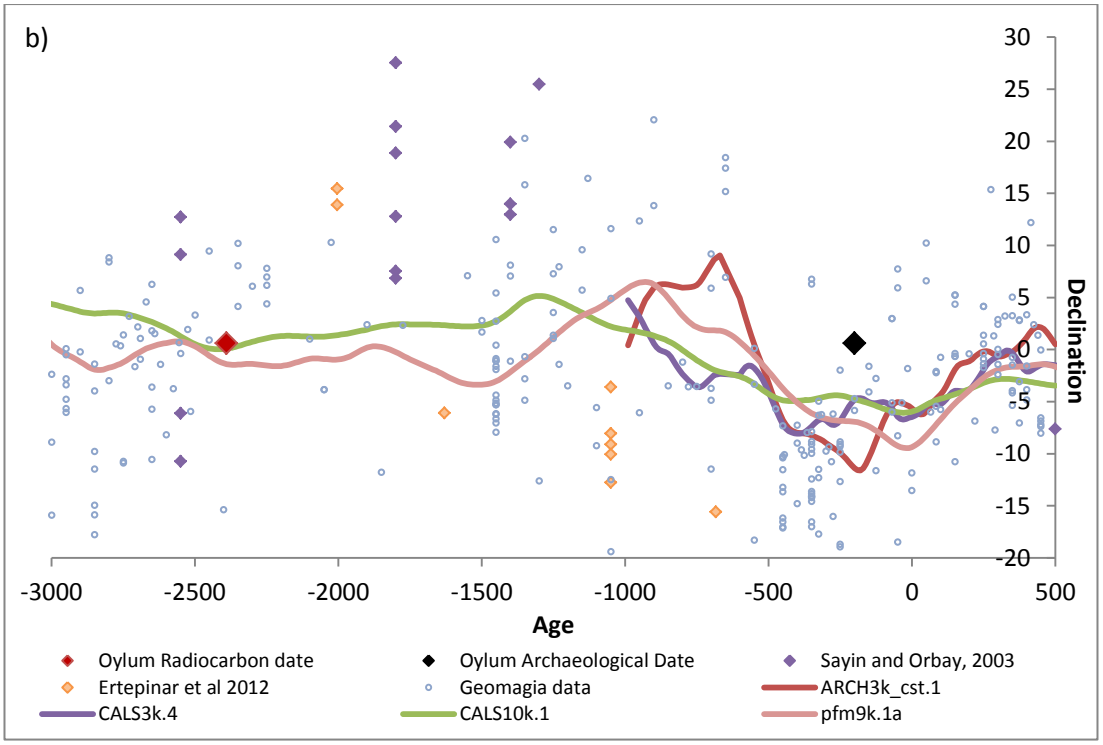

Figure 3.9: Comparison of the (a) declination and (b) inclination for Oylum Höyük obtained in this study. Due to the striking difference between the age of the feature based on the archaeological interpretation of the site and the age bracket determined from the radiocarbon, the inclination and declination measured in these blocks from Oylum Höyük has been plotted twice. The Red diamond is the Oylum data plotted using the radiocarbon age whilst the black diamond is the Oylum data plotted using the age based on archaeological evidence. These Oylum data are plotted with Turkish data (purple and orange) and GEOMAGIA50v2 data (open blue circles) and the global geomagnetic field models ARCH3k_cst.1 (red), CALS3k.4 (purple), CALS10k.1 (green) and pfm9k.1A(pink).

3.8.Determining the Magnetic Carriers

In order to characterise the magnetic carriers and heating history of the two blocks, experiments were carried at the University of Liverpool Geomagnetism Laboratory using the Variable Field Translation Balance (VFTB). The VFTB was used in two ways. The first way was to characterise the bulk magnetic carriers in each block. The second was to determine the temperature at which any alteration occurs. If alteration does occur it is likely that the temperature at which it occurs would represent the maximum temperature the blocks had been heated to in antiquity. This is based on the assumption that the magnetic minerals in the blocks are stable to the maximum temperature they previously reached in the kiln and unstable above this temperature. This will provide a minimum estimate of the maximum temperature reached in the kiln.

The sample preparation for all experiments run on the VFTB involved crushing the sample and removing any stone fragments (>0.5mm). This was done in the former case to reduce anisotropy effects and in the latter to prevent bias. Analysed samples weighed between 100mg and 200mg and the positions of the samples within the blocks with respect to each other are indicated in figure 3.10a and b. In addition to samples from the two blocks, samples from the nearby river, Akpýnar Suyu, were also analysed to see if there were any differences/ similarities between them and Blocks 1 and 2. Akpýnar River samples were analysed in order to confirm or refute the archaeological interpretation that the feature was constructed using clay from the river (see table 3.5 for details of experiments run on each sample).

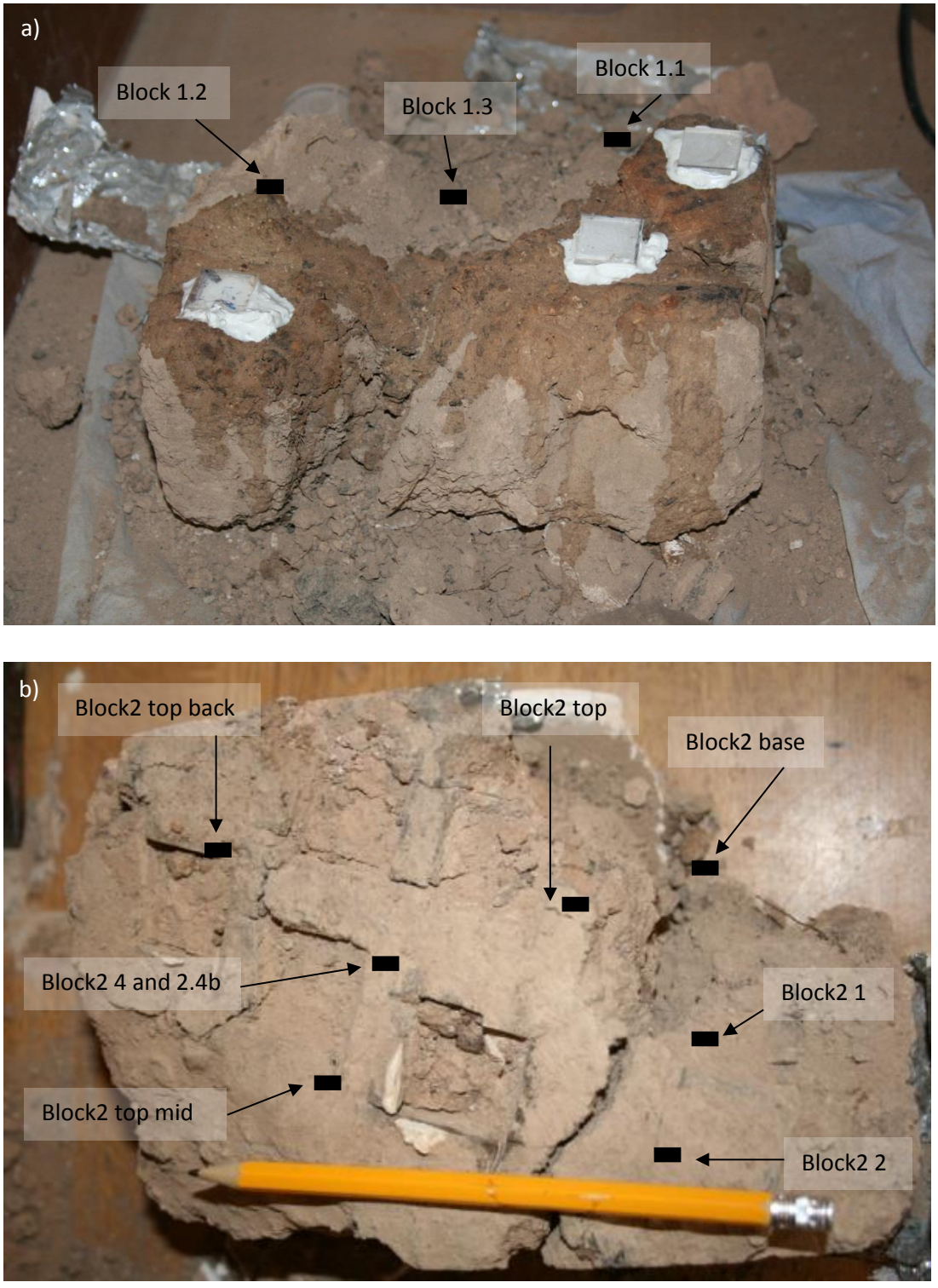

Figure 3.10: Photographs of Block 1 a) and Block 2 b) showing the location of the VFTB samples in the original block. The samples taken from the top of the block represent the top 5mm of the block.

Table 3.5 List of samples measured in order to determine the magnetic carriers and the thermomagnetic history of Blocks 1 and 2

Sample	VFTB experiments	Repeat VFTB experiments	Repeat heating experiments
Block 1.1	Y	-	-
Block 1.2	Y	-	-
Block 1.3	Y	-	-
Block 2.1	Y	-	-
Block 2.2	Y	-	-
Block 2 top	Y	-	Y
Block 2 base	Y	-	Y
Block 2 top back	Y	-	-
Block 2 top mid	Y	-	-
Block 2.4	Y	-	-
Block 2.4b	Y	Y	-
Akpýnar Suyu	Y	Y	-
Akpýnar Suyu	Y	-	-

Table 3.5 details the experiments run on samples from Block 1 and Block 2 with the aim of determining the magnetic carriers and the thermomagnetic history of Blocks 1 and 2. Repeat VFTB experiments column indicates which samples were subject to two suites of VFTB experiments with the aim of determining how stable the sample was to heating. Repeat heating experiments were repeat thermomagnetic experiments to increasing temperature. For more detail on each experiment, see main text.

The VFTB results for all the samples analysed show consistency between the two blocks and from top to bottom of Block 2 (figures 3.11-15). This consistency is not seen between the two randomly positioned samples from Block 1 (samples BK1S1 and BK11S2). It is noted that all samples are pseudosingle domain-like in their behaviour and plot within a very small area of the pseudo single domain region of a Day plot (figure 15). All samples contain a paramagnetic component but are dominated by a low coercivity phases like titanomagnetite. The thermomagnetic curves are irreversible for all samples and the heating curves typically have higher magnetisation than the cooling curves indicating that the heating created weaker magnetic minerals at the expense of stronger magnetic minerals (figure 12). The thermomagnetic curves are relatively linear suggesting the presence of either a range of grain sizes and or/ a range of magnetic carriers, most likely magnetite with a variety of compositions. A change in slope at ~580°C is observed for all samples and implies the presence of magnetite. It is noted that the river sample alone shows a change of slope in its heating curve at around 350°C. This is still present in the

cooling curve, although it is not as pronounced, and is interpreted to be maghemite which altered to a less magnetic phase e.g. haematite on heating and therefore is not present in the cooling curve. The IRM curves indicate that all the samples reached saturation at fields below 200 mT. It is noted that the greatest difference between samples from the same block is observed for samples from Block 1; sample BK1S1 and sample BK1S2, this implies heterogeneity within the block which is not observed between the samples from the base and top of Block 2. Sample BK1S2 is consistent with the river sample and with samples from Block 2 whilst BK1S1 has a greater intensity of magnetisation. It is also noted that the thermomagnetic curves from Block 2 are highly reversible whilst those from Block 1 are less reversible.

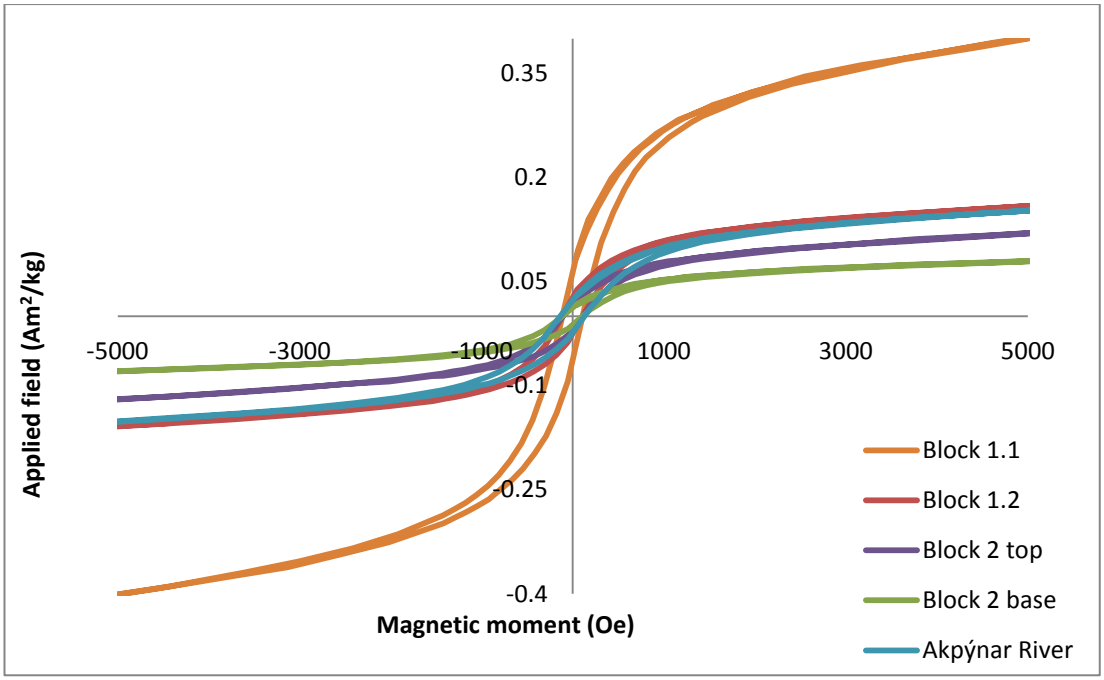

Figure 3.11: Hysteresis curves for a number of samples from Blocks 1 and 2 and for a sample from the Akpýnar River.

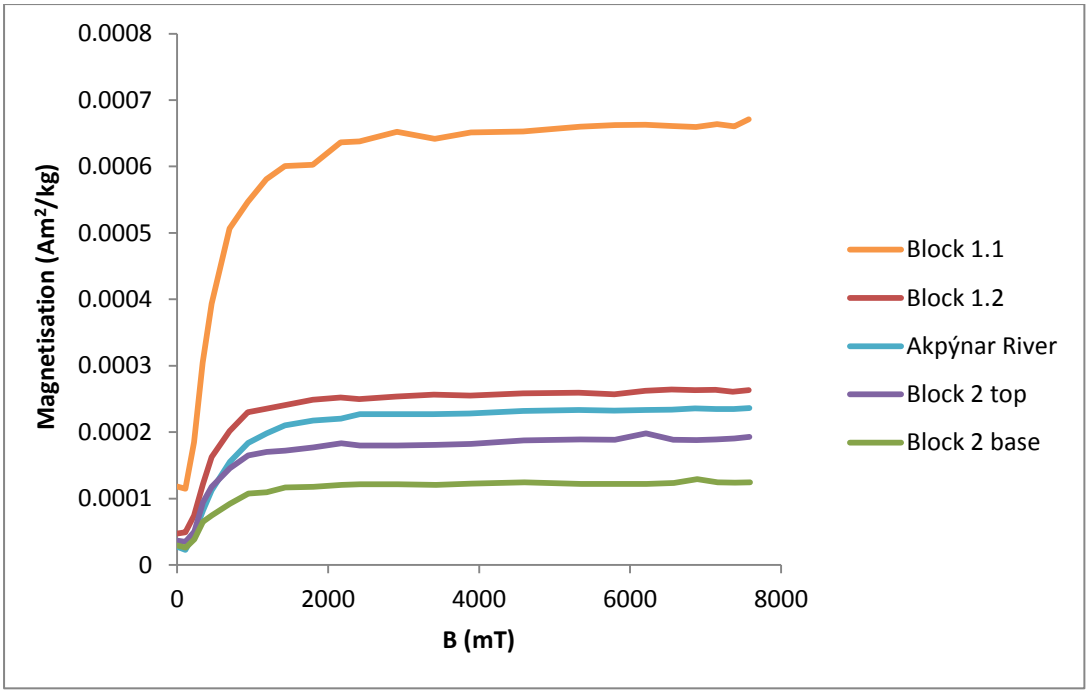

Figure 3.12: IRM curves for a number of samples from Blocks 1 and 2 and a sample from the Akpýnar River.

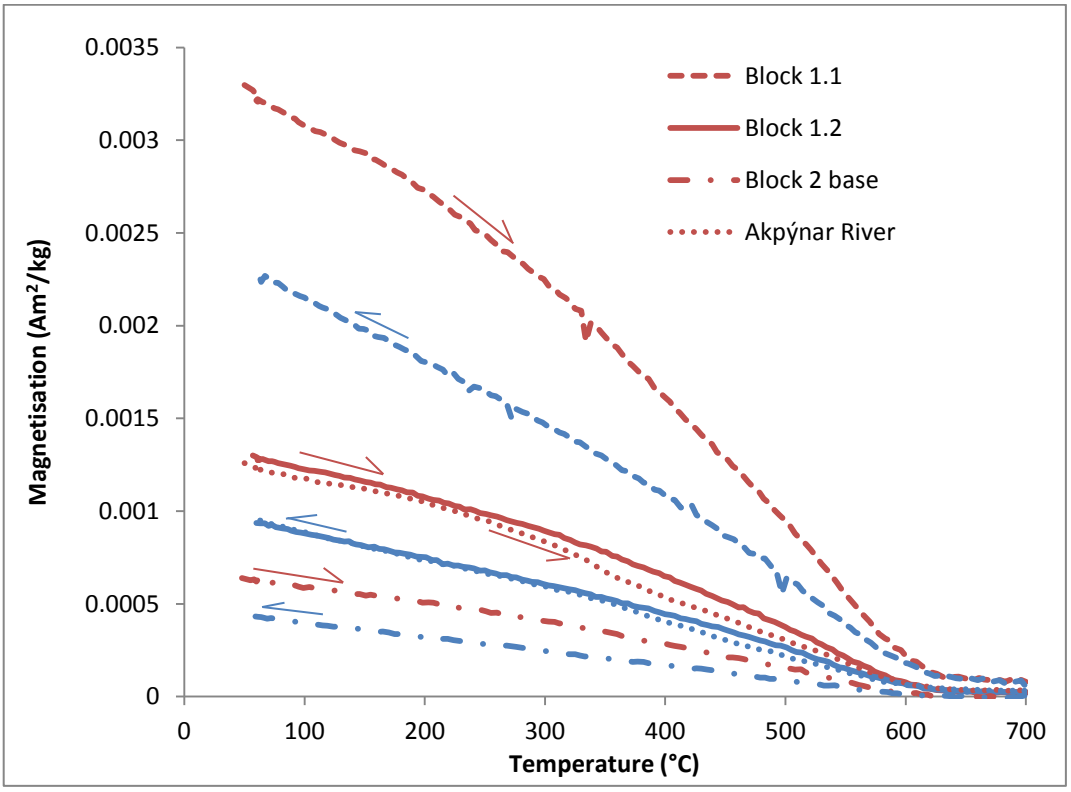

Figure 3.13: Thermomagnetic curves for samples from Blocks 1 and 2 and a sample from the Akpýnar River. Block 2 top is not shown here because it plotted on top of the result for sample Block 2 base front.

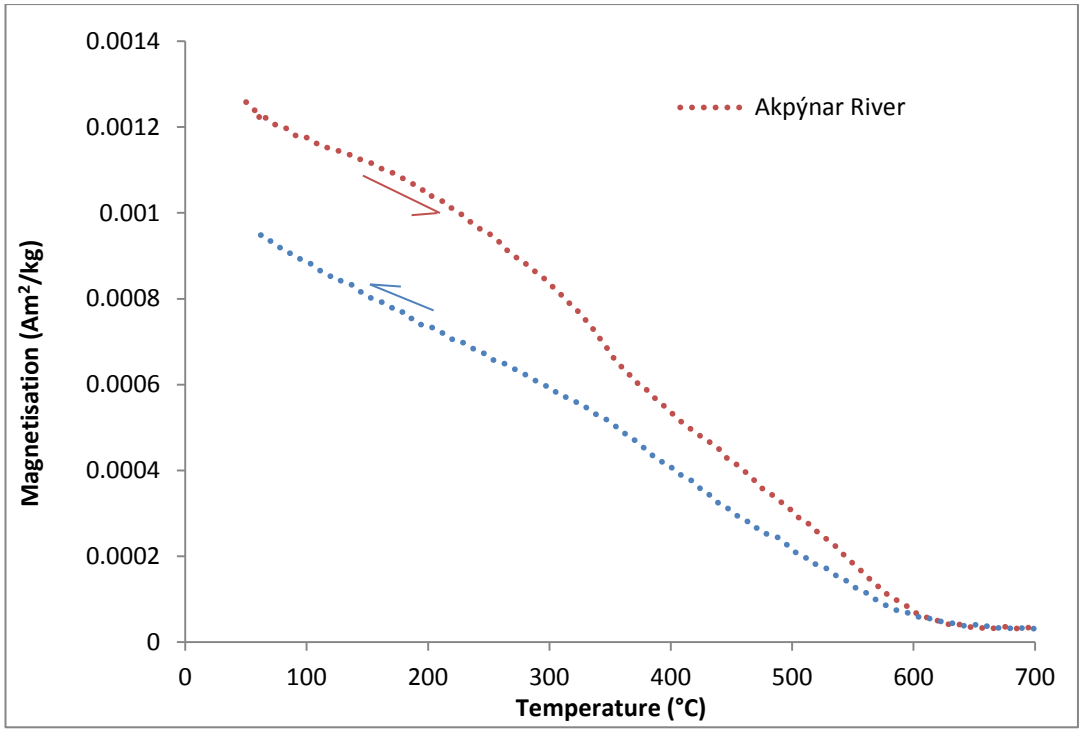

Figure 3.14: Thermomagnetic curve for a sample from the Akpýnar River clearly showing alteration on cooling.

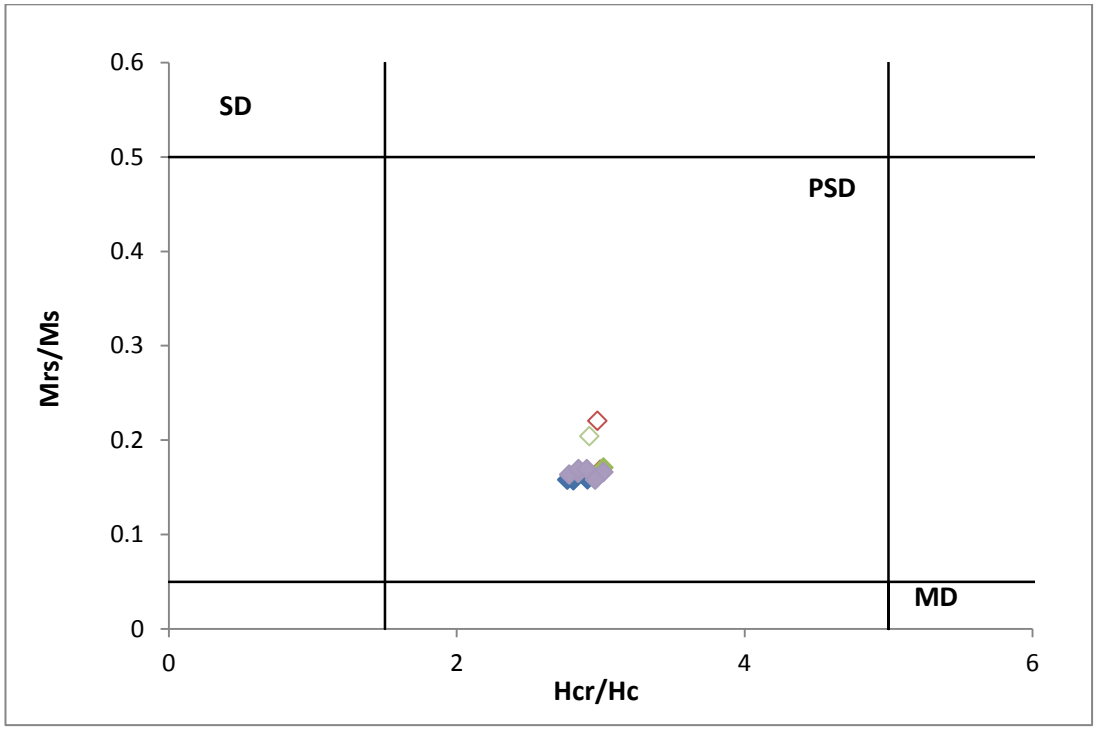

Figure 3.15: Day plot for Block 1 and Block 2 showing that there is significant homogeneity in grain domain states throughout the two samples. The purple data are from Block 2, the blue from Block 1, the red are river samples with an empty symbol indicating the sample had been analysed twice. The green diamonds are samples from Block 2. The result of a second heating of one of these samples is indicated by the hollow green diamond.

Table 3.6: Rock Magnetic Properties

Sample	M_s	M_{rs}	H_c	H_{cr}	H_{cr}/H_c	M_{rs}/M_s
Block 1.1	0.30	0.05	10.92	31.77	2.91	0.16
Block 1.2	0.12	0.02	10.81	29.93	2.77	0.16
Block 1.3	0.09	0.01	11.09	31.19	2.81	0.16
Block 2.1	0.15	0.03	11.12	31.65	2.85	0.16
Block 2.2	0.09	0.01	11.40	34.44	3.02	0.17
Block 2.top	0.14	0.02	11.08	30.84	2.78	0.16
Block 2 top back	0.08	0.01	11.10	31.60	2.85	0.17
Block 2 top mid	0.06	0.01	10.98	32.55	2.96	0.16
Block 2 base	0.08	0.01	11.10	32.24	2.91	0.17
Block 2.4	0.14	0.02	11.20	33.84	3.02	0.17
Block 2 4b	0.09	0.02	12.29	35.93	2.92	0.20
Akpýnar 1	0.11	0.02	13.18	39.54	3.00	0.17
Akpýnar 1b	0.09	0.02	16.38	48.78	2.98	0.22

Where Ms, saturation magnetisation; Mrs, saturation remanence; Hc, coercivity; Hcr, coercivity of remanence; Tc, Curie Temperature.

3.9. Determining the Temperature of Alteration

The second way the VFTB was used was to attempt to isolate the temperature to which the blocks had previously been heated. This was achieved using three different techniques on samples from the top and the base of Block 2. Following the destructive sub-sampling of Block 1 for the demagnetisation experiment, very little remained of Block 1 and it was not possible to carry out further experiments. It was expected that there would be a significant temperature gradient from the top to the bottom of each block. It was also anticipated that the top of both blocks was more likely to clearly record two components of magnetisation than the base. As it was not possible to determine the original base of the sample from what remained of Block 1, none of the following experiments were performed on samples from Block 1. The experiments are confined to Block 2 samples.

All three methods employed involved repeated heating experiments beginning at 300°C and reaching 700°C. The thermomagnetic curves for all these experiments were plotted on top of each other. This is shown in figure 3.16a and b for samples from the top and base of Block 2. In order to make the graphs clearer only the 600°C and 700°C steps are plotted. In both samples all the lower temperature steps plot on the 600°C curve so this curve is

representative of all the previous steps. The 700°C temperature step for both samples is less reversible than the 600°C step and has a lower magnetisation than all the previous steps.

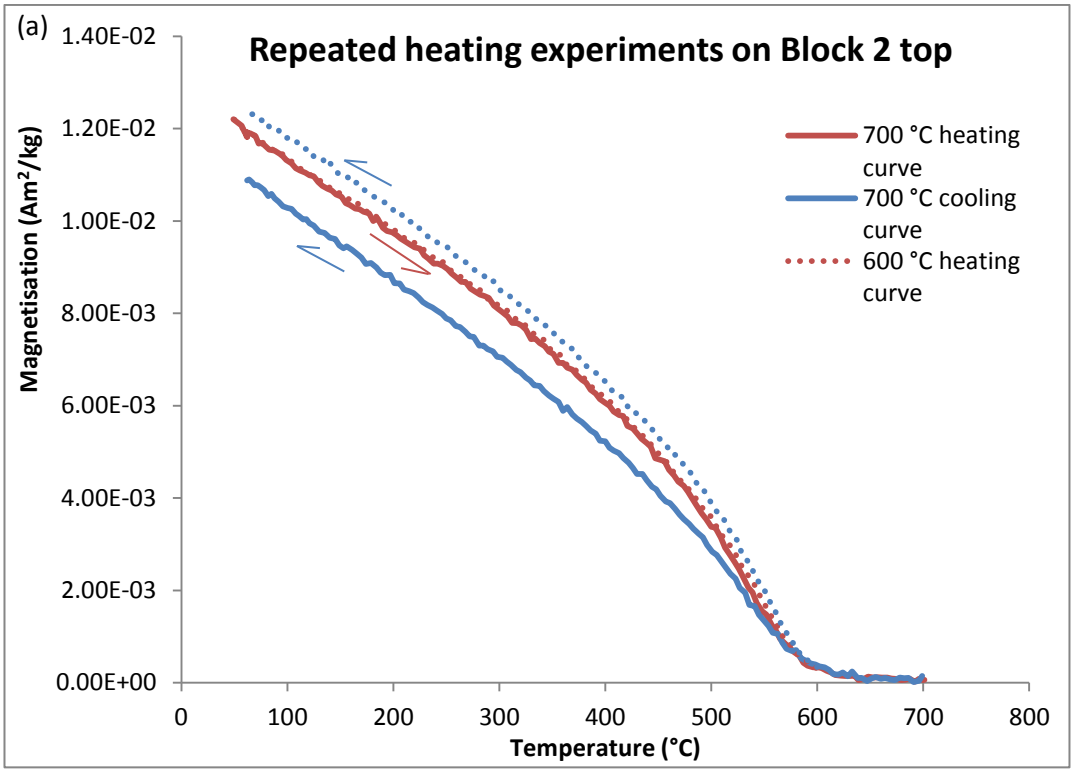

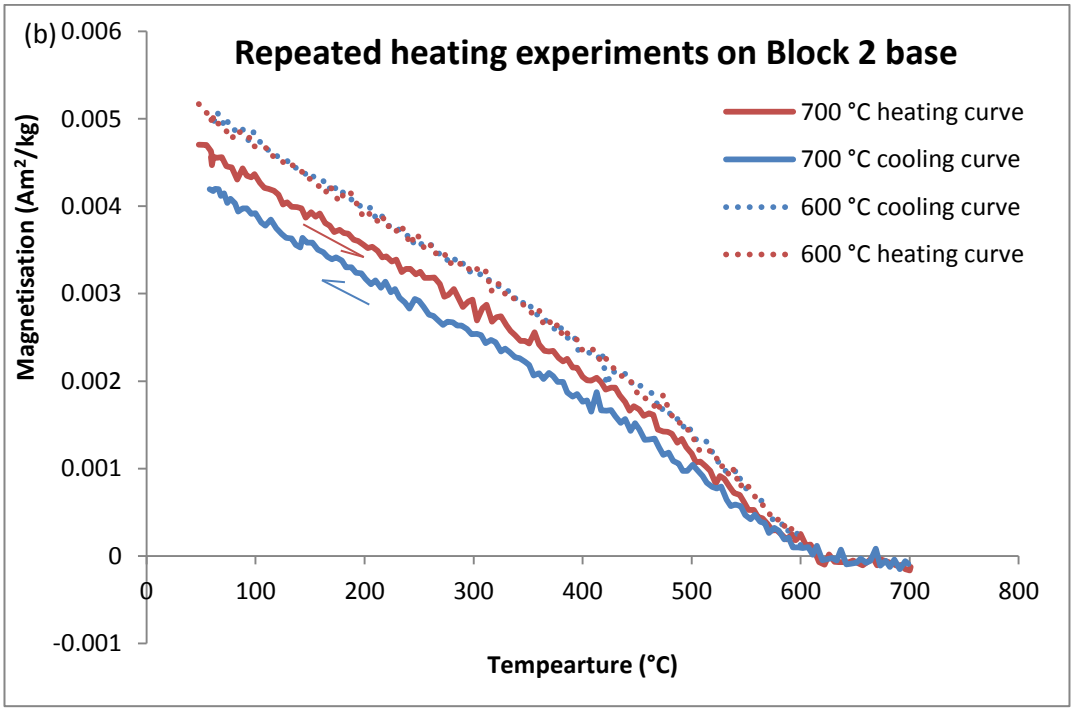

Figure 3.16a and b: Results of repeating thermogmagnetic experiments to increasing temperature on samples from the base and top of Block 2.

Further analysis of alteration temperatures was conducted using repeat magnetic saturation/temperature experiments at increasing temperatures following the work of Hrouda et al (2003). The experiments run are based on the principle that a sample that has been heated to a certain temperature, T_1, will not change its rock magnetic properties if it is heated again to T_1 in the laboratory under similar conditions. This is true if the magnetic minerals were in chemical equilibrium at T_1. When the sample is heated above T_1 the magnetic minerals are no longer in chemical equilibrium, resulting in changes in the rock magnetic properties. This concept assumes that post-baking weathering has not occurred.

The experiments conducted involved samples from both the top and the base of Block 2 (figure 3.10 b) with the aim of determining if Block 2 recorded a temperature gradient from its top to its base. If the temperature at which the sample switches from producing reversible to irreversible heating and cooling curves can be isolated then this temperature is inferred to be the previous highest temperature reached. This temperature is isolated by repeated progressive heating from room temperature to 700°C.

In a technique proposed by Hrouda et al (2003) an alteration index is calculated. This alteration index is a quantitative evaluation of the change in susceptibility after a whole cycle of heating and cooling has been run. Due to instrument constraints we considered instead the change in high field magnetisation after a whole cycle of heating and cooling had been run. It is acknowledged that mass magnetisation is a less sensitive indicator of change than susceptibility is.

The alteration index (as defined by Hrouda et al (2003) is as follows

$$A_{40}=100(k_{40}-K_{40})/K_{40} \qquad (3.1)$$

where k_{40} and K_{40} are the magnetisations on the cooling and heating curves at 40°C respectively. A positive index value indicates higher cooling than heating susceptibility, while a negative alteration indicates the opposite relationship. The temperature of 40°C was chosen by Hrouda et al (2003) because on cooling it can be reached more easily than the room temperature at the start of the experiment. Instrument differences meant that for this study, the most easily reached temperature using the VFTB was 60°C and so here the room temperature magnetisation was represented for practical reasons by the K_{60} and k_{60} magnetisation. This difference between this study and the work of Hrouda et al. (2003)

should not affect the calculated alteration because in each step of this experiment, the temperature window in which alteration occurred is significantly greater than 60°C.

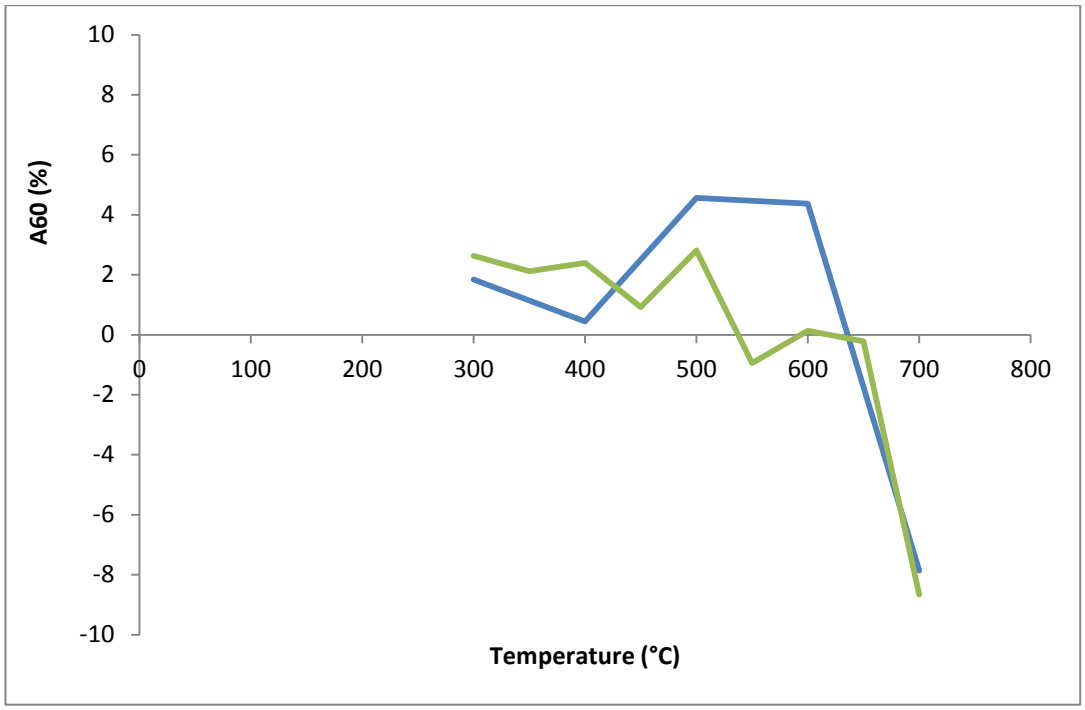

Figure 3.17: Change in the average A_{60} alteration index in individual heating/cooling runs of a sample from the top of Block 2. It is noted that the A_{60} alteration index is very low throughout the whole temperature range and the experiment is highly reversible. The green data are from the base of the block whilst the blue data are from the top.

Hrouda et al (2003) recorded alteration indices of up to 600%. As shown in figure 17 a maximum change of 12% is recorded by the sample from the top of the block between 600°C and 700°C whilst the maximum change seen in the sample from the base of the block is 10%, again observed between 600°C and 700°C. This small percentage change suggests that these two samples had either been heated to above 700 degrees previously or that alteration occurred regularly throughout the temperature range. There is no clear difference in the result for the subsample from the top of the block compared with that from the bottom of the block. This suggests no significant temperature gradient is recorded from the top of the block to the base. It is noted that this method assumes alteration due to lack of a previous heating to this temperature. In reality it may be due to heating in a different redox environment.

The third method employed in order to isolate the maximum heating temperature follows the work of Henry et al (2005) who studied changes in magnetic mineralogy in rocks

revealed by hysteresis loops differences measured after stepwise heating. Carrancho (2011) applied this method on samples from an experimental fire where the temperature was recorded by thermocouples. They found the method did not contradict the measured temperatures. The analysis involves using the hysteresis loop obtained as a difference loop between the two hysteresis loops measured after thermal treatment at two different temperatures. Here it is between hysteresis loops measured at room temperature after heating to 300°C and at 700°C for the top and base of Block 2. Significant evolution of the shape of such loop can arise when the ferrimagnetic part of the rock is affected by mineralogical alteration due to thermal treatment.

The difference hysteresis loop ($J_{Tj} - J_{Ti}$) presented in figures 3.18a and 3.19a are obtained by subtraction of the two intensities (J_{Tj} and J_{Ti}) measured at a given applied field value (H) for two successive temperatures Tj and Ti respectively, with Tj > Ti (Ti ≥ T0). The negative difference loop in Figure 3.19a is indicative of the disappearance of the ferrimagnetic phase. The positive difference loop in figure 3.18a is indicative of the occurrence of a new phase.

The half difference of magnetization between ascending and descending curves of a hysteresis loop as a function of the applied field is related to the acquisition of the remanent magnetization and is termed the 'remanent' curve (figures 3.18b and 3.19b). The 'induced' curve is the half sum of the magnetization in the descending and ascending curves as a function of the applied field (figures 3.18c and 3.19c) (Henry et al., 2005).

The difference loop for the top of Block 2 appears to show the formation of one ferrimagnetic phase. As the peak in the remanent curve is negative this indicates that the appearing phase has a lower coercivity than the original phase. The induced curve suggests the newly created component has a high saturation (the loop does not saturate) (figures 3.18 a-c). The difference loop for the base of Block 2 shows the disappearance due to transformation of one ferrimagnetic phase. The remanent curve is too noisy to be interpreted. The induced curve suggests that the disappearing phase had a high saturation value. The slight dip in the magnetisation either side of the y axis may be suggestive of a difference in measured coercivity following the disappearance of the ferromagnetic phase (figures 3.19a-c).

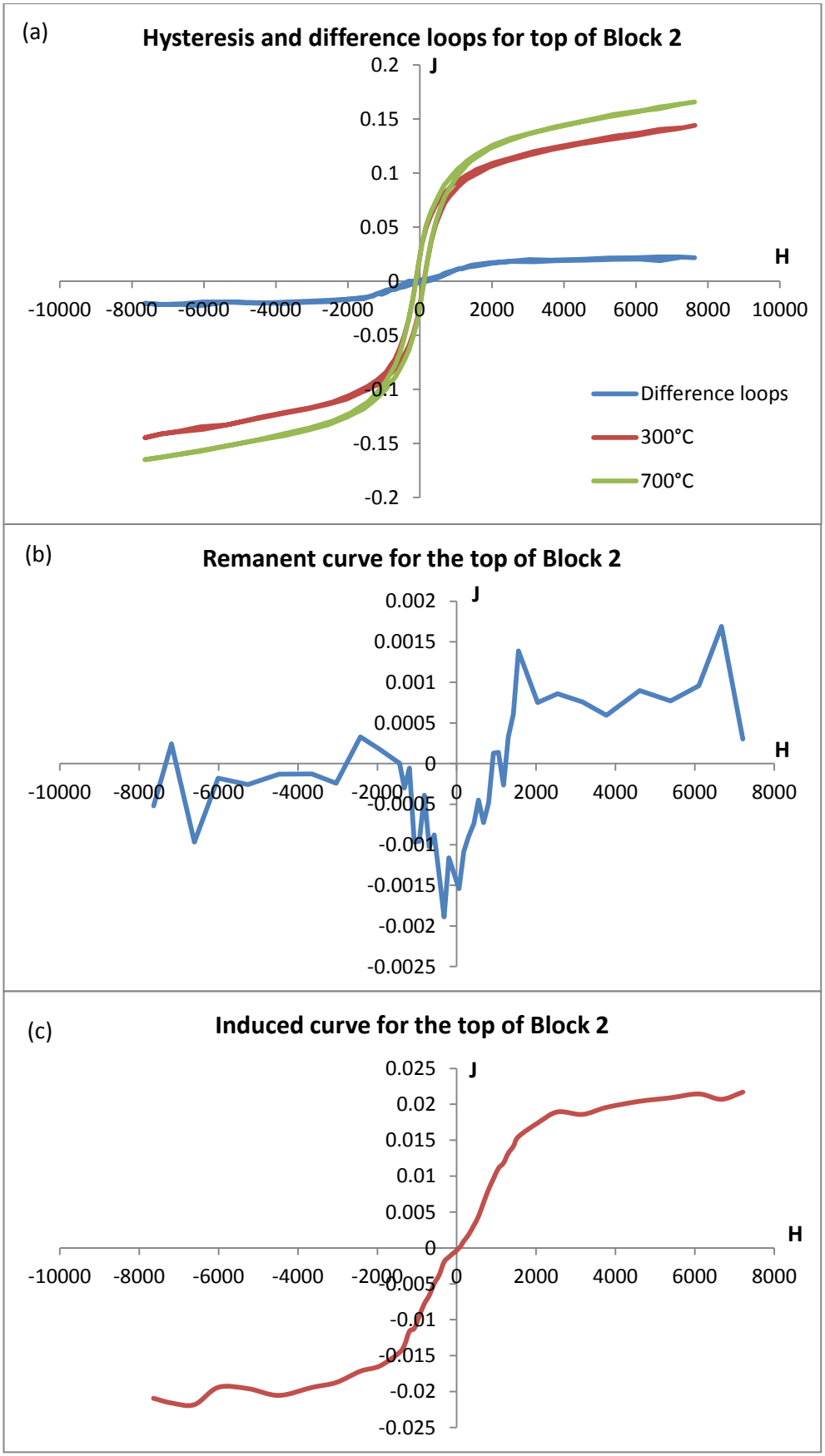

Figure 3.18: (a) Measured hysteresis loops after heating to 300°C and 700°C in a sample from the top of block 2. Also shown is the resultant difference loop for these two measurements. (b) remanent curve for the same sample, (c) induced curve for the sample.

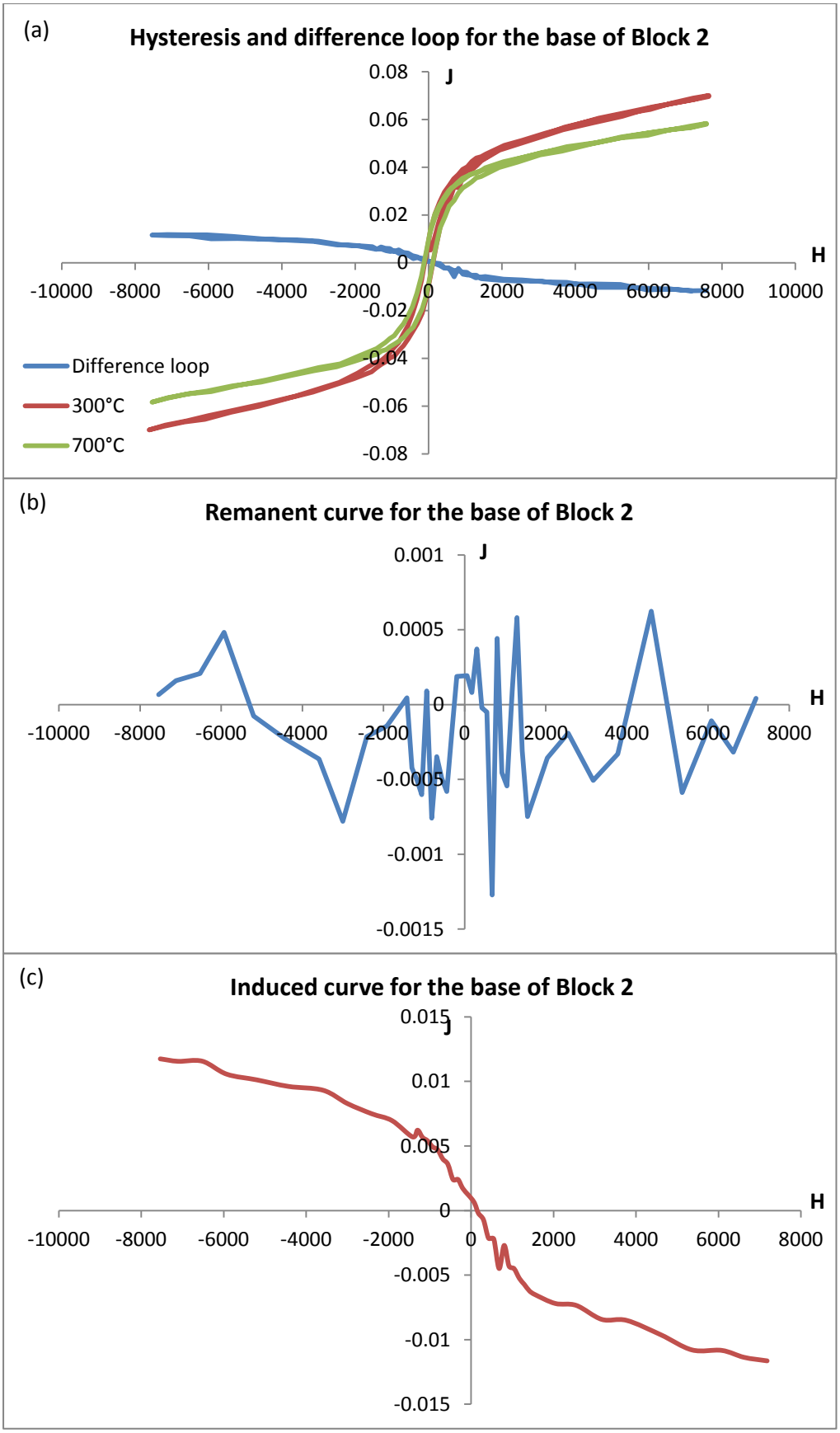

Figure 3.19: (a) Measured hysteresis loops after heating to 300°C and 700°C in a sample from the base of block 2. Also shown is the resultant difference loop for these two measurements. (b) remament curve for the same sample, (c) induced curve for the sample.

3.10. Discussion

3.10.1. Difficulties with the material

There were a number of difficulties encountered during this study. The first was the dryness of the blocks which made sub-sampling challenging. Block 1 was sub-sampled using two different methods: Method 1 involved the use of dilute sodium silicate to harden the surface of the block, a cement cap was then applied and the samples cut out using a hand-held mini saw. Method 2 also used sodium silicate to harden the surface which was then covered with Plaster of Paris. Samples were cut from these levelled, Plaster of Paris sections. The main problem with Method 2 is that in order to make the surface level a significant amount of Plaster of Paris was used meaning that an individual sample was more than 50% Plaster of Paris. Of the two methods employed, Method 1 was significantly better than Method 2. During the analysis of samples sub sampled using method 2 an unknown proportion of each of the samples was lost at high temperatures due to the disintegration of the Plaster of Paris. This introduced an unquantifiable error. Fortunately this only affected two subsamples from Block 1 (samples BK5 and BK6) and no samples from Block 2 as these were all subsampled using Method 1.

In addition to these laboratory difficulties, the field sampling (which was carried out by an archaeologist and not an archaeomagnetist) involved the removal of a significant, unknown amount of the top surface in order to get a levelled surface. This meant that the most-burnt material was removed prior to laboratory experiments. The consequence of this is that any temperature estimate calculated here would, therefore, only be a minimum estimate of the maximum temperature reached in the kiln. As the amount of material removed in the field is unknown, it is also impossible to extrapolate the temperature reached at the original surface.

The difficulty of sampling kiln material in comparison with other archaeological material has been studied by previous authors. During the manufacture of pottery and bricks in ancient times the raw material was pre-selected (Kovacheva et al., 1998). Consequently, bricks and pottery are in general more homogeneous and fine-grained than material taken from ovens and kilns with burnt soil layers containing the widest grain-size and mineralogical spectra of all studied archaeomagnetic material. In addition to this, kilns experience variable firing conditions which can produce heterogeneity in archaeomagnetic results (Spassov and Hus, 2006, Hrouda et al., 2003). The temperature to which clay plasters of ovens and kilns are

burnt depends on the particular usage of each structure e.g., multiple or single burning and the purpose of the structure – domestic, religious, manufacturing centre etc (Kovacheva and Jordanova, 2001). If a structure is multiply-fired then it is probably thermally stabilized (Spassov and Hus, 2006). The large difference in maximum heating temperatures and in the amount of secondary phases produced by hydration during burial within a particular feature are the major causes of non-uniformity in magnetic behaviour between individual specimens from kilns (Jordanova et al., 2003). Unfortunately due to ambiguity over its use, it is not clear what the firing conditions were like here and if the structure was repeatedly heated. The apparent stability before 600°C (as indicated by the alteration analysis shown in figures 3.15 and 3.17) may imply thermochemical stability and, in turn, repeated heating to 600°C.

3.10.2. Palaeothermometer Methods

The palaeo-thermometer methods of Henry (2005) and Hrouda (2003) do not apply cooling rate corrections despite the acknowledgement by Hrouda (2003) that the process of equilibrating magnetic minerals may take place at lower temperatures in nature than in the laboratory. The success of both experiments (in terms of being able to identify the temperature at which alteration occurs) relies on the ferrimagnetic composition of the sample under investigation. If this does not alter in the temperature window to which the sample had previously been heated then the method is not an accurate thermometer. Therefore these methods can only ever provide a biased view of alteration in a sample because it relies on the magnetic minerals present being able to record the temperature reached. If they are stable at the particular temperature reached in the original heating experiment then it will not be possible to recover information about the temperature of heating using this method.

3.10.3. Ambiguities of Results

The preliminary study of Block 1 samples indicated 2 components of magnetisation. However, these two components are not unambiguously seen in further experiments on Block 1 samples. As mentioned previously, both Block 1 and Block 2 were very dry samples. This meant that despite careful sub-sampling, it was invariably very destructive to take samples. Consequently when the second sets of subsamples (following the preliminary study) were taken the top surface of Block 1 had either crumbled away or had already been

sampled. This may explain the difference in the results between the preliminary study and the follow up study. As reported in Schnepp et al (2003) a temperature gradient within the floor of a bread oven can be 150 K/cm. This is significant as it may be that the initial subsampling removed evidence of this gradient. It is noted that at a depth of 3cm below the surface the temperature experienced would have been 450°C (if it was 600°C at the surface). It is possible that the second set of subsamples from Block 1 do not record two components of magnetisation because they did not experience it. The differences between Block 1 (two components preserved in some samples) and Block 2 (exclusively one component recorded) may be due to their original positions with respect to the fire. Unfortunately the exact position of the bricks with regards to the fire is unknown but they could not have been more than 150 cm from the heat source as the feature was 150 cm long. Compositionally the bricks appear to be identical therefore any differences in the temperature profiles within them will be a consequence of their position relative to the fire rather than due to differences between the samples.

3.11. Conclusions

The results of this study suggest that the bricks had previously been heated to between 600°C and 700°C. This represents a minimum estimate of the temperature reached at the base of the feature due to the removal of the top surface of the bricks in the field. The stability of the characteristic remanent magnetisation (ChRM) as it heads towards the origin indicates the sample had been previously heated to at least 580°C (the point at which less than 10% of the NRM remained in the samples and the experiment was ended). However, the irreversibility of the thermomagnetic curve suggests that it has not previously been heated to 700 degrees. The repeated heating and cooling curves suggested that the samples from the base and top of Block 2 were thermomagnetically stable to 600°C and alteration occurred between 600°C and 700°C. Following the method of Hrouda et al (2003) the a60 index did not unambiguously show alteration between these two temperatures in antiquity. The 10-12% change in the alteration index between 600°C and 700°C is insignificant when compared with the 600% changes seen by Hrouda et al (2003) in their study. It is acknowledged, however, that these authors used magnetic susceptibility as opposed to bulk magnetisation as the indicator of change and magnetic susceptibility is reportedly one of the most sensitive indicators of temperature change. The difference loops determined following the work of Henry et al (2005) indicate both the creation and the transformation of ferromagnetic minerals between 300°C and 700°C which implies the

samples were not thermo-chemically stable (consistent with the initial analysis of the repeat thermomagnetic curves). It is noted that the sample analysed from the base of the block was significantly paler in colour than that from the top.

As archaeomagnetic samples were exposed to high temperatures during ancient times, one normally expects that laboratory heating does not affect their magnetic mineralogy considerably (Spassov and Hus, 2006). This is only true, however, if the sample is magnetically stable. With this in mind the divergence on the cooling and heating curve is surprising as it indicates alteration. Once the samples had been heated to 700°C in the laboratory, subsequent heating and cooling curves to 700°C were reversible. This suggests that following the initial heating to 700°C and the creation of new stable minerals, the sample was subsequently thermomagnetically stable.

The results of the experiments run on Block 1 were inconsistent with the results of the preliminary study which also focused on Block 1. The results from this initial work indicated that two components of magnetisation were recorded by Block 1. The results for Block 1 presented here did not unambiguously indicate two components and the majority of the samples (4 out of 6) had either high α95 values or high MAD values. The demagnetisation of Block 2 showed one consistent component stable to high temperature which demagnetised towards the origin. All the results had α95 and MAD's of less than 10°. The directions from Block 2 were consistent with each other and with the expected field direction.

In summary, the evidence from Block 2 suggests the samples analysed here were only thermomagnetically stable to 600°C. In light of the inferred steep temperature gradient within the soil at the base of the feature and difficulties of sampling both in the laboratory and in the field, it is highly likely the oven itself was hotter than this. The stability of the remanence contained with Block 2 is consistent with it being heated to between 600°C and 700°C. Based on this evidence we therefore reject the hypothesis that the feature was a bread oven as the temperatures reached in the feature would have been far too high for baking bread. We therefore conclude that the feature is a lime kiln.

A further aim of this work was to determine whether the age given by radiocarbon dating was more or less likely to be the true age of the feature than the archaeological age (which was determined based on evidence from throughout the site, including architectural evidence). The age of the feature according to the archaeological interpretation of the site

is late 2nd century/ early 3rd century BC whilst the radiocarbon age of the sample found within the feature was 3640 to 3510 BC and the age of the samples found stratigraphically above are between 920 and 1270 BC. Unfortunately the directional data recorded in the blocks was consistent with the modelled and measured field values for both possible time periods. Intensity information from the samples might have helped constrain the age however no intensity experiments were carried out because the primary aim of the experiments was to determine archaeotemperatures.

It is not possible, based on the results presented here, to reject the hypothesis that the feature is composed of clay sourced from the nearby Akpýnar Suyu.

3.12. Further Work

The aim of this study was to identify the maximum temperature reached in the kiln during firing. This was difficult to establish for two main reasons:

1. The exact location of the blocks sampled with respect to the heat source was unknown.
2. An unknown amount of surface material was removed from the top of each block during field sampling.

In order to address these issues it would have been advantageous to have taken orientated samples along a transect with increasing distance from the heat source/ most highly vitrified area. This would have allowed the creation of a temperature profile for the feature which would be more useful than the spot readings determined here. It would also have enabled a more precise determination of the maximum temperature reached as well as additional measurements of the field at the time of firing. Calculating the field direction from a number of samples would have enabled the quantification of errors associated with the determination.

As Block 1 was effectively destroyed during the sampling process this study suffered from a lack of data from Block 1. This was particularly unfortunate because Block 1 showed more alteration than Block 2 in the original VFTB experiment, as well as evidence of two components of magnetisation (unlike Block 2). Any further work would involve both careful field sampling as well as careful subsampling of the material in order to preserve as much material as possible for subsequent experiments.

It would have been advantageous to study both the wall bricks and the roof tiles (in addition to the floor material studied here). It would be anticipated that the primary component of magnetisation in the wall bricks and the roof tiles would be from the original firing of the bricks and tiles during their creation. If a secondary component was recorded in them (particularly if it was recorded in the roof tiles) this would imply that the temperatures reached in the undefined kiln were very hot and therefore the feature more likely to be a lime kiln than a bread oven, further strengthening the conclusion reached here.

To try to prevent alteration due to oxidation during magnetic characterisation, experiments could be carried out in argon. If the observed alteration seen in figures 3.13 and 3.17 was due to oxidation then conducting the experiments in Argon would elucidate this. If the alteration is due to oxidation then this implies either that the area of the kiln from which this block was taken was anoxic or that alteration to the samples has occurred subsequent to the original heating. If an anoxic environment had been engineered by the makers of the feature then this will be significant for the archaeological interpretation of the kiln. If, however, the alteration is not due to oxidation (and is still observed when the experiments are carried out in Argon) then this implies the sample had not previously reached this temperature.

It would be illuminating to repeat the experiments of Hrouda et al (2003),this time measuring the changes in susceptibility as this is more sensitive to alteration than the change in mass magnetisation studied here. Repeating the experiments using susceptibility instead of magnetisation would confirm the reliability of the original experiments.

It would also be beneficial to carry out the same analysis (following Hrouda et al (2003) and Henry (2005)) on samples from the Akpýnar Suyu river as were carried out on the samples from the top and the base of Block 2. This would enable a more precise conclusion to be reached on the provenance of the clay used in the depression feature.

Due to the dryness of the material it would only have been suitable for a thermal intensity experiment. Due to the length of time this would have taken, it was deemed unbeneficial to carry out an archaeointensity experiment on the bricks. If the feature was resampled, along with other burnt features on the site, an archaeointensity value could potentially resolve the dating of the feature. As will be demonstrated in the following chapters, there

is now a considerable amount of intensity data collected from the Middle East between 500 and 0 BC.

4. An Archaeomagnetic Study of a Roman Bath in Southern France

4.1. Abstract

Absolute Thellier-Thellier archaeointensity determinations were conducted on 137 tiles and sedimentary blocks from 5 different structures from "Site de La Molère", Southern France in order to further constrain the archaeological interpretation of a relative age difference between structures. We present 89 new archaeointensity and 20 new directional results. Results range from 43µT to 83µT with averages of 57 (±8) µT in the 2nd and 68 (±7) µT in the 3rd century AD. The results fall into two groups, confirming the archaeological interpretation. In this chapter, the greater suitability of bricks and tiles for archaeointensity analysis over burnt sedimentary material is again in evidence.

4.2. Introduction

The field of archaeomagnetism is based on the principle that burnt archaeological materials such as tiles and fireplaces record the magnetic field at the time of their last heating. Archaeomagnetism is well established in Western Europe and France in particular (e.g. Chauvin et al., 2000; Thellier 1981; Bucur 1994; Genevey and Gallet 2002; Hervé 2013b; Genevey et al., 2013; Gomez-Paccard et al., 2012). If the material is well dated, it is possible to use the geomagnetic field information recorded within to contribute to the local secular variation (SV) record. SV records are crucial for the investigation of physical processes occurring deep in the Earth as well as being used for archaeomagnetic dating. It is possible to conduct archaeomagnetic dating in France for a number of time periods. This is achieved by comparing the magnetic record contained within burnt, undated, archaeological material with the existing, well defined French SV curve (e.g. as demonstrated by Le Goff et al (2002)).

The geomagnetic field is a vector quantity and has both direction (declination and inclination) and strength. In this chapter five contexts were studied. One of these contexts was composed of *in situ* material and provided directional and intensity information. The other four contexts were not *in situ* and from these intensity information was gathered. Displaced material does have the potential to provide information about the inclination of

the field at the time it was fired (Lanos, 1987, Lanos, 1998) if a sufficient amount of data is studied.

The type of material used for archaeointensity determination can influence the quality of the data produced and consequently how it is weighted in data compilations. In this study tiles, bricks and burnt sedimentary blocks were analysed using a modified Thellier-Thellier method (Thellier and Thellier, 1959) with partial thermoremanent magnetisation (pTRM) checks and applied anisotropy and cooling rate corrections. It is important to correct for the effect of magnetic anisotropy as neglecting to do so can lead to errors of up to 40% in the determination of the intensity (Rogers et al., 1979, Chauvin et al., 2000). Additionally, a cooling rate correction was applied as it has been shown experimentally and theoretically that the ability of a sample to acquire magnetisation is affected by the rate of cooling (Fox and Aitken, 1980, Halgedahl et al., 1980, Biggin et al., 2013, Genevey and Gallet, 2002).

In this chapter we present high quality archaeointensity data from 2nd and 3rd century AD Roman tiles, bricks and heated sedimentary blocks. The primary aim of this study was to verify the archaeological interpretation that the praefurnium , the hypocaust and one of the gutters, CAN4 were built prior to the construction of gutters CAN3 and CAN5. The second aim was to measure high quality archaeointensity data from the praefurnium, the hypocaust and the three gutters with accompanying directional data where possible..

4.3. The Archaeology of "Site de la Molère" in Saint-Jean-Poutge (Gers, Southern France) (43°43'41"N, 0°22'57"E) and Contextual Information About the Samples Analysed

Site de la Molère is located in the commune of Saint-Jean-Poutge in South Western France (figure 4.1). It was originally known as the Mutatio of Vanesia and is mentioned in the pilgrimage itinerary from Bordeaux to Jerusalem in 333AD (Colleoni, 2012). A severe drought experienced in 2003 revealed the outline of a building with characteristics consistent with known Roman Gaul road stations (figure 4.2). Excavation of the site by a French team from the University of Rennes 2 led by Fabien Colleoni began in 2009. The samples analysed in this study were collected during the excavation season in August 2012.

Site de la Molère was constructed alongside a road and was designed to provide amenities for travellers. It is approximately 1200m^2 in area and consists of a single large building with a number of rooms, some of which combine to make a spa roughly 100m^2 (figure 4.3). The bricks supporting the floor of the caldarium and tepidarium (within the spa) are remarkably well preserved and the heating channel widened significantly indicating a long period of

use (Colleoni, 2012). The site was abandoned in the first half of the 5th century and all useful material was removed from the site at this time.

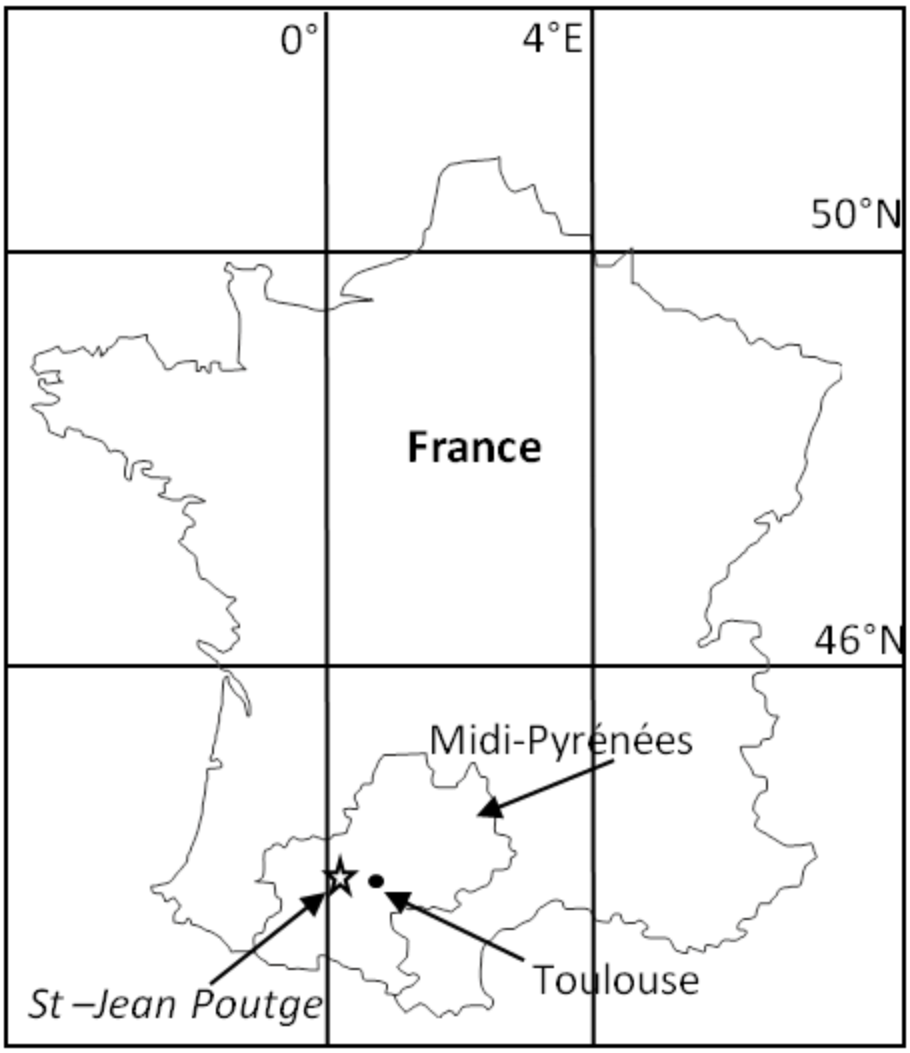

Figure 4.1. Map of France with the location of the Site de La Molère archaeological site indicated.

The construction of the building facade and northern courtyard has a *Terminus Post Quem* of the late first century AD. The spa was built during a different construction phase from the development of the building facade and courtyard but the absolute chronology prohibits a large time lag between these two events, of the order of a few decades at most. In the northern part of the baths, from west to east, we find the praefurnium and then the hypocaust. In the southern part of the baths there is a frigidarium (figure 4.3). The laying of the gutter CAN 4 is contemporary with the original manifestation of the baths. Its function was to collect rainwater and to drain the pools of the caldarium and the

frigidarium. During the second half of the second century, the baths were reorganized with the creation of a courtyard bordered on either side by galleries. In a fourth phase of modifications at the end of the third century or in the first third of the fourth century, two apses were built. The first was constructed within the hypocaust, not far from the praefurnium. The second apse, located in the east constituted a new frigidarium pool. Each pool had a gutter; CAN 3 was for the hot water pool and CAN5 the cold water pool. These two gutters meet in the south of the baths to form a single gutter towards the southern latrines (figure 4.3). The construction of these apses constituted a final architectural process.

From this site 5 separate contexts were sampled in August 2012 (figure 4.3).

Figure 4.2. Aerial photograph taken of a farmers field in St Jean Poutge. This photo was taken during an aerial survey of the region during the drought of 2003. The outline of a building is very clear (compare with the excavation plan seen in figure 4.3)


a)
b)
Building facade
Praefurnium
CAN4
Caldarium
apse
Courtyard
Hypocaust
Frigidarium
apse
CAN3
CAN5
N

.

Figure 4.3 a) Archaeological plan of the Site de la Molère archaeological site with the spa area indicated by a box. b) Sketch of the spa area where the archaeomagnetic study was focused. Note the locations of the sampled areas: the praefurnium, the hypocaust and gutters CAN3, CAN4 and CAN5. Note also that the praefurnium is to the North West of the hypocaust. It is emphasised that the archaeological interpretation of the site was that CAN3 and CAN5 were part of an extensional building phase in the 3rd century whilst the praefurnium, hypocaust and CAN4 are dated from the original construction of the spa in the 2nd century

Table 4.1: Chronological Evolution of the site:

Construction phase	Key features built	Features sampled	Date
1	Building facade and northern courtyard	None	Late first century AD
2	First phase of the spa area	The Praefurnium, Hypocaust and a gutter (CAN4)	Early to mid-2nd century AD
3	Extension to the spa area: creation of a courtyard bordered by galleries	None	Second half of the second century
4	Extension to the spa area: e.g. apse in the caldarium and gutter CAN3 and CAN5	The gutters CAN3 and CAN5	Late 3rd Century AD/ early 4th Century

4.4. Sampled Structures

The Praefurnium is the term given to the location of the fire within the spa which heated the hypocaust. Samples taken from the praefurnium were from four sedimentary blocks composed of sandstone, (variously coloured from yellow to red) and conglomerate (composed of a heterogeneous mix of relatively homogeneously sized pebbles) which lined the base of the praefurnium. From this context 26 *in situ* oriented cubes were taken plus three additional orientated cores taken from bricks located at the entrance to the praefurnium (see figures 4.4 and 4.5). During the sampling of these structures, cubes were cut using a circular saw The material between each of these cubes was chipped out with a

chisel (as seen in figure 4.4a and b) until the cubes were left proud. Each cube was then covered with plaster of Paris and the top made level using a spirit level (as seen in figure 4.4c). The cubes were then removed and cut into square samples at the laboratory following impregnation with waterglass (see figure 4.5).

a)

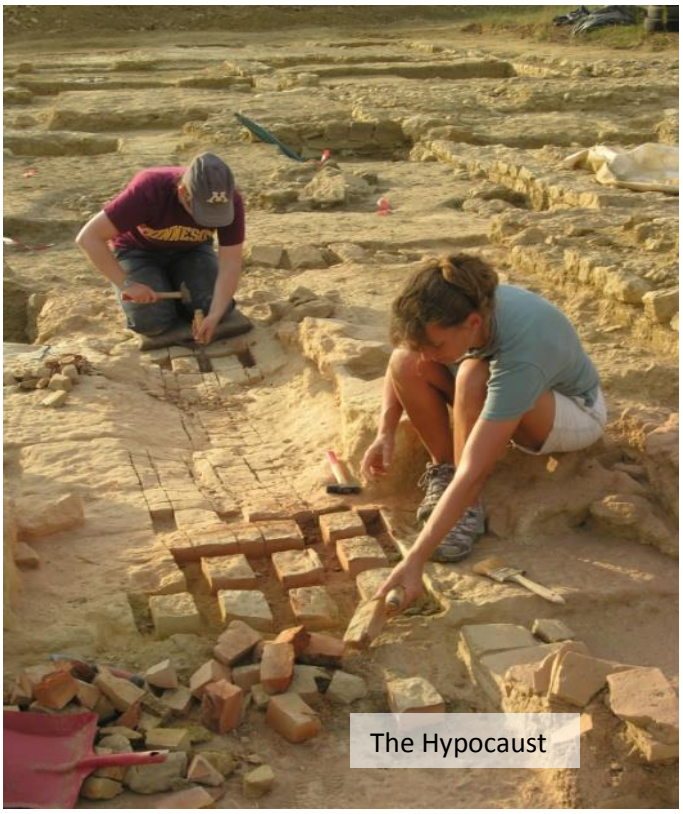

b)

c)

Figure 4.4: Photographs of the praefurnium during infield sampling. In a) and b) the praefurnium samples are being prepared whilst in c) the samples are being covered in Plaster of Paris so they retain their structural integrity during sampling. The location of the hypocaust is indicated in each photo. All the photographs were taken prior to the sampling of the hypocaust. Also indicated in c) is sample 14PB1 taken from the praefurnium.

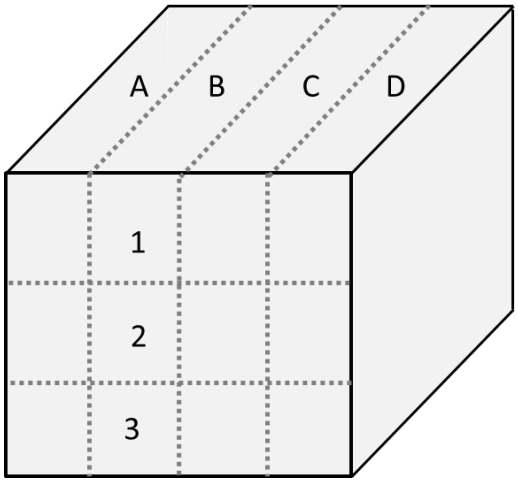

Figure 4.5: Sketch of a cube sample taken from the praefurnium (as seen in figure 4.4 c). Following impregnation with liquidglass, this block was then cut into vertical slices labelled A-D (as indicated in the cartoon above). These slices were then cut horizontally and numbered 1-3 with increasing distance from the heat source where 1 was exposed to the most heat. As the fire covered the entire of the Prafeurnium there was no difference between samples A-D. In this study only samples numbered 1 were used for an archaeointensity study or for rock magnetism experiments. See table 4.2 for examples of this.

The Hypocaust is the hollow space under the floor of the caldarium (the "hot room") into which hot air heated by the praefurnium was directed (figure 4.6). Here we sampled the topmost remaining bricks from the pillars of bricks that had originally supported the floor. This was accomplished by drilling cores into each brick using a handheld drill. The maximum number of bricks remaining in a pillar was 4 (up to a height above the ground level of around 30cm) (figure 4.6b). Although cores were taken from all of the bricks, only 20 cores were subject to an archaeointensity experiment. The cores which were subject to an archaeointensity experiment were taken from the uppermost remaining brick of each pillar. It is noted that the floor of the hypocaust is roughly 10 cm lower than the base of the praefurnium. The aim for this context was to determine if more than one heating event could be determined from the samples. If two heating events were preserved it is inferred they would represent the original firing of the bricks and the subsequent lower temperature heating due to proximity to the praefurnium whilst the baths were in use (as indicated in figure 4.6).

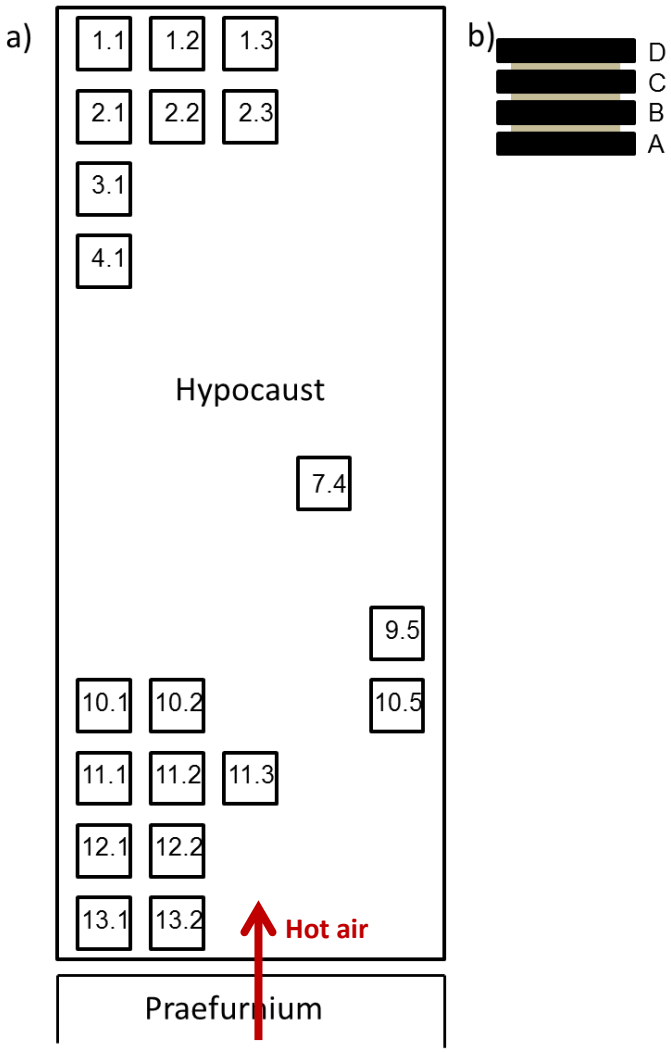

Figure 4.6: a) Plan view of the hypocaust indicating the sample and the sample naming convention. The hot air from the praefurnium was directed through the hypocaust, heating the floor above. This floor was supported by pillars of bricks. These bricks were separated by cement as seen in b). The letters in b) indicate the letter assigned to each brick dependent on its position within the pillar. In some cases only the lowest tile (a) remained in-situ whilst in others places four tiles remained. The cement between the tiles has weakened with time and the tiles are no longer fixed in position so could not be sampled as in-situ.

Tile-lined drains (or gutters) surrounded the praefurnium, hypocaust and other rooms in the spa and allowed hot and cold water to travel around the system. CAN4 was constructed in the 2nd Century and therefore dates from the 2nd construction phase. CAN3 and CAN5 are interpreted to have been built in the 3rd Century when the bathing area was extended. We sampled all available tiles from each context; 18 from CAN3, 21 from CAN4 and 52 from CAN5. Again we used a handheld drill to remove the samples. As the tiles had

been moved from their original firing location to their position in the base of the drain, the objective for CANs 3-5 was to determine the average archaeointensity at the time the tiles were fired. Un-orientated core samples (but oriented with respect to the tile edges) were drilled from these contexts (see figure 4.7 and 4.8). See table 4.2 for a full list of samples taken from all contexts.

Figure 4.7 Photograph of CAN5 taken following sampling. The cylindrical holes visible in each of the tiles are the result of core sampling for archaeointensity experimentation

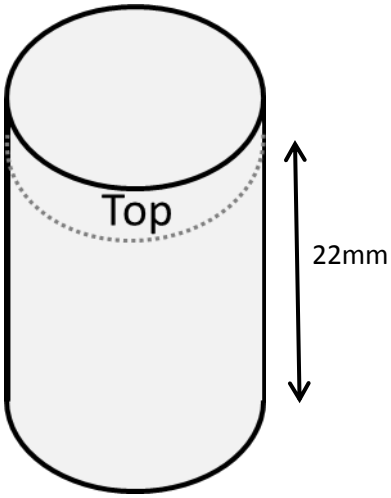

Figure 4.8: Cartoon of a representative core taken from CAN3, CAN4 and CAN5. Tops were taken off the core if the core top was uneven or longer than 22mm in length. These core tops were then used for rock magnetic analysis (in the case of CAN5) see table 4.2.

These five sampled structures have been dated using archaeological evidence including contemporary written material, coins found on site, structural styles as well as structural cross cutting relationships observed on the site.

Table 4.2 a)

Context	Context Code	Sample	Subsamples
The Praefurnium	32382B	10	10PA1
			10PA2
			10PA3
			10PB1
			10PB2
			10PB3
		11	11PA1
			11PA2
			11PA3
			11PB1
			11PB2
			11PB3
		12	12PA1
			12PA2
			12PA3
			12PB1

Context	Context Code	Sample	Subsamples
The Praefurnium	32382B	13	13PA1
			13PA2
			13PB1
			13PB2
			13PB3
		14	14PA1
			14PA2
			14PB1
			14PB2
		15	15PA1
			15PA2
			15PB1
			15PB2
		16	16PA1
			16PB1
		17	17PA1
			17PA2
			17PB1
			17PB2

Context	Context Code	Sample	Subsamples
The Praefurnium	32382B	18	18PA1
			18PB1
			18PC1
		19	19PA1
			19PA2
			19PA3
			19PB1
			19PB2
		20	20PA1
			20PB1
		21	21PA1
			21PA2
			21PB1
			21PB2
		22	22PA1
			22PA2
			22PB1
			22PB2

a continued)

Context	Context Code	Sample	Subsamples
The Praefurnium	32382B	23	23PA1
			23PA2
			23PB1
			23PB2
		24	24PA1
			24PA2
			24PB1
			24PB2
		25	25PA1
			25PA2
			25PA3
			25PB1
			25PB2
			25PB3
		26	26PA1
			26PA2
			26PB1
			26PB2

Context	Context Code	Sample	Subsamples
The Praefurnium	32382B	27	27PA1
			27PA2
			27PB1
			27PB2
		28	28PA1
			28PA2
			28PA3
			28PB1
			28PB2
			28PB3
		29	29PA1
			29PA2
			29PB1
			29PB2
		30	30PA1
			30PA2
			30PB1
			30PB2

Context	Context Code	Sample	Subsamples
The Praefurnium	32382B	31	31PA1
			31PA2
			31PB1
			31PB2
		32	32PA1
			32PA2
			32PB1
			32PB2
		33	33PA1
			33PA2
			33PB1
			33PB2
		34	34PA1
			34PA2
			34PB1
			34PB2
		35	35PA1
			35PB1
			35PB2

b)

Context	Context Code	Sample	Subsamples
The Hypocaust	32382C	11	11DT
			11DT1
			11CT1
			11BT1
			11AT1
		12	12CT
			12CT1
			12BT1
			12AT1
		13	13AT
			13AT1
		21	21CT
			21CT1
			21BT1
			21AT1
		22	22BT
			22BT1
			22AT1

Context	Context Code	Sample	Subsamples
The Hypocaust	32382C	23	23AT
			23AT1
		31	31CT
			31CT1
			31BT1
			31AT1
		41	41AT
			41AT1
		74	74BT
			74BT1
			74AT1
		95	95AT
			95AT1
		101	101BT
			101BT1
			101AT
		102	102AT1
			102AT
		105	105CT
			105CT1

Context	Context Code	Sample	Subsamples
The Hypocaust	32382C	105	105BT1
			105AT1
		111	111AT
			111AT1
		112	112AT
			112AT1
		113	113BT
			113BT1
			113AT1
		121	121AT
			121AT1
		122	122BT
			122BT1
			122AT1
		131	131BT1
			131AT
			131AT1
		132	132AT
			132AT1

c)

Context	Context Code	Sample	Sub sample
CAN3	32382D	300	300T
			300T1
		301	301T
			301T1
		302	302T1
			302T1
		303	303T
			303T1
		304	304T
			304T1
		305	305T
			305T1
		306	306T
			306T1
		307	307T
			307T1
		308	308T
			308T1

Context	Context Code	Sample	Sub sample
CAN3	32382D	309	309T
			309T1
		310	310T
			310T1
		311	311T
			311T1
		312	312T
			312T1
		313	313T
			313T1
		314	314T
			314T1
		315	315T
			315T1
		316	316T
			316T1
		317	317T
			317T1

d)

Context	Context Code	Sample	Sub sample
CAN4	32382E	100	100T
			100T1
		101	101T
			101T1
		102	102T
			102T1
		103	103T
			103T1
		104	104T
			104T1
		105	105T
			105T1
		106	106T
			106T1
		107	107T
			107T1
		108	108T
			108T1

Context	Context Code	Sample	Sub sample
CAN4	32382E	109	109T
			109T1
		110	110T
			110T1
		111	111T
			111T1
		112	112T
			112T1
		113	113T
			113T1
		114	114T
			114T1
		115	115T
			115T1
		116	116T
			116T1
		117	117T
			117T1

Context	Context Code	Sample	Sub sample
CAN4	32382E	118	118T
			118T1
		119	119T
			119T1
		120	120T
			120T1

e)

Context	Context Code	Sample	Sample
CAN 5	32382F	200	200T
			200T1
		201	201T
			201T1
		202	202T
			202T1
		203	203T
			203T1
		204	204T
			204T1
		205	205T
			205T1
		206	206T
			206T1
		207	207T
			207T1
		208	208T
			208T1

Context	Context Code	Sample	Sample
CAN 5	32382F	209	209T
			209T1
		210	210T
			210T1
		211	211T
			211T1
		212	212T
			212T1
		213	213T
			213T1
		214	214T
			214T1
		215	215T
			215T1
		216	216T
			216T1
		217	217T
			217T1

Context	Context Code	Sample	Sample
CAN 5	32382F	218	218T
			218T1
		219	219T
			219T1
		220	220T
			220T1
		221	221T
			221T1
		222	222T
			222T1
		223	223T
			223T1
		224	224T
			224T1
		225	225T
			225T1
		226	226T
			226T1

e continued)

Context	Context Code	Sample	Sample
CAN 5	32382F	227	227T
			227T1
		228	228T
			228T1
		229	229T
			229T1
		230	230T
			230T1
		231	231T
			231T1
		232	232T
			232T1
		233	233T
			233T1
		234	234T
			234T1
		235	235T
			235T1

Context	Context Code	Sample	Sample
CAN 5	32382F	236	236T
			236T1
		237	237T
			237T1
		238	238T
			238T1
		239	239T
			239T1
		240	240T
			240T1
		241	241T
			241T1
		242	242T
			242T1
		243	243T
			243T1
		244	244T
			244T1

Context	Context Code	Sample	Sample
CAN 5	32382F	245	245T
			245T1
		246	246T
			246T1
		247	247T
			247T1
		248	248T
			248T1
		249	249T
			249T1
		250	250T
			250T1
		251	251T
			251T1

Table 4.2. *All samples taken from the 5 contexts where a) shows the praefurnium samples, b) the hypocaust samples, c) CAN3 samples, d) CAN4 samples and e) CAN5 samples. Blue cells indicate those samples that were subject to an archaeointensity experiment, pink cells indicate samples on which rock magnetism experiments were carried out whilst green cells indicate samples which underwent a demagnetisation experiment.*

4.5. Experimental Procedure and Results

4.5.1. Rock Magnetism

A Magnetic Measurements Variable Field Translation Balance (MMVFTB) at the University of Liverpool was used to measure isothermal remanent magnetisation (IRM) acquisition curves, back field coercivity, hysteresis loops and Curie curves in order to determine the rock magnetic properties of the samples. Eleven samples from CAN5 and 10 samples from the praefurnium were analysed and the experiments were carried out in air.

All samples from CAN5 and half the samples from the praefurnium exhibited reversible heating and cooling curves indicating they were stable to heating to a temperature of 700°C (see figure 4.9). Six samples from CAN5 and 3 samples from the praefurnium were weakly ferromagnetic with curie curves dominated by paramagnetic components (1/t relationship observed). The remaining samples had a single high Curie temperature between 550°C and 580°C, therefore, these were inferred to be dominated by low Ti-titanomagnetite. For the majority of the weakly magnetised samples, the IRM curves are too noisy to interpret. For 3 of the CAN5 samples and 3 of the praefurnium samples the IRM is saturated by 300mT (Figure 4.7). The remaining eight CAN5 and seven praefurnium samples did not saturate by 300mT and with the exception of two samples all their hysteresis loops closed. The hysteresis loops of sample 235 from CAN5 and sample 35PA1 from the praefurnium did not close indicating the presence of a high coercivity mineral such as haematite. Haematite was not unambiguously seen in any other sample.

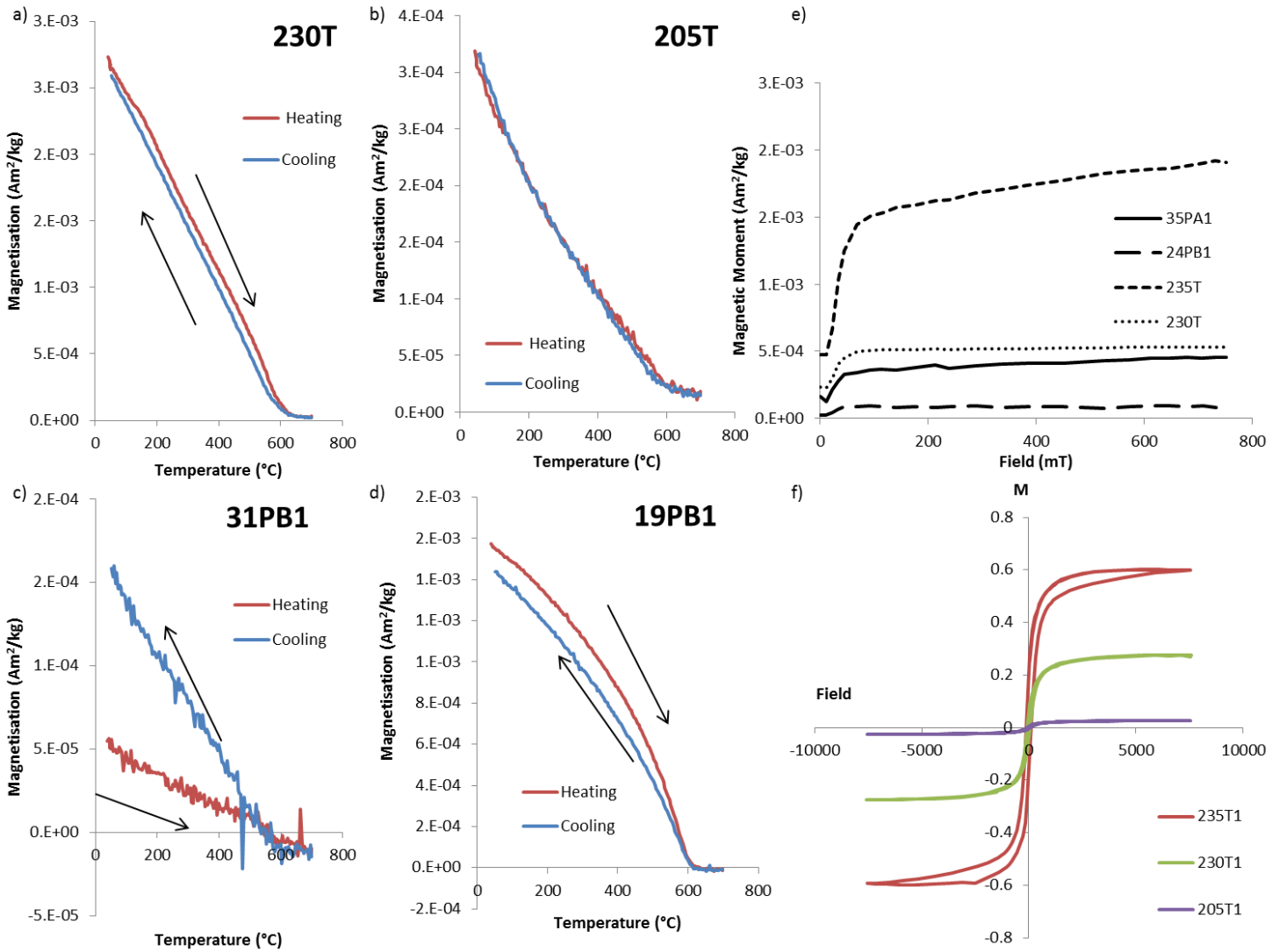
a)
230T
Heating
Cooling
Magnetisation (Am²/kg)
Temperature (°C)
b)
205T
Heating
Cooling
Magnetisation (Am²/kg)
Temperature (°C)
e)
35PA1
24PB1
235T
230T
Magnetic Moment (Am²/kg)
Field (mT)
c)
31PB1
Heating
Cooling
Magnetisation (Am²/kg)
Temperature (°C)
d)
19PB1
Heating
Cooling
Magnetisation (Am²/kg)
Temperature (°C)
f)
M
Field
235T1
230T1
205T1

Figure 4.9 a-d) Examples of thermomagnetic curves for samples from CAN5 (a) and (b) and the Praefurnium (c) and (d). The majority of the samples exhibited reversible curves (a,b and d). Note the change in slope observed around 580°C in a), b) and d) which indicates the presence of magnetite. e) Examples of isothermal remanent magnetisation curves for samples from the praefurnium (35PA1 and 24PB1) and from CAN5 (235T and 230T). 35PA1 and 235T did not saturate indicating the presence of a high coercivity mineral. Samples 230T1 and 24PB1 saturated in fields of 100mT. f) Hysteresis loops showing both closed and open loops as discussed in the text.

4.5.2. Directional Studies

The samples from the praefurnium (figure 4.4) were collected using the plaster cap method and were horizontally levelled using a bubble level and oriented using a magnetic and a sun compass. All the samples were brittle blocks and required consolidation using sodium silicate ("waterglass") in the laboratory, before being cut into cubic specimens of $8cm^3$ (figure 4.5). For all specimens from the praefurnium with stable and consistent natural remanent magnetization (NRM) (17 samples) directions were determined as part of the archaeointensity experiment.

Detailed stepwise thermal demagnetization was only performed on unorientated small core tops from the hypocaust (20 specimens – for sampling procedure see "archaeointensity studies" below) to identify if they contained one or two components of magnetisation. All other directional information comes from the intensity experiments.

It was not possible to determine robustly the inclination of the bricks and tiles (following the work of Lanos, 1987 and Lanos, 1998) because there were not enough samples per structures. In order to do this analysis, at least 100 samples would be required for a context and the maximum number of samples for a context was 52 from CAN5. The inclinations recorded by samples from CAN5 are scattered (table 4.3, figure 4.10 b).

Table 4.3 Directional results

Construction Age (AD)	Probable age of final use	Structure	N_{dir}/N_o	*Dec*	*Inc*	*k*	*α95*
2nd Century	5th Century	Praefurnium	17/26	-2.1°	58.8°	333	2.04°

Columns from left to right Construction Age, assigned construction age of context; Structure, type of structure; N_{dir}/N_0, number of samples over total samples used in the calculation of the site mean direction; Dec, average declination determined from the accepted archaeointensity experiments; Inc, average inclination determined from the accepted archaeointensity experiments; k precision parameter and α95, the radius of the 95% confidence circle (Fisher, 1953).

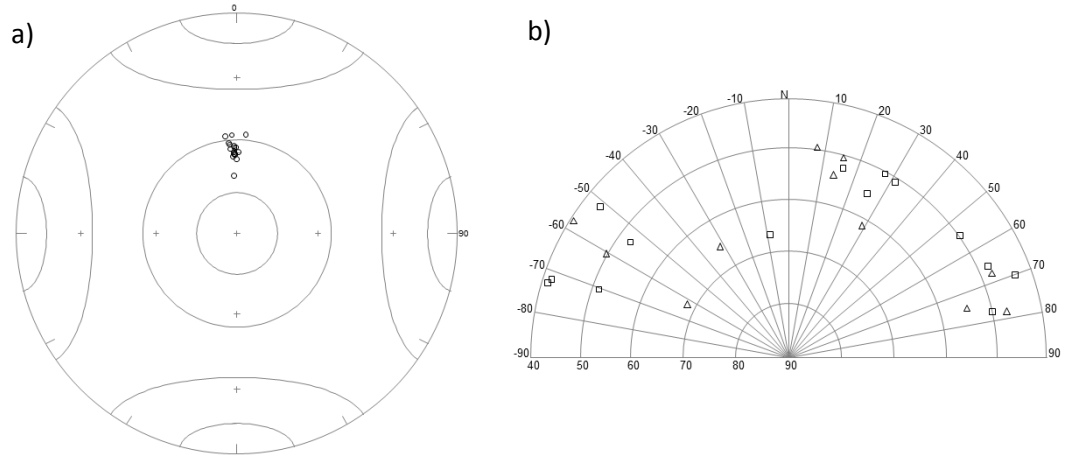

Figure 4 .10 a) Directional results for primary components recorded in samples from the praefurnium Plotted are 17 directions from the data set of 26. Six results were excluded from the calculation of the mean Dec and Inc because these samples altered during the archaeointensity experiment and a more magnetically susceptible mineral was created. In addition 3 samples (33PA1, 34PB1 and 35PB1) were excluded because the directions recorded by them were random with respect to each other and to the rest of the samples. Dec: -2.1°, Inc: 58.8°, k:333, α95:2.04°. The lines drawn on a) are used to determine the orientation of the feature during its original firing. This is particularly useful when considering objects which have subsequently moved such as tiles and bricks. However, it is only possible to do so for tiles if you have a sample set larger than 100 samples otherwise the calculated orientation angle is not statistically robust. This is because there are three possible orientations tiles can be fired in: flat, upright or on one edge. The lines indicate inclination 55° and 75°. : TMF inclination varies between these two values in Paris during the last millennia. If the measured inclination for the flat drilling position falls in this range, whatever the deviation angle is, then this is the right firing position. The two lines near 0°

correspond to upright firing position and the two lines near 90° correspond to on-edge firing position. Obviously in the preafurnium the samples have not been moved since firing so, as expected, they plot within 55° and 75°.

b) shows the directional results for CAN5. Plotted are the samples which gave successful intensity results. The results are plotted assuming the tiles were fired vertically on one side. Note the dispersive nature of this data set and the small number of samples making it impossible to determine a reliable average inclination for CAN5.

Both intensity and demagnetisation experiments were carried out at Rennes 2 Laboratory using a Magnetic Measurements Thermal Demagnetizer (MMTD) oven and measured with either a 2G cryogenic magnetometer or a Molspin spinner magnetometer. Low-field susceptibility was measured after each heating step using a Bartington MS2 susceptibility meter in order to monitor mineralogical changes.

All the praefurnium samples with the exception of 3 were taken from the sandstone blocks or conglomeratic blocks forming the floor of the praefurnium (figure 4.11). The other three samples were taken from bricks at the entrance to the praefurnium. All the samples from the praefurnium had a small viscous overprint which was removed by 100°C in all cases except one (where it was removed by 200°C see figure 4.13). For the majority of samples the primary component headed towards the origin before alteration occurred at around 470°C or 500°C. Alteration was typically indicated by a change in slope of the Arai plot, however, six samples showed a significant increase in their magnetic susceptibility at 370°C and were not included in the archaeointensity or directional calculations. All accepted results have an MAD of less than 5° (figure 4.13). Two of the brick samples taken from the entrance to the praefurnium have two components of magnetisation, samples 33PA1 and 35PB1. The secondary component is found between 100°C and 320-370°C and the primary component is from 320-370°C to 550°C. The secondary component is inferred by a change in orientation of the remanent magnetisation on the orthogonal vector plots (see Figure 4.13d).

It is noted that as the directional values are determined from the Thellier-Thellier archaeointensity method the values determined contain an implicit assumption that the samples were solely composed of single domain grains.

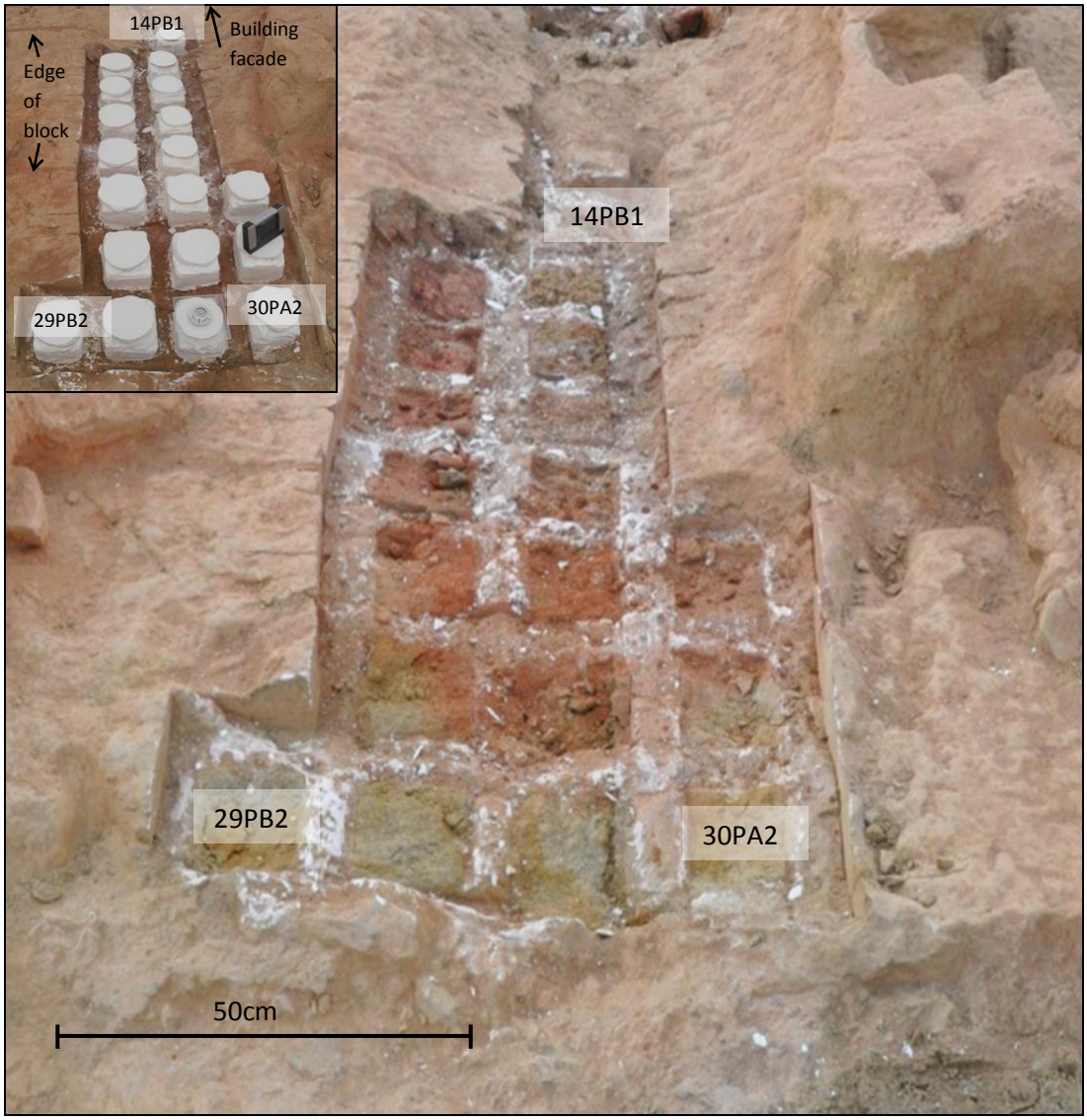

Figure 4.11. Photograph of the praefurnium following the removal of the samples. As can clearly be seen the composition of the sedimentary blocks making up the preafurnium is variable (with the finer grained mudstone found near to the viewer). The colour difference seen may also be indicative of the degree of heating and/or oxygenation that the various areas of the fireplace experienced. Insert shows the praefurnium prior to sample removal; the individual samples can clearly be seen. The join between the praefurnium and the hypocaust is in the foreground of the picture. The two samples which contained two components of magnetisation, 33PA1 and 35PB1 were taken from where the photographer is standing. 19 of the 26 samples taken from the praefurnium can be seen here, additional samples (33PA1, 34PB1 and 35PB1) were taken from where the photographer is standing whilst the remaining four samples, 10PA1, 11PB1, 12PA1 and 13PA1 were taken off the top of the picture (towards the building facade)

4.5.3. Archaeointensity Studies

The unoriented (displaced) samples collected were from bricks found in the hypocaust and tiles from CANs 3-5. From these locations ~5cm long cores were taken using a portable,

water cooled, hand-held drill. The field sampling method involved drawing a line parallel to the short edge of the tile (if one existed) at roughly 10cm distance. Samples were taken along this line. This was done to ensure the core was taken perpendicular to the inferred firing orientation (on a tile edge) whilst at a sufficient distance from the edge of the tile to reduce the chance of sampling an area significantly affected by shape anisotropy (Lanos, 1987, Kovacheva et al., 2009). In the laboratory, these cores were cut to 10.8 cm^3 cores with a diameter of 25 mm and a height of 22 mm.

For 135 specimens from the praefurnium, hypocaust and CANs 3-5, values of archaeointensity were determined using the classical Thellier-Thellier archaeointensity protocol (Thellier and Thellier, 1959) with pTRM checks (Coe, 1967). At each temperature step, specimens were heated and cooled twice in air, first in a laboratory field ($+F_{lab}$) and secondly in the opposite field ($-F_{lab}$). The strength of the laboratory field was 60µT and applied along the z axis of the specimens (for cores this was the long axis). Twelve temperature steps were carried out from 100°C to 575°C. Low field susceptibility was measured after each heating step.

The TRM anisotropy tensor was determined on all specimens following the procedure described by Chauvin et al (2000). Six successive heatings were performed with a laboratory field applied along the +Z, -Z, +X, -X, +Y, -Y axis of each specimen, once the NRM had been demagnetised to 70% of its initial value. A thermal stability check was then performed with a laboratory field applied along the +Z axis. The alteration factor determined via the stability check had to be less than 5% for the anisotropy correction to be applied. Where this condition was met, samples were individually corrected for anisotropy (figure 4.12)

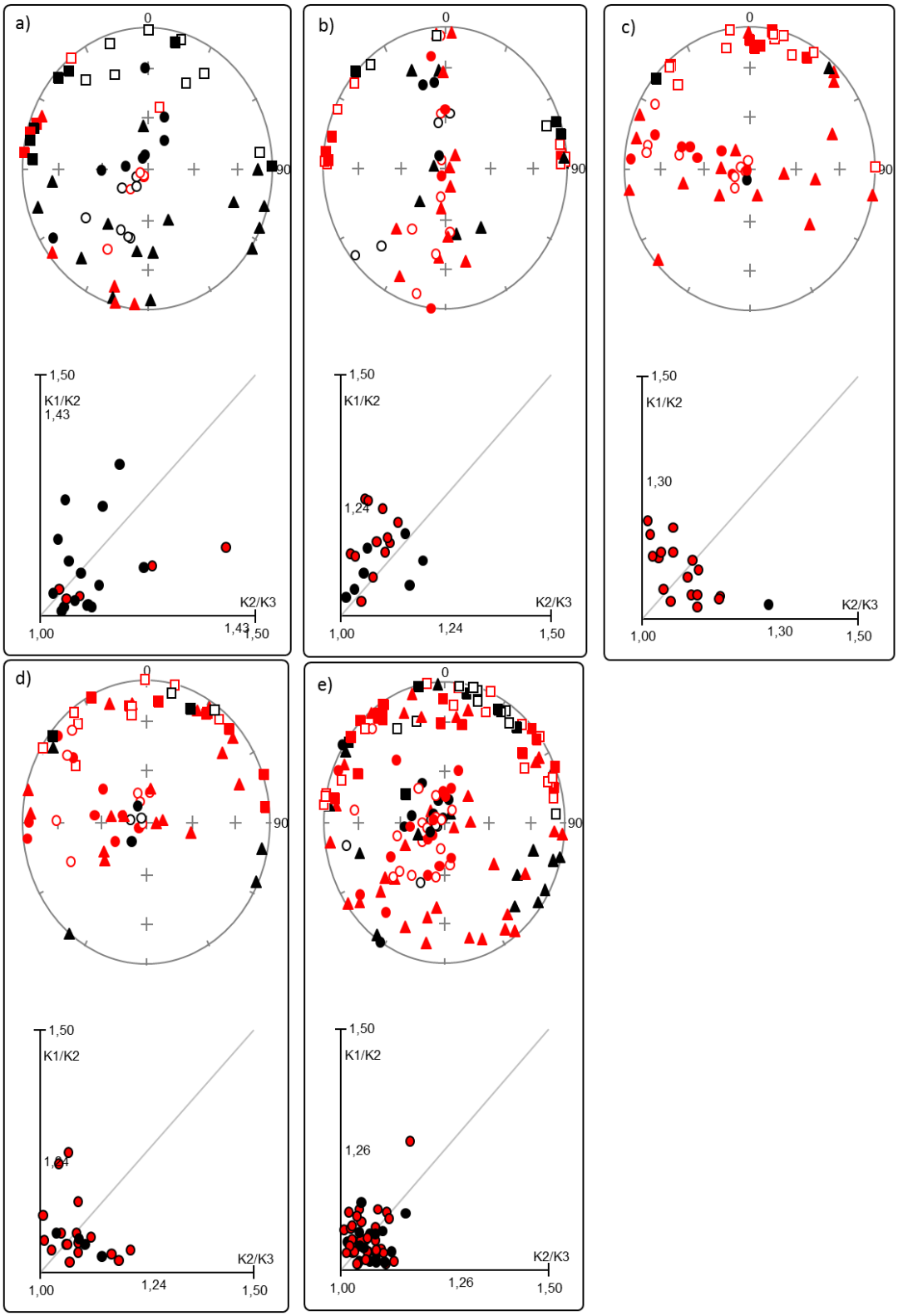

Figure 4.12 Flinn and Polar anisotropy diagrams for all 5 contexts. Red data was accepted whilst black data was rejected. a) The praefurnium, b) the hyposcaust, c) CAN3, d) CAN4, e) CAN5. Two results from CAN5 are not shown in this diagram because they had such strong anisotropy they skewed the graph and obscured the other results.Triangles represent the maximum anisotropy direction, circles represent the minimum whilst squares represent the intermediate direction.

Cooling rate corrections were also individually applied to each archaeointensity value determined. The method involved four heating steps (as described by Gomez-Paccard et al, 2006). The first and second steps are classical Thellier-Theller (1959) ($+F_{lab}$ and $-F_{lab}$) steps with a fast cooling (around 1.5 hours). The third $+F_{lab}$ step is carried out with a slow cooling rate and finally the fourth $-F_{lab}$ step with a fast cooling is a stability check. If this stability check indicated the TRM acquisition of the sample changed between the second and fourth steps by more than 10% then the correction was not applied. Additionally, the cooling rate correction was only applied when it was larger than the alteration factor. The slow cooling rate ideally should mimic the original cooling of the archaeomagnetic material when it was last heated. A cooling rate was fixed at around 20hrs (0.5/min). This rate was selected following Hervé et al (2013a) who followed the same rate for large kilns. Mineralogical changes and the acquisition of chemical remanent magnetization during successive laboratory heatings were indicated by negative pTRM-checks and/or obvious distortion of the NRM direction. pTRM checks were considered positive if at a given temperature step, the difference between the original pTRM and the pTRM check did not exceed 10% of the total TRM acquired.

Selection criteria were applied in order to ensure that only reliable archaeointensity estimates were chosen to calculate the mean archaeointensity. Building on the criteria adopted by Hervé et al (2013) the following selection criteria were applied:

a) NRM fraction factor *f* greater than 0.4, with the minimum number of selected points defining this *f* being 5 *(Coe et al., 1978)*,
b) Maximum angular deviation (MAD) lower than 5° (Kirschvink, 1980)
c) Deviation angle (DANG) lower than 5° (Selkin and Tauxe, 2000)
d) The ratio of the standard error of the slope to the absolute value of the slope (β) lower than 0.05 (Kissel and Laj, 2004)
e) Cumulative Difference Ratio (CDRAT) lower than 10 from a minimum number of 3 consecutive accepted checks (Selkin and Tauxe, 2000)

Table 4.4: Archaeointensity results

Construction Age (AD)	**Age of final heating (AD)**	**Structure**	**Name**	N_{int}/N_o	***F*± SEM (μT)**	F_a± SEM (μT)	F_{acr} ± SEM (μT)	***Ave CR Corr. (%)***
2nd Century	400 ±25	Praefurnium	Praefurnium	4/26	67±12	64±13	64±11	3
2nd Century	125 ±25	Hypocaust	Hypocaust	13/20	63±10	60±8	56±7	9
3rd Century	300 ±25	Gutter	CAN3	17/18	75±6	72±7	68±6	8
2nd Century	125 ±25	Gutter	CAN4	17/21	70±4	65±4	58±8	15
3rd Century	300 ±25	Gutter	CAN5	34/52	73±6	70±5	68±7	9

Columns from left to right: Construction Age, assigned age of context; Age of final heating (AD), estimated date when structures were most recently exposed to heating. With the exception of the Praefurnium the construction age and the age of final heating are identical. In the case of the Praefurnium, it is presumed that the Praefurnium was in use throughout the occupation of the site and therefore the date of final heating of the Praefurnium corresponds to the date of the abandonment of the site in the first half of the 5th Century; Structure, type of structure; Name, Context name used in this study; N_{int}/N_o*, number of accepted archaeointensity results over number of samples subjected to the Thellier-Thellier protocol; F ± s.d. mean archaeointensity and standard deviation determined from the archaeointensity protocol with no corrections applied,* F_a *± s.d., mean archaeointensity and standard deviation corrected for anisotropy effects;* F_{acr} *± s.d., mean archaeointensity corrected for anisotropy and cooling rate effects with standard deviation, Ave CR Corr (%) mean cooling rate correction applied to all samples from a context.*

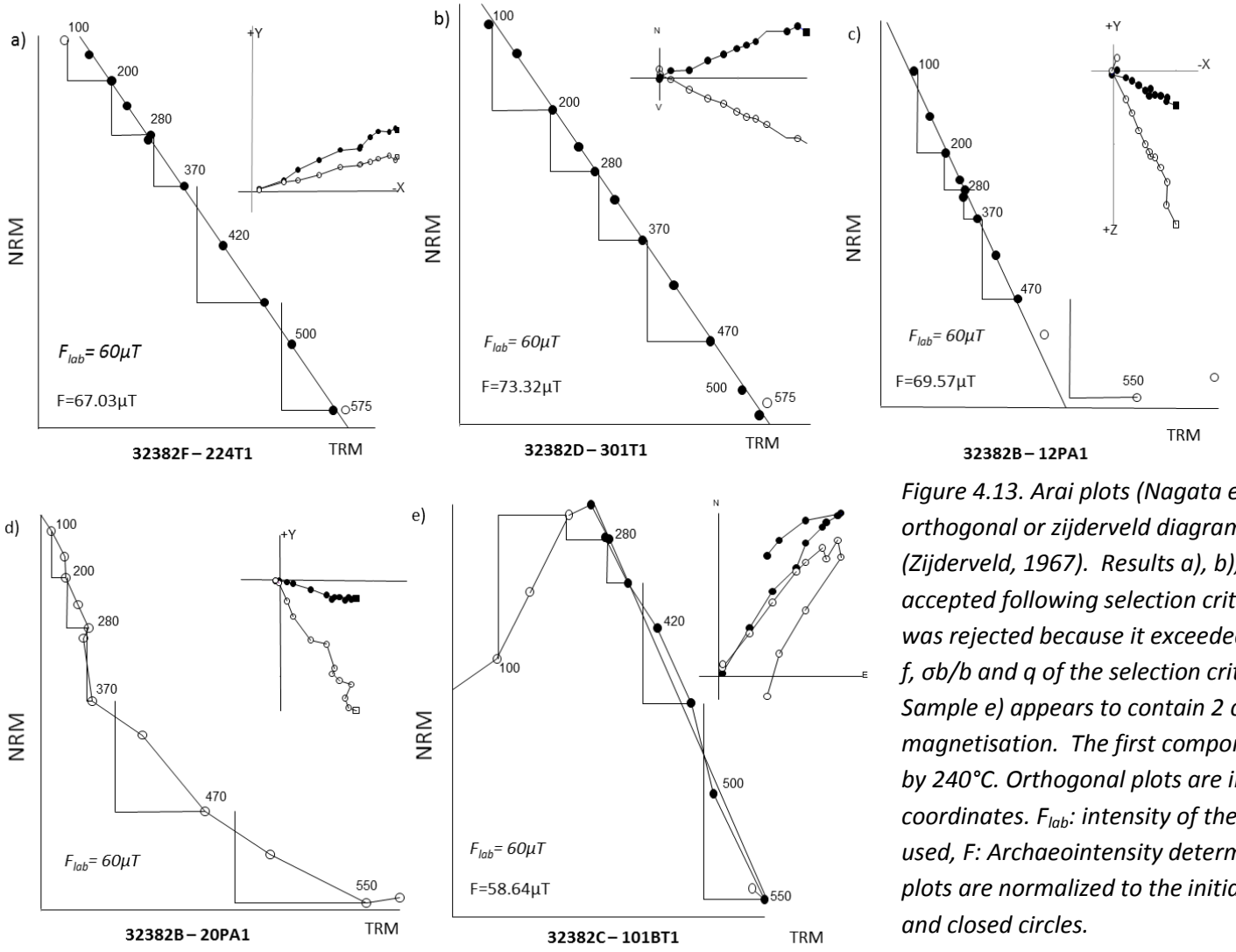

Figure 4.13. Arai plots (Nagata et al., 1963) with orthogonal or zijderveld diagrams as insets (Zijderveld, 1967). Results a), b), c) and e) were accepted following selection criteria. Sample d) was rejected because it exceeded the limits set for f, σb/b and q of the selection criteria (see text). Sample e) appears to contain 2 components of magnetisation. The first component is removed by 240°C. Orthogonal plots are in sample coordinates. F_{lab}: intensity of the laboratory field used, F: Archaeointensity determined. NRM-TRM plots are normalized to the initial NRM intensity and closed circles.

Twenty one samples contained a viscous remanent magnetization (VRM), characteristically easily identifiable in the Arai plot (figure 4.13a). This VRM was typically removed by 200°C and the primary magnetisation then headed towards the origin. In total 85 intensity results were accepted and 52 were rejected so the study as a whole had a 62% success rate although for individual structures the success rate was as high as 94% for CAN 3 and as low as 15% in the praefurnium (table 4.4).

Eighteen rejected samples had high CDRAT values (greater than 10% of the total TRM acquired) implying consistent alteration occurred during the experiment resulting in an over- or under- estimation of the archaeointensity from the Arai plot. Additionally 21 samples were rejected because β was greater than 0.05. This was the most commonly missed criteria for samples from the praefurnium (16 out of 21 rejected samples). Alteration during the anisotropy experiment was uncommon and only 8 samples from the entire sample set recorded alteration factors greater than 5%. In contrast, alteration frequently occurred during the cooling rate experiment, with 36 samples recording alteration factors greater than the cooling rate correction factor. Thirty samples had cooling rate experiment alteration factors greater than 10%. Successful results range from 45μT to 94μT (before cooling rate and anisotropy corrections were applied) and from 44-83μT once all corrections were applied. The archaeointensity results gathered from the hypocaust and CANs 3-5 were typically of very high quality with an acceptance rate of over 65%. The samples were typically strongly magnetised and stable during archaeointensity analysis (distortion in the direction or the linearity of the Arai plot, implying alteration, was typically not observed below 470°C). For individual results see appendix 4.8.

Obvious mineralogical alterations occurred on 6 specimens from the praefurnium that were rejected (their low field susceptibility increased threefold following the 370° temperature step). For all other specimens, the archaeointensity was computed from the first temperature step following the removal of the VRM to the last step before any CRM acquisition, indicated either by a pTRM check with a DRAT greater than 10% or by a distortion of the NRM direction or by a change in the direction of the Arai plot (as seen in figure 4.12 e).

4.6. Discussion

4.6.1. Data Quality

There is a clear difference in archaeointensity success rate between samples from the praefurnium and the other sampled areas (see table 4.4). The praefurnium has a 15% success rate compared with 65%: the lowest success rate from any of the other sampled structures. The material sampled from the praefurnium is burnt sandstone and burnt fine grained conglomerate with a sandy matrix whereas all the other samples are clay tiles with a high concentration of magnetic minerals in their matrix. The praefurnium samples typically had a significantly lower NRM than those from the other structures. The results of the rock magnetic analysis on praefurnium and CAN5 samples suggest that both contexts have the same magnetic carrier: Titanomagnetite with low titanium content. The main difference between the praefurnium and CAN5 is the reversibility of the thermomagnetic curves and the strength of the NRM. The irreversibility of the thermomagnetic curve for a number of the samples from the praefurnium implies either that the sandstone/ conglomerate in the praefurnium had not previously reached 700°C or that it did so under different circumstances i.e. in a reducing environment as opposed to the oxidizing environment in the VFTB. Alternatively, alteration may have occurred subsequent to the last heating to 700°C. A number of praefurnium samples showed evidence of alteration or multi domain behaviour during the archaeointensity experiment (concave-up Arai plots were recorded). The magnetic susceptibility of six samples from the praefurnium increased sharply during the course of the archaeointensity experiment. Either this is further evidence that the samples had not reached temperatures in excess of 420°C during their original heating or the addition of water glass to the sample as a consolidator caused appreciable changes in the magnetic susceptibility (Kostadinova et al., 2004). Regardless of the root of the differences, the relative weakness of the magnetic carrier within the samples from the praefurnium contributed to their low success rate in the archaeointensity experiments as the weak signal meant it was difficult to distinguish the signal from the noise. This reaffirms the suitability of using materials composed solely of burnt clay (e.g. bricks, tiles and pottery) for archaeomagnetic study as burnt clay typically contains a strong remamence.

4.6.2. Number of Components

One of the objectives of this study was to determine if there were one or two components of magnetisation observable in samples from the hypocaust. If there was evidence of two components of magnetisation the interpretation would be that the primary component represented the initial firing of the bricks in their kiln whilst the secondary component would represent their subsequent heating due to their proximity to the praefurnium. It would only be possible to record this subsequent heating if the bricks themselves reached sufficiently high temperatures in the second event (>100°C) for it to be recorded by their magnetic minerals. It is also essential that the orientation of the primary field recorded within the bricks is sufficiently different to the orientation of the secondary component.

In the hypocaust, seven samples showed evidence of two components of magnetisation (figure 4.13e). These seven samples were positioned close to the praefurnium, although it is noted that not all of the samples close to the praefurnium and none of the samples more than 2.5m straight line distance from the praefurnium entrance showed evidence of two components of magnetisation (figure 4.13). This is consistent with a strong temperature gradient existing across the hypocaust meaning that those samples that recorded a secondary overprint were generally located closest to the praefurnium. This secondary component of magnetisation was removed by 240°C in all cases. This is in agreement with the findings of Goulpeau (1994) who was able to plot two isotherms in a hypocaust they studied at 250°C and 300°C. It was not possible to precisely determine how far into the hypocaust this thermal gradient was felt as the sampling was restricted to those bricks remaining on site (Figure 4.14).

As mentioned previously, not all samples record two components. We can think of three possible mechanism to explain this: 1) Some of the samples may not contain magnetic minerals capable of recording the lower temperature secondary component, 2) as the bricks are no longer in their firing position, they are randomly oriented with respect to their NRM in the hypocaust. Therefore in some (probably rare) cases it is possible that the secondary component of magnetisation was in the same orientation as (or very near to) the primary component and therefore the secondary component is not apparent as it is masked by the primary component or 3) there were perturbations in the isotherm. As the samples were not sampled as *in situ* material it was not possible to calculate the site mean for the secondary component of magnetisation. The samples were not *in situ* because the cement between the bricks had weakened over time and was no longer acting as an

adhesive. Consequently it was not possible to sample the bricks without them moving. The samples were, therefore, unorientated. The average inclination for the 2nd component is 62° but the results are quite spread from 54-77° so it is not possible to conduct archaeomagnetic dating on the secondary component (see table 4.5).

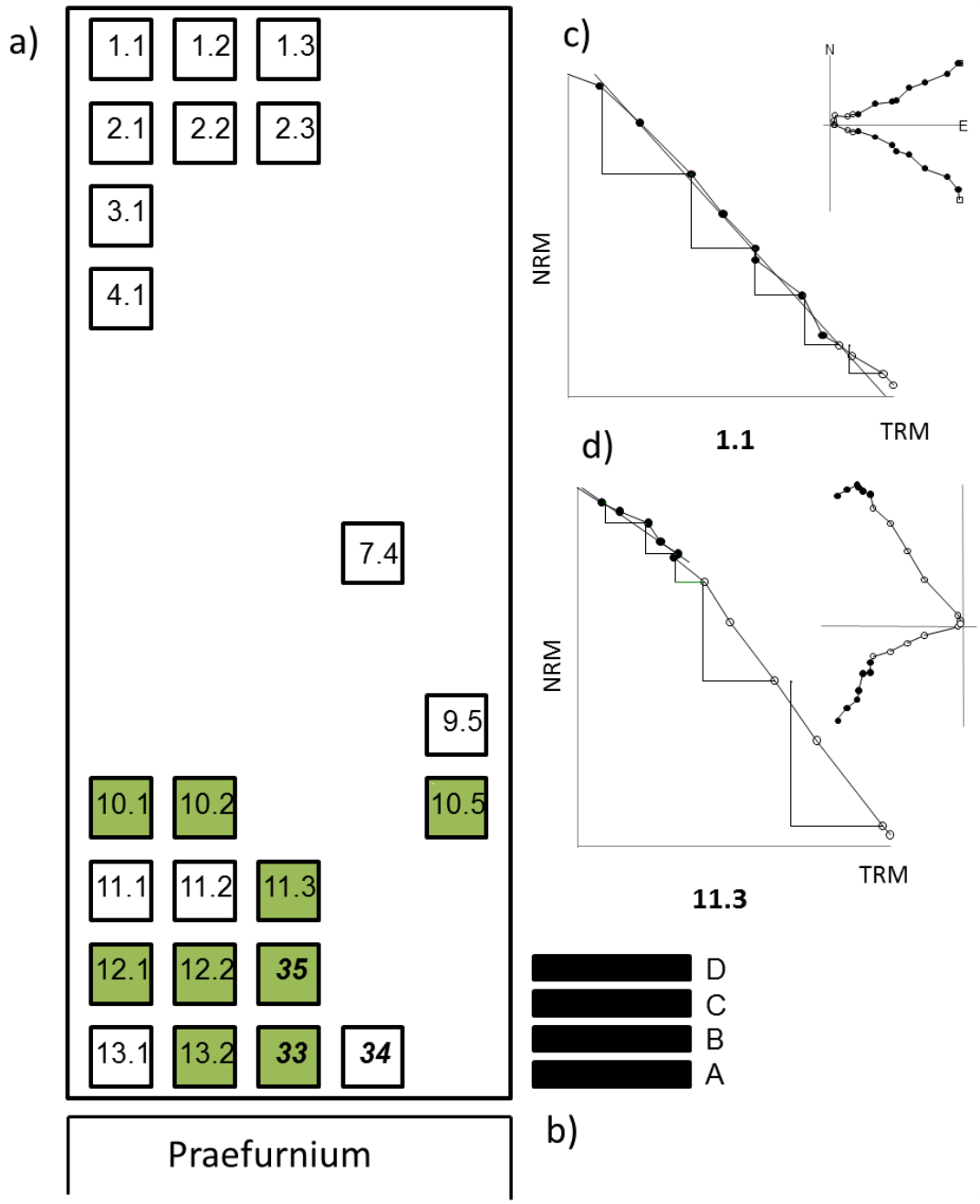

Figure 4.14. Plan view of the hypocaust with squares indicating where bricks remained in their original position within the hypocaust. For ease of sampling, the hypocaust was divided into vertical columns (as you look down on the plan view) which were numbered 1 to 5 and rows numbered 1 to 13 (a). Hence the brick in the bottom left was given the sample name 131A because it was on the 13th row if you count towards the praefurnium and it was the first brick as you worked from left to right.

Each brick was either found as a single brick or as a stack of bricks, up to a maximum of 4 bricks. The topmost remaining brick in each stack was selected for analysis and these were labelled A to D (from bottom to top as indicated in b). To return to sample 131A, we see that in this case only the lower-most brick was left in the stack. It is inferred that during the heating of the praefurnium the topmost brick would reach the highest temperature. It was also inferred that a temperature gradient might be observed across the context, from row 13 to row 1. Green squares in a) indicate bricks which showed evidence of two components of magnetism (see representative Arai plot from sample 11.3 in (d)) with the primary component interpreted to correspond to the initial firing of the brick in the kiln (location unknown) they were manufactured in. The secondary component is a record of the heat the samples were exposed to due to their proximity to the praefurnium. Bricks labelled 33-35 were sampled as part of context B and 33 and 35 also contained two components of magnetism. Sample 34 was very noisy and it was difficult to determine the number of components of magnetisation it contained. Although it was possible to get a direction from samples 33-35 (because they were sampled as in-situ material), the directions they recorded were inconsistent with others from the praefurnium and with each other. It is noted that the samples which showed evidence of two components of magnetisation were located closest to the praefurnium. Also shown in (c) is an Arai plot for a brick containing 1 component of magnetization, sample 1.1.

Interestingly, two samples from the praefurnium also showed evidence of two components of magnetisation. The samples that showed these two components were located at the join between the praefurnium and the hypocaust and were taken from a wall composed of bricks oriented parallel with the strike of the praefurnium. Again, it is interpreted that these bricks recorded both their initial firing and then their subsequent heating in the praefurnium.

Table 4.5: Direction of the secondary component of magnetisation

Context	Sample	T1-T2	Inc	Dec	MAD	DANG
The Hypocaust	101BT1	0-240	61.2	241.1	5.40	42.07
	102AT1	0-200	54.3	-34.9	6.62	65.06
	105CT1	0-200	54.9	254.4	8.49	66.40
	113BT1	0-320	60.1	4.1	11.39	51.80
	121AT1	0-240	77.0	153.1	13.70	72.14
	122BT1	0-200	67.9	-5.7	8.74	95.44
	132AT1	0-200	59.3	75.4	21.51	102.23
The Praefurnium	33PA1	100-320	62.3	-19.5	4.12	55.72
	35PB1	100-320	63.3	-8.5	4.64	33.32

Context, name of the sampled context; sample, name of the sample, T1-T2, chosen temperature range; Inc, measured inclination; Dec, measured declination, MAD, Mean Angular Deviation of the directional fit to the paleomagnetic vector on a vector component diagram; DANG, Deviation angle.

4.6.3. Impact of Corrections on Archaeointensity Results

The addition of anisotropy and cooling rate corrections in this study; had no effect, reduced the scatter or increased the scatter in the recorded archaeointensity results (table 4.4, figure 4.15). The hypocaust behaves as might be expected with the implementation of each additional correction leading to a reduction in the scatter. The three gutters all behave differently with some corrections increasing the scatter and some decreasing the scatter. The tiles lining the gutters are rectangular with lips on both of the long edges and are interpreted to be originally designed as roofing tiles (tegulae). It is highly likely that the tiles are reused and may not have been created in the same firing. Therefore they do not have to give consistent archaeointensity results although it is presumed that they were fired at relatively similar times and therefore should give similar results. A variety of firing origins may explain the large range in cooling rate corrections determined for CAN4 where the calculated corrections ranged from -0.3% to 23% (see figure 4.15). For each context there are an insufficient number of accepted archaeointensity results which has prevented the application of robust statistical tests to try and isolate tiles from different firings.

The highest recorded cooling rate correction factor was 23%. This correction factor is higher than a number of previous studies which have cooling rate ranges of 2% to 16% from bricks (Hill et al., 2008) 3% to 18% from potsherds (Genevey and Gallet, 2002) 2% - 14% from ceramics (Goguitchaichvili et al., 2012) and 3% to 9% from kilns (Hill et al., 2007) although why this is so is unclear. It is noted that applying the corrections does lead to greater consistency between determined archaeointensities from each century (56±7 and 58±8 for the 2nd Century and 68±6 and 68±7 for the 3rd century) therefore justifying the application of the corrections.

Whilst the praefurnium samples were heated together meaning the addition of corrections would be expected to reduce the scatter, there were only four successful archaeointensity results recorded from this context. In addition, one of these samples experienced significant alteration during the cooling rate experiment and therefore the cooling rate correction was not applied to this result. With such a small population, it is not surprising that the results from the praefurnium have large error bars (±11). The conglomeratic samples from the praefurnium are relatively heterogeneous in terms of mineral size especially in comparison to the uniformly fine grained clay used to make tiles. Applied corrections for cooling rate and anisotropy are therefore expected to be significant.

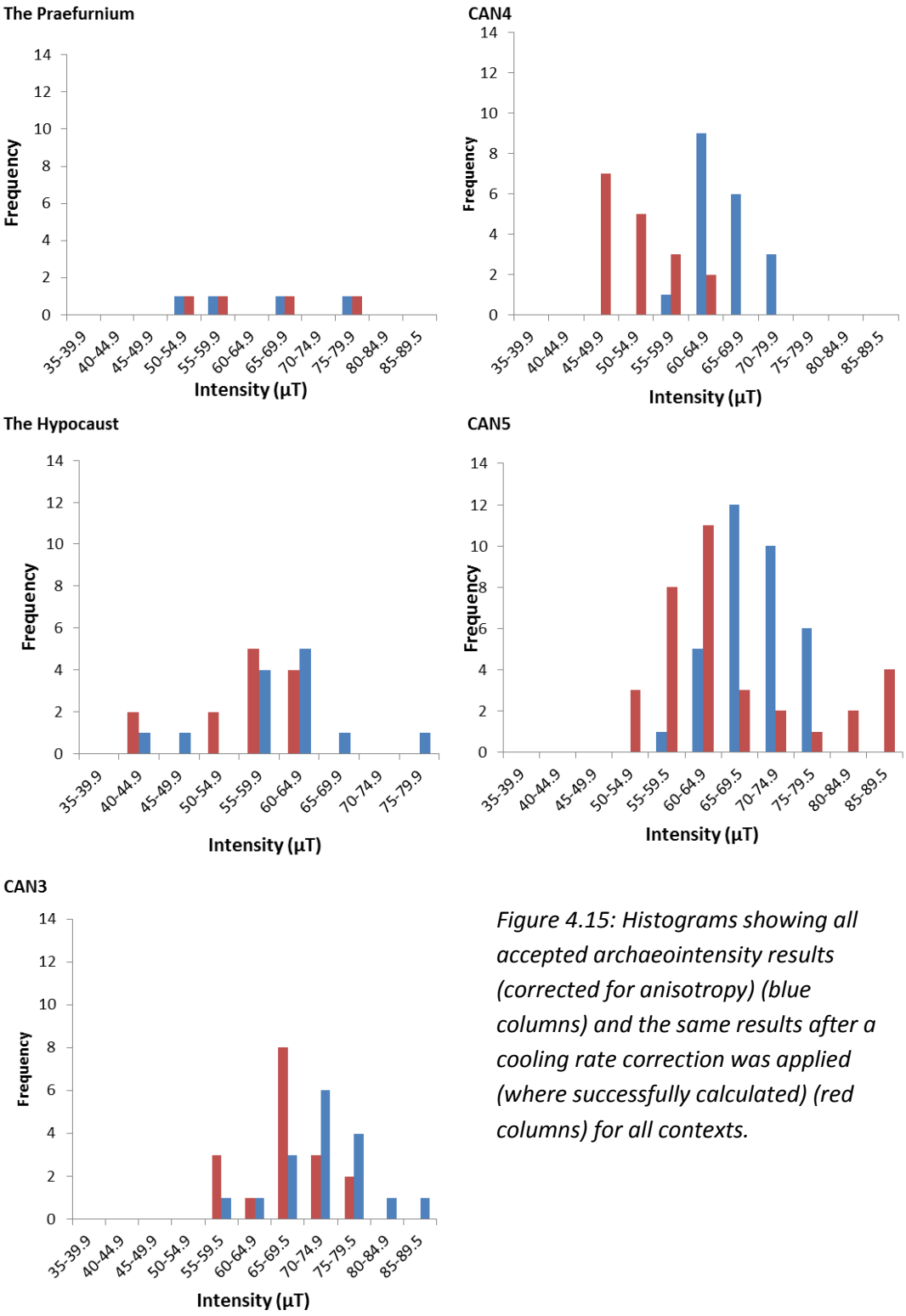

Figure 4.15: Histograms showing all accepted archaeointensity results (corrected for anisotropy) (blue columns) and the same results after a cooling rate correction was applied (where successfully calculated) (red columns) for all contexts.

4.6.4. Relative Ages

Figure 4.16 and table 4.4 show that the average calculated archaeointensity values for four of the contexts cluster in two groupings corresponding to the two different assigned ages. This confirms the differences in relative ages between the 2nd phase of construction and the 3rd phase. The age assigned to the different features determined from archaeological evidence is early 2nd century AD or 3rd century AD. For the samples from the early 2nd century AD, the age probability of the samples is uniformly distributed over 50 years whilst the samples from the 3rd century AD have an age probability uniformly distributed over 100 years. As a consequence of the lack of variability in archaeointensities over this time period, comparison of these results with those published on the GEOMAGIA database (Korhonen et al., 2008, Donadini et al., 2006) for France does not more closely constrain the age of the features.

As full vector field information was measured for the praefurnium, it was possible to conduct archaeomagnetic dating for this context using Philippe Lanos' ChronoModel 1.1 software. As seen in figure 4.17, the declination, inclination and intensity values measured for the praefurnium correspond to four time periods:88 AD ±80 at 16% probability. 399 AD ± 96 at 41% probability, 1058 ± 73 at 28% and 1523 ± 27 at 10% probability. Using the archaeological evidence, the second of these dates is preferred. It is difficult to get a precise date for this time period because there was a relative hiatus in the intensity in France between 100AD to 600AD (as can be seen in the secular variation curve plotted in figure 4.16) whilst over the same time period declination increased very slowly. This means there could potentially be relatively little difference between the field recorded when the praefurnium was first used and that recorded by its last usage. It is plotted in figure 4.16 at 399 AD ± 96 although it is noted that the intensity data was used in the Chronomodel software to date the praefurnium.

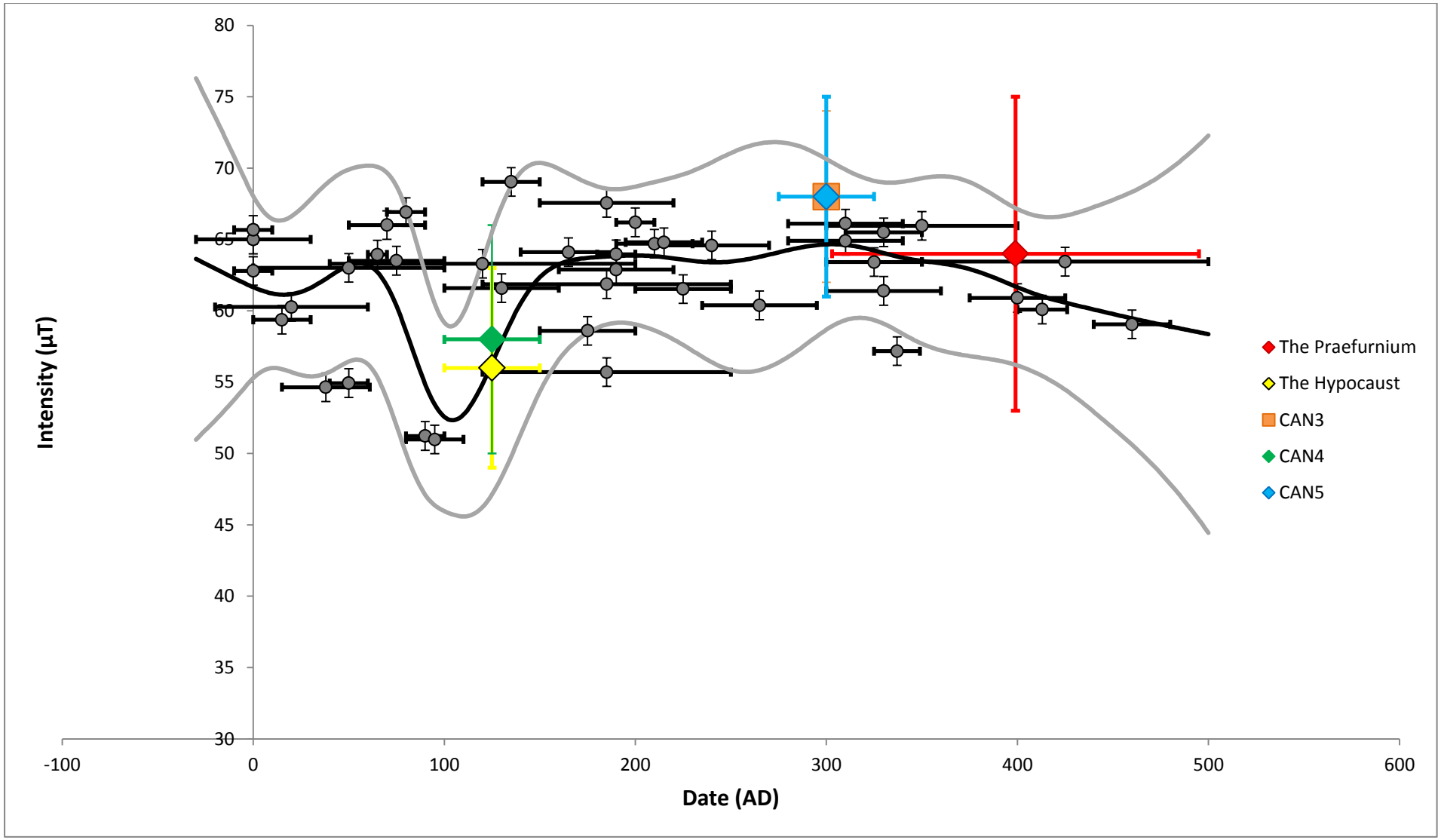
80
75
70
65
60
55
50
45
40
35
30
Intensity (µT)
-100
0
100
200
300
400
500
600
Date (AD)
The Praefurnium
The Hypocaust
CAN3
CAN4
CAN5

Figure 4.16

Intensity results from this study (coloured diamonds) plotted with all the French archaeointensity data in the Geomagia database (black circles) (Donadini et al., 2006, Korhonen et al., 2008) relocated to Site de la Molère. Horizontal error bars represent the beginning and end of the date assigned to the structure whilst the intensity value for each structure (displayed as a diamond) is plotted in the centre of the archaeological age estimate. Also plotted is a secular variation curve (red line) for St-Jean-Poutge calculated by Philippe Lanos with the blue lines indicating the error envelope for this curve. As can be seen, all the intensity values determined here plot within this error envelope. Whilst the intensity calculated for CAN3 and CAN 5 is consistent with the modelled intensity over the majority of the time period plotted, the intensity values determined for the hypocaust and CAN4 are lower than the average intensity measured over between 0 and 500 BC. The intensity is, however, consistent with field strengths experienced in a certain time periods: between 0 and 150 AD, around the middle of the 3rd century AD or after the middle of the 4th century. Combined with the archaeological evidence, the most probable age for the hypocaust and CAN4 is 0 – 150 AD. The archaeological age for the hypocaust and CAN4 is early 2nd Century AD. The vertical error bars are 1 standard deviation plus or minus the mean of the average intensity calculated for the level. Note that as CAN3 and CAN5 gave identical results they plot on top of each other.

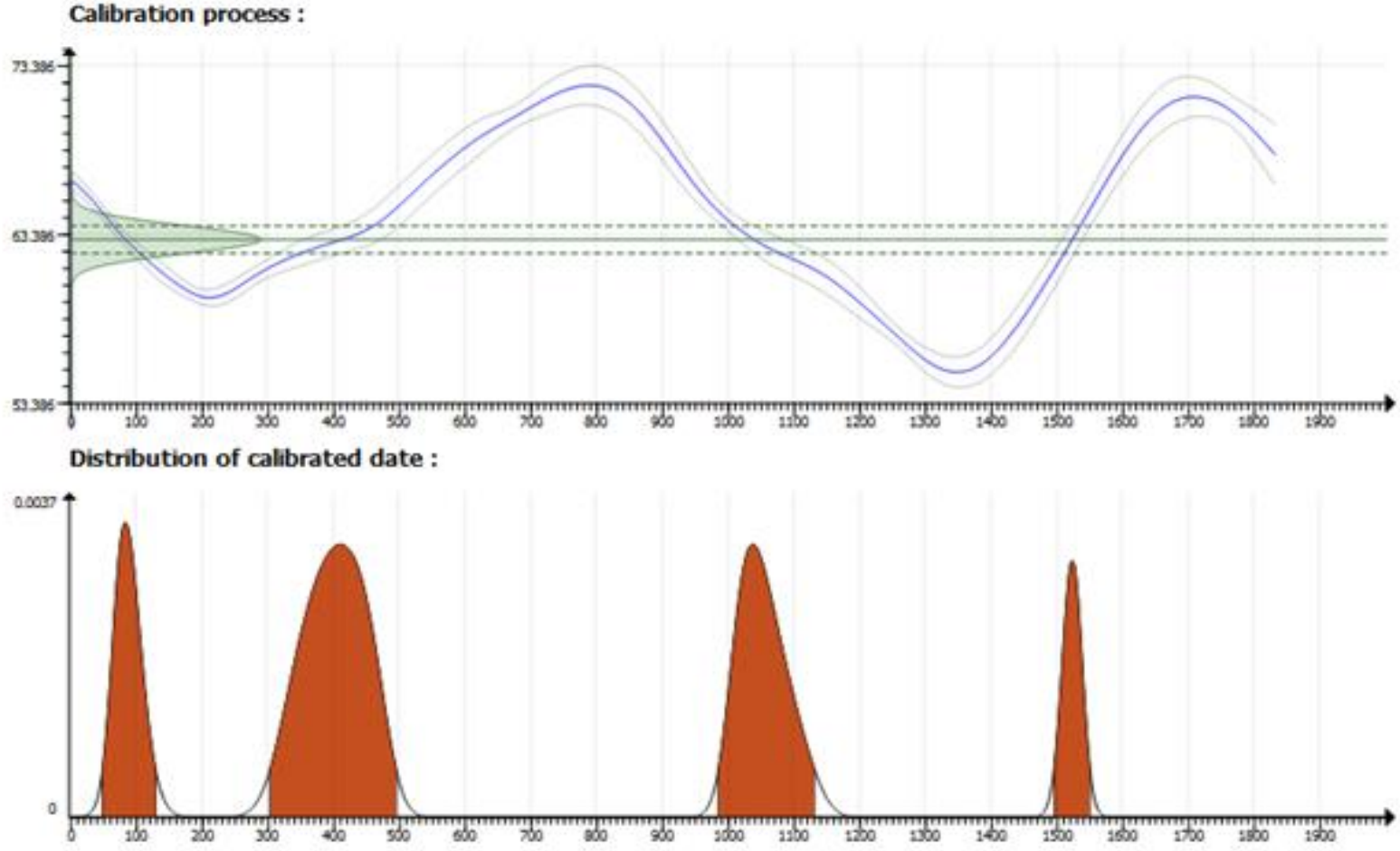
Calibration process :
73.386
63.386
53.386
0
100
200
300
400
500
600
700
800
900
1000
1100
1200
1300
1400
1500
1600
1700
1800
1900
Distribution of calibrated date :
0.0037
0

Figure 4.17. ChronoModel 1.1 prediction of the age of the praefurium based on the measured declination, inclination and intensity values. The predicated calendar dates are:48 AD ; 128 AD at 16%, 303 ; 494 AD at 41%, 985 AD; 1130 AD at 28% and 1496 AD ; 1549 AD at 10%. Based on archaeological evidence, the preferred archaeomagnetic date for the praefurnium is 399 AD ±96.

4.7. Conclusions

The results of this study cautiously confirm the archaeological interpretation that the features were constructed during two different construction events, separated in time. This is a difficult time period to study due to the lack of variability in the intensity of the field and so this study would have been strengthen by the addition of directional data. Where directional data was available, for the praefurnium, four potential calendar dates were proposed by the ChronoModel 1.1 dating software. Using archaeological information, the final heating of the praefurnium most likely occurred at 399 AD ± 96 (see figure 4.17). The site is thought to have been abandoned in the 5th century. The field vector data from the praefurnium does not contradict this conclusion.

It is acknowledged that whilst the intensity measured from features of the same age appear to group together (CAN4 and the Hypocaust for example) all five average intensity values are within the error envelopes of each other. The values determined for the early 2nd Century AD (56 ±7 and 58 ±8) appear to potentially confirm that the field was slightly lower at 100 AD before returning to former levels by 200 AD (see figure 4.16). If there was a decrease in field strength during this time period then the intensity plotted here reflects a period of increasing field strength, back to pre-100 AD values. Significantly more data is needed from 100 AD before this interpretation can be confirmed.

This study highlights the value to the archaeologist of collaborating with archaeomagnetists as archaeomagnetism can provide independent verification of dates/ interpretations and can determine if a sample has been subject to heating on more than one occasion. The value for the archaeomagnetist of working on archaeological sites is that it can either provide us with data for the construction of secular variation curves or it provides us with data with which to test geomagnetic field models e.g. Korte and Constable (2011).

The difference in success rate between burnt clay samples and burnt sedimentary material is striking. This study serves to reinforce the superiority of clay as a recorder of geomagnetic field behaviour.

4.8. Appendix

Context	Sample	T_1-T_2	β	N	f	g	q	MAD	DANG	CDRAT	No. Of checks	F	Ani Alt (%)	L1	L2	L3	Ani Corr	Fa	CR Alt (%)	CR Corr (%)	Facr
The Praefurnium	10PA1	100-500	0.057	10	0.765	0.860	11.6	2.3	0.7	0.2	4	61.1	1.6	1.028	1.013	0.958	2.4	59.583	15.4	32.7	40.1
	11PB1	100-470	0.070	9	0.728	0.829	8.6	2.0	1.1	5.7	4	64.1	4.1	1.048	1.028	0.924	4.0	61.597	4.8	15.6	51.99
	12PA1	100-470	0.034	9	0.591	0.845	14.6	2.1	0.9	3.2	4	72.0	5.6	1.055	1.016	0.929	3.4	69.566	11.9	28.5	49.71
	13PA1	100-470	0.049	9	0.744	0.846	12.8	2.8	1.2	7.2	4	73.8	37.5	1.204	1.058	0.738	9.9	66.532	11.4	24.1	50.53
	14PB1	100-470	0.049	9	0.649	0.825	10.9	2.5	5.6	-6.1	4	54.0	4.3	1.187	0.968	0.845	8.2	49.58	-1.8	-6.8	52.97
	15PA1	100-420	0.152	8	0.290	0.839	1.6	1.6	7.8	-26.5	3	79.0	7.9	1.094	0.985	0.922	2.8	76.786	-4.3	-5.3	80.83
	16PA1	100-550	0.042	11	0.890	0.883	18.9	1.5	0.5	3.5	5	53.8	2.1	1.050	0.997	0.954	2.1	52.626	-3.7	0.9	52.14
	17PA1	370-550	0.091	5	0.643	0.687	4.9	3.0	0.7	-0.5	3	28.2	3.5	1.248	0.951	0.801	7.1	26.155	-4.0	-8.6	28.41
	18PC1	100-550	0.051	11	0.879	0.837	14.3	4.7	6.6	7.2	5	35.2	2.0	1.020	1.014	0.965	-1.8	35.862	-0.7	7.8	33.06
	19PA1	100-500	0.028	10	0.610	0.750	16.6	1.6	1.8	4.9	4	60.1	2.9	1.141	1.037	0.822	8.1	55.211	2.8	-2.6	56.64
	20PA1	100-370	0.162	7	0.439	0.778	2.1	2.7	10.4	-0.6	3	114.1	0.9	1.049	1.028	0.923	1.8	112.1	-0.4	6.3	105
	21PB1	200-500	0.057	8	0.701	0.772	9.5	1.4	0.7	3.6	3	52.4	1.7	1.135	1.034	0.831	13.2	45.475	-0.1	-7.4	48.84
	22PA1	100-420	0.066	8	0.300	0.787	3.6	1.4	5.4	1.4	3	69.3	7.3	1.039	0.996	0.965	1.1	68.554	-2.0	6.3	64.25
	23PB1	100-420	0.059	8	0.459	0.734	5.7	1.5	3.0	4.6	3	67.4	10.1	1.082	1.021	0.896	5.5	63.728	3.0	10.0	57.35
	24PA1	100-370	0.034	7	0.341	0.801	8.0	0.7	2.7	-6.9	3	91.7	2.7	1.087	1.001	0.912	5.0	87.076	-0.2	1.9	85.39

The Praefurnium	25PB1	100-420	0.045	8	0.438	0.780	7.5	1.5	3.6	-3.2	3	81.3	1.9	1.041	1.009	0.949	2.4	79.374	-1.4	3.9	76.32
	26PA1	100-370	0.061	7	0.450	0.712	5.2	2.2	4.9	23.0	3	45.5	-	-	-	-	-	-	-	-	45.51
	27PA1	100-370	0.445	7	0.700	0.620	1.0	4.0	8.9	9.0	3	142.6	-	-	-	-	-	-	-	-	142.6
	28PB1	100-420	0.085	8	0.446	0.800	4.2	1.5	2.7	-4.9	3	77.7	1.3	1.045	1.016	0.939	5.2	73.654	0.0	6.1	69.19
	29PB2	100-370	0.652	11	0.728	-14.807	-16.5	2.5	3.2	-1177.5	4	13.7	-	-	-	-	-	-	-	-	13.71
	30PA2	100-370	0.451	12	0.519	-13.285	-15.3	3.9	11.5	18.4	4	29.2	-	-	-	-	-	-	-	-	29.21
	31PA1	100-370	0.134	7	0.456	-1.931	-6.5	2.2	2.5	13.2	3	45.6	-	-	-	-	-	-	-	-	45.62
	32PB1	100-370	0.805	8	-1.687	-0.266	0.6	3.6	4.1	73.2	4	152.6	-	-	-	-	-	-	-	-	152.6
	33PA1	370-550	0.035	5	0.598	0.622	10.6	2.1	2.8	11.9	3	79.8	0.7	1.167	0.943	0.890	19.7	64.07	-1.5	-17.8	75.46
	34PB1	240-550	0.061	10	0.770	0.794	10.0	10.6	11.5	20.4	5	40.6	0.5	1.049	1.032	0.919	8.8	37.02	1.6	7.6	34.21
	35PB1	320-550	0.036	6	0.386	0.721	7.7	3.3	1.5	6.5	2	62.9	0.3	1.114	0.964	0.923	0.0	62.897	0.0	7.9	57.94
												67±12						64±13			64±11

The Hypocaust	11DT1	100-420	0.032	8	0.773	0.842	20.2	3.5	6.4	0.8	3	58.7	2.2	1.109	0.976	0.915	12.8	51.195	2.7	2.8	49.74
	12CT1	100-470	0.016	9	0.783	0.800	38.0	5.7	7.2	-3.0	4	70.8	2.3	1.029	0.994	0.977	1.8	69.52	-0.9	-2.0	70.89
	13AT1	150-500	0.030	9	0.835	0.813	22.7	4.5	6.9	9.0	4	56.7	1.8	1.045	0.994	0.960	3.5	54.705	-3.9	7.5	50.63
	22BT1	100-420	0.026	8	0.936	0.805	29.5	1.9	2.0	-0.9	3	46.7	1.4	1.133	1.018	0.850	9.5	42.297	-	-	-
	23AT1	150-470	0.024	7	0.945	0.785	30.5	2.1	3.2	1.7	3	57.9	1.8	1.168	0.943	0.889	1.6	56.927	1.3	2.5	55.48
	31CT1	150-471	0.029	8	0.813	0.833	23.3	2.2	2.8	7.0	3	61.3	1.1	1.036	1.007	0.957	2.5	59.76	-0.9	-4.0	62.16
	41AT1	200-370	0.020	5	0.776	0.677	26.5	1.3	0.8	0.2	2	59.0	3.1	1.089	0.968	0.942	-2.6	60.546	0.7	-6.1	64.22
	74BT1	200-500	0.024	8	0.657	0.820	22.1	1.8	1.1	6.1	3	58.4	1.5	1.125	0.978	0.897	-0.5	58.685	0.5	-0.5	58.95
	95AT1	200-500	0.030	8	0.621	0.726	15.0	6.6	6.5	6.0	3	44.0	0.1	1.169	0.960	0.870	19.9	35.233	5.0	4.8	33.54
	101BT1	240-550	0.042	8	1.740	0.805	33.8	2.2	2.0	9.5	4	63.6	0.5	1.156	0.989	0.855	7.9	58.64	2.5	7.2	54.39
	102AT1	240-550	0.038	8	0.598	0.826	13.1	3.7	3.5	17.0	4	49.7	2.2	1.077	0.998	0.925	8.8	45.315	5.2	-1.3	45.91
	105CT1	240-470	0.022	6	0.982	0.700	31.9	2.0	1.6	-1.0	3	50.2	2.8	1.074	0.989	0.936	3.4	48.491	7.4	9.9	43.68
	111AT1	200-500	0.021	8	0.826	0.769	30.2	1.3	2.0	1.4	2	71.1	0.7	1.089	0.973	0.937	-6.3	75.529	3.1	15.7	63.68
	112AT1	200-550	0.014	9	0.909	0.840	53.2	1.2	0.2	0.8	4	67.2	2.4	1.170	0.945	0.885	8.3	61.58	0.8	5.1	58.47
	113BT1	370-550	0.015	5	0.678	0.733	32.4	1.6	1.5	4.4	3	85.0	2.4	1.164	0.978	0.858	18.5	69.282	1.3	7.1	64.38
	121AT1	240-500	0.031	7	0.763	0.774	18.9	2.1	3.8	0.0	3	75.6	1.2	1.133	0.987	0.881	16.9	62.831	1.8	16.9	52.21
	122BT1	240-500	0.015	7	0.731	0.780	38.4	2.0	2.2	6.8	3	60.9	1.7	1.138	0.982	0.881	2.9	59.126	2.2	2.8	57.48
	131AT1	100-550	0.030	11	0.820	0.868	24.1	3.9	4.4	4.7	5	65.0	0.4	1.117	0.990	0.893	1.4	64.069	5.2	13.6	55.36
	132AT1	240-550	0.030	8	0.882	0.766	22.2	1.6	1.2	12.9	4	59.5	1.3	1.026	0.996	0.978	12.7	51.991	-3.2	26.1	38.4
	21CT1	0-575	2.714	12	0.060	0.109	39.3	12.0	1.0	3.7	3	51.1	1.5	1.090	1.028	0.882	-	-	-	-	-
												63±10						60±8			56±7

CAN3	300T1	100-470	0.026	9	0.707	0.822	22.6	1.5	2.4	4.9	4	71.4	0.9	1.044	1.011	0.945	6.0	67.16	-0.2	1.3	66.3
	301T1	100-550	0.008	11	0.929	0.891	101.6	1.8	1.7	2.1	4	72.0	1.5	1.055	0.997	0.948	-1.8	73.323	0.6	12.9	63.84
	302T1	200-550	0.021	8	0.603	0.821	23.6	2.5	2.2	-9.8	3	64.1	3.3	1.141	0.963	0.896	7.7	59.119	0.7	0.9	58.58
	303T1	110-550	0.014	11	0.923	0.888	58.1	1.0	0.3	1.9	4	79.7	1.8	1.092	0.973	0.934	6.8	74.308	-0.6	8.7	67.85
	304T1	100-420	0.017	8	0.932	0.826	44.3	1.7	0.7	1.9	3	78.0	1.5	1.109	0.979	0.912	3.2	75.515	-14.8	-21.7	91.9
	305T1	100-550	0.020	11	0.985	0.859	41.5	1.2	1.0	1.3	4	79.3	2.0	1.112	0.997	0.891	2.7	77.134	2.1	4.3	73.79
	306T1	100-550	0.024	11	0.992	0.881	36.3	1.0	1.0	1.7	4	75.2	1.7	1.101	0.971	0.928	-1.8	76.534	-5.7	9.6	69.19
	307T1	100-550	0.012	11	0.977	0.876	69.5	1.1	1.2	1.8	4	73.5	1.9	1.105	1.007	0.889	-12.1	82.406	0.1	7.2	76.45
	308T1	0-575	0.071	12	0.870	0.726	8.9	5.4	5.6	18.8	4	44.6	6.9	1.101	1.072	0.827	16.7	37.108	2.0	16.5	30.99
	309T1	200-470	0.033	7	0.711	0.671	14.7	0.9	0.9	3.1	3	94.3	0.3	1.083	1.039	0.877	18.4	76.868	0.9	7.6	71
	310T1	100-500	0.022	10	0.821	0.836	30.6	1.0	0.5	2.8	4	76.5	0.8	1.088	1.005	0.908	6.9	71.162	1.2	5.6	67.17
	311T1	100-500	0.025	9	0.628	0.845	21.2	1.3	1.5	-9.5	4	75.9	0.3	1.068	1.020	0.913	8.3	69.593	2.1	1.2	68.75
	312T1	100-550	0.018	10	0.819	0.872	39.4	1.9	0.6	7.9	4	70.1	3.0	1.072	1.023	0.905	10.6	62.674	0.2	8.8	57.14
	313T1	100-550	0.010	11	0.866	0.893	78.3	1.6	2.5	3.6	4	66.8	0.9	1.090	0.968	0.942	-1.9	68.096	-15.8	-11.3	75.82
	314T1	100-550	0.017	11	0.989	0.871	51.8	1.4	1.4	3.6	4	74.8	3.3	1.114	0.952	0.934	2.2	73.102	-1.8	18.2	59.79
	315T1	100-470	0.024	9	0.569	0.845	19.7	1.1	2.9	2.5	3	73.6	2.0	1.054	1.032	0.914	4.2	70.548	1.5	2.2	69.01
	316T1	100-550	0.018	11	0.983	0.847	46.6	1.1	0.8	1.5	4	77.5	1.1	1.079	1.040	0.881	-10.1	85.355	1.7	17.8	70.16
	317T1	100-420	0.017	8	0.504	0.818	24.9	1.5	3.0	1.1	3	72.4	2.2	1.130	0.943	0.928	5.0	68.801	-16.6	1.0	68.14
												75±6						72±7			68±6

CAN4	100T1	100-320	0.022	6	0.580	0.038	19.8	1.9	4.1	4.6	3	63.3	2.8	1.077	0.966	0.957	-0.6	63.64	4.9	21.5	49.95
	101T1	100-470	0.026	9	0.838	0.008	27.2	4.3	4.9	5.0	4	66.5	0.3	1.074	1.038	0.888	13.4	57.61	7.0	13.0	50.10
	102T1	100-470	0.038	9	0.704	0.051	15.1	3.4	5.1	2.2	3	66.1	3.8	1.035	1.017	0.948	-4.4	69.03	10.9	18.7	56.09
	103T1	100-550	0.012	9	0.716	0.791	48.7	4.3	3.0	-0.1	4	70.5	2.9	1.056	1.001	0.943	7.3	65.373	10.7	22.2	50.85
	104T1	100-420	0.018	8	0.631	0.017	27.4	1.6	1.5	3.0	3	67.1	1.8	1.053	1.016	0.931	8.1	61.69	6.0	14.1	53.00
	105T1	100-550	0.019	11	0.915	0.042	43.2	3.2	4.2	3.9	4	68.6	3.0	1.038	0.996	0.966	-2.3	70.24	5.3	16.0	59.00
	106T1	100-470	0.040	9	0.750	0.005	15.7	1.9	1.1	2.9	3	73.0	1.2	1.070	1.047	0.883	10.1	65.65	-0.9	6.3	61.50
	107T1	100-470	0.039	9	0.818	0.002	16.8	2.8	2.4	2.5	3	69.1	0.2	1.067	1.008	0.925	9.4	62.55	4.7	17.6	51.55
	108T1	100-370	0.046	7	0.882	0.110	14.8	4.0	4.6	5.0	3	72.9	3.7	1.045	0.983	0.972	-1.4	73.90	13.0	36.8	46.72
	109T1	100-370	0.030	7	0.750	0.040	20.1	2.7	3.8	2.7	3	69.9	3.9	1.068	0.991	0.942	3.3	67.62	15.1	32.8	45.43
	110T1	100-470	0.026	9	0.715	0.010	22.7	2.0	1.8	6.2	4	67.2	2.1	1.057	1.003	0.940	6.7	62.64	8.7	23.2	48.09
	111T1	100-420	0.026	8	0.786	0.064	24.5	2.3	2.4	0.6	3	74.6	4.5	1.079	1.002	0.919	4.2	71.49	23.1	33.5	47.52
	112T1	150-470	0.032	8	0.802	0.002	21.1	1.3	1.6	5.1	3	81.9	0.6	1.093	1.047	0.861	19.3	66.13	0.0	19.7	53.12
	113T1	100-370	0.018	7	0.659	0.032	28.7	1.8	1.8	2.7	3	66.5	4.8	1.154	0.944	0.902	8.5	60.86	16.1	25.1	45.62
	114T1	100-420	0.082	8	0.773	0.026	7.4	4.2	3.0	5.0	3	68.9	0.8	1.071	1.014	0.915	7.8	63.51	19.4	16.0	53.37
	115T1	100-420	0.030	8	0.646	0.031	17.5	1.8	1.3	3.1	3	66.4	3.1	1.121	0.980	0.898	6.3	62.25	13.1	9.6	56.26
	116T1	150-420	0.040	7	0.573	0.800	11.5	3.9	5.3	-14.7	2	74.8	5.8	1.065	0.987	0.947	7.4	69.24	9.1	24.8	52.09
	117T1	100-420	4.428	8	0.080	0.081	9.1	12.0	0.8	2.3	3	77.4	0.8	1.065	1.035	0.901	-	-	-	-	-
	118T1	100-420	0.029	8	0.761	0.019	20.7	3.0	1.5	2.7	4	66.9	1.5	1.084	1.013	0.903	9.8	60.33	8.7	17.4	49.81
	119T1	100-370	0.010	7	0.963	0.014	79.0	3.5	2.0	5.0	3	72.1	0.9	1.174	0.944	0.882	13.1	62.63	7.8	-0.3	62.82
	120T1	0-575	0.237	12	0.609	0.848	2.2	10.4	4.6	8.5	4	48.9	3.1	1.074	1.006	0.920	-	-	-	-	-
												70±4						65±4			58±8

.

CAN 5	200T1	100-420	0.030	8	0.730	0.833	20.4	2.2	4.2	2.6	3	73.5	2.4	1.057	1.017	0.926	11.1	65.36	-11.9	8.9	59.55
	201T1	100-550	0.024	11	0.947	0.873	34.1	2.1	178.2	14.0	5	60.8	2.0	1.033	1.017	0.950	0.0	60.80	2.6	8.6	55.59
	202T1	100-420	0.034	8	0.695	0.845	17.5	2.0	4.2	0.8	4	71.5	2.6	1.111	0.995	0.894	-11.1	79.36	-2.3	2.2	77.59
	203T1	100-370	0.017	7	0.732	0.824	36.2	1.6	2.7	2.9	3	78.0	1.2	1.045	1.010	0.945	1.6	76.72	-28.3	8.3	70.32
	204T1	100-370	0.025	7	0.769	0.829	25.3	1.7	1.4	2.7	3	62.3	3.2	1.040	1.031	0.928	-0.1	62.32	-19.5	17.7	51.26
	205T1	100-370	0.027	7	0.759	0.832	23.8	2.8	6.0	2.6	3	70.5	2.6	1.055	0.977	0.968	1.4	69.49	-16.2	15.1	59.02
	206T1	100-420	0.022	8	0.793	0.852	30.1	2.1	4.1	1.9	3	69.8	3.0	1.063	0.982	0.955	-1.7	71.04	-9.6	16.7	59.19
	207T1	150-370	0.019	6	0.444	0.738	17.2	1.5	4.3	1.6	2	65.3	3.5	1.045	1.008	0.947	0.0	65.26	6.6	15.8	54.95
	208T1	100-550	0.016	10	0.426	0.880	23.1	1.7	9.5	9.1	4	63.9	1.3	1.033	0.996	0.971	0.0	63.86	-18.3	-7.0	68.32
	209T1	100-370	0.014	7	0.715	0.827	42.0	1.7	2.8	-0.1	3	75.2	1.6	1.049	0.994	0.958	4.4	71.84	-25.9	5.1	68.20
	210T1	100-420	0.018	8	0.756	0.849	35.2	3.6	7.2	-2.1	3	59.8	4.2	1.123	1.007	0.870	-2.7	61.40	1.2	6.6	57.37
	211T1	100-420	0.023	8	0.800	0.850	29.8	2.4	3.9	3.2	3	71.8	3.4	1.094	0.974	0.932	-3.1	73.99	-2.2	-11.7	82.66
	212T1	100-420	0.019	8	0.673	0.850	30.1	1.9	3.4	1.0	3	76.0	2.3	1.060	1.000	0.940	6.4	71.15	-9.3	-13.4	80.72
	213T1	100-420	0.028	8	0.741	0.846	22.5	2.4	4.4	0.2	3	72.9	4.6	1.020	1.011	0.969	1.8	71.54	-21.6	17.4	59.12
	214T1	100-550	0.022	11	0.908	0.888	35.9	1.1	0.7	10.5	5	65.7	2.0	1.062	1.025	0.912	0.0	65.70	2.8	9.2	59.68
	215T1	100-420	0.028	8	0.773	0.842	23.3	2.5	4.2	2.2	3	73.8	3.4	1.084	0.998	0.918	9.6	66.71	0.0	5.9	62.74
	216T1	100-370	0.023	7	0.735	0.832	26.6	1.8	4.0	3.2	3	76.7	2.4	1.065	1.007	0.927	8.5	70.19	-8.5	-2.0	71.58
	217T1	100-370	0.033	7	0.795	0.831	20.1	2.8	5.3	3.6	3	72.6	2.5	1.074	1.002	0.924	0.0	72.63	-9.5	-8.8	79.04
	218T1	100-550	0.030	11	0.965	0.883	28.1	3.1	3.8	18.1	5	49.6	2.7	1.047	1.004	0.949	0.0	49.56	4.3	12.2	43.50
	219T1	100-550	0.034	11	0.907	0.870	23.1	1.7	1.2	9.1	4	58.0	2.5	1.040	1.022	0.939	0.0	57.95	3.1	8.1	53.27
	220T1	0	0.325	12	0.335	0.879	0.9	12.0	1.0	-2.1	4	15.6	6.0	1.105	0.972	0.924	-	-	-	-	-

	221T1	100-370	0.017	7	0.755	0.828	35.9	2.3	4.8	-0.6	3	71.8	4.3	1.048	0.998	0.954	4.5	68.54	-11.0	6.0	64.44
	222T1	150-470	0.019	8	0.693	0.809	30.2	1.3	1.2	10.9	4	61.2	2.5	1.042	0.987	0.970	0.0	61.21	3.8	9.4	55.45
	223T1	100-550	0.022	11	0.947	0.872	38.3	1.4	0.4	10.9	5	64.9	1.1	1.026	1.010	0.964	0.0	64.91	2.4	8.1	59.65
	224T1	150-550	0.011	10	0.909	0.864	72.9	1.3	0.3	9.7	5	75.4	1.6	1.051	1.034	0.915	11.1	67.03	1.9	11.8	59.09
	225T1	100-370	0.009	7	0.790	0.830	71.4	1.3	2.0	2.2	3	73.7	2.4	1.080	0.985	0.936	0.9	73.00	-26.3	18.4	59.58
	226T1	100-550	0.022	11	0.900	0.860	34.4	1.7	1.0	8.2	5	67.7	2.9	1.370	1.146	0.484	-35.3	91.54	1.8	9.0	83.30
	227T1	100-550	0.016	11	0.922	0.873	51.3	1.1	0.3	10.2	5	63.1	1.1	1.041	1.029	0.929	0.0	63.08	1.5	6.6	58.90
	228T1	150-550	0.010	10	0.983	0.876	86.9	1.2	0.7	9.4	4	72.3	1.5	1.055	0.997	0.947	5.1	68.66	2.8	10.1	61.73
	229T1	150-500	0.088	9	76.822	0.815	4.4	1.5	174.3	-0.2	3	76.8	3.7	1.071	0.998	0.931	0.0	76.82	4.7	11.5	67.98
	230T1	100-420	0.017	8	0.821	0.852	42.0	2.1	2.1	4.1	3	64.6	3.0	1.032	1.014	0.954	3.0	62.69	-14.2	1.7	61.62
	231T1	150-500	0.028	9	0.510	0.839	15.1	2.6	8.8	8.8	3	59.9	3.2	1.083	1.005	0.912	0.0	59.90	5.8	7.4	55.46
	232T1	100-370	0.027	7	0.691	0.827	21.4	2.3	4.1	2.4	3	79.3	2.5	1.068	0.980	0.952	4.7	75.54	-21.2	-23.1	92.96
	233T1	100-370	0.064	7	0.574	0.783	7.0	5.7	12.9	4.1	3	54.6	3.3	1.036	1.023	0.941	0.0	54.60	6.0	7.2	50.68
	234T1	150-500	0.014	9	0.730	0.813	41.7	1.0	0.4	1.0	5	85.4	2.7	1.109	0.986	0.905	9.7	77.10	-0.5	10.0	69.35
	235T1	150-500	0.012	9	0.735	0.839	49.6	1.3	2.1	1.4	4	79.1	1.0	1.216	0.962	0.822	12.1	69.55	1.0	12.3	61.02
	236T1	100-550	0.013	11	0.948	0.893	63.1	1.7	0.8	2.6	4	73.7	1.2	1.083	0.969	0.949	0.9	73.01	-19.4	-30.1	94.99
	237T1	100-420	0.025	8	0.864	0.833	28.4	1.5	1.2	4.3	3	66.6	1.0	1.032	0.999	0.969	3.3	64.41	1.9	1.1	63.73
	238T1	100-500	0.015	10	0.872	0.849	48.1	1.0	1.1	5.4	4	70.1	1.8	1.352	1.155	0.492	-40.5	98.58	3.6	7.3	91.41
	239T1	150-370	0.745	6	0.614	0.745	25.5	1.1	0.9	3.9	2	64.1	2.7	1.063	0.990	0.946	0.0	64.06	7.7	15.8	53.91
	240T1	150-470	0.805	7	0.712	0.805	12.7	4.0	4.2	-8.2	2	73.6	3.4	1.048	1.000	0.953	0.0	73.57	-18.6	8.2	67.56

CAN 5	221T1	100-370	0.017	7	0.755	0.828	35.9	2.3	4.8	-0.6	3	71.8	4.3	1.048	0.998	0.954	4.5	68.54	-11.0	6.0	64.44
	222T1	150-470	0.019	8	0.693	0.809	30.2	1.3	1.2	10.9	4	61.2	2.5	1.042	0.987	0.970	0.0	61.21	3.8	9.4	55.45
	223T1	100-550	0.022	11	0.947	0.872	38.3	1.4	0.4	10.9	5	64.9	1.1	1.026	1.010	0.964	0.0	64.91	2.4	8.1	59.65
	224T1	150-550	0.011	10	0.909	0.864	72.9	1.3	0.3	9.7	5	75.4	1.6	1.051	1.034	0.915	11.1	67.03	1.9	11.8	59.09
	225T1	100-370	0.009	7	0.790	0.830	71.4	1.3	2.0	2.2	3	73.7	2.4	1.080	0.985	0.936	0.9	73.00	-26.3	18.4	59.58
	226T1	100-550	0.022	11	0.900	0.860	34.4	1.7	1.0	8.2	5	67.7	2.9	1.370	1.146	0.484	-35.3	91.54	1.8	9.0	83.30
	227T1	100-550	0.016	11	0.922	0.873	51.3	1.1	0.3	10.2	5	63.1	1.1	1.041	1.029	0.929	0.0	63.08	1.5	6.6	58.90
	228T1	150-550	0.010	10	0.983	0.876	86.9	1.2	0.7	9.4	4	72.3	1.5	1.055	0.997	0.947	5.1	68.66	2.8	10.1	61.73
	229T1	150-500	0.088	9	76.822	0.815	4.4	1.5	174.3	-0.2	3	76.8	3.7	1.071	0.998	0.931	0.0	76.82	4.7	11.5	67.98
	230T1	100-420	0.017	8	0.821	0.852	42.0	2.1	2.1	4.1	3	64.6	3.0	1.032	1.014	0.954	3.0	62.69	-14.2	1.7	61.62
	231T1	150-500	0.028	9	0.510	0.839	15.1	2.6	8.8	8.8	3	59.9	3.2	1.083	1.005	0.912	0.0	59.90	5.8	7.4	55.46
	232T1	100-370	0.027	7	0.691	0.827	21.4	2.3	4.1	2.4	3	79.3	2.5	1.068	0.980	0.952	4.7	75.54	-21.2	-23.1	92.96
	233T1	100-370	0.064	7	0.574	0.783	7.0	5.7	12.9	4.1	3	54.6	3.3	1.036	1.023	0.941	0.0	54.60	6.0	7.2	50.68
	234T1	150-500	0.014	9	0.730	0.813	41.7	1.0	0.4	1.0	5	85.4	2.7	1.109	0.986	0.905	9.7	77.10	-0.5	10.0	69.35
	235T1	150-500	0.012	9	0.735	0.839	49.6	1.3	2.1	1.4	4	79.1	1.0	1.216	0.962	0.822	12.1	69.55	1.0	12.3	61.02
	236T1	100-550	0.013	11	0.948	0.893	63.1	1.7	0.8	2.6	4	73.7	1.2	1.083	0.969	0.949	0.9	73.01	-19.4	-30.1	94.99
	237T1	100-420	0.025	8	0.864	0.833	28.4	1.5	1.2	4.3	3	66.6	1.0	1.032	0.999	0.969	3.3	64.41	1.9	1.1	63.73
	238T1	100-500	0.015	10	0.872	0.849	48.1	1.0	1.1	5.4	4	70.1	1.8	1.352	1.155	0.492	-40.5	98.58	3.6	7.3	91.41
	239T1	150-370	0.745	6	0.614	0.745	25.5	1.1	0.9	3.9	2	64.1	2.7	1.063	0.990	0.946	0.0	64.06	7.7	15.8	53.91
	240T1	150-470	0.805	7	0.712	0.805	12.7	4.0	4.2	-8.2	2	73.6	3.4	1.048	1.000	0.953	0.0	73.57	-18.6	8.2	67.56

CAN 5	241T1	100-470	0.018	9	0.862	0.859	40.5	2.1	2.8	3.3	4	81.4	2.2	1.105	1.001	0.894	17.2	67.33	-11.7	-12.3	75.64
	242T1	100-370	0.049	7	0.663	0.810	11.1	2.6	4.8	1.5	3	71.3	0.8	1.020	1.009	0.971	2.0	69.89	8.8	15.2	59.29
	243T1	100-370	0.038	7	0.720	0.829	15.7	2.0	3.6	0.9	3	72.8	3.0	1.035	1.000	0.965	2.0	71.34	-16.0	13.1	61.99
	244T1	150-550	0.018	10	0.843	0.881	41.9	1.2	0.6	11.0	4	67.4	1.6	1.048	1.017	0.935	0.0	67.38	-	11.2	59.83
	245T1	100-420	0.015	8	0.871	0.831	49.1	1.7	2.0	6.3	4	74.4	2.0	1.049	0.989	0.962	4.5	71.08	6.9	8.8	64.86
	246T1	100-420	0.016	8	0.838	0.827	44.4	1.5	1.1	4.1	3	72.7	2.0	1.038	0.993	0.969	3.1	70.46	0.9	5.1	66.85
	247T1	100-420	0.020	8	0.751	0.845	31.1	0.9	0.9	4.5	3	67.5	1.8	1.026	0.994	0.980	1.5	66.50	-0.1	2.7	64.67
	248T1	100-420	0.006	8	0.840	0.827	106.9	1.4	1.6	2.9	3	78.3	2.0	1.055	1.021	0.924	5.9	73.71	0.0	2.9	71.56
	249T1	100-420	0.009	8	0.819	0.835	75.2	1.0	0.9	2.0	3	76.9	1.9	1.084	0.977	0.938	-2.7	78.91	-15.2	9.8	71.14
	250T1	100-500	0.020	10	0.813	0.852	34.2	1.6	0.9	8.8	4	68.5	2.0	1.053	1.014	0.933	0.2	68.41	1.2	5.3	64.80
	251T1	150-550	0.013	10	0.860	0.863	55.1	0.9	0.4	6.3	3	69.5	2.0	1.064	0.999	0.937	2.0	68.06	1.9	10.8	60.70
												73±6						70±5			68±7

Context, name of the sampled context; Sample, name of the sample; T1-T2, chosen temperature range; β, ratio of standard error of the slope to the absolute value of the slope; N, number of points used to define a linear segment of the Arai diagram; f, the NRM fraction used for the best-fit on an Arai diagram; g, 'gap factor' normalised error of the slope and quality factor according to Coe et al. (1987) q, quality factor; MAD, Mean Angular Deviation of the directional fit to the paleomagnetic vector on a vector component diagram; DANG, Deviation angle; CDRAT, cumulative DRAT where a DRAT is the maximum absolute difference produced by a pTRM check, normalized by the length of the best-fit line; No of checks, number of accepted pTRM checks; F, measured intensity; Ani Alt, Anisotropy Alteration, alteration occuring during the anisotropy experiment; L1, L2, L3, the Anistropy tensor; Ani Corr, Anisotropy correction, determined anisotorpy correction per sample; Fa, intensity value corrected for anisotropy; CR Alt, Alteration occuring during the cooling rate experiment; Cooling rate correction, measured cooling rate correction per sample; Facr, cooling rate and anistropy corrected intensity value. Grey rows indicate accepted results.

5. Increasing the Duration of the 1000 BC Geomagnetic Intensity High: The First Continuous Archaeointensity Data set from Turkish Potsherds

5.1. Abstract

Here we present new archaeointensity data recorded in potsherds and burnt mud brick from two Bronze Age archaeological sites in Southern Turkey: Tell Atchana and Kilise Tepe. Microwave Coe and IZZI experiments were run on 128 potsherds and thermal IZZI experiments were run on 18 mudbricks. Archaeointensity values spanning 2200BC to 1305BC are reported from 56 pot sherds and 17 mud bricks from Tell Atchana. Two Microwave Coe method archaeointensity values from 800-600 BC are also reported from the archaeological site Kilise Tepe. Recently published archaeointensity values from neighbouring countries suggest that there was a period of relatively high field intensity at 1000 BC, the exact duration of which has been the subject of much debate. The key result of this study extends the geographic range of this intensity high and increases its duration as we record a field of 84μT (153 ZAm^2) in Southern Central Turkey at ~700BC which is nearly twice the present value of the field. This makes the geomagnetic field behaviour at 1000 BC more reasonable from a geophysical perspective than suggested by previous work in this region. We also present evidence that the strength of the geomagnetic field was consistent with current field values for the 1000 years prior to this and was relatively stable, only varying by 16μT between 2200 BC and 1300 BC.

5.2. Introduction

Archaeomagnetism is the study of burnt or fired archaeological artefacts; in situ features studied include kilns, ovens and fires whilst commonly studied ex situ artefacts include tiles, bricks and ceramics. The importance of archaeomagnetism in revealing short

timescale changes in the strength of the geomagnetic field has been highlighted in recent years by studies from the Levant and Middle East. Results have been published from archaeomagnetic studies in Syria and Iran (Gallet et al., 2006, Gallet et al., 2003, Gallet and Le Goff, 2006, Genevey et al., 2003, Gallet et al., 2008, Gallet et al., 2014) as well as Jordan and Israel (Ben-Yosef et al., 2009, Ben-Yosef et al., 2008b, Shaar et al., 2011) and also Turkey (Ertepinar et al., 2012). The focus of recent research has been on the Levant and Middle East between ~3000 BC and 0 BC partly because Gallet et al., (2006) proposed that there were four 'archaeomagnetic jerks' recorded in Middle Eastern data. An archaeomagnetic jerk has been defined as a period of intensity maxima coinciding with a sharp cusp in geomagnetic field direction with time characteristics intermediate between geomagnetic jerks and magnetic excursions (Gallet et al., 2003). These four archaeomagnetic jerks are proposed to have occurred at ~2800-2600 BC, ~2100-1900 BC, ~1750-1500 BC and 1100-750BC. The latter of these proposed jerks is coincident in time with two periods of exceptionally high field intensity recorded in Southern Jordan and Israel (Ben-Yosef et al., 2009, Shaar et al., 2011) and dubbed geomagnetic spikes. A geomagnetic spike is defined as a very short episode of exceptionally high field intensity in excess of 200 ZAm^2 (104 μT) (Ben-Yosef et al., 2009). During one geomagnetic spike, geomagnetic virtual axial dipole moments in excess of 250 ZAm^2 (114.7 μT) were measured. The duration of the two proposed "geomagnetic spikes" in the 10^{th} and 9^{th} Centuries BC (Shaar et al., 2011) is contentious particularly as the authors speculate that the peak of each spike may be as short as a few years. Additionally the rate of change recorded by these authors seems to imply that geomagnetic field strength can increase dramatically over an extraordinarily short time period.

Such exceptional field strength changes (~4-5μT/ year) are impossible to model mathematically with our current understanding of core surface-flow (Livermore et al., 2014) and are 40 to 50 times larger than typical present-day values. Livermore et al., (2014) propose two possible solutions to this contradiction. Either the rate of change is less than reported (intensity itself is lower or the spike longer) or the field was truly exceptional around 1000 BC and behaved significantly differently to today.

Compared to its neighbouring countries, Syria and Bulgaria, there have been very few archaeomagnetic studies based in Turkey. This is surprising considering the long cultural heritage of Turkey. Prior to 2014, we are only aware of 5 papers published on archaeomagnetic studies in Turkey (Saribudak and Tarling, 1993, Bucha and Mellaart, 1967,

Bammer, 1964, Sayin and Orbay, 2003, Ertepinar et al., 2012). The results of these papers are sporadic in time and location varying from the study of a single Neolithic site, Çatalhöyük in southern Anatolia (Bucha and Mellaart, 1967) to the study of 15 sites occupied from 7900BC to 1750 AD in central Anatolia (Sayin and Orbay, 2003). Such a dispersed data set means that geomagnetic field models for Turkey are relatively unconstrained by local data and rely heavily on data published for Bulgaria and Syria. Of these 5 papers only 3 reported archaeointensity data. This is consistent with data sets from other countries as archaeointensity is generally neglected due to the inherent experimental difficulties associated with determining archaeointensities. As a consequence of the lack of a local secular variation curve it is, therefore, also not currently possible to conduct archaeomagnetic dating in Turkey.

Ertepinar et al., (2012) focused on five mounds occupied between 2500 and 700 BC in south eastern Turkey and the directional results they determined were comparable with the global geomagnetic field models CALS7k.2, ARCH3k_cst.1 and CALS3k.4 (Korte et al., 2009, Korte and Constable, 2005, Donadini et al., 2009, Korte and Constable, 2011) and data from GEOMAGIA50v2 (Donadini et al., 2006). The authors used microwave and conventional thermal Thellier methods to calculate archaeointensities on four furnaces and a mud-brick wall. The excellent agreement shown between the microwave and thermal Thellier-Thellier results in this paper is further proof of the equivalence of the two methods. The intensities determined from the furnaces were slightly higher than the CALS7k.2 model and in agreement with data from GEOMAGIA50v2 and previously published Middle Eastern data. The results from the mud-brick wall, however, suggest a high intensity of 100.8µT (177 ZAm^2) at ~1000BC, a result which is in striking agreement with Shaar et al., (2011) and Ben-Yosef et al., (2009) and their proposed geomagnetic spikes.

The aim of this study was to determine if pottery from Turkey recorded high field intensities between 2200 and 700 BC and therefore could contribute to determining exactly the duration and geographic extent of the intensity high around 1000BC. A further motivation of this study is to gather archaeointensity data for Turkey because there is a dearth of previous studies based in the country. The results of this study will help to narrow the data gap over Turkey and so increase the accuracy of field models.

5.3. Archaeological Background

5.3.1. Tell Atchana (36.237° N, 36.384° E)

Tell Atchana is located on the western side of the Amuq plain in the Hatay Province of Southern Turkey, within 2km of the current border with Syria (figure 5.1) (see Woolley (1955) for a detailed site description). It is a region of major cultural importance and the valley holds one of the largest expanses of level, arable land situated within South-East Turkey. The African-Dead Sea Rift system carved out a major North-South route that links Malatya and the Sakçegözü to the north, through the Amuq, to the Beqa'a, Jordan Valley and Gulf of Aqaba further south. Countless migrating people and animals have moved and been constrained along this natural corridor and its landscapes have provided unique combinations of resource niches for human exploitation. The Amuq plain is framed by the metaliferous Amanus and Taurus mountain ranges to the west and north (Yener et al., 2000).

Figure 5.1: Geographic map of Turkey with the two sites indicated by grey stars.

Tell Atchana is an oval settlement mound measuring 750m in length by ~300m in width and the elevation of the site slopes from about 9m at the north-western end to the level of the plain in the southwest (figure 5.2). The succession of temples, palaces and town defences have confirmed the city's prominence (Stein, 1997). Archaeological investigation of Tell Atchana has taken place in two discrete phases; the first took place discontinuously between 1937 and 1949 and was carried out by the British archaeologist Sir Leonard Woolley. The second has been led by K.Aslihan Yener beginning with the Amuq Valley Regional Project in 1995. Renewed excavation at the site began in 2000 and is ongoing. The samples in this study come from both of these excavation phases at the site (see appendix 3 for photographs of all the samples from Tell Atchana).

Figure 5.2: Aerial photograph of Tell Atchana from Google Earth.

The modern excavation has re-evaluated the original Woolley chronology and found it to be broadly correct for Levels 1-7 which marks the limit of the current excavation (Yener, 2013). It is therefore assumed that the chronology proposed by Woolley for the earlier levels, although not yet reassessed, is also broadly correct. It is acknowledged, however, that there are number of errors in Woolley's work (many of which are in stark contrast with modern excavation methods: Akar, 2013). A number of authors over the years have re-evaluated the chronology of Tell Atchana based on Woolley's original work and the tablets found on site and have proposed their own chronologies (see table 5.1), however, only

Yener has re-excavated the site. Yener et al., (2013) proposed a revised chronology based on fine-grained relational stratigraphy, dendrochronlogy, radiocarbon sampling from Levels III-I, ceramic seriation and textual data (Yener, 2013). The most significant dating control is that the stratigraphy of the site unambiguously determines the older and younger structures as is typical of most multi-level tells (Kostadinova-Avramova et al., 2014).

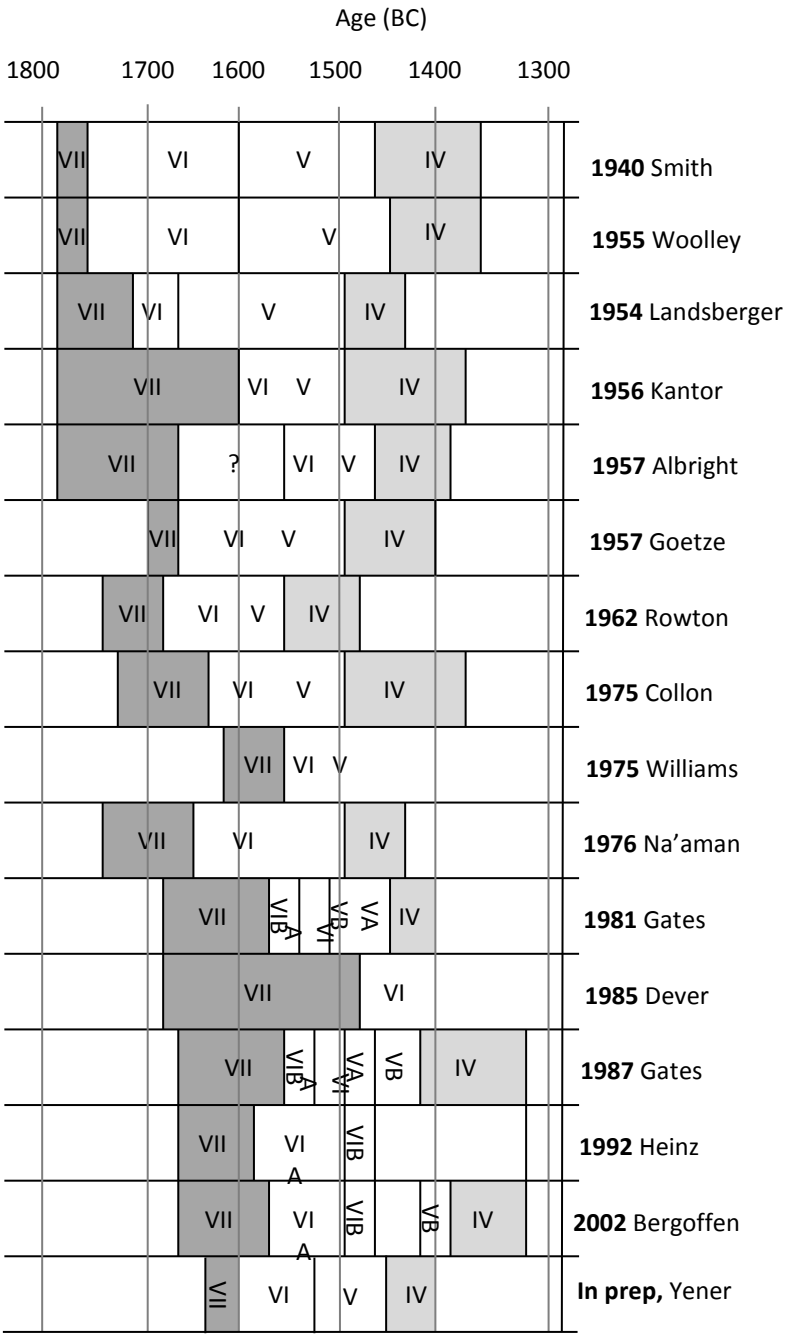

Table 5.1: Chart of previous and current chronologies for levels IV-VII of Tell Atchana, redrawn from Yener et al., (2013). Notice that the start date of Level IV only varies by 150 years whilst the end of Level IV varies over a 200 year interval.

The stratigraphy of the site has been subdivided into a sequence of 18 occupation levels numbered from Level 0 to Level 17/ 18. One hundred and twenty eight potsherds from 15 of these levels form the bulk of this study (for photographs of all these samples, see 5.14 Appendix 3). In addition to the potsherds analysed, 18 mud brick cores taken from a stratigraphic sequence of four brick pavements in use sequentially from Level 7 - Level 4 were also analysed (figure 5.3). The mudbricks formed the floors of buildings which were burnt down during a number of different fires. The archaeointensity recorded in the mudbricks, therefore, dates from the destruction of the building. It is unlikely they had been burnt before this as mudbricks are traditionally dried in the sun. The potsherd sample set begins at Level 2/3 which represents occupation of the site from between 1320 and 1305 to 1400BC and continues to Level 17/18 which began at ~2200 BC. The samples are stratigraphically controlled and dated using the Middle Chronology (Yener, pers com). The site has also been radiocarbon dated. Samples from Levels 2/3 to Level 9 span the time period from 1305 BC to 1675 BC (these dates have been supplied by the archaeologists and represent the earliest estimated age for the beginning of Level 2 (1305 BC) and the latest date for the end of Level 9 (1675 BC)). Samples from these levels were collected as part of the Yener excavation whilst samples from Levels 10 to Level 17/18 (covering the time period 1650 BC to 2200 BC, where 1650 BC represents the earliest proposed start date for Level 10 and 2200 BC the proposed end date for Level 17/18) were collected during the Woolley excavation. In the interests of clarity, the Woolley Levels are identified here using Arabic numerals: this in contrast to Woolley's original work where the levels were numbered using Roman numerals. For example Woolley's Level XVI is referred to here as Level 16.

Figure 5.3: Cross section of a stratigraphic sequence of mud bricks that formed pavements from Level 7 (towards the base of the pictures) to Level 4 (towards the top of the pictures) which were sampled for archaeomagnetic analysis. Locations of drilled cores, analysed in this study, can be easily seen. a) shows the entire building whilst b) is a close up of one corner of the building. The location of b is indicated in a) with a red star.

5.3.1.1. Dating of Tell Atchana

It is acknowledged that there is considerable debate in the archaeological community over which Middle Eastern dating chronology is the best, for more detail see Bietak and Czerny (2003). Suffice to say that the use of either the Lower or Upper Chronology instead of the Middle Chronology would lead to a ~ ±50 year change in the date of at least one level at Tell Atchana. This is partly because the dating of the transition from the Middle Bronze Age II to the Lower Bronze Age I has a discrepancy of up to 100 years between the three chronologies. In this chapter, we have used the Middle Chronology as this is favoured by the archaeologists excavating the site.

Confusion has arisen since the original excavation by Woolley associated with Level 17/18. In Woolley's original publications, there is no mention of an 18th Level, Level 17 is the deepest he excavated. However, in the depot containing all the samples Woolley excavated, there are a number of samples clearly labelled as Level 18. As samples from

both Level 17 and Level 18 show characteristics of Amuq J culture (Horowitz, pers comm.) samples labelled as Level 17 and Level 18 have been grouped together into Level 17/18. The Amuq J culture has been dated to c. 2200-2000 BC (Braidwood and Braidwood, 1960). For a full list of samples from Tell Atchana and details of experiments run on them see tables 5.2 and 5.3

5.3.2. Kilise Tepe (36.840° N, 33.926° E)

Kilise Tepe (formerly known as Maltepe) is located in the Mersin province of Southern Turkey on the left bank of the Göksu River (figure 5.1). Excavation of the site began in 1994 and revealed Iron Age, Hellenistic and Byzantine layers in addition to the Late Bronze Age record of surface sherds gathered by Mellaart and French in 1965 (Hansen and Postgate, 1999, Baker et al., 1995). Thin section analysis of the 8 sherds from 6 levels of this site studied here was carried out by Carl Knappett (Postgate and Thomas, 2011) and focused on establishing the provenance of the sherds. This sample set represents occupation of the site from 1200 BC to 600 BC (Hansen and Postgate, 1999). See table 5.4 for a full sample list.

The various levels of the site have been dated using dendrochronolgy (the Late Bronze Age levels), dateable finds e.g. stone stamp seals with the name and title of an official in hieroglyphs (Hansen and Postgate, 1999), pottery typology as well as stratigraphic controls.

Table 5.2 List of samples

Location	Type	Level	No. of Potsherds	Sample Name	VFTB sample code	MW Demag Code	MW Coe Code	MW IZZI Code	CR Code
Tell Atchana	Potsherd	2/3	9	TA L2.3-1	TA L2.3-1	2.3-1D	2.3-1I	-	-
				TA L2.3-2	TA L2.3-2	2.3-2D	2.3-2I	-	L23-2C
				TA L2.3-3	TA L2.3-3	2.3-3D	2.3-3I	-	-
				TA L2.3-4	TA L2.3-4	2.3-4D	2.3-4I	-	-
				TA L2.3-5	TA L2.3-5	2.3-5D	2.3-5I	-	-
				TA L2.3-6	TA L2.3-6	2.3-6D	2.3-6I	-	-
				TA L2.3-7	TA L2.3-7	2.3-7D	2.3-7I	-	L237CR
				TA L2.3-8	TA L2.3-8	2.3-8D	2.3-8I	-	-
				TA L2.3-9	TA L2.3-9	2.3-9D	2.3-9I	-	-
Tell Atchana	Potsherd	4	10	TA L4-1	TA L4-1	L4-1D	L4-1I	-	L4-1CR
				TA L4-2	TA L4-2	L4-2D	L4-2I	-	-
				TA L4-3	TA L4-3	L4-3D	L4-3I	-	-
				TA L4-4	TA L4-4	L4-4D	-	L4-4I	-
				TA L4-5	TA L4-5	L4-5D	L4-5A	L4-5I	-
				TA L4-6	TA L4-6	L4-6D	L4-6I	-	L4-6IC
				TA L4-7	TA L4-7	L4-7D	L4-7I	-	-
				TA L4-8	TA L4-8	L4-8D	L4-8I	-	-
				TA L4-9	TA L4-9	L4-9D	L4-9I	-	-
				TA L4-10	TA L4-10	L4-10D	L4-10I	-	-

Location	Type	Level	No. of Potsherds	Sample Name	VFTB sample code	MW Demag Code	MW Coe Code	MW IZZI Code	CR Code
Tell Atchana	Potsherd	5	10	TA L5-1	TA L5-1	L5-1D	L5-1I	-	-
				TA L5-2	TA L5-2	L5-2D	L5-2I	-	-
				TA L5-3	TA L5-3	L5-3D	L5-3I	-	-
				TA L5-4	TA L5-4	L5-4D	L5-4I	-	-
				TA L5-5	TA L5-5	L5-5D	L5-5I	-	-
				TA L5-6	TA L5-6	L5-6D	L5-6I	-	L5-6CR
				TA L5-7	TA L5-7	L5-7D	L5-7I	-	L5-7IC
				TA L5-8	TA L5-8	L5-8D	L5-8I	-	-
				TA L5-9	TA L5-9	L5-9D	L5-9I	-	-
				TA L5-10	TA L5-10	L5-10D	L5-10I	-	-

Tell Atchana	Potsherd	7/8	9	TA L7.8-1	TA L7.8-1	L78-1D	L78-1I	-	-
				TA L7.8-2	TA L7.8-2	L78-2D	-	-	-
				TA L7.8-3	TA L7.8-3	L78-3D	L78-3I	-	-
				TA L7.8-4	TA L7.8-4	L78-4D	-	-	-
				TA L7.8-5	TA L7.8-5	L78-5D	L78-5I	-	L78-5C
				TA L7.8-6	TA L7.8-6	L78-6D	L78-6I	-	-
				TA L7.8-7	TA L7.8-7	L78-7D	L78-6I	-	-
				TA L7.8-8	TA L7.8-8	L78-8D	L78-8I	-	-
				TA L7.8-9	TA L7.8-9	L78-9D	L78-9I	-	-

Location	Type	Level	No. of Potsherds	Sample Name	VFTB sample code	MW Demag Code	MW Coe Code	MW IZZI Code	CR Code
Tell Atchana	Potsherd	9	8	TA L9-1	TA L9-1	L9-1D	L9-1I	L9-1Ib	L9-1IC
				TA L9-2	TA L9-2	L9-2D	L9-2I	-	-
				TA L9-3	TA L9-3	L9-3D	L9-3I	-	-
				TA L9-4	TA L9-4	L9-4D	L9-4I	-	-
				TA L9-5	TA L9-5	L9-5D	L9-5I	-	L9-5CR
				TA L9-6	TA L9-6	L9-6D	L9-6I	-	-
				TA L9-7	TA L9-7	L9-7D	L9-7I	-	-
				TA L9-8	TA L9-8	L9-8D	L9-8I	-	L9-8CR

Tell Atchana	Potsherd	10	8	TA WD L10-1	TA WD L10-1	L10-1D	L10-1I	-	L10-1C
				TA WD L10-2	TA WD L10-2	L10-2D	L10-2I	-	-
				TA WD L10-3	TA WD L10-3	L10-3D	L10-3I	-	-
				TA WD L10-4	TA WD L10-4	L10-4D	L10-4I	-	L104CR
				TA WD L10-5	TA WD L10-5	L10-5D	10-5IA	L10-5I	-
				TA WD L10-6	TA WD L10-6	L10-6D	L10-6I	-	-
				TA WD L10-7	TA WD L10-7	L10-7D	L10-7I	-	-
				TA WD L10-8	TA WD L10-8	L10-8D	L10-8I	-	L108CR

Location	Type	Level	No. of Potsherds	Sample Name	VFTB sample code	MW Demag Code	MW Coe Code	MW IZZI Code	CR Code
Tell Atchana	Potsherd	12 a	9	TA WD L12a-1	TA WD L12a-1	L12a1D	L12a1I	-	-
				TA WD L12a-2	TA WD L12a-2	L12a2D	L12a2I	-	-
				TA WD L12a-3	TA WD L12a-3	L12a3D	-	-	-
				TA WD L12a-4	TA WD L12a-4	L12a4D	L12A4I	L12A4A	12A4CR
				TA WD L12a-5	TA WD L12a-5	L12a5D	L12a5I	-	-
				TA WD L12a-6	TA WD L12a-6	L12a6D	L12a6I	-	-
				TA WD L12a-7	TA WD L12a-7	L12a7D	L12a7I	-	-
				TA WD L12a-8	TA WD L12a-8	L12a8D	L12a8I	-	L12A8C
				TA WD L12a-9	TA WD L12a-9	L12a9D	L12a9I	-	-

Tell Atchana	Potsherd	12 b	10	TA WD L12b-1	TA WD L12b-1	L12b1D	L12b1I	-	12B1CR
				TA WD L12b-2	TA WD L12b-2	L12b2D	L12b2I	-	12B2CR
				TA WD L12b-3	TA WD L12b-3	L12b3D	L12b3I	-	-
				TA WD L12b-4	TA WD L12b-4	L12b4D	L12b4I	-	-
				TA WD L12b-5	TA WD L12b-5	L12b5D	L12b5I	-	-
				TA WD L12b-6	TA WD L12b-6	L12b6D	L12b6I	-	12B6CR
				TA WD L12b-7	TA WD L12b-7	L12b7D	L12b7I	-	-
				TA WD L12b-8	TA WD L12b-8	L12b8D	12b8IA	L12b8I	L12B8C
				TA WD L12b-9	TA WD L12b-9	L12b9D	L12b9I	-	-
				TA WD L12b-10	TA WD L12b-10	12b10D	12b10I	-	-

Location	Type	Level	No. of Potsherds	Sample Name	VFTB sample code	MW Demag Code	MW Coe Code	MW IZZI Code	CR Code
Tell Atchana	Potsherd	12 c	8	TA WD L12c-1	TA WD L12c-1	L12c1D	L12c1I	-	L12C1C
				TA WD L12c-2	TA WD L12c-2	L12c2D	-	-	-
				TA WD L12c-3	TA WD L12c-3	L12c3D	L12c3I	-	-
				TA WD L12c-4	TA WD L12c-4	L12c4D	L12c4I	-	-
				TA WD L12c-5	TA WD L12c-5	L12c5D	L12c5I	-	-
				TA WD L12c-6	TA WD L12c-6	L12c6D	-	-	-
				TA WD L12c-7	TA WD L12c-7	L12c7D	L12c7I	-	12C7CR
				TA WD L12c-8	TA WD L12c-8	L12c8D	L12c78I	-	-

Tell Atchana	Potsherd	13	9	TA WD L13-1	TA WD L13-1	L13-1D	L131II	L13-1I	L131CR
				TA WD L13-2	TA WD L13-2	L13-2D	-	-	-
				TA WD L13-3	TA WD L13-3	L13-3D	L13-3I	-	-
				TA WD L13-4	TA WD L13-4	L13-4D	L13-4I	-	-
				TA WD L13-5	TA WD L13-5	L13-5D	L13-5I	-	-
				TA WD L13-6	TA WD L13-6	L13-6D	L13-6I	-	-
				TA WD L13-7	TA WD L13-7	L13-7D	-	-	-
				TA WD L13-8	TA WD L13-8	L13-8D	L13-8I	L13-8A	-
				TA WD L13-9	TA WD L13-9	L13-9D	L13-9I	-	-

Location	Type	Level	No. of Potsherds	Sample Name	VFTB sample code	MW Demag Code	MW Coe Code	MW IZZI Code	CR Code
Tell Atchana	Potsherd	14	7	TA WD L14-1	TA WD L14-1	L14-1D	L141IA	L14-1I	-
				TA WD L14-2	TA WD L14-2	L14-2D	-	L14-2I	-
				TA WD L14-3	TA WD L14-3	L14-3D	L14-3I	-	-
				TA WD L14-4	TA WD L14-4	L14-4D	L14-4I	-	-
				TA WD L14-5	TA WD L14-5	L14-5D	L14-5I	-	-
				TA WD L14-6	TA WD L14-6	L14-6D	L14-6I	-	L146CR
				TA WD L14-7	TA WD L14-7	L14-7D	L14-7I	-	L14-7C

Tell Atchana	Potsherd	15	9	TA WD L15-1	TA WD L15-1	L15-1D	L15-1I	-	-
				TA WD L15-2	TA WD L15-2	L15-2D	L15-2I	-	-
				TA WD L15-3	TA WD L15-3	L15-3D	L15-3I	-	-
				TA WD L15-4	TA WD L15-4	L15-4D	-	-	-
				TA WD L15-5	TA WD L15-5	L15-5D	L15-5I	-	L15-5C
				TA WD L15-6	TA WD L15-6	L15-6D	L15-6I	-	-
				TA WD L15-7	TA WD L15-7	L15-7D	L15-7I	-	-
				TA WD L15-8	TA WD L15-8	L15-8D	L15-8I	-	-
				TA WD L15-9	TA WD L15-9	L15-9D	L15-9I	-	-

Location	Type	Level	No. of Potsherds	Sample Name	VFTB sample code	MW Demag Code	MW Coe Code	MW IZZI Code	CR Code
Tell Atchana	Potsherd	16	7	TA WD L16-1	TA WD L16-1	L16-1D	L16-1I	-	-
				TA WD L16-2	TA WD L16-2	L16-2D	-	L16-2I	-
				TA WD L16-3	TA WD L16-3	L16-3D	-	-	-
				TA WD L16-4	TA WD L16-4	L16-4D	L16-4I	-	L16-5C
				TA WD L16-5	TA WD L16-5	L16-5D	L16-5I	-	L166CR
				TA WD L16-6	TA WD L16-6	L16-6D	L16-6I	-	-
				TA WD L16-7	TA WD L16-7	L16-7D	-	-	-
Tell Atchana	Potsherd	17/18	15	TA WD L17.18-1	TA WD L17.18-1	L17-1D	L17-1I	-	L17-1C
				TA WD L17.18-2	TA WD L17.18-2	L17-2D	L17-2I	-	-
				TA WD L17.18-3	TA WD L17.18-3	L17-3D	L17-3I	-	-
				TA WD L17.18-4	TA WD L17.18-4	L17-4D	L17-4I	-	-
				TA WD L17.18-5	TA WD L17.18-5	L17-5D	L17-5I	-	-
				TA WD L17.18-6	TA WD L17.18-6	L17-6D	L17-6I	-	-
				TA WD L17.18-7	TA WD L17.18-7	L17-8D	L17-8I	-	-
				TA WD L17.18-11	TA WD L17.18-11	L18-1D	L18-1I	-	-
				TA WD L17.18-12	TA WD L17.18-12	L18-2D	L18-2I	-	-
				TA WD L17.18-13	TA WD L17.18-13	L18-3D	L18-3I	-	-
				TA WD L17.18-14	TA WD L17.18-14	L18-4D	L18-4I	-	L18-4C
				TA WD L17.18-15	TA WD L17.18-15	L18-5D	L18-5I	AT302I	L18-5C
				TA WD L17.18-16	TA WD L17.18-16	L18-6D	L18-6I	-	-
				TA WD L17.18-17	TA WD L17.18-17	L18-7D	-	AT303I	-
				TA WD L17.18-18	TA WD L17.18-18	L18-8D	L18-8I	-	-

Table 5.2: List of Tell Atchana potsherds analysed in this thesis indicating the sample codes used in each experiment. Where there is a dash in the cell it indicates that no experiments of this type were carried out on this sample. Location, the archaeological site where samples were found; type, material being studied; Level, archaeological level samples were found in; No. of potsherds, number of samples of this type from this site and level; sample name, name of parent sample; VFTB sample code, name of subsample which was subject to a suite of VFTB experiments; MW demag code, name of subsample subjected to a microwave demagnetisation experiment, MW coe code, name of subsample subjected to a microwave, coe method, archaeointensity experiment; MW IZZI code, name of subsample subjected to a microwave IZZI method archaeointensity experiment, CR code, name of subsample subjected to a cooling rate experiment.

Site	Location	Type	Context code	No. of bricks	Sample Name	VFTB sample code	AMS experiment code	Themal IZZI Code	CR Code
Tell Atchana	Level 4 Palace pavements	Burnt mudbricks	15	1	TA15.3	TA15.3V	TA15.3	TA15.3	15.3
			16	1	TA16.4Br	TA16.4BrV	TA16.4Br	TA16.4Br	16.4
			17	8	TA17.23	TA17.23V	TA17.23	TA17.23	-
					TA17.18	TA17.18V	TA17.18	TA17.18	-
					TA17.9	TA17.9V	TA17.9	TA17.9	17.9
					TA17.8	TA17.8V	TA17.8	TA17.8	-
					TA17.5	TA17.5V	TA17.5	TA17.5	-
					TA17.3	TA17.3V	TA17.3	TA17.3	17.3
					TA17.21	TA17.21V	TA17.21	TA17.21	-
					TA17.2	TA17.2V	TA17.2	TA17.2	-
			18	9	TA18.8A	TA18.8AV	TA18.8A	TA18.8A	-
					TA18.13	TA18.13V	TA18.13	TA18.13	-
					TA18.17	TA18.17V	TA18.17	TA18.17	-
					TA18.28	TA18.28V	TA18.28	TA18.28	18.28
					TA18.28A	TA18.28AV	TA18.28A	TA18.28A	-
					TA18.16	TA18.16V	TA18.16	TA18.16	-
					TA18.31	TA18.31V	TA18.31	TA18.31	-
					TA18.4B	TA18.4BV	TA18.4B	TA18.4B	-
					TA18.22	TA18.22V	TA18.22	TA18.22	18.22

Table 5.3: List of Tell Atchana burnt mud bricks analysed in this thesis indicating the sample codes used in each experiment. Where there is a dash in the cell it indicates that no experiments of this type were carried out on this sample. Site, the archaeological site where samples were found; location, the location within the archaeological site where the samples were found; type, material being studied; context code, archaeological context where samples were found; No. of bricks, number of samples of this type from this site. Location and context; sample name, name of parent sample; VFTB sample code, name of subsample which was subject to a suite of VFTB experiments; AMS experiment code, name of subsample subjected to AMS analysis, Thermal IZZI code, name of subsample subjected to a thermal IZZI method archaeointensity experiment, CR code, name of subsample subjected to a cooling rate experiment.

Location	Type	Level	Unit	Sample Name	VFTB sample code	MW Demag Code	MW Coe Code	MW IZZI Code	CR Code
Kilise Tepe	Potsherd	IIa	5502	120	KT120	S120D	KT120I	KT120b	-
		IIa	5502	121	KT121	KT121D	-	-	-
		IId	1541	116	KTS116	KTS116	KT116I	KT116b	-
		IId	5864	141	KTS141	KT141D	-	S141I	-
		I/II	1124	142	KTS142	KT142D	KT142I	S142Ib	-
		IIe	1924	148	KTS148	KTS148	KT148I	S148Ib	-
		IIf	1783	150	KT150	KTS150	KT150I, KT150R	KT150b	KT150CR
		IIf	1783	155	KT155	KTS155	KT155I, KT155R	KT155b	KT155CR

Table 5.4: List of Tell Kilise potsherds analysed in this thesis indicating the sample codes used in each experiment. Where there is a dash in the cell it indicates that no experiments of this type were carried out on this sample. Location, the archaeological site where samples were found; type, material being studied; Level, archaeological level samples were found in; Unit; archaeological unit within the level where sample was found;; sample name, name of parent sample; VFTB sample code, name of subsample which was subject to a suite of VFTB experiments; MW demag code, name of subsample subjected to a microwave demagnetisation experiment, MW coe code, name of subsample subjected to a microwave, coe method, archaeointensity experiment, where there are two codes this indicates that MW Coe experiments were run on two subsamples from this parent sample; MW IZZI code, name of subsample subjected to a microwave IZZI method archaeointensity experiment, CR code, name of subsample subjected to a cooling rate experiment.

5.4. Rock Magnetic Properties

For 154 samples from both sites isothermal remanent magnetisation (IRM) acquisition curves, back field coercivity, hysteresis loops and Curie curves up to 700°C were measured using a Magnetic Measurements Variable Field Translation Balance (MMVFTB) at the University of Liverpool. A ~100-200mg sample from each sherd/ mud brick was measured.

5.4.1. Tell Atchana Potsherds

All the potsherds from Tell Atchana are magnetically strong which is most likely due to the high magnetite content of the clay source material. The local Orontes river sand is up to 40% magnetite (Hadi Özbal, pers comm.) which is consistent with the local origin of the sherds. The source of this magnetite is likely to be the eroded basalt flow in the middle Orontes valley as well as the foothills southwest of the site between Antakya and Orontes where there are Ophiolite outcrops (Horowitz, in prep). The Plain Ware potsherds are not thought to have been heated to above 650°C due to the presence of intact bioclasts of both micro and nano-fossils (Horowitz, in prep.). Both of these two findings are consistent with the results of the thermomagnetic curves which confirm the dominance of magnetite/ titanomagnetite.

With the exception of one sample from Tell Atchana, saturation at fields of less than 300mT was observed in all of the IRM experiments. Three types of thermomagnetic curve were identified, all of which are highly reversible indicating they were stable to heating to a temperature of 700°C (see figures 5.4 and 5.5). All samples show a gradient change at around 580°C indicating the presence of magnetite. All samples plot within the pseudo-single domain region of the Day plot (see figure 5.6).

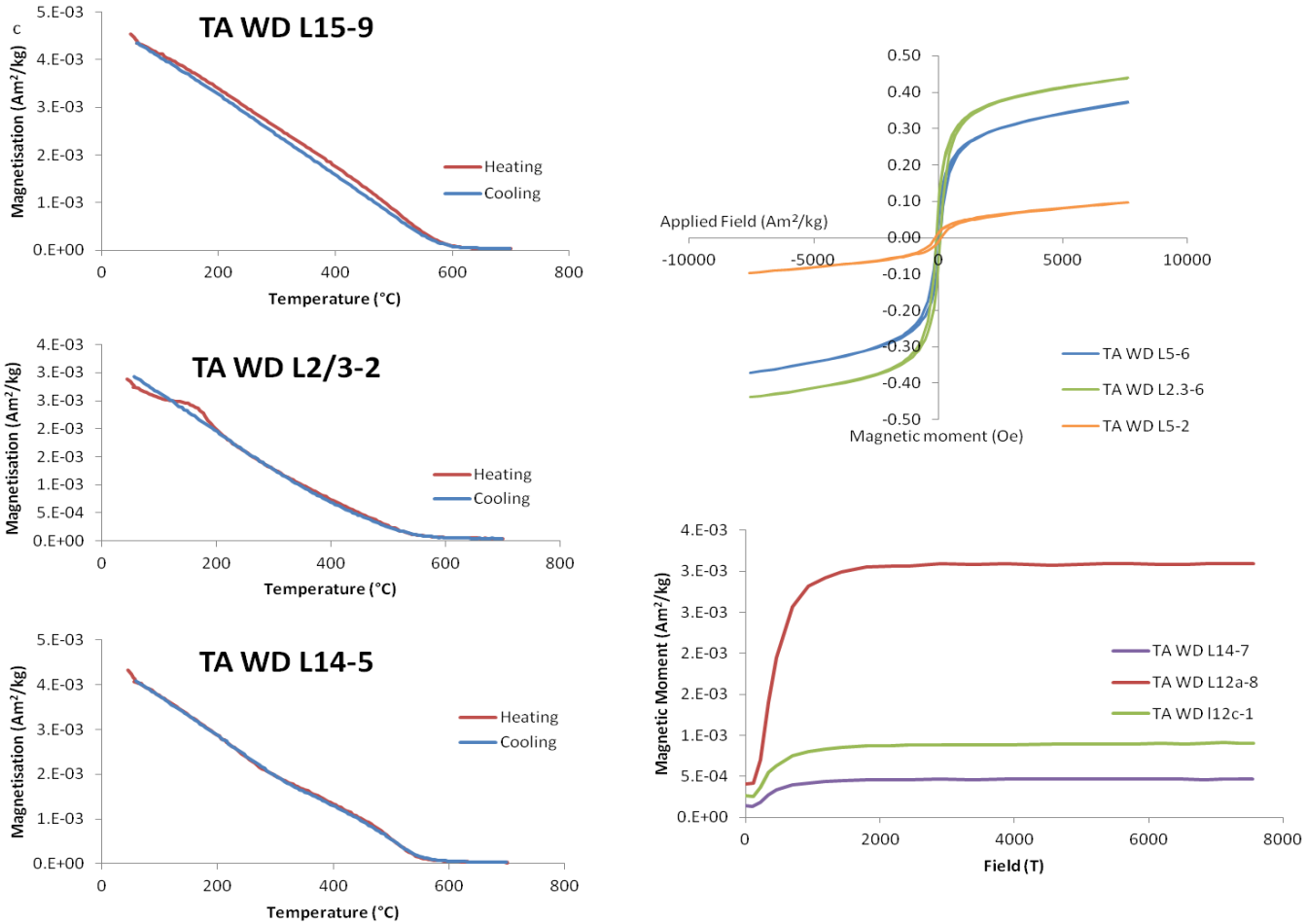

Figure 5.4: Representative thermomagnetic curves, hysteresis loops and IRM curves for Tell Atchana potsherds.

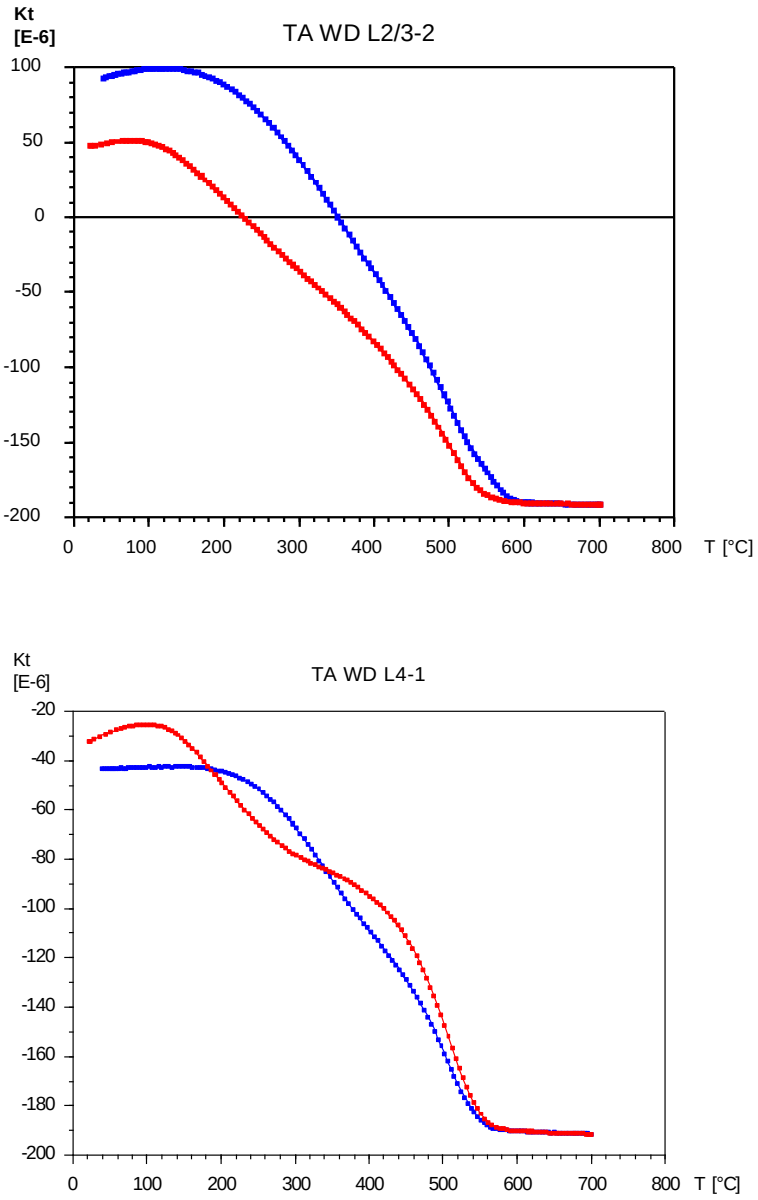

Figure 5.5: Temperature vs susceptibility experiments carried out in argon for samples TAWD L2/3-2 and TAWD L4-1 which showed a low temperature component in the initial thermomagnetic curve measured in the VFTB.

In addition to the signal from titanomagnetite, in samples L2/3-2 and L4-1 there is a low temperature signal which is destroyed on heating. To determine if this low temperature signal was a result of an oxidation reaction, thermomagnetic curves were measured in argon using the Kappabridge at the University of Liverpool. These experiments were run on two of the samples that showed this feature (figure 5.5). The result for sample L4-1 is consistent with the original experiment and implies the presence of a mineral with a Curie

Temperature around 250°C. In contrast to this, the thermomagnetic experiment carried out in Argon for L2/3-2 shows irreversible behaviour which is inconsistent with that observed in the original thermomagnetic experiment. Despite some similarities, this result is inconsistent with the high coercivity, thermally stable, low unblocking temperature mineral (HCSLT) reported in McIntosh et al. (2011, 2007) and often seen in archaeological samples, as all the hysteresis loops close implying the presence of low coercivity minerals.

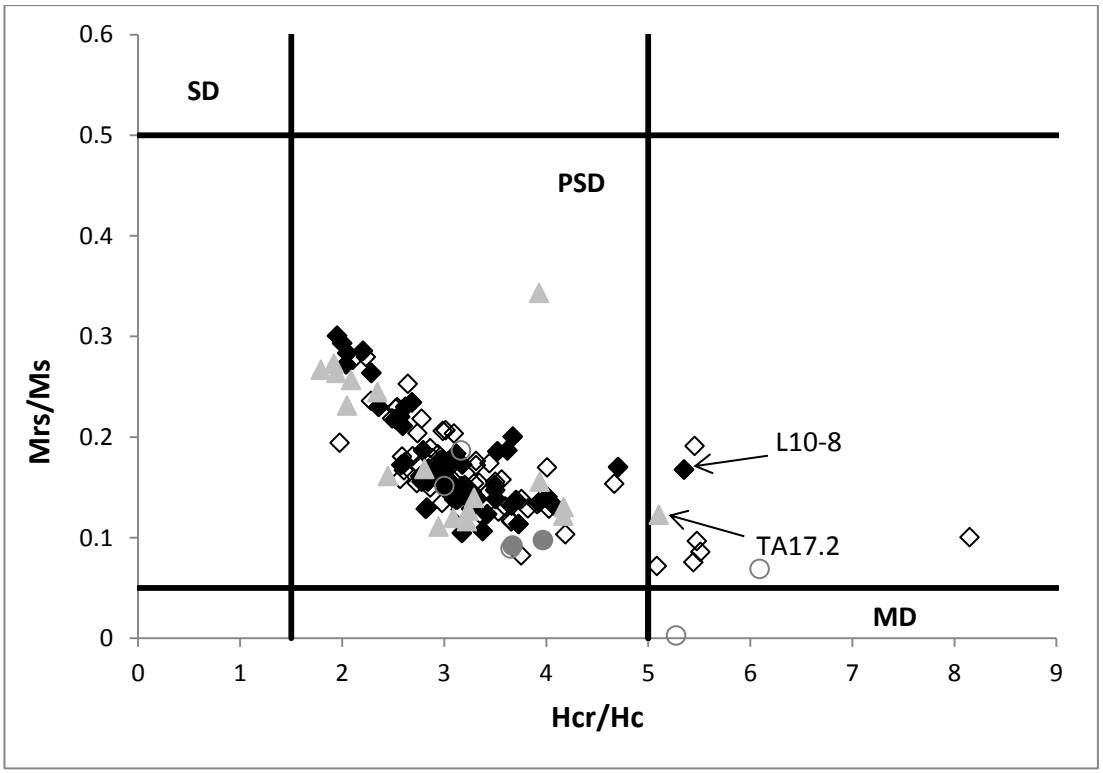

Figure 5.6: Day plot of all samples Day et al. (1977): Tell Atchana pot sherds (diamonds); Tell Atchana mud brick pavements (triangles) and Kilise Tepe potsherds (circles). The solid symbols represent those samples for which the archaeointensity results were accepted. The open symbols represent rejected samples. The region of the plot which encloses single domain (SD), pseudo-single domain (PSD) and multidomain (MD) grains is indicated. As can be seen all the accepted samples plot within the PSD region of the Day plot except for potsherd L10-8 and mudbrick TA17.2 which both plot on the edge of this region.

5.4.2. Tell Atchana Mud Brick Cores

IRM saturation occurred in fields of less than 200mT for all of the mud brick samples. All thermomagnetic curves are highly reversible above 400°C but below this temperature the cooling part of the curve is always above the heating curve suggesting the creation of a more magnetic mineral. Where a change in the curvature of the thermomagnetic curve is unambiguous it is between 475°C and 540°C implying the presence of titanomagnetite with

varying titanium contents. For five samples, it was very difficult to isolate the exact point where the curvature of the thermomagnetic curve changed over the temperature interval 350-600°C as it was very gradual, therefore preventing a more precise identification of the Curie Temperature of the component minerals.

5.4.3. Kilise Tepe Potsherds

Four of the eight Kilise Tepe samples show two clear Curie temperatures, the first at ~300°C, the second at ~580°C implying the presence of Ti- rich titanomagnetite and magnetite. Three of the other samples have curved thermomagnetic curves where it is impossible to isolate a Curie temperature. The remaining one sample has a Curie temperature of ~550°C due to the presence of Ti-poor titanomagnetite. The IRM curve for all the samples saturate in fields of less than 150mT.

5.5. Archaeointensity Investigation

5.5.1. Microwave Archaeointensity Experiments

A 14GHz microwave system (MWS) combined with a low temperature Tristan SQUID magnetometer was used to conduct intensity experiments (Shaw and Share, 2007). For the microwave experiments, subsamples were drilled perpendicular to the surface of the sherd. Each subsample had a diameter of 5 mm and was between 1 and 5 mm in length. The specimens were mounted on a quartz glass tube, using negative vacuum pump pressure, before being inserted into the MWS. The microwave frequency was then individually tuned to optimise the absorption of each individual sample. As heating of the bulk sample is minimised during microwave experiments, an acquired Thermal Remanent Magnetisation (TRM) in the MWS is denoted as T_MRM.

Prior to intensity measurements, demagnetization experiments were conducted on 128 Tell Atchana potsherds and 8 Kilise Tepe samples. Of these, 6 Kilise Tepe and 114 Tell Atchana pot sherds were selected for archaeointensity experiments. The majority of the remainder were rejected because they lacked a stable component of remanence which demagnetised towards the origin. This may have been caused by insufficient heating or by pot movement during firing. Additionally 3 samples were rejected due to technical difficulties during sample preparation.

For each selected potsherd, a subsample was subjected to a full microwave demagnetisation/ remagnetisation experiment with a field applied parallel to the Natural

Remanent Magnetisation (NRM). We followed either the Coe protocol (Coe, 1967) or an IZZI procotol (Tauxe and Staudigel, 2004). Repeat pT_MRM checks were carried out to monitor possible alteration (Coe, 1967). Repeat zero field checks were made as an additional alteration check and also to detect Multi-Domain (MD) grains when following the Coe protocol (Riisager and Riisager, 2001). It is recognised that applying the field parallel to the NRM direction will mask MD behaviour (Yu and Dunlop, 2003).

5.5.2. Thermal Archaeointensity Experiments

Thermal experiments were conducted on 19 core samples (diameter: 2.5cm, length 1.2-1.8cm) taken from mud bricks which had formed brick pavements at Tell Atchana (figure 5.3). The experiments were carried out using the Magnetic Measurements Thermal Demagnetising Oven with an air conditioning cooling system and measured on an AGICO JR6 magnetometer at Liverpool University Geomagnetism Laboratory. The experiments followed the IZZI protocol with the field applied either sub parallel or anti-parallel with additional alteration checks (Tauxe and Staudigel, 2004, Yu et al., 2004). Up to 14 double heating steps were applied between 100°C and 525°C with pTRM checks after every second step. By 525°C all the samples had less than 10 % of their starting NRM remaining.

5.6. Anisotropy Corrections

Pottery has been shown to be strongly anisotropic (Chauvin et al., 2000) due to the preferential alignment of magnetic grains presumed to be related to the moulding of the clay. This can lead to an error in the intensity estimation of up to 40% (Rogers et al., 1979). In order to mitigate the effects of anisotropy in the sherds, the field was applied parallel to the NRM direction. To confirm that anisotropy was not biasing the results, the angle between the pTRM acquired at the last step used for the best-fit segment and the applied field direction (denoted as γ (Paterson et al., 2014)) was checked for a subset (23/128) of the samples and found to always be <5°. For the cores taken from the bricks, the anisotropy of magnetic susceptibility (AMS) was individually measured for all samples prior to the archaeointensity analysis. These experiments were carried out on the Kappabridge at the University of Liverpool Geomagnetism Laboratory (table 5.5). All of the samples have $0 < T < 1$ (where T is the shape factor) and therefore their anisotropy of magnetic susceptibility is an oblate ellipsoid. Five of the nineteen samples have T values greater than 0.5. All the samples have AMS values of less than 2%.

Table 5.5: Anisotropy of Magnetic Susceptibility for the brick cores

Sample	L	F	P	T
TA 15-3	1.002	1.008	1.010	0.598
TA16-4	1.009	1.016	1.025	0.275
TA18-13	1.002	1.014	1.015	0.802
TA18-16	1.005	1.005	1.010	0.063
TA18.22	1.004	1.007	1.011	0.267
TA18.28	1.008	1.015	1.023	0.281
TA18-28A	1.004	1.018	1.022	0.605
TA18-31	1.009	1.010	1.019	0.061
TA18-4B	1.006	1.019	1.025	0.548
TA18-7	1.001	1.009	1.011	0.787
TA18-8A	1.003	1.008	1.011	0.381
TA17.18	1.006	1.008	1.014	0.104
TA17.2	1.006	1.007	1.013	0.091
TA17.21	1.002	1.011	1.013	0.699
TA17.23	1.000	1.012	1.013	0.923
TA17.3	1.005	1.013	1.018	0.415
TA17.5	1.008	1.015	1.024	0.293
TA17.8	1.009	1.013	1.022	0.207
TA17.9	1.007	1.009	1.016	0.166

L, magnetic lineation; F, magnetic lineation; P, anisotropy degree; T, shape factor

5.7. Cooling Rate Correction

Numerous studies have demonstrated the potential significance of cooling rate both theoretically and experimentally. These studies found that for an assemblage of single domain (SD) grains TRM increases with slower cooling (e.g. Fox and Aitken, 1980; Halgedahl et al., 1980). The importance of applying a cooling rate correction for samples containing pseudo single domain (PSD) and multi-domain (MD) states is less clear, some recent studies suggest that in coarse grains the cooling rate effect is indistinguishable from zero (Biggin et al., 2013, Ferk et al., 2014) whilst others believe TRM decreases with slower cooling (Papusoi, 1972, Yu, 2011, McClellandbrown, 1984, Muxworthy and Heslop, 2011, Winklhofer et al., 1997). It is less vital in studies of archaeological materials to apply a cooling rate correction than it is in studies of certain geological materials. The cooling rate for clays is closer to the laboratory cooling rate than it is for large igneous bodies when cooling may take thousands of years (Halgedahl et al., 1980). Polleti et al., (2013) demonstrated that similar experimental behaviour is observed between microwave and thermal procedures despite the different ways in which energy is transferred into the spin

system. It is, therefore, necessary to apply cooling rate corrections to microwave determined archaeointensity results.

5.7.1. Cooling Rate Experiments on the Potsherds

The method followed involved 3 steps. The first step was a Coe method archaeointensity (AI) experiment, as previously described. The sample was demagnetised until 10% of the starting NRM remained. The second step was in a custom-made oven housed at the University of Liverpool Geomagnetism Laboratory where the samples were heated to 600°C and held at this temperature for 30 minutes. The samples were then allowed to cool in the oven which has thick thermal insulation and no fan. The samples were left in the oven, in a field, for 48 hours and then a repeat AI experiment was performed using the microwave system. The cooling rate correction factor was then calculated using the following equation from Poletti et al., (2013):

$$fMW = \frac{56}{AI\_CR} \tag{5.1}$$

where 56 is the laboratory field and AI_CR represents the MW archaeointensity estimation. The corrected archaeointensity (AIC) is given by:

$$AIC = AI.fMW \tag{5.2}$$

AIC is the product of the cooling-rate correction and the MW archaeointensity measured in the original AI experiment (fMW).

Studies by Gomez-Paccard et al (2006) and Genevey and Gallet (2003) found that the choice of cooling time was not critical as the mean correction factors at 5, 10 and 30 hours were roughly similar (Genevey et al., 2003).

Cooling rate experiments were only carried out on samples that showed neither visible sign of physical alteration (e.g. colour changes or melt spots) nor evidence of alteration on the Arai diagram or orthogonal vector plots. A cooling rate correction was applied to each calculated archaeointensity value and was determined following a cooling rate experiment on one or two sherds from every level (see tables 5.2-5.5 for more detail on which samples cooling rate experiments were conducted on). In all cases a blanket cooling rate correction

was applied across a level as it was not possible to determine individual cooling rate corrections because a number of samples showed evidence of alteration towards the end of the archaeointensity experiment.

5.7.2. Cooling Rate Experiment for the Mud Brick Cores

Due to the lengthy nature of the cooling rate experiment followed for the potsherds, it was not possible to follow the same method on the mud brick cores which had originally been subjected to a thermal archaeointensity experiment. Accordingly, a modified version of that followed by Gómez-Paccard et al (2006) was adopted on six samples, 1 from mud brick pavement (mbp) TA15, 1 from mbp TA16, 2 from mbp TA17 and 2 from mbp TA18. The method followed involved two additional steps after the original archaeointensity experiment was completed. Both steps were to 525°C (the maximum temperature reached in the initial experiment). The first step involved holding the sample at temperature for 30 minutes and then allowing it to cool slowly over a period of 24 hours in the cooling rate oven at the University of Liverpool. This first step is termed A_{slow} and is defined as $(pTRM_{slow}\text{-}pTRM_{A525})/ pTRM_{A525}$. Where pTRM is the measured pTRM following this initial step and $pTRM_{A525}$ is the last infield step of the experiment. The second step again involving heating the sample to 525°C but was followed by fast cooling (at the same cooling rate as in all the previous steps). This second step was an alteration check on the TRM acquisition capacity of the samples and is denoted as A_{fast}. The alteration was defined by $(pTRM_{fast}\text{-}pTRM_{A525})/pTRM_{A525}$. This alteration factor estimates the amount of magneto-chemical changes which occur during the first (slow cooling) and/or the second (rapid cooling) steps. Such changes could introduce an error in the correction factor which is estimated by comparing TRMs acquired during the A_{fast} and the A_{525} step. The mudbrick archaeointensity results were only corrected for cooling rate effect when the correction factors were bigger than the alteration factors (figure 5.7).

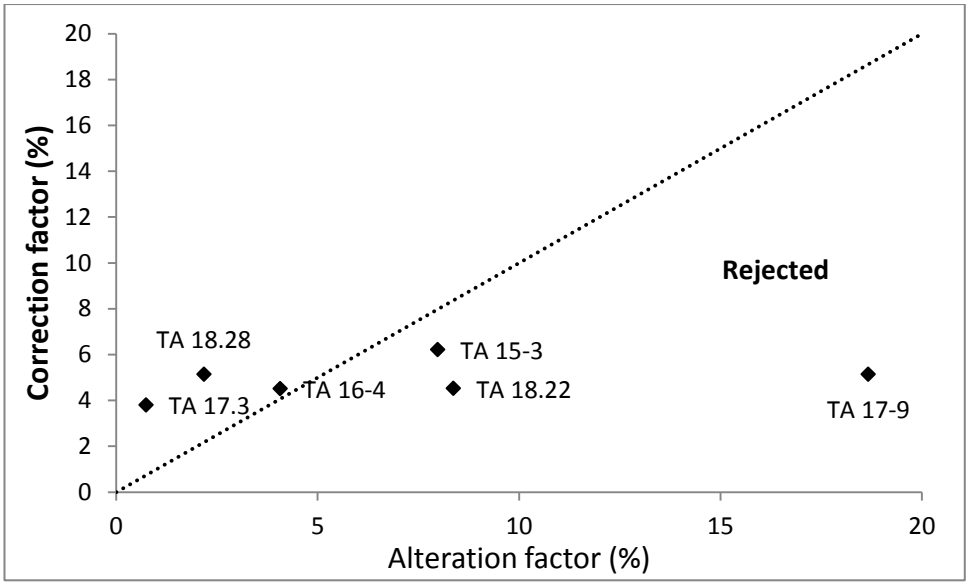

Figure 5.7: Absolute values of the effect of cooling rate upon TRM acquisition (correction factor) plotted against the variations of the TRM acquisition capacity (alteration factor) for mud brick samples, for cooling times of 24 hours.

5.8. Selection Criteria for Archaeointensity Determinations

For both microwave and thermal experiments, we used similar selection criteria to those described by Ertepinar et al., (2012) which are a modification of Coe et al., (1978) and Selkin and Tauxe (2000):

1. The number of points (N) defining the slope is greater than or equal to 5
2. The ratio of standard error of the slope to absolute value of the slope (β) is smaller than 0.1
3. The lower acceptance limit for the NRM fraction (f) is greater than or equal to 0.4 using the formula described by Coe et al., (1978).
4. The acceptance criterion of quality factor (q) was reduced to 1.
5. The upper acceptance limits for maximum angular deviation (MAD) and α are taken as 10% (Kirschvink, 1980)
6. pTRM checks were deemed to have been successful if the ratio of the difference between the check and the relevant TRM value to the length of the selected NRM-TRM segment (DRAT) was smaller than 7% (Selkin and Tauxe, 2000) and the cumulative DRAT (CDRAT), defined as the sum of all the DRATs, should be less than 20% (Kissel and Laj, 2004).
7. Three successful, consecutive, pTRM checks (Kissel and Laj, 2004).

Following the criteria applied by Gallet et al., (2006), where the mean archaeointensity value was calculated at the sherd level from two (or more) subsamples, the individual intensities calculated from these sherds must have a standard deviation <5(μT) or <10% of the mean. We used the average of the intensity value for the sherds. Where two measurements were made per sherd and one failed to meet the criteria outlined above then the other result was accepted.

5.9. Archaeointensity Results

From the sample set of 128 Tell Atchana potsherds, 18 Tell Atchana mud bricks and 8 Kilise Tepe potsherds, 16 samples were deemed unsuitable for a archaeointensity experiment following the result of a demagnetisation experiment (see 5.14 appendix 1). In total archaeointensity experiments were carried out on 120 individual sherds and 19 archaeointensity experiments were run on sister subsamples of these sherds. The results from Tell Atchana range from 53.3±7.9μT to 37.4±2.7μT. Over the duration of the occupation of the site the field fluctuated rapidly between this maximum and minimum. The highest field value was recorded for the lowest level, Level 17/18 which represents the earliest occupation level of the site, ~2200-2000 BCE. The lowest average intensity value recorded was from the mud brick pavement fragments: 37.4±2.7μT, approximately 1424 ± 24 BC. The lowest average intensity results from the potsherds were 38.6 ± 2.1 μT and 38.5 ± 1.9 μT for Levels 9 (1644 ±19 BC) and Level 15 (1925 ±25 BC).

Fifty-six individual potsherds from Tell Atchana passed all the criteria detailed above resulting in a success rate of 43%, whilst 17 of the 18 brick cores were successful, giving a success rate of 94% and 2 samples from Kilise Tepe were accepted giving a success rate of 25% (table 5.6). Most rejected microwave intensity results had a CDRAT greater than 20% with 44 samples failing this criterion. Additionally 18 samples had f values less than 0.4 and α values greater than 10°. Fifteen samples had β >0.1. With the exception of five of the 56 accepted Tell Atchana potsherds samples, all the samples contained a viscous remanent magnetisation (VRM) which was removed by a low microwave power (figure 5.8).

Nine of the Kilise Tepe experiments failed because they had a CDRAT of greater than 20%. Of these, six experiments recorded f values of less than 0.5 and 4 experiments had q values less than 3.

The mud brick samples had a success rate of 94% with 17 out of 18 samples passing all the acceptance criteria. The one sample which did not meet the criteria had a check greater

than 7% indicating alteration had occurred during the experiment. All samples showed evidence of a VRM which was removed by 200°C in 15 of the 18 samples. For the remaining samples it was removed by 300°C. The mudbrick samples gave very consistent behaviour with very little zigzagging present indicating MD grains did not affect the result.

The main criteria which samples failed to meet were related to the CDRAT and DRAT values. Rejected results from samples from Levels 2/3 to Level 10 from Tell Atchana, with CDRATs >20% typically showed a consistent trend of negative DRATs which individually passed (were less than 7%) but cumulatively failed. As the checks are consistently negative, the calculated intensity is probably an overestimation of the archaeointensity. However, it is not known why this consistent alteration occurred. For samples from lower levels (Level 10-Level 17/18) we still see this consistent pattern of negative DRATS cumulating in a large CDRAT, however, we also see many more individual DRATS failing (>7%). This perhaps implies a difference in composition or heating history and that these samples are more prone to alteration during an archaeointensity experiment. The success rate per level was >50 % for the majority of levels with the notable exception of Level 7/8, Level 12c, Level 13 and Level 16 where the success rate was as low as 22% (maximum 37%). For these levels only 2 or 3 successful individual results were recorded.

Table 5.6: A*verage archaeointensity results for each level from both sites*

Site	Level	Age bracket (BC)	Plotted Age (BC)	Material	N_{int}/N_0	F±s.d. (μT)	Fcr±s.d. (μT)
Tell Atchana	2/3	1400 - 1320/1305	1357 ± 44	sherds	6/9	60.6±11.2	50.3±9.3
	4	1450/1425 - 1400	1419 ± 19	sherds	5/10	64.7±7.5	45.0±3.1
	TA17	1600/1575 - 1400	1424 ± 24	bricks	7/8	38.9±2.8	37.4±2.7
	TA18	1600/1575 - 1400	1472 ± 24	bricks	9/9	44.3±2.6	42.0±2.5
	TA16	1600/1575 - 1400	1520 ± 24	bricks	1/1	41.5	39.6
	TA15	1600/1575 - 1400	1568 ± 24	bricks	1/1	45.7	-
	5	1525/1500 – 1450/1425	1476 ± 37.5	sherds	4/10	66.7±6.1	52.0±4.7
	7/8	1675/1650 – 1600/1575	1607 ± 18.75	sherds	2/9	54.4±9.1	46.8±7.9
	9	1675/1650 – 1600/1575	1644 ± 18.75	sherds	4/8	46.4±2.2	38.5±1.9
	10	1800 - 1675/1650	1680 ± 17	sherds	3/8	56.0±11.0	50.4±9.9
	12a	1800 - 1675/1650	1714 ± 17	sherds	3/9	52.1±5.2	45.9±5.9
	12b	1800 - 1675/1650	1748 ± 17	sherds	7/10	52.9±4.0	45.0±2.8
	12c	1800 - 1675/1650	1782 ± 17	sherds	2/8	54.1±3.5	48.2±3.0
	13	2000-1800	1825 ± 225	sherds	1/9	53.3±1.8	43.7±1.5
	14	2000-1800	1875 ± 25	sherds	3/7	56.2±4.3	46.7±3.5
	15	2000-1800	1925 ± 25	sherds	3/7	45.5±2.5	38.6±2.1
	16	2000-1800	1975 ± 25	sherds	2/7	56.1±6.3	46.0±5.2
	17/18	2200-2000	2100 ± 100	sherds	6/15	49.4±7.3	53.3±7.9
Kilise Tepe	IIa	LBA/ Iron Age	-	sherds	0/2	-	-
	IId	1150 (destruction age)	-	sherds	0/2	-	-
	I/II	Helenistic/ LBA	-	sherds	0/1	-	-
	IIe	LBA/ Iron Age	-	sherds	0/1	-	-
	IIf	800-600	700 ±100	sherds	2/2	102.1±6.3	84.7±6.2

Site, site where samples were taken; level, context samples were found in; age bracket, archaeologically assigned age bracket for the level; plotted age, when the data is plotted on graphs, the intensity value is plotted in the middle of the archaeological age estimate with the ± indicating number of years between this value and the beginning and end of the age estimate. Where there is a range of values given for the beginning or end of an age estimate, the middle of these two values is taken as the end/ beginning of the time period; material, type of remains studied; N_{int}/N_0*, where* N_{int} *is the number of accepted intensity results for the level and* N_0 *is the total number of samples studied from that level; F±s.d. average uncorrected intensity result per level with one standard deviation plus and minus the mean; Fcr ±s.d. cooling rate corrected intensity result per level with one standard deviation plus and minus the mean.*

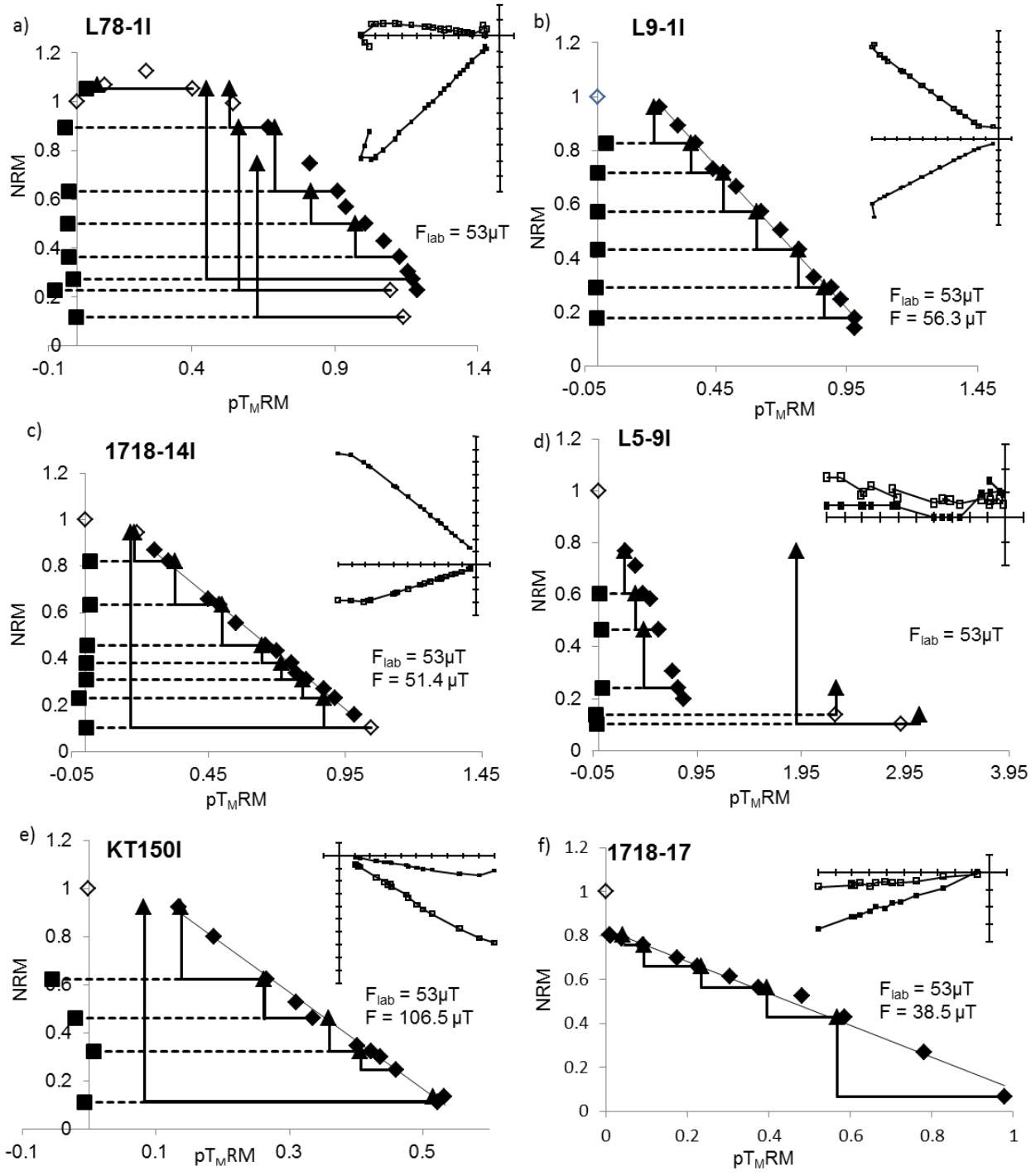

Figure 5.8: Accepted and rejected Arai plots for Tell Atchana potsherds (a-d), Kilise Tepe potsherd (e) and a mud brick core rom Tell Atchana (f) where NRM is the Natural Remanent Magnetisation and pT_MRM is the partial microwave Thermal Remanent Magnetisation. F_{lab} is the field applied during the intensity experiment. F is the calculated archaeointensity. The result for potsherd L5-9 (d) was rejected because it failed the CDRAT criteria. Open symbols represent rejected points whilst full symbols represent points used to calculate the intensity. Inserts are Orthogonal vector plots for the samples where open symbols represent the horizontal component and closed symbols represent the vertical component.

For Level 16, only four out of a sample set of seven were suitable for archaeointensity experiments and of these only two gave successful archaeointensity results. The remaining two results for this level were rejected because they had an α value of greater than 10. Interestingly the four samples deemed unsuitable for archaeointensity analysis all failed to establish a constant direction of demagnetisation and therefore were rejected. For Level 7/8 two samples were also rejected prior to running an archaeointensity experiment because they did not establish a constant demagnetisation direction. An intensity experiment on another sample was rejected because it demagnetised very quickly and differently to its sister sample. Of the remaining six samples, four of them were rejected either because they failed the DRAT criterion or they failed the CDRAT criterion. It is interesting to note that in contrast to these, eight results from Level 12b were accepted (out of ten samples) and therefore it would appear from this limited data set that at certain time periods the pottery used at Tell Atchana site was more suitable for archaeointensity analysis than at other times. This could be for a number of reasons; compositional, manufacturing or firing differences, amongst others. It would be interesting to explore further what made the samples from some levels more successful than the samples from others. This could be accomplished through a number of means. In order to establish more closely the differences between the pottery types, microscopy or SEM studies could help establish the magnetic carriers, as could additional rock magnetism investigations e.g. low temperature thermomagnetic curves. A more detailed study of the amount of variability observed within a sherd could also have benefits beyond this study. These archaeomagnetic investigations could usefully be accompanied by archaeological ones on the provenance and heating history of sherds as these factors would also influence the suitability of sherds for archaeomagnetic analysis.

Archaeointensity acceptance criteria is an ongoing and interesting debate most recently addressed by Paterson et al.(2014) and we have also attempted to investigate it here. There is a plethora of different criteria used and each of these can be applied with different cut off limits. For this data set, the most significant was the CDRAT criterion and a number of samples failed on this alone. A cut off limit of 20% is more lenient than has been applied in other studies e.g. PICRIT 03 (Kissel and Laj, 2004) and is more lenient than the recommended modifications made by Paterson et al. (2014). However, for most contexts studied here, it was found that modifying this criterion led to a maximum change in the calculated intensity of 3μT. Applying the PICRIT03 criteria (Kissel and Laj, 2004) (as

modified by Paterson et al. (2014)) led to a success rate of 33% whereas applying more lenient CDRAT criterion gave a success rate of 49%.

5.10. Applying Different Criteria

There is a lack of coherence in the palaeo- and archaeomagnetic community about intensity criteria with most authors applying their own criteria. In an attempt to address this, Paterson et al. (2014) presented a compilation of standard definitions for archaeointensity statistics to help remove ambiguities. One of these is a modification of the PICRIT03 criteria proposed by Kissel and Laj (2004). Using this modified PICRIT03, the thresholds of which are reported in table 5.7, 75% of the calculated archaeointensity values from Tell Atchana potsherds, were rejected and for four levels only 1 result was accepted. It was found that applying less stringent criteria (termed "applied criteria") increased the acceptance rate from 25% to 43% (32 accepted results under the modified PICRIT03, 56 under the less stringent "applied criteria") without changing the mean values by more than 3 μT (Table 5.8). It is noted that the standard deviation of the mean for the average archaeointensity values calculated using the less stringent criteria had a greater standard deviation than the standard deviation determined for the mean archaeointensity results calculated using the modified PICRIT03 results.

Using the applied criteria instead of the modified PICRIT03 criteria did not change the overall trend shown by the data with all the peaks and troughs being maintained (Figure 5.9). The maximum difference in the standard deviation of the mean determined for each level using both criteria's was 3.6 μT (Table 5.8)

It is noted that the average intensity calculated for Kilise Tepe, context IIf, was consistent for both criteria, increasing our confidence in the accuracy of this result.

Note: The mud brick samples were excluded from this analysis as all the results except for one passed both sets of criteria. This serves to emphasise the quality of the data from the mud brick samples

Table 5.7: Acceptance criteria applied to archaeointensity results.

Criteria	**Applied criteria**	**Modified PICRIT03 (Kissel and Laj, 2004, Paterson et al., 2014)**
N	≥ 5	≥ 4
β	≤ 0.1	≤ 0.1
f	> 0.4	≥0.35
q	≥ 1	≥ 2
MAD	≤ 10	≤ 7
α	≤ 10	N/A
DRAT	< 7	≤ 10
CDRAT	< 20	≤ 11
pTRM checks	≥ 3	≥ 3

Table 5.8

			Applied criteria		Modified PICRIT 03		int diff.
Site	**Context**	**Age range (BC)**	**Fcr ± sd**	**N**	**Fcr ± sd**	**N**	**(μT)**
Tell Atchana	L2/3	1400 - 1320/1305	50.3±9.3	7	50.7±8.7	3	-0.41
	L4	1450/1425 - 1400	47.2±5.5	6	47.2±3.5	3	0.02
	L5	1525/1500 – 1450/1425	52.0±4.7	4	50.5±4.5	3	1.50
	L7/8	1675/1650 – 1600/1575	46.8±7.9	4	-	0	-
	L9	1675/1650 – 1600/1575	38.5±1.9	3	40.4	1	-1.87
	L10	1800 - 1675/1650	50.4±9.9	3	50.4±9.9	3	0.00
	L12a	1800 - 1675/1650	45.9±5.9	2	43.0±1.9	2	2.90
	L12b	1800 - 1675/1650	45.0±2.8	7	43.8±3.2	4	1.21
	L12c	1800 - 1675/1650	48.2±3.0	2	50.3	1	-2.15
	L13	2000-1800	43.7±1.5	2	43.2	1	0.48
	L14	2000-1800	46.7±3.6	5	49.1±2.8	2	-2.43
	L15	2000-1800	38.6±2.1	3	40.1	1	-1.47
	L16	2000-1800	46.0±5.2	2	48.2±5.3	3	-2.25
	L17/18	2200-2000	53.3±7.9	6	52.2±8.7	5	1.10
Kilise Tepe	IIf	800-600	84.7±6.2	4	83.2±5.0	3	1.50

Site, sampled site; Context, sampled context; Age range (BC), estimated age range of context; Fcr± sd, cooling rate corrected average intensity for context with 1 standard deviation plus and minus the mean; N, number of samples from this context which passed the criteria; int diff., total difference between average intensity values determined when applying the different criteria's.

Figure 5.9

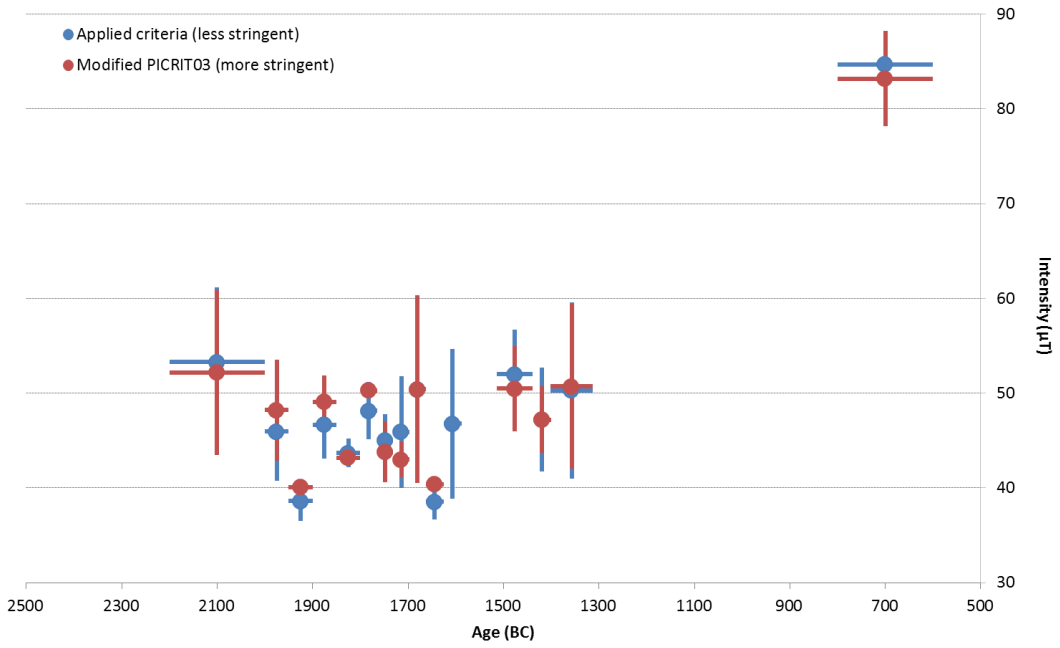

Figure 5.9: Intensity results for Tell Atchana applying more (modified PICRIT03) and less (applied criteria) stringent criteria. Note, as seen in table 5.8 no sample from level 7/8 was accepted under the modified PICRIT03 criteria. Additionally, the same samples were accepted under both criteria sets for level 10 therefore these results plot on top of one another.

As the applied criteria did not change the overall trend of the data and increased the number of accepted results whilst not significantly changing the calculated intensity, the more lenient criteria were applied to this data set.

5.11. Cooling rate results

As mentioned previously, determining an accurate cooling rate correction is crucial to the accuracy of the result. It was possible to run cooling rate experiments on 3 of the 10 Level 12b samples. The ten samples from Level 12b were placed into two groups based on their physical characteristics. Five samples are orange-red in colour with red decorative lines (for the purposes of this discussion dubbed “pottery type 1”). The remaining five samples are pale grey in colour sometimes with black decorative lines (“pottery type 2”). The average cooling rate correction for pottery type 1 is 0.81 (0.8 and 0.81) whilst for type 2, the value obtained from a single sample is 0.94. As can be seen from table 5.9, the average intensity determined when applying an individual cooling rate correction as opposed to applying a blanket correction are within the error estimate of each other. It is therefore deemed reasonable to apply a blanket cooling rate correction per level.

Table 5.9:

Comparing the effect of applying individual and blanket cooling rate corrections on the average intensity for Level 12b

	Average intensity for Level 12b (μT)	**Standard deviation**	**Range (μT)**
No cooling rate correction applied	52.94	3.25	10.83
Individual cooling rate corrections	46.72	3.52	9.52
Blanket cooling rate correction	45.00	2.76	9.21

It was not possible to carry out individual cooling rate corrections on all samples most frequently because alteration occurred at the end of the intensity experiment. Blanket cooling rate corrections were therefore applied for all samples from a level. On average, the cooling rate correction factor was 0.85 with the two largest correction factors being 0.73 for Level 4 and 0.78 for Level 5. Most unusually, a positive correction factor of 1.08 was recorded for Level 17/18. For the majority of levels it was only possible to carry out one cooling rate correction experiment.

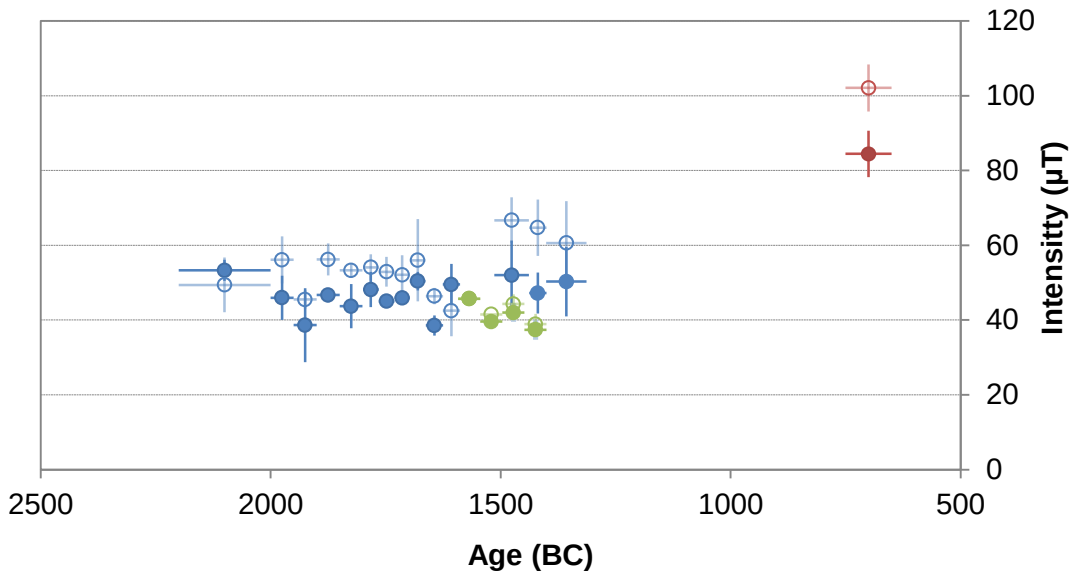

Figure 5.10. Archaeointensity data obtained from this study shown with and without cooling rate correction where full symbols are the cooling rate corrected results and open symbols are the non-cooling rate corrected results. Blue values are determined from Tell Atchana potsherds, green values are from Tell Atchana mud bricks and the red value is from Kilise Tepe potsherds. The horizontal error bars represent the age range for potsherds. The archaeointensity determined is plotted in the centre of this age bracket. Vertical error bars are one standard deviation plus and minus the mean of the average intensity for that level.

Despite having to reject 50% of the cooling rate correction experiments carried out on the brick cores due to alteration during the cooling rate experiment, it was possible to determine a cooling rate correction for mud brick samples TA16.4, TA17.3 and TA18.28. It is noted that the corrections were consistent with each other and were 4.5%, 3.8% and 5.1% respectively. Alteration was seen to affect all samples, however, most strikingly in sample TA17-9 where the alteration factor was 18% (see figure 5.7).

For interest, the results from Tell Atchana and Kilise Tepe (both corrected and uncorrected) are plotted in 5.14 Appendix 2. These results are plotted against previously published data from the region and model curves to demonstrate the impact of applying a cooling rate correction. The cooling rate corrected results are more consistent with previously published data than the results which are not cooling rate corrected. See 5.14 Appendix 2 for more discussion of this.

5.12. Discussion

The geomagnetic field in the Middle East over the time period from 3000-0 BC is marked by at least one period of high field intensity. This chapter reports high quality archaeointensity data from Turkey for a continuous time period from ~2200 BC to 1320/1305BC. Additionally a spot reading from two individual Kilise Tepe potsherds from ~700 BC is also reported. The time period considered here spans a staccato archaeomagnetic jerk which according to Gallet et al., (2006) began with a strong increase in the geomagnetic field intensity between ~1750 and 1500 BC, followed by a moderate increase between ~1500 and 1200-1100 BC and culminating in another strong increase up to ~750 BC. The results presented here indicate the field fluctuated throughout this time period beginning with a high of 53.3 ±7.9 μT before dropping to a low of 38.6± 2.1μT and then rising again to 52.0±4.7μT with a maximum mean increase of 14 μT observed between ~1644 ±19 and ~1476 ±38 BC which is consistent with the increase observed by Gallet et al. (2006) between ~1750 and 1500 BC. Excluding the results from the mud bricks (which are notably lower than the results from the potsherds, see below for more discussion of this) the field then maintains this higher intensity until the end of the occupation of the site (figure 5.11). It is noted, however, that the field only varies by 16 μT over the entire duration of the occupation of Tell Atchana and the maximum field value measured of 53.3 μT is only 6 μT higher than observed today at Ankara.

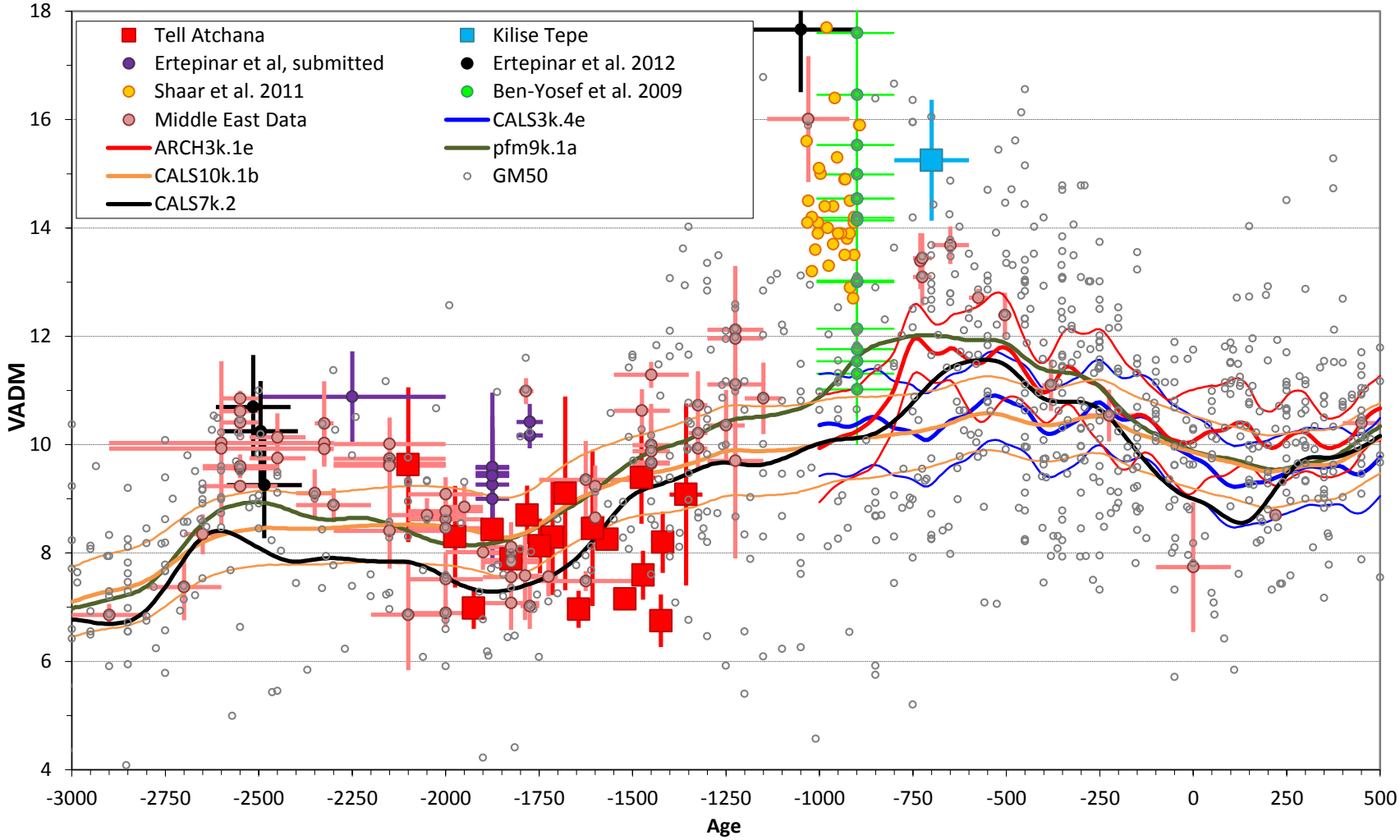
Tell Atchana
Kilise Tepe
Ertepinar et al, submitted
Ertepinar et al. 2012
Shaar et al. 2011
Ben-Yosef et al. 2009
Middle East Data
CALS3k.4e
ARCH3k.1e
pfm9k.1a
CALS10k.1b
GM50
CALS7k.2
VADM
Age
18
16
14
12
10
8
6
4
-3000
-2750
-2500
-2250
-2000
-1750
-1500
-1250
-1000
-750
-500
-250
0
250
500

Figure 5.11. Archaeointensity results from this chapter (Tell Atchana: red squares, Kilise Tepe: blue square) plotted against other recent papers from the Middle East and the Levant. Results from the Middle East (Genevey et al., 2003, Gallet et al., 2006, Gallet et al., 2008, Gallet et al., 2014, Gallet and Le Goff, 2006) are plotted in pink. Of particular interest are the data from (Shaar et al., 2011) (yellow data); (Ertepinar et al., 2012) (black data); Ertepinar et al. (submitted) (purple data), (Ben-Yosef et al., 2009) (green data) and GEOMAGIA50 (grey data, labelled as GM50 in the key) (Donadini et al., 2006 and Korhonen et a., 2008). Model predictions for this location from CALS7k.2 (Korte and Constable, 2005), CALS3k.4e (Korte and Constable, 2011), CALS10k.1b(Korte et al., 2011) ARCH3k_CST.1 (Korte et al., 2009) and pfm9k.1a (Nilsson et al., 2014). All results are plotted as VADMs. Horizontal error bars are errors associated with the age estimate whilst vertical error bars are errors associated with the calculated intensity. The results from this study (squares) are plotted in the middle of their age bracket with the error bars stretching from the beginning to the end of the assigned age. Notice that the data from Tell Atchana (red squares) is consistent with the data from the Middle East (pink circles) and GEOMAGIA50 (grey circles). The data from the mud bricks (~1600-1400 BC) is lower than this published data. The field during the occupation of Tell Atchana is relatively low compared with the field immediately before (2600 BC to 2000 BC) and after (1250 BC to 0BC). The data from Kilise Tepe (blue square) is roughly 1 VADM greater than any other data measured over this time period and about 2 VADMs less than the values measured by Etrepinar et al. (2012), Ben-Yosef et al. (2009) and Shaar et al. (2011).

The two samples of White Painted IV type from Level IIf of Kilise Tepe which record a high intensity are thought to be local following petrographic and chemical analysis. All sherds of this type have extremely standardized fabric and contain serpentine and foraminifera consistent with local clay sources (Hansen and Postgate, 1999, Postgate and Thomas, 2011). This high average field strength of 84µT was recorded by two Kilise Tepe samples. One sherd gave an average value of 80µT with values of 80.0 µT and 80.6 µT being recorded for sister samples. The other successful Kilise Tepe sherd gave an intensity of 89 µT. This average field value of 84 µT for 800-600 BC represents an increase in the strength of the field in Turkey by a factor of 2 over the time range 1305-700 BC. This is a much less dramatic temporal variability than that claimed by Shaar et al (2011) of > 70 ZAm^2 over less than a few decades. Whilst it is acknowledged that the data set presented here does not extend over the time period studied by Shaar et al., (2011) it is possible that the feature they describe (a spike lasting less than 30 years) is a longer lived event than they have observed. Potentially the field strength decayed over at least 300 years with the effects felt over a larger area, not just the Levant. This would be more consistent with the models of Livermore et al. (2014) than with the exceptionally rapid event proposed by Shaar et al (2011).

It is noted that the intensity values determined for the mud bricks were lower than the intensity values determined from the potsherds with the exception of a single non-cooling rate-corrected mud brick sample from Level TA15. Note: all the other mud brick results were cooling rate corrected. It is not clear why there is a disparity between the different artefacts. The composition of mud bricks and potsherds is different as mud bricks frequently contain dung, straw and other available materials whilst potsherds are much more compositionally homogenous. However, both the potsherds and the mudbricks contained a relatively strong, clear primary component without too much ambiguity in the interpretation so we do not believe composition to be the reason for the different calculated values. The mud bricks were burnt during a series of fires which destroyed the buildings they formed the floor of. It is therefore possible that the bricks cooled a lot quicker than the cooling rate correction we applied here, however, it is difficult to estimate the exact cooling rate. Alternatively, as the intensity values for the mud bricks are more consistent with the intensity values for the Level 9 potsherds it is possible the mud bricks are older than originally thought. However, other than this discrepancy in the calculated intensity values, we have no other reason to doubt the dating of the mudbricks or the potsherds as they were both collected during the most recent excavation by K.Aslihan Yener.

The cooling rate correction determined for Level 17/18 from sample L17/18-15 gave a negative (-0.07) ΔTRM whilst all the other cooling rate corrections were positive. It is proposed that this result was influenced by the presence of MD grains in the sample. There is experimental and theoretical support for the theory that the cooling rate effect is smaller and of revered sign in samples containing uniquely MD grains (Papusoi, 1972, Yu, 2011, McClellandbrown, 1984, Muxworthy and Heslop, 2011, Winklhofer et al., 1997), however, this was not observed by Biggin et al. (2013) in their study of assemblages of pseudo-single domain, multi-domain and interacting single domain grains nor by Ferk et al. (2014).

5.13. Conclusions

The results presented here demonstrate the stability of the geomagnetic field in Southern Turkey from ~2200 BC to ~1300 BC. The mean intensity values per archaeological level had a range over the time period of 16μT. The average field strength at this time was 47μT which is comparable with the average field in Turkey (Ankara) in 2014 which was also 47μT. This is the first continuous archaeointensity data set from a single location in Turkey.

The single data point recorded from locally produced pottery found at Kilise Tepe is a robust result which has been reproduced experimentally. The mean, cooling rate corrected value of 84μT is almost double both the current field and the average field over the 1000 years studied here. This result is equivalent to a VADM of 152 ZAm^2 which is less than the 204 ZAm^2 and 251 ZAm^2 reported by Shaar et al. (2011) and Ben-Yosef et al.(2009). Two possibilities are suggested to explain this. Either this result is from the field returning to a lower strength and so represents the decreasing part of the ~1000 BC geomagnetic "spike". This interpretation necessitates it being a longer lived event than proposed by previous authors (Shaar et al., 2011). Alternatively it is the signal of another short lived, high field intensity event.

The high field recorded during the age bracket 600-800 BC is consistent with the VADM of 180 ZAm^2 reported by Ertepinar et al., (2012) from Arslantepe for the time period 1200-9000 BC. Arslantepe is located in the East of Turkey. If the two results are from one continuous period of high geomagnetic field strength then the result presented here extends the geographic extent of the Levant intensity high at 1000BC into central Anatolia.

5.14. Appendix 1: Results tables

Site	Type	Sample	N	F	β	F	g	q	MAD	α95	α	w	CDRAT	Exp type	CR Corr	Fcr	*VADM*
Tell Atchana	Potsherd	L2.3-1I	9	60.6	0.058	0.587	0.838	9.7	1.4	0.4	1.6	3.7	-14.8	1	0.830	50.3	
		L2.3-2I	11	49.0	0.023	0.501	0.865	18.9	0.7	0.4	1.5	6.3	-9.0	1	0.830	40.7	
		L2.3-3I	7	84.7	0.210	0.638	0.676	3.3	2.8	2.2	5.4	1.5	-14.3	1	-	-	
		L2.3-4I	9	68.9	0.026	0.690	0.866	29.7	1.0	0.5	1.6	11.2	11.7	1	0.830	57.2	
		L2.3-5I	8	48.4	0.037	0.635	0.756	12.0	1.9	0.5	0.8	4.9	-28.0	1	-	-	
		L2.3-6I	12	65.8	0.025	0.705	0.875	24.9	1.0	1.5	4.6	7.9	-0.4	1	0.830	54.6	
		L2.3-7I	11	41.2	0.026	1.002	0.888	26.2	4.6	1.5	4.6	8.7	-17.4	1	0.830	34.2	
		L2.3-8I	13	68.4	0.020	0.516	0.919	23.4	2.2	0.3	2.5	7.1	-8.1	1	0.830	56.8	
		L2.3-9I	11	70.1	0.043	0.574	0.886	15.5	1.1	0.2	1.1	5.2	-13.4	1	0.830	58.2	
				60.6±11.2												***50.3±9.3***	***9.1***
Tell Atchana	Potsherd	L4-1I	9	58.6	0.028	0.623	0.832	18.8	0.9	1.3	3.6	7.1	-0.8	3	0.730	42.7	
		L4-2I	9	64.9	0.040	0.705	0.863	18.4	2.4	1.6	4.4	7.0	-27.0	1	-	-	
		L4-3I	9	77.5	0.040	0.461	0.828	9.5	7.2	1.8	6.5	3.6	-7.4	1	-	-	
		L4-4I	9	104.6	0.376	0.645	0.625	1.1	2.3	1.4	6.9	0.4	38.1	2	-	-	
		L4-5I	12	67.9	0.042	0.780	0.897	16.6	1.7	0.5	1.8	5.3	2.5	2	0.730	49.6	
			5	64.6	0.062	0.406	0.721	4.7	3.0	1.2	0.6	2.7	16.3	1	0.730	47.2	
		L4-6I	8	61.9	0.039	0.700	0.834	17.3	1.0	0.3	0.7	7.1	-11.9	1	0.730	45.2	
		L4-7I	12	56.4	0.022	0.725	0.894	31.1	1.1	0.6	2.4	9.8	15.0	1	0.730	41.2	
		L4-8I	12	75.3	0.021	0.796	0.873	47.2	11.3	2.3	3.2	14.9	-33.2	1	-	-	
		L4-9I	8	57.2	0.025	0.555	0.822	19.4	2.4	5.9	16.7	7.9	-16.7	1	-	-	
		L4-10I	19	66.8	0.010	0.825	0.931	80.4	0.5	0.3	1.4	19.5	-1.0	1	0.730	48.8	
				64.7±7.5												***45.0±3.0***	***8.2***

Site	Type	Sample	N	F	β	F	g	q	MAD	α95	α	w	CDRAT	Exp type	CR Corr	Fcr	*VADM*
Tell Atchana	Potsherd	L5-2I	7	63.6	0.106	0.503	0.773	4.4	2.4	1.1	4.8	2.0	-3.8	1	-	-	
		L5-3I	11	58.3	0.015	0.721	0.890	45.6	5.0	1.7	5.8	15.2	-4.1	1	0.780	45.5	
		L5-4I	7	72.5	0.060	0.661	0.800	12.0	0.8	0.2	0.3	5.4	-13.0	1	0.780	56.5	
		L5-6I	12	69.3	0.016	0.844	0.841	44.0	0.9	0.3	0.8	9.1	-5.7	1	0.780	54.1	
		L5-7I	18	66.5	0.010	0.833	0.911	78.9	0.6	0.2	0.9	19.7	-2.9	1	0.780	51.9	
		L5-8I	5	66.6	0.176	0.430	-0.364	-0.9	9.8	1.1	6.0	10.7	-35.1	1	-	-	
		L5-9I	8	57.3	0.043	0.571	0.815	11.7	3.9	1.5	3.0	4.8	-28.0	1	-	-	
		L5-10I	7	64.5	0.106	0.251	0.791	2.3	9.1	0.9	12.6	1.0	-14.8	1	-	-	
				66.7±6.1												***52.0±4.7***	***9.4***
Tell Atchana	Potsherd	L7.8-1I	8	66.7	0.033	0.665	0.866	17.6	1.0	0.4	1.4	6.2	-4.0	1	-	-	
		L7.8-3I	8	54.3	0.025	0.556	0.850	19.1	3.8	0.6	1.9	7.8	-16.9	1	0.860	46.7	
		L7.8-5I	9	44.7	0.040	0.651	0.858	11.7	3.1	0.8	3.7	4.4	-15.9	1	0.860	38.4	
		L7.8-6I	11	75.0	0.446	0.831	0.867	2.3	1.5	0.6	2.1	0.8	-66.5	1	-	-	
		L7.8-8I	8	37.1	0.060	0.433	0.835	6.0	5.8	2.9	14.2	2.5	40.8	1	-	-	
		L7.8-9I	9	52.0	0.029	0.757	0.849	21.6	1.0	1.5	5.3	8.2	13.3	1	-	-	
				49.5±6.8												***42.6±5.9***	***8.5***
Tell Atchana	Potsherd	L9-1I	14	56.3	0.020	0.819	0.911	38.2	0.6	0.3	1.2	11.0	-7.4	1	-	-	
			12	49.0	0.046	0.692	0.880	13.2	0.5	0.4	1.2	4.2	-0.6	2	-	-	
		L9-2I	16	44.2	0.016	0.799	0.917	46.7	0.6	0.8	3.5	12.5	11.9	1	0.830	36.7	
		L9-3I	5	56.8	0.026	0.285	0.739	8.6	4.5	0.7	5.6	5.0	-21.7	1	-	-	
		L9-4I	9	50.3	0.043	0.389	0.845	7.6	3.3	0.8	5.8	2.9	-21.6	1	-	-	
		L9-5I	13	46.3	0.017	0.823	0.899	38.3	0.9	0.3	0.5	11.5	-12.8	1	0.830	38.5	
		L9-6I	9	47.8	0.036	0.609	0.836	12.9	1.7	0.8	1.6	4.9	-22.9	1	-	-	
		L9-7I	9	49.3	0.094	0.478	0.868	4.1	3.2	1.2	2.2	1.6	-21.7	1	-	-	
		L9-8I	12	48.7	0.023	0.789	0.881	30.3	1.3	0.7	3.1	9.6	-6.5	1	0.830	40.4	
				46.4±2.2												***38.5±1.9***	***7.0***

Site	Type	Sample	N	F	β	F	g	q	MAD	α95	α	w	CDRAT	Exp type	CR Corr	Fcr	*VADM*
Tell Atchana	Potsherd	L10-1I	12	50.6	0.010	0.647	0.901	55.6	0.9	0.4	1.4	17.6	-1.6	1	0.900	45.6	
		L10-2I	11	48.2	0.023	0.390	0.886	13.6	1.4	1.5	7.5	4.5	-57.5	1	-	-	
		L10-3I	11	92.0	0.036	0.615	0.939	16.1	7.7	2.9	15.4	5.4	0.0	1	-	-	
		L10-4I	11	68.6	0.019	0.795	0.877	37.1	1.7	0.6	1.4	12.4	-9.1	1	0.900	61.8	
		L10-5I	7	61.4	0.089	0.600	0.771	5.2	4.8	1.3	3.6	2.3	-31.4	2	-	-	
			9	50.4	0.019	0.752	0.894	35.5	0.9	0.3	1.5	13.4	-26.6	1	-	-	
		L10-6I	11	53.4	0.101	0.889	0.841	7.5	2.5	2.2	6.3	2.5	-63.4	1	-	-	
		L10-7I	13	54.1	0.031	0.532	0.893	15.5	0.6	0.3	1.1	4.7	-92.7	1	-	-	
		L10-8I	13	48.7	0.017	0.830	0.912	39.9	1.7	0.5	1.6	12.0	-10.9	1	0.900	43.8	
				56.0±11.0												***50.4±9.9***	***9.1***
Tell Atchana	Potsherd	L12a-1I	7	52.4	0.076	0.243	0.794	2.5	5.7	6.6	19.5	1.1	-62.7	1	-	-	
		L12a-2I	13	48.0	0.019	0.780	0.874	33.4	0.5	2.3	7.2	10.1	-31.8	1	-	-	
		L12a-4I	13	54.5	0.032	0.833	0.888	22.9	4.6	1	3.5	6.9	-5.7	2	0.880	48.0	
			9	59.3	0.040	0.616	0.536	8.3	0.6	2.4	4.1	3.1	-13.8	1	0.880	52.2	
		L12a-5I	12	50.4	0.018	0.787	0.899	39.7	0.3	4	11.2	12.6	-3.4	1	-	-	
		L12a-6I	10	54.5	0.038	0.828	0.837	18.4	0.6	0.2	0.2	5.8	-21.9	1	-	-	
		L12a-7I	12	55.6	0.027	0.848	0.895	29.6	2.1	1	2.3	9.3	-49.3	1	-	-	
		L12a-8I	14	47.4	0.009	0.892	0.892	84.8	0.4	0.4	1.2	24.5	-2.9	1	0.880	41.7	
		L12a-9I	11	61.3	0.060	0.761	0.868	12.8	6.3	1.9	7.5	4.3	-31.6	1	-	-	
				52.1±5.2												***45.9±5.9***	***8.3***

Site	Type	Sample	N	F	β	F	g	q	MAD	α95	α	w	CDRAT	Exp type	CR Corr	Fcr	*VADM*
Tell Atchana	Potsherd	L12b-1I	17	56.0	0.015	0.761	0.900	44.2	0.5	0.4	2.2	8.4	-17.0	1	0.850	47.6	
		L12b-2I	15	52.9	0.014	0.805	0.918	53.0	1.1	0.3	1.2	14.7	-4.1	1	0.850	45.0	
		L12b-3I	13	80.8	0.209	0.853	0.868	3.5	31.6	10.1	26.2		-168.9	1	-	-	
		L12b-4I	8	52.9	0.030	0.557	0.813	15.1	2.2	0.8	2.4	6.2	-42.0	1	-	-	
		L12b-5I	15	51.4	0.020	0.811	0.908	34.9	3.6	2.4	7.1	9.7	-2.5	1	0.850	43.7	
		L12b-6I	8	55.3	0.010	0.541	0.850	49.1	2.9	0.6	3.5	20.0	-7.7	1	0.850	47.0	
		L12b-7I	9	53.6	0.041	0.620	0.838	12.8	0.8	0.5	1.8	4.8	-12.6	1	0.850	45.6	
		L12b-8I	8	47.8	0.034	0.701	0.806	16.7	1.9	1	3.5	6.8	10.6	1	0.850	40.6	
			14	45.1	0.044	0.718	0.903	14.7	3.4	1	2.4	4.3	10.9	2	0.850	38.4	
		L12b-9I	8	52.9	0.123	0.541	0.800	3.5	0.6	1.3	1.6	1.4	-23.6	1	-	-	
		L12b-10I	11	54.9	0.018	0.621	0.861	31.6	1.5	1.2	4.0	10.5	-15.7	1	0.850	46.7	
				52.9±4.0												***45.0±2.8***	***8.1***
Tell Atchana	Potsherd	L12c-1I	11	51.7	0.020	0.871	0.879	37.5	0.9	0.6	1.3	12.5	-13.8	1	0.890	46.0	
		L12c-3I	8	78.2	0.226	0.451	0.724	5.8	0.5	2.6	3.7	2.4	-33.9	1	-	-	
		L12c-4I	10	44.7	0.049	0.723	0.762	11.3	0.6	0.7	2.9	4.0	-22.7	1	-	-	
		L12c-5I	9	52.9	0.105	0.925	0.894	7.9	3.0	3.9	10.7		-53.1	1	-	-	
		L12c-7I	17	56.5	0.086	0.854	0.889	9.4	0.6	0.4	1.9	2.4	-7.4	1	0.890	50.3	
		L12c-8I	8	43.7	0.063	0.236	0.839	2.6	13.4	3.4	29.3	1.1	-5.9	1	-	-	
				54.1±3.5												***48.2±3.0***	***8.7***
Tell Atchana	Potsherd	L13-1I	8	51.8	0.024	0.598	0.848	21.2	1.1	1	2.5	8.6	-12.8	1	0.820	42.5	
			9	52.2	0.044	0.836	0.839	16.1	3.7	2	5.0	6.1	7.5	2	0.820	42.8	
		L13-3I	9	54.5	0.023	0.870	0.842	136.3	0.6	0.3	1.0	51.5	-19.2	1	0.820	44.7	
		L13-4I	12	54.6	0.020	0.856	0.888	37.9	0.5	0.4	1.4	12.0	22.9	1	-	-	
		L13-5I	17	52.4	0.107	0.839	0.925	7.3	21.3	15.5	47.9		-5.3	1	-	-	
		L13-6I	6	57.3	0.160	0.243	0.551	0.8	4.2	1.2	7.2		-113.2	1	-	-	
		L13-8I	6	62.0	0.184	0.538	0.699	2.0	1.5	4.8	7.8		-32.7	1	-	-	
		L13-9I	12	52.7	0.048	0.743	0.891	13.7	1.6	3.4	12.5	4.3	-2.2	1	-	-	
				53.3±1.8												***43.7±1.5***	***7.9***

Site	Type	Sample	N	F	β	F	g	q	MAD	α95	α	w	CDRAT	Exp type	CR Corr	Fcr	*VADM*
Tell Atchana	Potsherd	L14-1I	6	61.2	0.073	0.731	0.701	7.0	1.9	1.2	2.8	3.5	-41.4	2	-	-	
			9	46.0	0.035	1.131	0.848	27.4	4.7	5.9	14.4	10.4	-14.9	1	-	-	
		L14-2I	8	50.0	0.079	0.647	0.835	6.8	2.0	0.9	2.5	2.8	15.9	2	0.830	41.5	
		L14-3I	16	54.8	0.028	0.413	0.894	13.2	1.4	0.3	0.2		17.0	1	0.830	45.5	
		L14-4I	11	72.7	0.176	0.500	0.874	3.4	1.8	4.1	13.4	1.1	-44.9	1	-	-	
		L14-5I	9	58.1	0.060	0.803	0.859	11.5	2.2	1.6	5.5	8.1	-13.7	1	0.830	48.2	
		L14-6I	13	56.8	0.023	0.857	0.892	35.3	1.4	0.4	1.6	10.6	-5.5	1	0.830	47.1	
		L14-7I	13	61.6	0.008	0.862	0.906	103.6	1.9	0.7	3.4	31.2	9.5	1	0.830	51.1	
				56.2±4.3												***46.7±3.5***	***8.4***
Tell Atchana	Potsherd	L15-1I	11	50.4	0.037	0.808	0.878	18.5	0.8	0.4	1.5	6.2	-67.4	1	-	-	
		L15-2I	7	46.6	0.049	0.621	0.691	7.7	2.4	1.5	4.1	3.5	-11.7	1	0.850	39.6	
		L15-3I	13	53.4	0.062	0.830	0.870	11.7	2.2	0.7	1.2	3.5	-90.7	1	-	-	
		L15-5I	10	54.9	0.025	0.869	0.859	31.2	1.5	0.8	0.9	11.0	-26.9	1	-	-	
		L15-6I	10	60.5	0.017	0.732	0.837	35.1	0.5	0.3	112.0	12.4	-14.2	1	-	-	
		L15-7I	9	47.2	0.041	0.868	0.813	17.4	3.9	1.4	3.9	6.6	-10.0	1	0.850	40.1	
		L15-8I	11	42.6	0.057	0.554	0.876	6.8	5.5	1	6.9	2.3	-12.8	1	0.850	36.2	
		L15-9I	14	56.2	0.020	0.710	0.899	32.0	0.9	0.4	1.8	9.2	-21.2	1	-	-	
				45.5±2.5												***38.6±2.1***	***7.0***
Tell Atchana	Potsherd	L16-2I	8	64.1	0.045	0.809	0.829	14.9	1.9	6.8	11.1	6.1	-9.1	2	-	-	
		L16-4I	12	57.4	0.019	0.919	0.883	41.8	6.8	2.8	11.5	13.2	-21.2	1	-	-	
		L16-5I	16	60.5	0.015	0.634	0.914	38.3	0.3	0.7	1.5	10.2	9.4	1	0.820	49.6	
		L16-6I	18	51.6	0.007	0.702	0.915	86.4	0.6	1.1	4.7	22.2	9.7	1	0.820	42.3	
				56.1±6.3												***46.0±5.2***	***8.3***

Site	Type	Sample	N	F	β	F	g	q	MAD	α95	α	w	CDRAT	Exp type	CR Corr	Fcr	*VADM*
Tell Atchana	Potsherd	L17/18-1I	11	47.0	0.017	0.763	0.877	38.9	0.9	0.2	1.0	13.0	8.5	1	1.080	50.8	
		L17/18-2I	10	35.7	0.092	0.795	0.823	7.1	4.1	1.2	3.7	2.5	-5.6	1	1.080	38.5	
		L17/18-4Ib	10	53.6	0.017	1.001	0.841	49.1	0.6	0.3	0.9	17.3	-58.2	1	-	-	
		L17/18-5I	9	53.0	0.065	0.489	0.796	6.0	6.9	1.9	16.0	2.3	-67.5	1	-	-	
		L17/18-6I	9	64.1	0.060	0.472	0.833	6.5	8.0	2	10.7	2.5	-17.1	1	-	-	
		L17/18-7I	9	53.9	0.028	0.615	0.844	18.5	0.9	1.1	4.0	10.2	-20.6	1	-	-	
		L17/18-11I	11	66.8	0.047	0.740	0.868	17.3	2.6	1.8	4.4	5.8	-53.6	1	-	-	
		L17/18-12I	10	60.3	0.017	0.717	0.723	31.4	0.6	1.1	4.3	11.1	27.4	1	-	-	
		L17/18-13I	10	54.3	0.055	0.712	0.866	11.5	0.4	0.6	2.4	4.1	-16.0	1	1.080	58.6	
		L17/18-14I	13	51.4	0.017	0.710	0.882	37.1	0.5	1.8	8.4	11.2	-2.6	1	1.080	55.5	
		L17/18-15I	11	53.1	0.061	0.865	0.889	12.5	3.9	1.6	6.9	4.2	-1.8	2	1.080	57.3	
			10	52.4	0.018	0.714	0.885	35.1	2.6	1.5	6.3	12.4	2.2	1	1.080	56.6	
		L17/18-16I	9	40.0	0.111	0.754	0.728	4.9	3.3	2.5	7.2	1.9	-40.9	1	-	-	
		L17/18-17I	11	55.3	0.049	0.804	0.901	14.8	1.9	0.8	0.9	4.9	2.2	2	1.080	59.7	
		L17/18-18I	8	69.2	0.176	0.743	0.793	4.4	7.0	6.9	7.9	1.8	-102.4	1	-	-	
				49.4±7.3												***53.3±7.9***	***9.6***

Site, name of site; Type, material studied, Sample, name of the sample; N, number of points used to define a linear segment of the Arai diagram; F, measured intensity; β, ratio of standard error of the slope to the absolute value of the slope; f, the NRM fraction used for the best-fit on an Arai diagram; g, 'gap factor' normalised error of the slope and quality factor according to Coe et al. (1987) q, quality factor; MAD, Mean Angular Deviation of the directional fit to the paleomagnetic vector on a vector component diagram; α95, radius of a cone of 95% confidence; CDRAT, cumulative DRAT where a DRAT is the maximum absolute difference produced by a pTRM check, normalized by the length of the best-fit line; Exp type, 1) Microwave Coe method with field applied parallel, 2) Microwave IZZI method with field applied anitparallel, 3) Microwave IZZI method with field applied parallel; CR Corr, Cooling Rate correction as determined from a cooling rate experiment and checked for alteration; Fcr, intensity result which has been cooling rate corrected; VADM Virtual Axial Dipole Moments calculated for these corrected intensity values Accepted results are highlighted in grey. Mean intensity per context with standard deviation reported in bold italics.

Site	Type	Sample	N	F	β	F	g	q	MAD	α95	Fit Dec	Fit Inc	Mean Dec	Mean Inc	α	w	CDRAT	Exp type	CR Corr	Fcr	*VADM*
Tell Atchana	Orientated mud brick	TA15.3	13	***45.7***	0.012	0.638	0.889	46.2	4.4	1.1	149.2	50.2	144.3	51.7	3.4	13.9	0.3	4			***6.8***
		TA16.4	13	***41.5***	0.028	0.667	0.890	21.1	2.8	0.8	216.5	-7.9	214.3	-8.8	2.4	6.3	8.7	4	0.955	***39.6***	***7.6***
		TA18.13	13	47.0	0.066	0.775	0.904	10.6	3.6	1.1	344.2	-38.2	343.9	-41.1	2.9	3.2	10.0	4	0.949	44.6	
		TA18.16	12	45.5	0.035	0.769	0.896	19.9	3.4	1.1	285.8	28.0	285.4	28.1	0.4	6.3	2.1	4	0.949	43.2	
		TA18.22	14	45.7	0.016	0.787	0.915	44.2	2.8	0.9	115.0	-1.6	112.7	-1.0	2.4	12.8	10.2	4	0.949	43.3	
		TA18.28	11	45.2	0.028	0.610	0.396	8.8	2.3	0.9	201.6	78.8	192.1	79.5	1.9	2.9	1.5	4	0.949	42.8	
		TA18.29	11	46.7	0.025	0.663	0.872	23.4	2.5	1.1	62.6	29.1	61.0	27.5	2.1	7.8	7.6	4	0.949	44.3	
		TA18.31	13	44.6	0.032	0.696	0.901	19.6	3.3	1.3	60.6	30.3	55.8	28.6	4.5	5.9	10.8	4	0.949	42.3	
		TA18.4B	13	43.4	0.030	0.711	0.895	21.1	3.4	1.1	227.5	-39.6	223.5	-39.0	3.2	6.4	10.3	4	0.949	41.1	
		TA18.7	12	38.5	0.033	0.735	0.839	18.8	2.4	3.3	264.3	16.0	265.6	18.8	3.1	5.9	3.6	4	0.949	36.6	
		TA18.8A	14	42.2	0.049	0.777	0.891	14.1	4.0	1.0	221.5	-57.3	224.5	-57.4	1.6	4.1	3.7	4	0.949	40.0	
				44.3±2.6																***42.0±2.5***	***7.2***
		TA17.18	9	39.3	0.038	0.914	0.801	19.1	2.5	0.9	56.6	-47.5	58.1	-47.2	1.1	7.2	0.4	4	0.962	37.8	
		TA17.2	10	37.9	0.051	0.791	0.869	13.4	4.9	1.3	149.1	50.3	142.6	52.0	4.4	4.7	7.5	4	0.962	36.4	
		TA17.21	9	35.3	0.054	1.009	0.769	14.3	1.5	0.8	257.1	-21.8	257.3	-22.8	1.0	5.4	0.0	4	0.962	33.9	
		TA17.23	10	36.5	0.011	0.703	0.875	54.1	3.3	1.1	98.0	-55.5	94.3	-55.3	2.1	6.0	10.3	4	0.962	35.1	
		TA17.5	10	44.0	0.019	0.846	0.865	38.2	2.1	0.8	262.8	37.6	264.1	38.7	1.5	13.5	5.7	4	0.962	42.3	
		TA17.8	10	39.1	0.043	0.836	0.860	16.7	3.0	1.1	150.5	41.4	146.8	43.6	3.5	5.9	3.0	4	0.962	37.6	
		TA17.9	12	39.9	0.020	0.791	0.894	35.7	4.5	1.6	294.3	36.6	298.3	36.1	3.3	11.3	-0.3	4	0.962	38.4	
		TA17.3	11	38.7	0.059	0.634	0.835	9.0	3.1	1.2	48.1	36.8	49.6	35.8	1.6	3.0	19.5	4	0.962	37.2	
				38.9±2.8																***37.4±2.7***	***8.3***

Site, name of site; Type, material studied, Sample, name of the sample; N, number of points used to define a linear segment of the Arai diagram; F, measured intensity; β, ratio of standard error of the slope to the absolute value of the slope; f, the NRM fraction used for the best-fit on an Arai diagram; g, 'gap factor' normalised error of the slope; q, quality factor according to Coe et al. (1987); MAD, Mean Angular Deviation of the directional fit to the paleomagnetic vector on a vector component diagram; α95, radius of a cone of 95% confidence; Fit Dec and Inc, fitted dec and inc describe the mean directions anchored to the origin, determined using "Plotcore 2.1" by Alan McCormack; Mean Dec and Inc, describe the mean directions when not anchored to the origin again determined using "Plotcore 2.1"; CDRAT, cumulative DRAT where a DRAT is the maximum absolute difference produced by a pTRM check, normalized by the length of the best-fit line; Exp type, 4) Thermal IZZI method with the field applied antiparallel; CR Corr, Cooling Rate correction as determined from a cooling rate experiment and checked for alteration; Fcr, intensity result which has been cooling rate corrected; VADM Virtual Axial Dipole Moments calculated for these corrected intensity values. Grey rows represent accepted results. Mean intensity per context with standard deviation reported in bold italics.

5.14 Appendix 2: Cooling rate and non-cooling rate corrected results plotted with previously published data

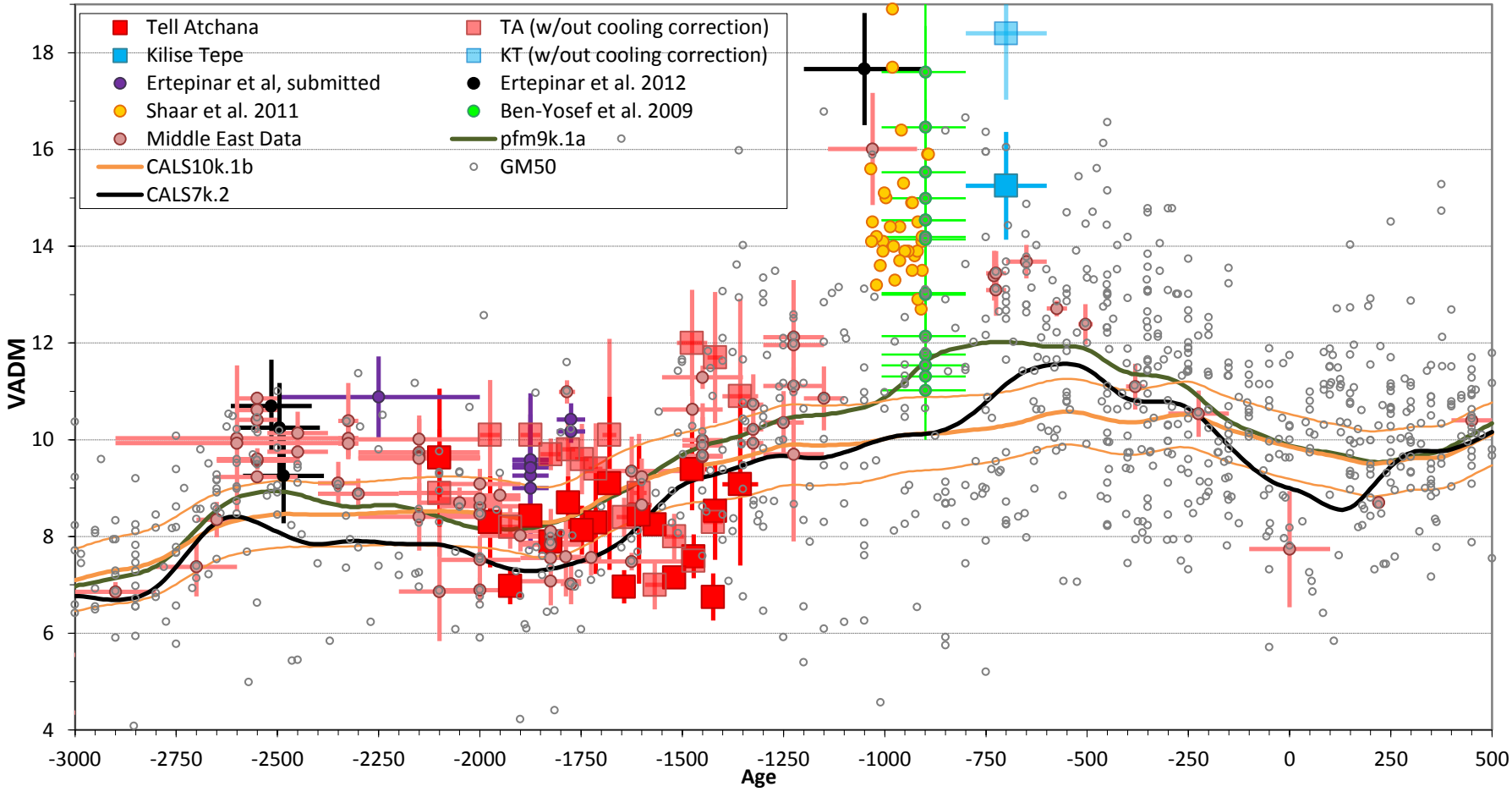

Figure 5.12 . Cooling rate corrected and ***non cooling rate corrected*** *archaeointensity results from this study (Tell Atchana: red/* ***pale red*** *squares, Kilise Tepe: blue/* ***pale blue*** *square) arhcaeointensity results plotted against other recent papers from the Middle East and the Levant. Results from the Middle East (Genevey et al., 2003, Gallet et al., 2006, Gallet et al., 2008, Gallet et al., 2014, Gallet and Le Goff, 2006) are plotted in pink. Of particular interest are the data from (Shaar et al., 2011) (yellow data); (Ertepinar et al., 2012) (black data); Ertepinar et al. (submitted) (purple data) and (Ben-Yosef et al., 2009) (green data) , model predictions for this location from CALS7k.2 (Korte and Constable, 2005), CALS3k.4e (Korte and Constable, 2011), CALS10k.1b(Korte et al., 2011) ARCH3k_CST.1 (Korte et al., 2009) and pfm9k.1a (Nilsson et al., 2014) All results are plotted as VADMs. Horizontal error bars are errors associated with the age estimate whilst vertical error bars are errors associated with the calculated intensity.*

This figure is partly plotted for interest and partly because the paper by Suttie et al. (2011) demonstrated that applying corrections to archaeomagnetic data can actually worsened the consistency of the fit between historical data and archaeomagnetic data. Note how not applying the correction improves the correlation with the recent work of Ertepinar et al (submitted) (purple circles) whilst decreasing the correlation with data from Gallet and Genevey. If time had permitted, it would have been interesting to investigate the reasons behind this. The most obvious explanations are that it is either related to the material being studied or to the cooling rate correction applied in Ertepinar et al (submitted).

The non cooling rate corrected result for Kilise Tepe is striking and much higher than the majority of the data from Shaar et al. (2011) and Ben-Yosef et al. (2009)

5.14 Appendix 3: Photographs of samples

Tell Atchana level 2.3

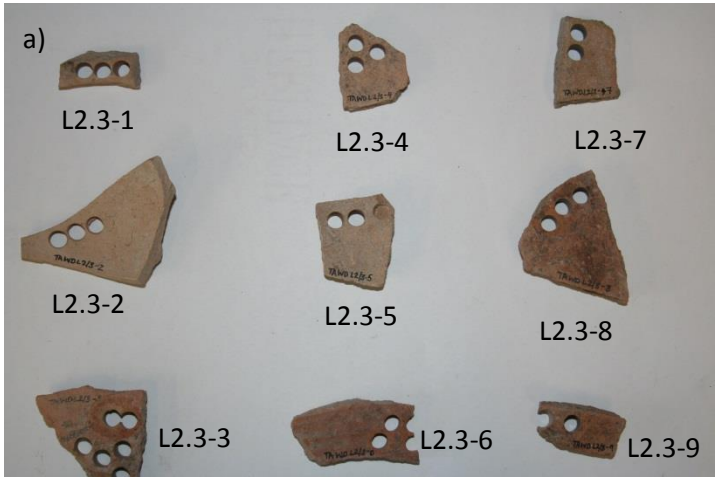

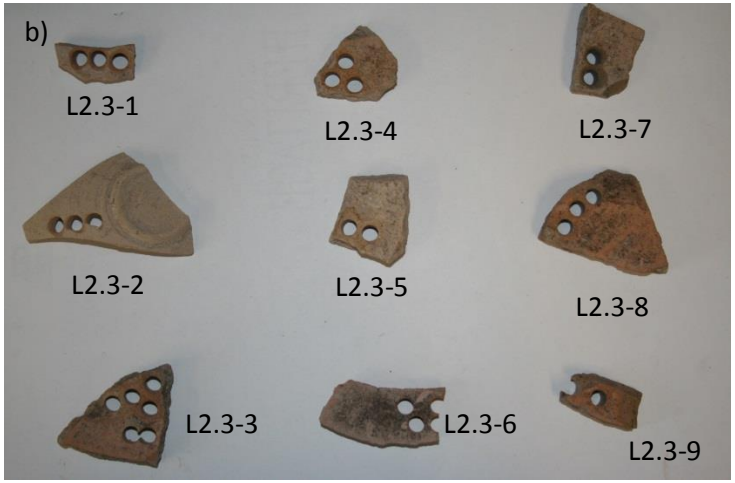

Tell Atchana level 4

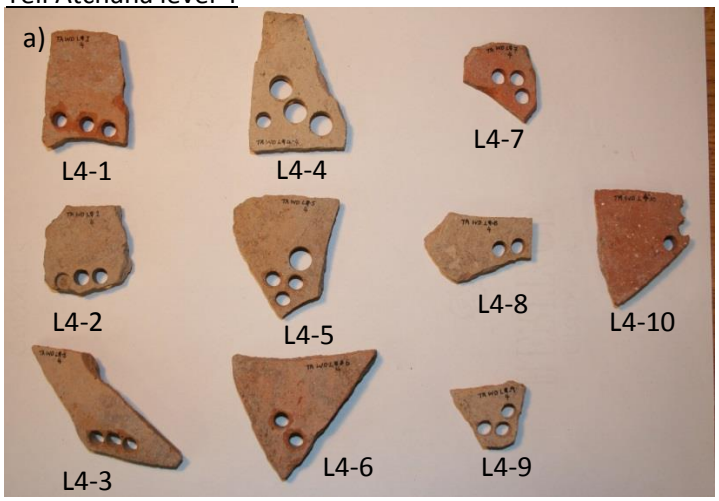

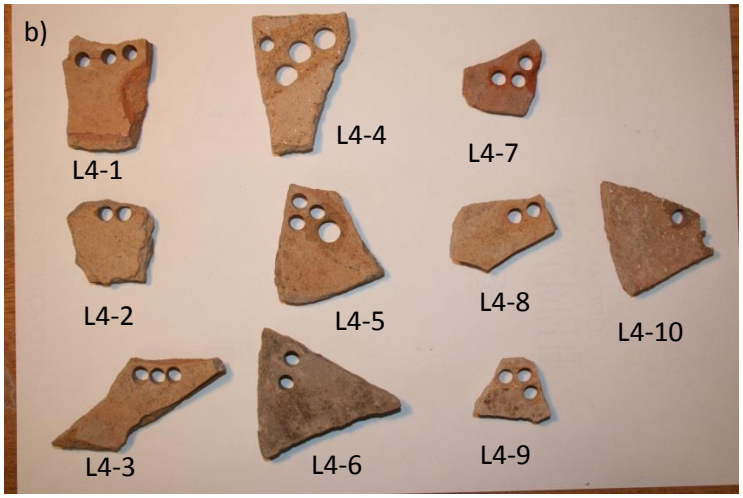

Tell Atchana level 5

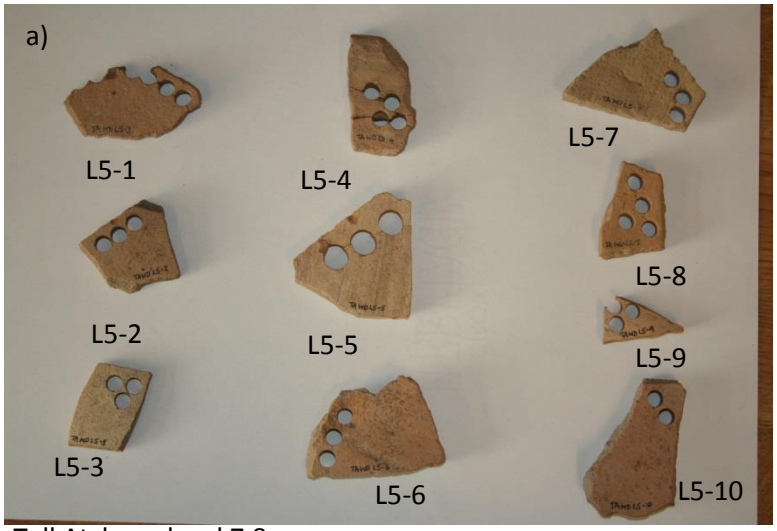

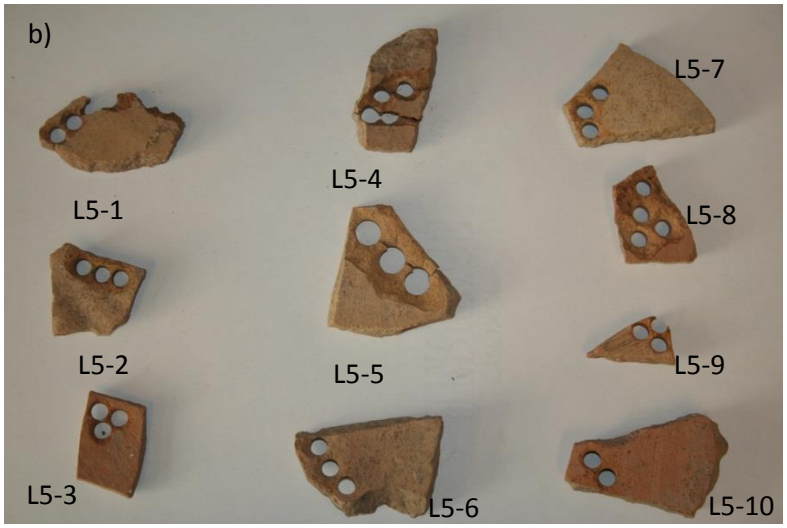

Tell Atchana level 7.8

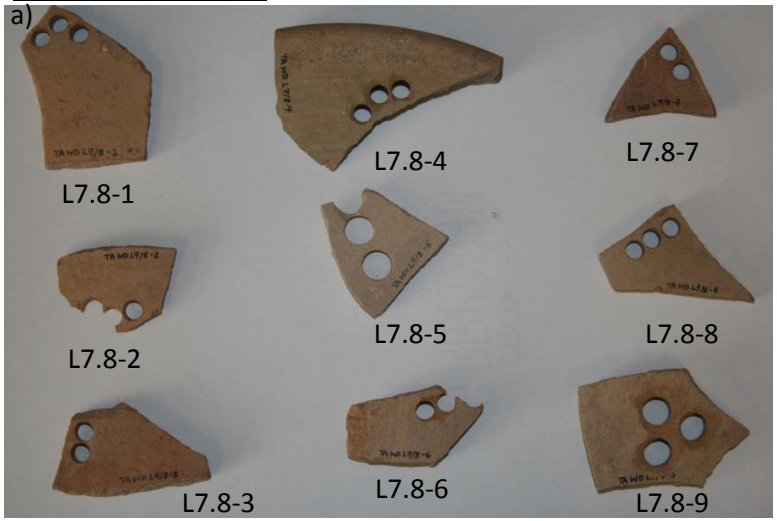

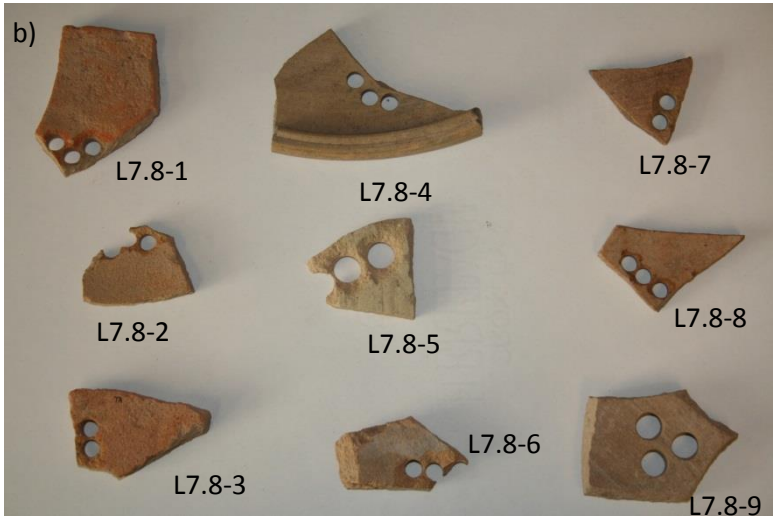

Tell Atchana level 9

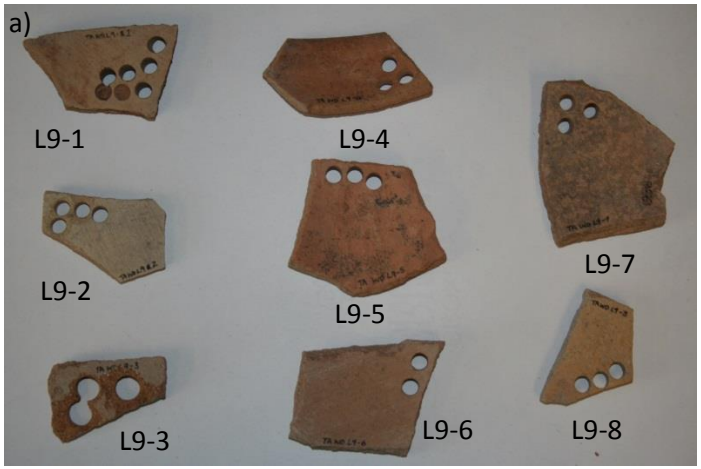

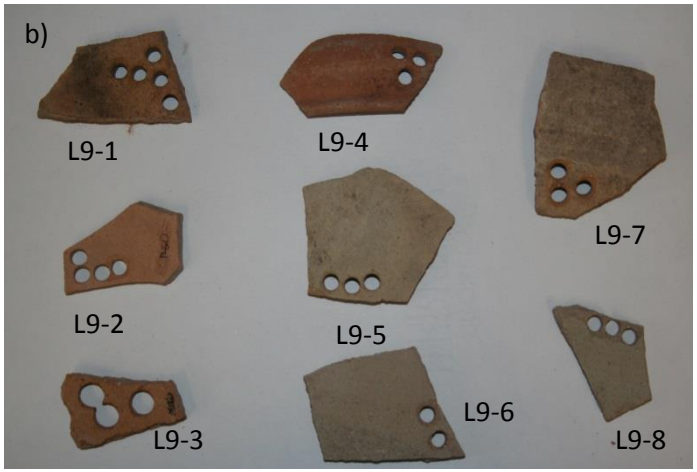

Tell Atchana level 10

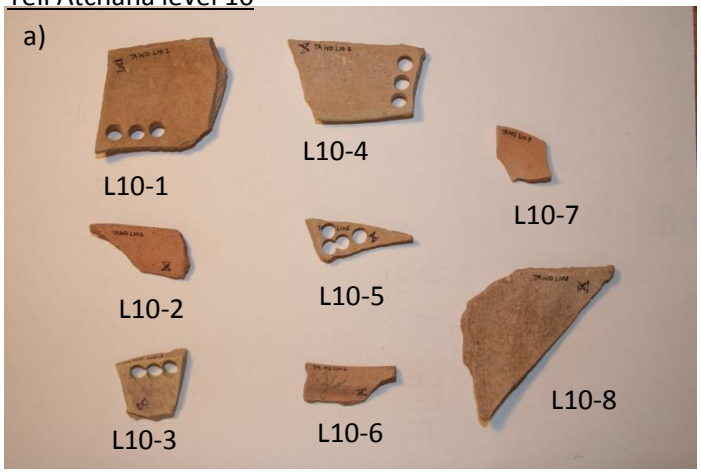

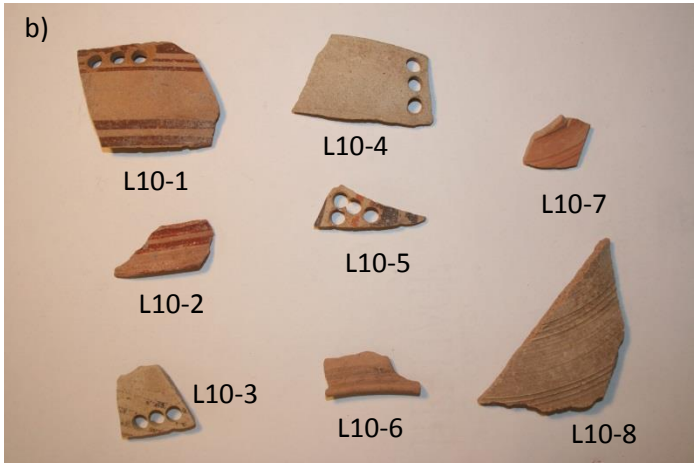

Tell Atchana level 12a

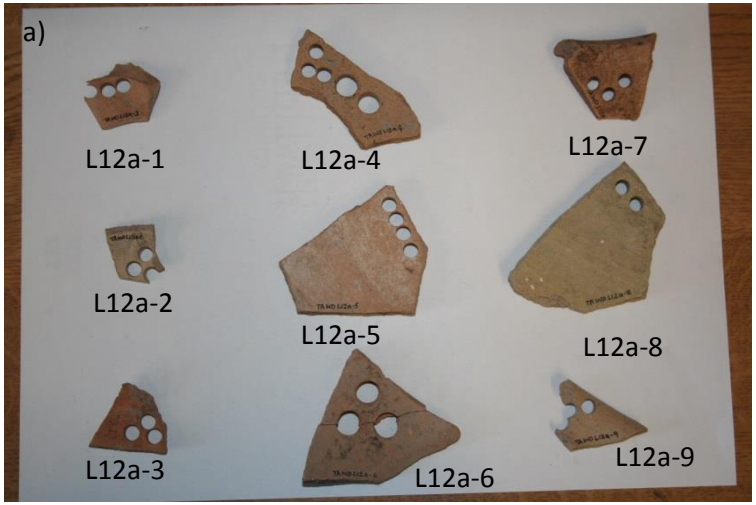

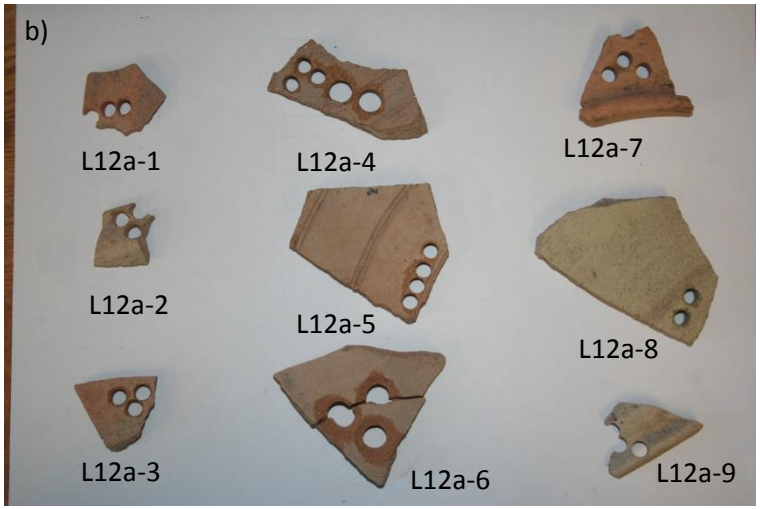

Tell Atchana level 12b

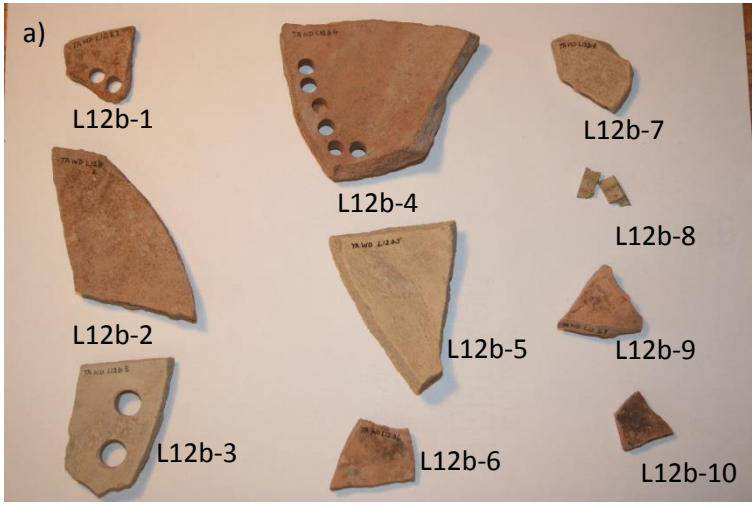

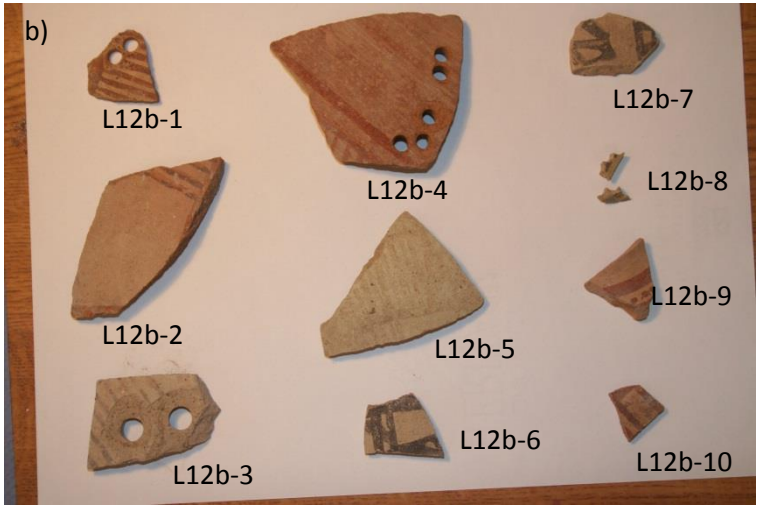

Tell Atchana level 12c

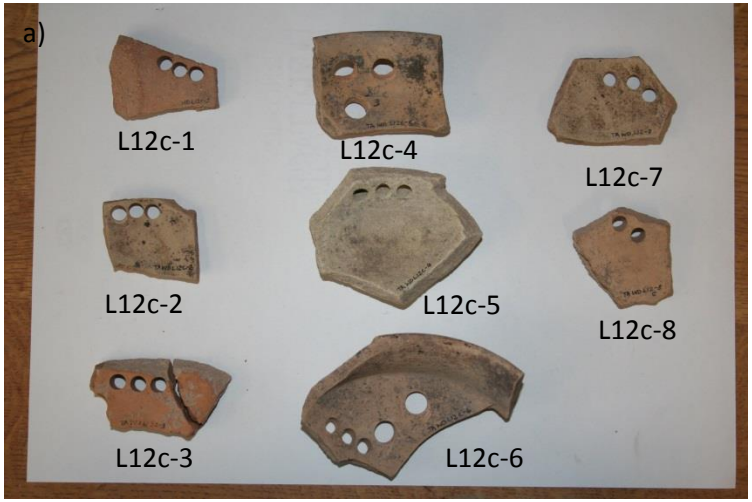

Tell Atchana level 13

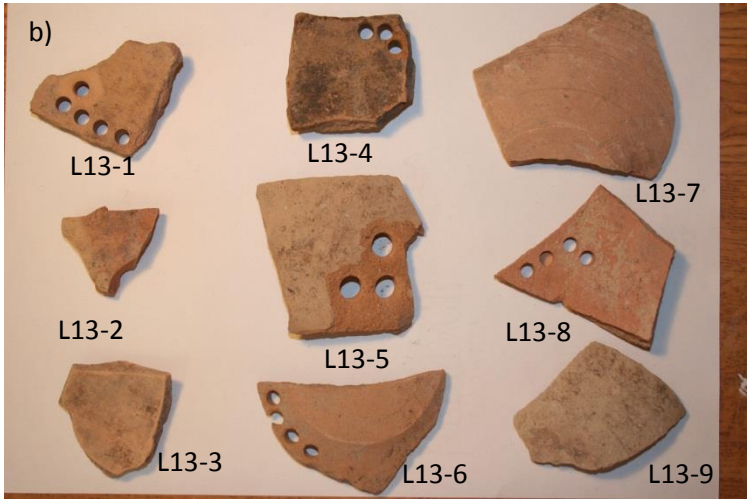

Tell Atchana level 14

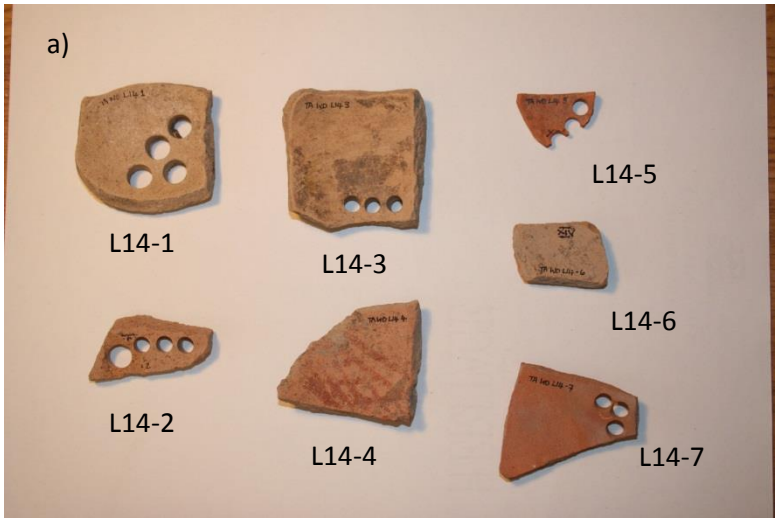

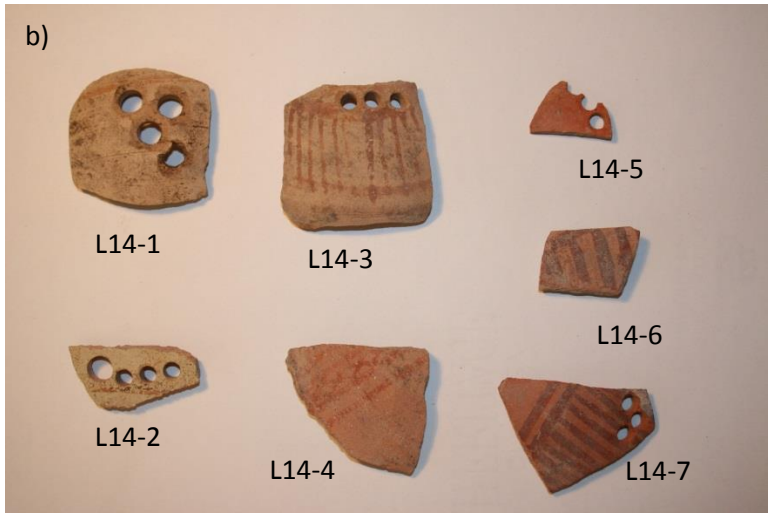

Tell Atchana level 15

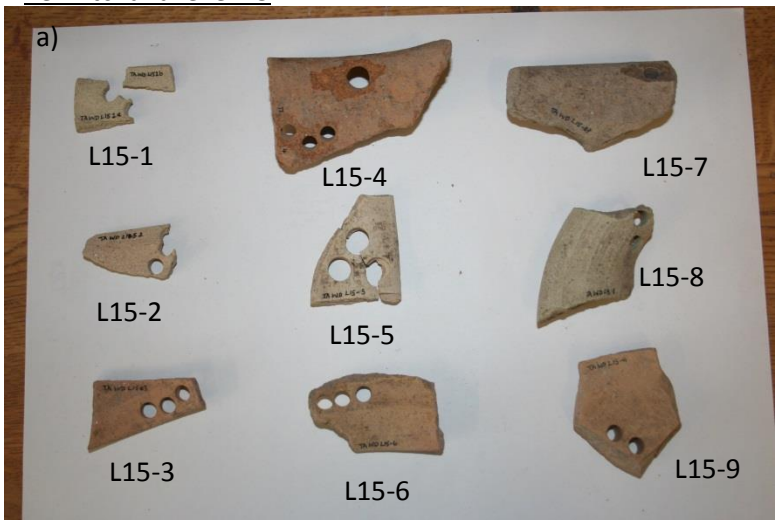

Tell Atchana level 16

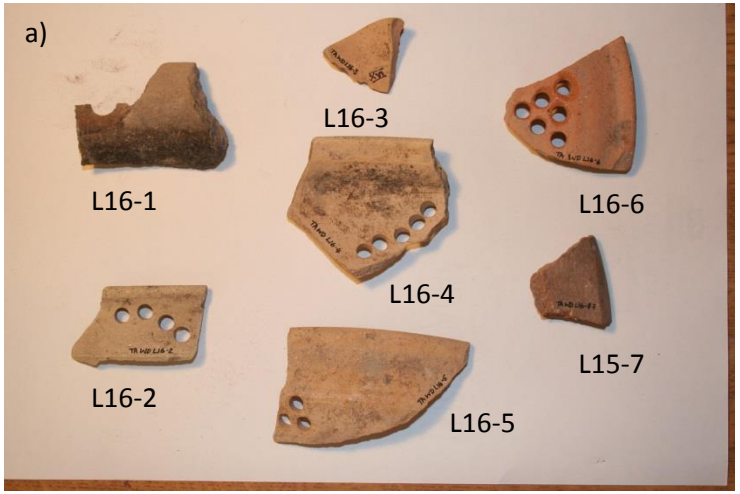

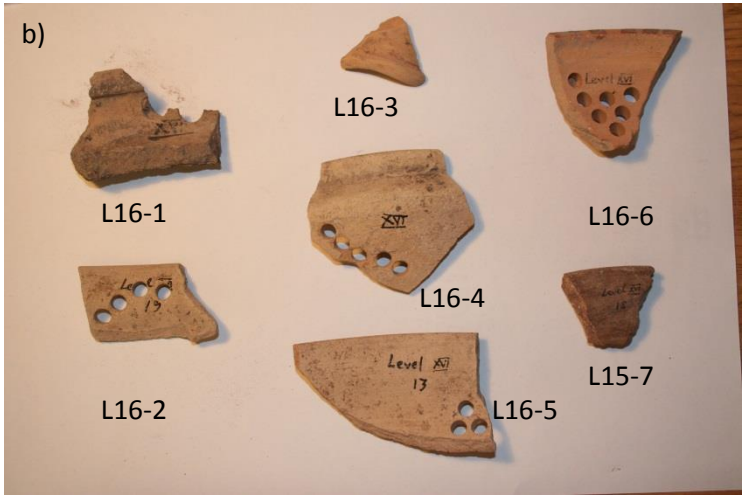

Tell Atchana level 17.8

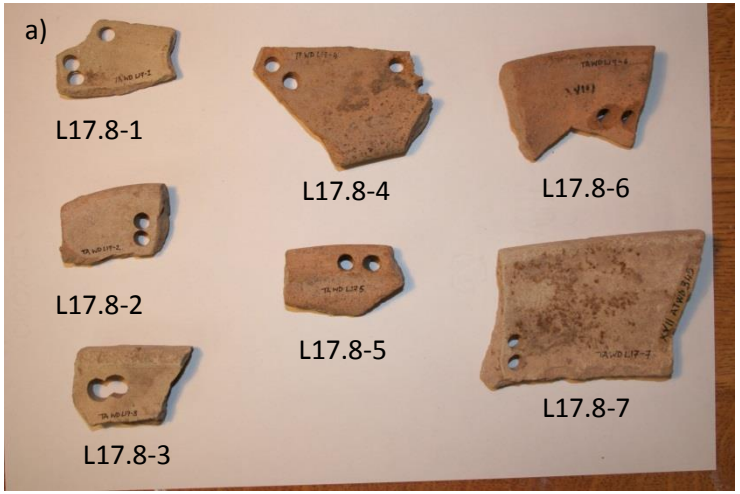

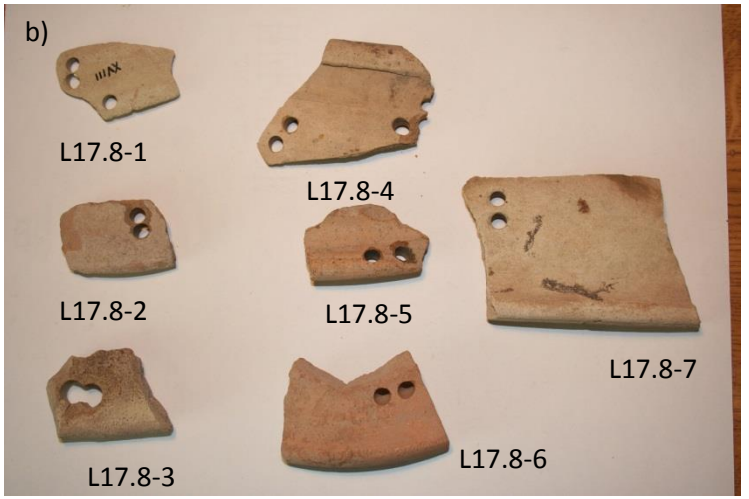

Tell Atchana level 17.8

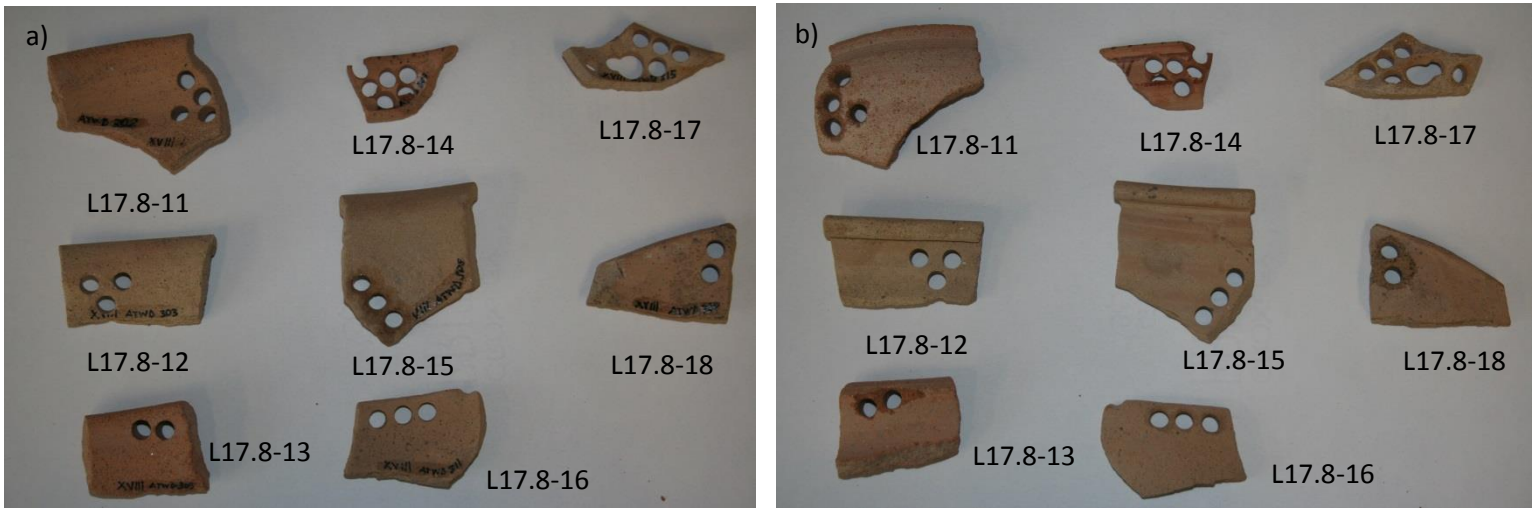

Photographs shows all the Tell Atchana potsherds with the sample names indicated next to the sample. Photographs labelled a) show one side of the sherds whilst b) shows the reverse of the same ample. The small holes in the samples are 5mm in diameter and represent subsamples taken for analysis. In each photograph, the sherds are lying on a piece of A4 paper. The larger holes are 7mm in diameter and again indicate where subsamples were taken for analysis. Note the close proximity of the holes to each other. Note also the differences in decoration and thickness of the sherds analysed.

6. Archaeointensity Results from Cypriot Bronze Age Pottery Sherds

6.1. Abstract

The findings of a number of recent archaeomagnetic studies based in the Middle East have suggested that exceptional geomagnetic field conditions were experienced in this region during the Bronze Age. In spite of this, it is remarkable how few studies have been based in Cyprus considering its rich cultural heritage. This study presents some of the first archaeointensity data from Cypriot potsherds. We have studied 34 potsherds from two archaeological sites in Cyprus: Marki *Alonia* and Bellapais *Vounous*. Marki *Alonia* was occupied from 2400 BC to 1900 BC. The samples studied from the necropolis of Bellapais *Vounous* all date from the Early Cypriot I-II period (c.2240-2100 BC). We conducted Coe method archaeointensity experiments with pTRM and zero field steps on these samples using the microwave system at Liverpool University Geomagnetism Laboratory. The archaeointensity values measured are consistent with previously published results. An average archaeointensity was calculated of 56.0±11µT over the time period 2400-2250 BC, 48.6 ±4 µT from 2250-2100 BC and 43.3±3 µT from 2100-1900 BC. The data reported in this study and in other papers suggests that the overall trend in the Middle East was for decreasing field strength over this time period. We found no evidence in Cypriot pottery to support the presence of a relative intensity maximum between 2100 and 1900 BC as proposed by previous authors.

6.2. Introduction

Archaeomagnetism is the study of burnt archaeological material which has retained a record of the geomagnetic field at the time it was last heated. Commonly studied recorders of the magnetic field include pottery e.g. Tema et al., (2012), tiles and bricks e.g. Chauvin et al., (2000) and kilns and hearths e.g. Hervé et al. (2013b). Using archaeomagnetic and palaeomagnetic recorders of known age and provenance, changes in the geomagnetic field of the Earth both spatially and temporally can be modelled e.g. CALS10kb (Korte et al., 2011), ARCH3k_cst.1 (Korte et al., 2009), CALS3k.4 (Korte and Constable, 2011). Such models are limited by the quality and quantity of available field

information. In locations where a local secular variation (SV) curve has been constructed from well dated archaeological material it is possible to use the SV curve for dating e.g. Casas et al., (2013)

A thorough knowledge of the evolution of the field over time allows us to better understand geodynamo processes occurring in the core as well as enabling us to construct better field models and constrain local secular variation curves. In order to possess this thorough knowledge, full vector field information (declination, inclination and intensity) is required from as many different locations and times as possible. There are still many key questions to be answered about geomagnetic field behaviour including (but not limited to) elucidating the exact relationship, if any, between the geomagnetic field and climate (e.g. Gallet et al., 2006) determining the maximum possible rate of change in field intensity and determining the maximum possible field intensity (e.g. Shaar et al., 2011) . In order to answer these questions we need directional and intensity data from all time periods gathered from across the globe. Many authors have highlighted the bias in the existing archaeomagnetic data set towards directional data from Western Europe from the recent past e.g. Korte et al., (2011), Pétronille et al., (2012), Kostadinova-Avramova et al (2014).

Considering the recent volume of papers focused on archaeointensity in the Middle East e.g. Gallet et al. (2006), Gallet and Le Goff (2006), Ertepinar et al. (2012), Ben-Yosef et al. (2009), Shaar et al. (2011) the lack of published work centred in Cyprus is surprising. There are only two papers known to the author: Aitken et al. (1984) and Shaar et al. (2015). The former of these two papers reports results from 5 Cypriot sherds as part of a broader study of geomagnetic intensity in Egypt and Western Asia. Cyprus has a long cultural heritage and history of trade and immigration from neighbouring countries including the Levant and Anatolia (Webb and Frankel, 1999). Attention has lately turned to Cyprus, however, in particular to its abundant slag deposits (Ben-Yosef et al., 2011, Shaar et al. 2015). Copper slag has recently been exploited as a recorder of the geomagnetic field and has the potential to provide a very high resolution time series (Ben-Yosef et al., 2009, Ben-Yosef et al., 2008b, Shaar et al., 2011). This high temporal resolution means that very short timescale events can potentially recorded (Shaar et al., 2011).

Nonetheless, there is still a role to be played by sherds, as they are ubiquitous across archaeological sites. Sherds can provide information over a longer time sequence than most slag deposits e.g. 2000 years as reported in Genevey and Gallet (2002). If we gather archaeointensity values from Cypriot sherds we will gain an understanding of the longer

wavelength trends in the field behaviour for a location where very few previous archaeomagnetic studies have been based and no secular variation curve exists.

The aim of this chapter is to gather archaeointensity data from Cyprus over the time period 2400 BC – 1900 BC using samples from two Bronze Age Cypriot archaeological sites; Marki *Alonia* and Bellapais *Vounous*.

A further aim of this study is to look at the ability of cooking pots to stably record the magnetic field. Cooking pots would have been exposed to repeated heating during the course of their use which would have caused considerable thermal stress. This may affect the ability of such pots to reliably record the magnetic field. Additionally, if archaeomagnetism can be used to identify cooking pots this would have significant ramifications for archaeologists as the identification of cooking pots is not always straight forward.

6.3. Archaeological Sites Studied

6.3.1. Context

The Early and Middle Bronze Age in Cyprus lasted from about 2400 to 1700 BC (Frankel, 2014, Webb, 2014, Knapp, 2013). For much of this time the predominant pottery type in many areas of the island was Red Polished Ware. This hand-made pottery was produced in a variety of shapes and styles, with chronological and regional differences. Detailed typological studies provide the basis for a fine-scale relative chronology (Stewart, 1962, Bolger and Webb, 2013) which is now reinforced by stratigraphy and radiocarbon dating (Peltenburg, 2013, Manning, 2013b, Manning, 2013a). All sherds sampled come from hand-made vessels, fired to various temperatures, but probably not more than 800 or 900^{o}C (for a recent review of these ceramic fabrics see Webb in Bolger and Webb 2013). The harder, coarser fabrics (e.g. Drab Polished Ware), and in particular those used for cooking pots (Red Polished Philia Coarse Ware and Red Polished Coarse Ware), were fired at higher temperatures than the softer, finer ones. Cooking pots would have been subject to repeated heating when in use.

6.3.2. Marki *Alonia*

Marki *Alonia* is a Bronze Age village in central Cyprus which was occupied from about 2400 BC to 1900 BC (Frankel and Webb, 2006). It is located on the Alykos River, on the edge of the north-eastern foothills of the Troodos mountain range (figure 6.1) and was excavated

during the 1990s by the Australian Cyprus Expedition under the direction of David Frankel and Jennifer Webb of La Trobe University. The site has produced an unparalleled stratigraphic and architectural sequence from the earliest manifestations of the Early Cypriot Bronze Age (the Philia facies) through to the earlier part of the Middle Bronze Age (Frankel and Webb, 2000). In addition to pottery typology and site stratigraphy, the site has been dated using radiocarbon.

We have studied 28 sherds from this site which have been taken from contexts dated between 2400 BC and 1900 BC. The majority of these sherds are Red Polished Ware. During the Philia phase finer quality vessels were brought into the site from elsewhere on the island. Later the majority of pottery vessels were locally made.

Figure 6.1: Map of Cyprus with black circles indicating the location of Marki Alonia and Bellapais Vounous.

6.3.3. Bellapais *Vounous*

The necropolis of *Vounous* is located on the north coast of Cyprus (figure 6.1). During the 1930s Cypriot (Dikaios, 1940), Australian (Stewart and Stewart, 1950) and French (Dunn-Vaturi, 2003) expeditions excavated several hundred of the rock-cut chamber tombs. Six Red Polished Ware sherds from the Australian excavations at this site have been studied here. All date from the Early Cypriot I-II period (c.2250-2100 BC)

6.4. Materials

In this study a total of 34 sherds were measured, 6 from Bellapais *Vounous* and 28 from Marki *Alonia* (see Table 6.1 and 6.9. appendix 2). They fall into 3 chronological groups: Philia Early Cypriot Phase (c. 2400-2250 BC), Early Cypriot I-II (c. 2250-2100 BC) and Early Cypriot III/ Middle Cypriot I (c. 2100-1900 BC). Five different pottery wares are represented.

Table 6.1: List of samples

Period	**Age (BC)**	**Site**	**Pottery Type**	**No. of sherds**	**Samples**
Philia Early Cypriot	c. 2400 - 2250	Marki *Alonia*	Red Polished Philia Ware	11	CPEC1, CPEC2, CPEC3, MPEC4, MPEC5, MPEC6, MPEC7, MPEC8, MPEC9, MPEC10, MPEC11, MPEC12
			Red Polished Philia Coarse Ware	1	CPEC3
Early Cypriot I-II	c. 2250 - 2100	Marki *Alonia*	Red Polished Ware	1	CEC4
		Bellapais *Vounous*	Red Polished Ware	6	BVEC1, BVEC2, BVEC3, BVEC4, BVEC5, BVEC5, BVEC6
Early Cypriot III/ Middle Cypriot I	c. 2100 - 1900	Marki *Alonia*	Red Polished Ware	10	ECMC5, ECMC6, ECMC9, ECMC11, ECMC12, ECMC13, ECMC14, ECMC15, ECMC16, ECMC17
			Red Polished Coarse Ware	2	ECMC7, ECMC8
			Drab Polished Ware	3	CDPW9, CDPW10, ECMC10

Period, archaeological time period samples belong to; Age (BC), Dates in BC which define the period; Site, archaeological site where the samples were found; Pottery type, name given to the pottery group samples belong t, no. of sherds, number of pottery sherds found on this site within this time period of a particular pottery type which were analysed in this chapter; Samples, name given to each of the samples analysed in this chapter with their position in the table indicative of the period, site and pottery type they belong to. See 6.9 Appendix 1 for more details on the pottery types.

6.5. Methods

6.5.1. Characterising the Magnetic Properties of the Samples

The bulk magnetic properties of each pot sherd were determined using the Magnetic Measurements Variable Field Translation Balance (VFTB) at the University of Liverpool Geomagnetism Laboratory. Isothermal remanent magnetisation (IRM) acquisition curves, back field coercivity, hysteresis loops and curie curves up to 700°C in an ambient field of up to 700mT were measured. Each sherd subsample measured weighed between 100 – 200 mg.

The results of the IRM experiments indicate that all samples contain a low coercivity phase and are saturated in fields of less than 300mT (figure 6.2). Three of the six samples from Bellapais *Vounous* (all Red Polished Ware) and four of the eleven Red Polished Philia Ware samples from Marki *Alonia* show a dominance of paramagnetic components in their hysteresis loops. After removal of the paramagnetic contribution from all the results, the saturation magnetisation (M_s), remanent magnetisation (M_{rs}), coercivity of remanence (H_{cr}) and the coercivity (H_c) were determined and displayed as a Day Plot (Day et al., 1977) (figure 6.3). All the samples plotted within the Pseudo Single Domain (PSD) field of the Day plot. Four samples of Early Cypriot III/ Middle Cypriot I Red Polished Ware and one of Drab Polished Ware showed alteration on heating producing a more magnetic phase on cooling. All other samples showed either highly reversible heating curves or alteration on heating to produce a less magnetic phase apparent in the cooling curve (figure 6.2). There are three main types of thermomagnetic curves observed in this data set which are:

1. A linear curve with a slight change in slope at ~580°C. These curves are typically highly reversible. This type is representative of the bulk of the data set.
2. A sudden, curved, change of slope at ~580°C. This is observed in two samples of Red Polished Ware and two samples of Red Polished Coarse Ware.
3. Two gradient changes observed, the first between 250°C and 300°C, the second around 580°C. This type was observed in three samples of Red Polished Ware and in one sample of Red Polished Philia Ware.

All three types of thermomagnetic curves have a change in slope at around 580°C, and so the inferred dominant magnetic carrier is magnetite. This interpretation is supported by the low coercivity observed in each sample.

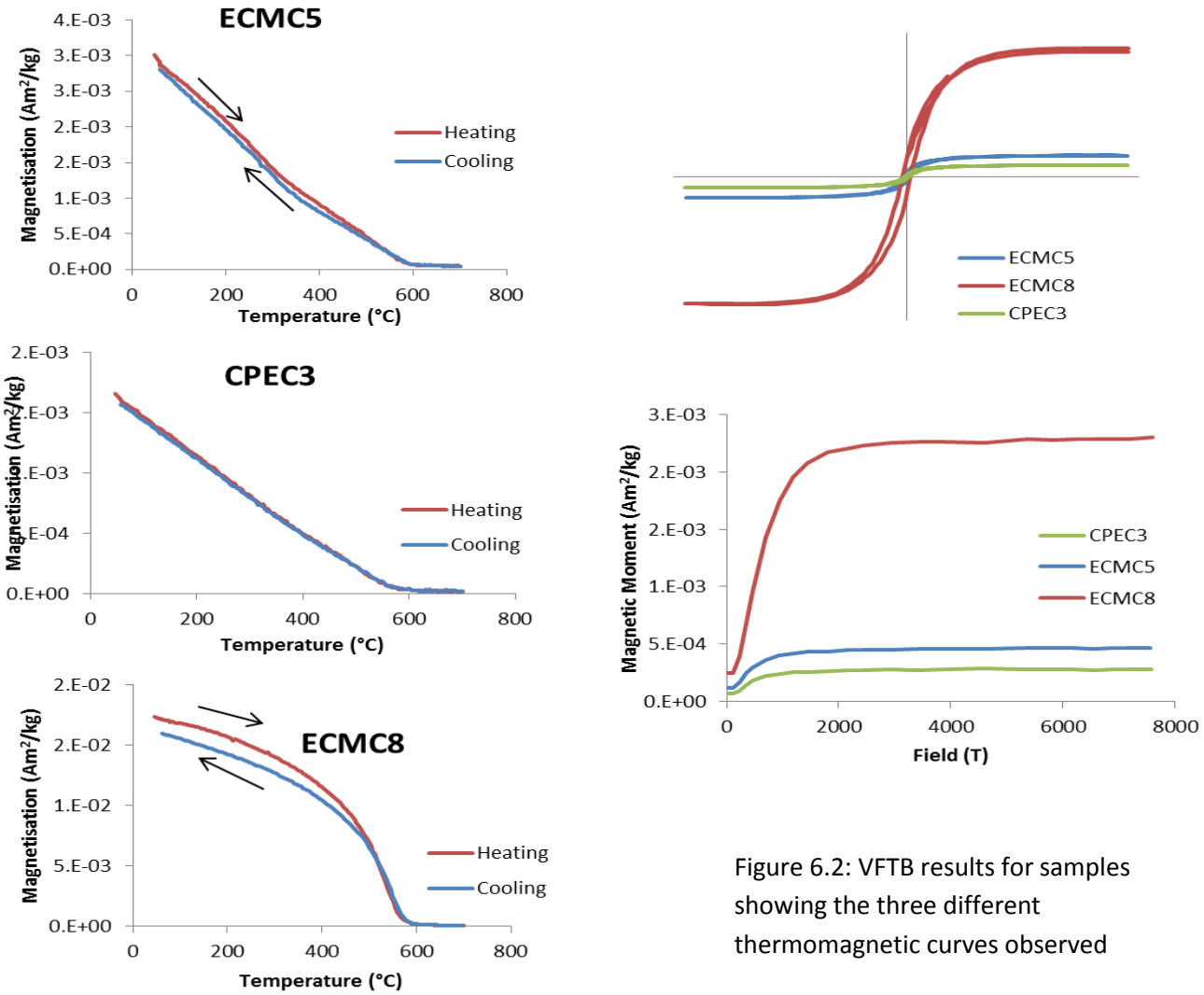

Figure 6.2: VFTB results for samples showing the three different thermomagnetic curves observed

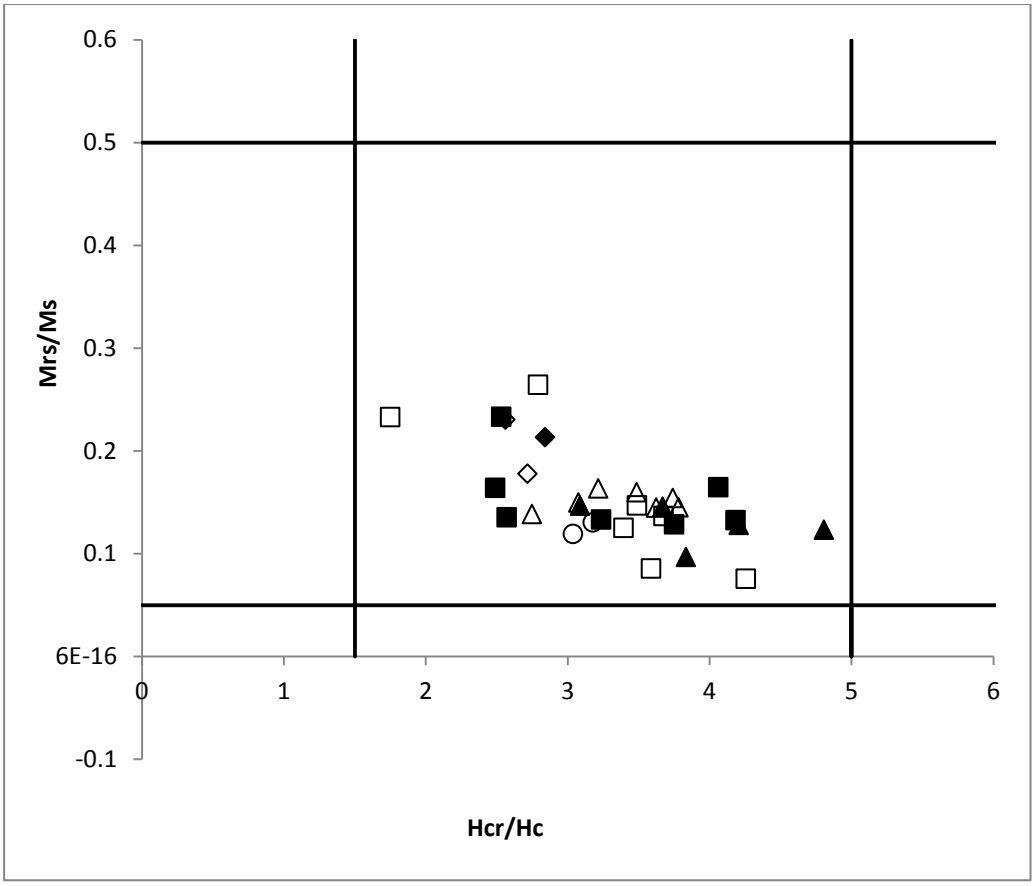

Figure 6.3: Day plot for all samples where solid symbols indicate samples which gave accepted archaeointentsity results and open symbols indicate samples which gave rejected archaeointensity results. Squares = Red Polished Ware, Triangles = Red Polished Philia Ware, Circles = Red Polished Coarse Ware, Diamonds = Drab Polished Ware

6.5.2. Demagnetisation and Intensity Experiments

Subsamples with a diameter of 5mm and a length of 1- 5mm were drilled perpendicular to the surface of each sherd. Three subsamples were drilled per sherd and all were taken in close proximity to each other (within an area 20 x 20 mm). One subsample was used to determine the bulk magnetic properties of the sample. The second subsample was demagnetised and the results of this demagnetisation experiment shaped the subsequent archaeointensity experiment. The final subsample was subjected to a full intensity experiment. All demagnetisation and archaeointensity experiments were conducted on the 14GHz microwave system (MWS) combined with a low temperature Tristan SQUID magnetometer (Shaw and Share, 2007) based at the University of Liverpool Geomagnetism Laboratory. The subsamples were mounted on a quartz glass tube using negative vacuum pump pressure before being inserted into the MWS. The microwave cavity was then tuned

in order to optimise the power absorbed by each individual sample. During a microwave experiment, the bulk sample is not heated, and so an acquired 'TRM' in the MWS is denoted as T_MRM.

Prior to intensity measurements, demagnetization experiments determined the suitability of the sherd for intensity experiments and also established if it contained a viscous remanent magnetisation. Six samples from Marki *Alonia* (samples CPEC2, ECMC7, CPEC3, MPEC6, EMC12 and MPEC5) and 1 from Bellapais *Vounous* (sample BVEC6) were deemed unsuitable for archaeointensity experiments following the demagnetisation experiment. For the majority of these sherds this was because they lacked a stable component of remanence heading towards the origin. This may have been caused by insufficient heating or by pot movement during firing. Additionally, one sample did not demagnetise when subject to microwaves even when the time and/or the power was increased (sample MPEC6 from Marki *Alonia*). One sample fell apart during the intensity experiment and therefore wasn't suitable for further microwave experiments (sample EMC14 from *Marki Alonia*).

As mentioned previously, one subsample from each sherd was subjected to a full intensity experiment with the field applied parallel to the direction of the Natural Remanent Magnetisation (NRM). Experiment steps followed the Coe protocol including repeated pT_MRM checks which were carried out to monitor possible alteration (Coe et al., 1978). Repeat zero field checks were made as an additional alteration check for multi-domain (MD) behaviour. It is acknowledged that applying the field parallel to the NRM reduces the sensitivity of zero field checks (Yu and Dunlop, 2003).

6.5.3. Archaeointensity Criteria

The archaeointensity criteria applied follows SELCRIT2 (Biggin et al., 2007) as modified by Paterson et al., (2014) with the addition of a CDRAT criteria. Accordingly, the number of points (N) defining the slope had to be greater than or equal to 5 and the ratio of the standard error of the slope to absolute value of the slope (β) smaller than 0.1. The lower acceptance limit for the fraction of remanence (FRAC) (Shaar and Tauxe, 2013) is 0.35 and the acceptance criterion of quality factor (q) was set to 1 (Coe et al., 1978). The upper acceptance limits for maximum angular deviation (MAD) and α (Kirschvink, 1980) are taken as 15%. pTRM checks were deemed successful if the ratio of the difference between the check and the relevant TRM value to the length of the selected NRM-TRM segment (DRAT)

(Selkin and Tauxe, 2000) was smaller than 10%. The cumulative DRAT (CDRAT) (Kissel and Laj, 2004), defined as the sum of all the DRATs, must be less than 11%. Here we have used the CDRAT limit proposed by Paterson et al., (2014) to be applied when using the PICRIT 03 criteria (Kissel and Laj, 2004) as the original SELCRIT criterial does not include a CDRAT criterion. A CDRAT criterion was applied because CDRAT is very effective at eliminating results with systematic bias introduced by consistent alteration throughout the experiment. The DRATtail (Biggin et al., 2007) must be less than 10%.

6.5.4. Anisotropy Effects

A number of authors e.g. Rogers et al. (1979), Chauvin et al. (2000) have reported a significant anisotropy of the thermoremanent magnetisation in pottery and tiles which originates from the preferential alignment of grains along one easy axis. This is most likely induced during the creation of the ceramic artefact particularly in wheel-thrown pottery. At least one pottery type studied here (Red Polished Ware) is exclusively hand-built and vessels were pinched, coiled or formed in a mould (Webb, 1994). For both wheel and hand-made pottery, if the clay is worked into a particular orientation it is probable that the plate-like clay particles become aligned during fabrication and cause a similar alignment of the magnetic minerals (Yang et al., 1993). In order to minimize the effects of anisotropy and the angular difference between the TRM and the applied field, the laboratory field in the microwave was applied in the direction of the natural remanent magnetisation. To confirm that results were not biased by anisotropy, the angle between the pTRM acquired at the last accepted experiment step and the applied field direction, γ, was checked for all accepted samples and found to always be <7.5 .

6.5.5. Cooling Rate Effect

The rate of cooling of the sample in nature and in the laboratory will be influenced by the local environment and for practical reasons is quicker in the laboratory. If a sample is allowed to cool slowly it will gain more thermoremanent magnetisation than a sample that cools over a shorter amount of time. This is because the sample spends longer at any given temperature allowing more domain states to populate the higher magnetisation state. The magnitude of this difference depends on the domain state of the magnetic carriers and the cooling rate. In an assemblage of ideal, non-interacting single domain (SD) grains, the archaeointensity measured in the lab with its faster cooling time is an overestimate of the archaeointensity if an appropriate correction is not made. This has been demonstrated

theoretically and experimentally e.g. Fox and Aitken (1980), Halgedahl et al. (1980). The cooling rate effect is less significant in samples with pseudo-single-domain (PSD) states: if a sample containing PSDs cooled over a 24 hour period then the laboratory estimate will be an over-estimation of 4% compared to the 15% measured for ideal SD grains (Biggin et al., 2013).

Poletti et al., (2013) demonstrated that samples behave in a similar way when subjected to microwaves as they do during thermal experiments in spite of the different way in which energy is transferred into the samples spin system between the two methods. They confirmed that the cooling rate effect biases the results from microwave experiments and therefore it is just as important to correct for this in microwave studies as it is in thermal.

A cooling rate experiment was run on one sample of Drab Polished Ware, one sample of Red Polished Ware and three samples of Red Polished Philia Ware. Only a small number of cooling rate experiments were run as there were very few samples suitable as many samples showed alteration towards the end of the original archaeointensity experiment. Additionally, a number of samples had melt spots induced by the microwaves. Cooling rate experiments were only carried out on samples that showed neither sign of physical alteration (i.e. melt spots) nor evidence of alteration on the Arai diagram or orthogonal vector plots. Unfortunately no samples from Bellapais *Vounous* fitted these criteria so the cooling rate correction for these samples has been determined from a sherd of the same type (Red Polished Ware) from Marki *Alonia.* The cooling rate determined from one sample of Red Polished Ware and one sample of Drab Polished Ware was applied to all samples of this pottery type (Table 6.2). For samples of Red Polished Philia Ware where the cooling rate was determined directly then this was applied to the result. However, for samples of Red Polished Philia Ware where a cooling rate correction was not calculated directly, an average of the two determined cooling rates was calculated and applied.

Table 6.2: Calculated cooling rate corrections

Sample	Applied field	Intensity	Pottery type	fMW	Description of pot	Age (BC)
CEC4cr	56	66.80	RPW	0.83	Small open vessel	2250-2100
MPEC8cr	62	72.49	RPPW	0.81	Large closed vessel	2400-2250
MPEC12C	51	50.56	RPPW	0.95	Small open vessel	
MPEC9C	55	66.77	RPPW	0.82	Large-closed vessel	
EMCXcr	54	68.45	DPW	0.79	Medium to large closed vessel	2100-1900

Where sample refers to the sample from which the subsample was taken, Applied field is the field applied in the cooling rate oven, intensity is the intensity recorded by the sherd following the cooling rate experiment, Pottery type is the assigned pottery typology where RPW is Red Polished Ware, RPPW is Red Polished Philia Ware and DPW is Drab Polished Ware, fMW is the cooling rate correction factor, Description of Pot is the archaeological interpretation of the original pot the sherd came from, Age is the age range assigned to the samples based on their typology and context.

The method followed to determine the cooling rate correction involved 3 steps. The first step was a Coe method archaeointensity (AI) experiment, as previously described. During this step, the sample was demagnetised until 10% of the starting NRM remained. The Arai diagrams and orthogonal vector plots were then consulted and only samples which showed no evidence of alteration were selected for a cooling rate experiment. The second step was in a custom-made oven at the University of Liverpool Geomagnetism Laboratory where the samples were heated in a field to 600°C and held at temperature for 30 minutes. The oven itself has thick thermal insulation and no fan. The samples were then left to cool in the oven in a field for 24 hours as studies by Gomez-Paccard et al (2006) and Genevey and Gallet (2003) found that the choice of cooling time was not critical. The mean correction factors at 5, 10 and 30 hours were found to be roughly similar (Genevey et al., 2003) and using a longer cooling time only led to a small increase in the correction factors (Gomez-Paccard et al., 2006).

Finally, a repeat PI experiment was performed on the samples, again using the microwave system. The cooling rate correction factor, fMW was then calculated using the following equation from Poletti et al., (2013):

$$fMW = \frac{56}{AI\_CR} \tag{6.1}$$

where *AI_CR* represents the MW archaeointensity estimation, 56 is the laboratory field and the corrected archaeointensity (AIC) is given by:

$$AIC = AI.fMW \tag{6.2}$$

AIC is the product of the cooling-rate correction and the MW archaeointensity measured in the original AI experiment.

For a summary of all the experiments run on samples from Marki *Alonia* and Bellapais *Vounous*, please see table 6.3

Table 6.3

Site	Type	Sample Name	VFTB sample code	MW Demag Code	MW Coe Code	Repeat MW Coe	CR Code
Marki Alonia	Potsherd	CPEC1	MT-MA-CPEC1	CPEC1D	CPEC1I	-	-
		CPEC2	MT-MA-CPEC2	CPEC2D	-	-	-
		CPEC3	MT-MA-CPEC3	CPEC3D	-	-	-
		MPEC4	MT-MA-MPEC4	MPEC4D	MPEC4I	MPEC4R	-
		MPEC5	MT-MA-MPEC5	MPEC5	-	-	-
		MPEC6	MT-MA-MPEC6	MPEC6	-	-	-
		MPEC7	MT-MA-MPEC7	MPEC7D	MPEC7I	-	-
		MPEC8	MT-MA-MPEC8	MPEC8D	MPEC8I	-	MPE8CR
		MPEC9	MT-MA-MPEC9	MPEC9D	MPEC9I	PEC9RI	MPEC9C
		MPEC10	MT-MA-MPEC10	PEC10D	PEC10I	-	-
		MPEC11	MT-MA-MPEC11	PEC11D	PEC11I	-	-
		MPEC12	MT-MA-MPEC12	PEC12D	PEC12I	-	PEC12C
		CEC4	MT-MA-CEC4	CEC4-D	CEC4-I	-	CEC4CR
		ECMC5	MT-MA-ECMC5	ECMC5D	ECMC5I	ECMC5R	-
		ECMC6	MT-MA-ECMC6	ECMC6D	ECMC6I	-	-
		ECMC7	MT-MA-ECMC7	ECMC7D	-	-	-
		ECMC8	MT-MA-ECMC8	ECMC8D	ECMC8I	-	-
		ECMC9	MT-MA-ECMC9	ECMC9D	ECMC9I	-	EM9CR
		ECMC10	MT-MA-ECMC10	EMC10D	EMC10I	-	EMCXCR
		ECMC11	MT-MA-ECMC11	EMC11D	EMC11I	-	-
		ECMC12	MT-MA-ECMC12	EMC12D	-	-	-
		ECMC13	MT-MA-ECMC13	EMC13D	EMC13I	-	-
		ECMC14	MT-MA-ECMC14	EMC14D	EMC14I	-	-
		ECMC15	MT-MA-ECMC15	EMC15D	EMC15I	-	-
		ECMC16	MT-MA-ECMC16	EMC16D	EMC16I	-	EM16CR
		ECMC17	MT-MA-ECMC17	EMC17D	EMC17I	-	-
		CDPW9	MT-MA-CDPW9	CDPW9D	CDPW9I	-	-
		CDPW10	MT-MA-CDPW10	DPW10D	DPW10I	-	-

Site	Type	Sample Name	VFTB sample code	MW Demag Code	MW Coe Code	Repeat MW Coe	CR Code
Bellapais Vounous	Potsherd	BVEC1	MT-BVEC1	BVEC1D	BVEC1I	-	-
		BVEC2	MT-BVEC2	BVEC2D	BVEC2I	-	-
		BVEC3	MT-BVEC3	BVEC3D	BVEC3I	-	-
		BVEC4	MT-BVEC4	BVEC4D	BVEC4I	-	-
		BVEC5	MT-BVEC5	BVEC5D	BVEC5I	-	-
		BVEC6	MT-BVEC6	BVEC6D	-	-	-

Table 6.3: Site, Archaeological site where samples were found; Type, type of archaeological material studied; Sample Name, name given to the sample; VFTB sample code, name given to the subsample which underwent analysis on the VFTB; MW Demag code, name given to the subsample which underwent a demagnetisation experiment on the microwave; MW Coe code, name given to the subsample which underwent a Coe method microwave archaeointensity experiment; Repeat MW Coe, name given to the second subsample from the sample to undergo a Coe method microwave archaeointensity experiment; CR Code, name assigned to subsamples subjected to a cooling rate experiment.

6.6. Results

6.6.1. Archaeointensity Results

In total 13 samples from a sample set of 34 gave acceptable archaeointensity results, meaning the total success rate was 38%. Of these, five are Red Polished Philia Ware, one is Drab Polished Ware and eight were Red Polished Ware. Three successful results were recorded for samples from Bellapais *Vounous*, giving a success rate of 50% for this site. Ten successful results were recorded from Marki *Alonia* samples (table 6.4) resulting in a success rate of 36% for Marki *Alonia*. With the exception of two of the ten accepted results, all the samples showed evidence of a viscous remanent magnetisation which was typically removed at low power. The most commonly missed criteria was the DRAT criteria with 9 archaeointensity results rejected because they had a DRAT greater than 10%. This contributed to the failure of 13 samples to reach the CDRAT criteria of less than 11% alteration. One sample had a FRAC value lower than 0.35 and 2 samples had a DRATtail greater than 10%. One sample recorded an α of greater than 15%.(figure 6.4)

Applying a cooling rate correction reduced the standard deviation of the mean intensity from 4.7 μT to 4.0 μT for the Early Cypriot I-II period and from 5.9 μT to 3.2 μT in the Early Cypriot III/ Middle Cypriot I. However, the standard deviation about the mean intensity increased for the Philia Early Cypriot period from 10.2 μT to 11.0 μT. This is because unlike the other time periods where the cooling rate correction was a constant correction, for the Red Polished Philia Ware samples from the Philia Early Cypriot, three cooling rate corrections were calculated: 0.81, 0.82 and 0.95. These corrections were either applied directly to the sample for which they had been calculated or averaged to make an average correction of 0.86. This was then applied to those samples where it was not possible to directly calculate the cooling rate.

Age(BC)	Site	Type	Sample	F	N	β	FRAC	g	q	delCK	DRAT	CDRAT	α	MAD (fixed)	DRAT tail	γ	fMW	FCR	Ave. F	VADM
2400-2250	MA	RPPW	PEC12I	**69.9**	6	0.041	0.625	0.738	10.2	2.0%	2.1%	-3.7%	0.7	0.4	0.0	1.2	0.95	**66.4**		
			MPEC11I	**61.5**	9	0.074	0.709	0.841	6.4	3.9%	4.6%	-5.8%	1.6	1.0	0.1	6.6	0.86	**52.9**		
			MPEC8I	**60.7**	11	0.016	0.784	0.855	39.5	5.0%	4.5%	-9.9%	3.4	2.9	0.0	2	0.81	**49.2**		
			MPEC9I	**52.6**	13	0.018	0.751	0.911	34.1	1.6%	1.8%	1.2%	0.9	0.8	0.0	0.9	0.82	**43.1**		
			MPEC4I	**79.5**	9	0.057	0.489	0.855	8.1	3.4%	3.6%	-4.5%	0.8	0.9	0.1	2.7	0.86	**68.4**		
			CPEC1I	**42.5**	7	0.022	0.561	0.783	21.4	13.5%	17.8%	16.8%	0.9	0.6	0.1	0.2				
			PEC7IB	**59.8**	11	0.035	0.774	0.797	16.0	5.4%	5.1%	-16.2%	1.1	2.4	0.0	5.3				
			PEC10I	**90.9**	9	0.078	0.532	0.858	8.9	8.5%	5.3%	6.8%	6.3	3.5	0.0	1.2			***56.0±11.0***	***10.3***
				64.8±10.2																
2250-2100	BV	RPW	BVEC1I	**60.7**	15	0.025	0.789	0.919	27.3	8.0%	7.1%	8.0%	0.5	0.7	0.0	1.9	0.83	**50.4**		
			BVEC2I	**56.6**	13	0.046	0.834	0.901	14.8	4.7%	4.3%	4.9%	0.8	0.7	0.0	4	0.83	**47.0**		
			BVEC3I	**53.0**	6	0.059	0.382	0.751	4.6	2.0%	3.9%	-7.8%	6.6	1.3	0.0	2	0.83	**44.0**		
	MA		CEC4-I	**63.9**	10	0.012	0.850	0.871	59.7	6.5%	5.1%	2.1%	0.8	0.5	0.0	6.1	0.83	**53.0**		
	BV		BVEC5I	**70.4**	13	0.030	0.760	0.903	21.6	4.9%	4.1%	-15.0%	0.3	0.7	0.0	3				
			BVEC4	**77.2**	7	0.070	0.396	0.737	4.7	32.3%	41.1%	-49.5%	6.3	2.4	0.0	6.8			***48.6±4.0***	***8.9***
				58.6±4.7																
2100-1900	MA	DPW	EMC10I	**50.5**	8	0.011	0.524	0.851	40.0	2.2%	3.2%	2.5%	1.1	0.5	0.0	7.1	0.79	**39.9**		
			ECMC11I	**56.0**	7	0.071	0.541	0.799	5.4	3.7%	5.2%	-6.7%	1.9	0.9	0.1	6.6	0.79	**44.2**		
		RPW	EMC17I	**54.7**	8	0.020	0.454	0.846	16.5	2.7%	4.8%	-9.8%	0.7	0.3	0.0	4.8	0.79	**43.2**		
			ECMC5I	**61.2**	7	0.009	0.659	0.731	47.5	2.6%	2.9%	-5.1%	2.8	1.4	0.0	1.6	0.79	**48.3**		
			ECMC6I	**38.6**	7	0.058	0.652	0.768	8.9	15.1%	18.3%	18.9%	2.0	1.6	0.0	2.3				
		RPCW	ECMC8I	**29.8**	10	0.046	0.547	0.873	9.8	8.0%	13.5%	48.3%	1.9	1.2	0.0	31.3				
		RPW	ECMC9I	**29.5**	8	0.045	0.489	0.818	11.4	5.3%	7.5%	-23.2%	1.0	1.2	0.0	60.1				
		DPW	DPW10I	**59.8**	11	0.079	0.646	0.881	9.4	9.2%	7.3%	11.5%	15.1	9.1	0.0	41				
		RPW	EMC15I	**61.2**	10	0.039	0.612	0.858	11.3	13.0%	15.3%	-30.4%	1.2	0.9	0.1	4.7				
			EMC16I	**31.9**	10	0.064	0.473	0.844	6.3	11.1%	19.8%	-15.8%	3.2	2.2	0.1	5.7				
			EMC13I	**32.3**	8	0.068	0.280	0.846	3.3	4.0%	13.1%	-27.3%	2.4	0.6	0.0	2.4				
			EMC14I	**64.8**	7	0.036	0.354	0.762	6.7	10.8%	21.5%	11.5%	4.3	0.8	0.2	1.9				
		DPW	CDPW9I	**37.4**	11	0.034	0.593	0.877	16.1	8.1%	10.7%	22.0%	2.6	2.1	0.0	4.7				
				56.3±5.9															***43.9±3.2***	***8.2***

Table 6.4: Microwave archaeointensity results from potsherds from three different time periods. Rejected results are in italics. MA is for Marki Alonia samples, BV is for Bellapais Vounous samples; F is the calculated intensity; N number of points used to define a linear segment of the Arai diagram; β is the ratio of the standard error of the slope to the absolute value of the slope; FRAC is the NRM fraction used for the best-fit on an Arai diagram determined entirely by vector difference sum calculation; g is the gap factor; q is the quality factor; δCK is the maximum absolute difference produced by a pTRM check, normalized by the total TRM; DRAT, Maximum absolute difference produced by a pTRM check, normalized by the length of the best-fit line; CDRAT, cumulative DRAT; α, angular difference between the anchored and free-floating best-fit directions on a vector component diagram; MAD(fixed), Maximum Angular Deviation of the anchored directional fits to the paleomagnetic vector on a vector component diagram, DRATtail, Maximum absolute difference produced bya pTRM tail check, normalized by the length of the best-fit line; CR, Cooling Rate correction; Fcr, cooling rate corrected intensity value; Ave. F, Mean intensity for accepted archaeointensity results

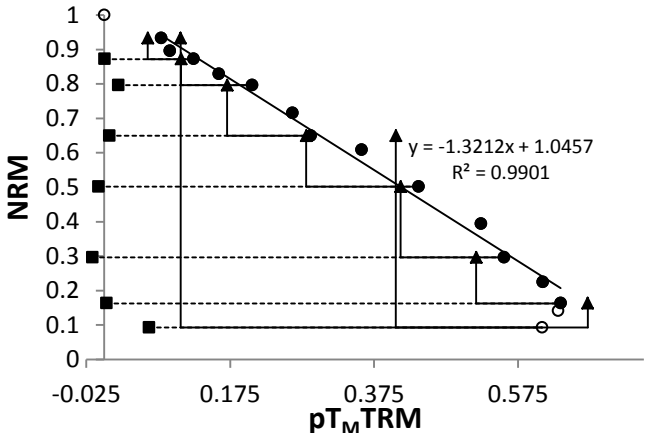
NRM
y = -1.3212x + 1.0457
R² = 0.9901
pTMTRM

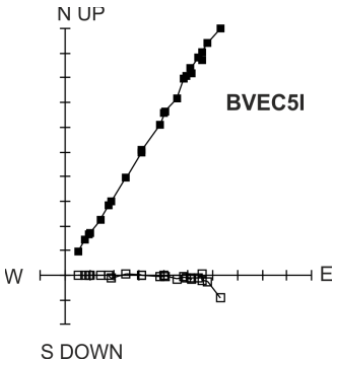
N UP
BVEC5I
W
E
S DOWN

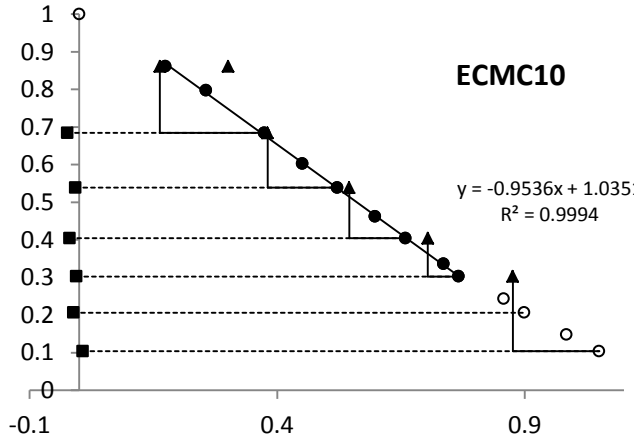
ECMC10
y = -0.9536x + 1.0351
R² = 0.9994

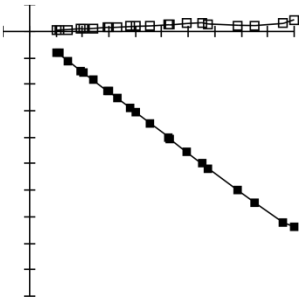

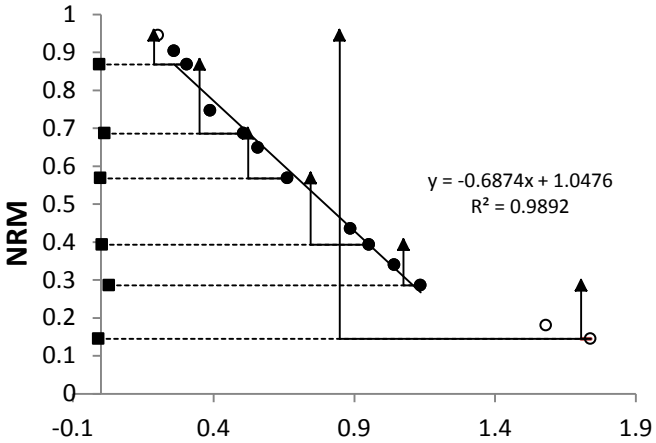
NRM
y = -0.6874x + 1.0476
R² = 0.9892

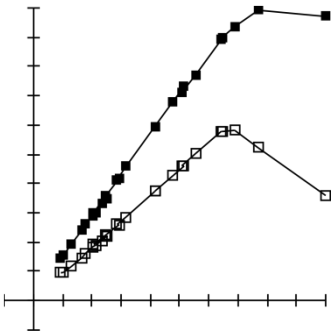

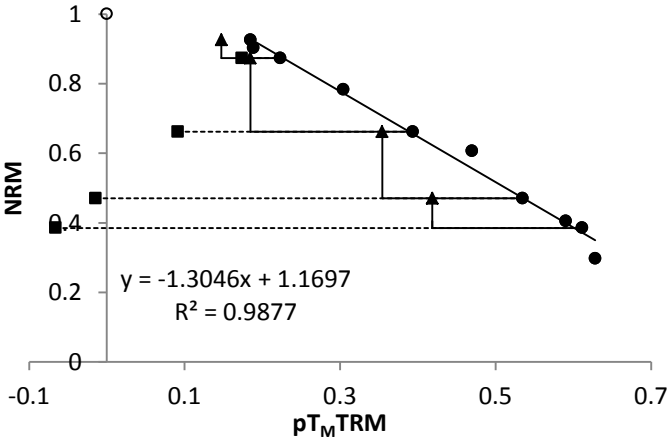
NRM
y = -1.3046x + 1.1697
R² = 0.9877
pTMTRM

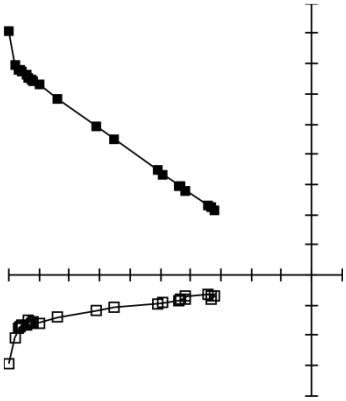

Figure 6. 4. Arai and Orthogonal vector plots for representative samples from Bellapais Vounous (a) and Markia Alonia (b-d). a) and c) were rejected for failing the CDRAT criteria, whilst d) failed the DRAT criteria. b) was accepted.

6.6.2. Influence of Pottery Typology on Archaeointensity Success Rate

There is no apparent pattern in the samples which were unsuccessful/ successful which could be related to pottery type as sherds from the two most populous wares in this sample set (Red Polished Ware and Red Polished Philia Ware) gave both successful and unsuccessful results. For the remaining three wares: Red Polished Philia Coarse Ware (1 sample in data set), Drab Polished Ware (1 sample) and Red Polished Coarse Ware (2 samples in data set) it is not possible to determine if the pottery type influenced their success rate as there were too few samples of each.

Four of the 34 samples were either from cooking pots or suspected of being from cooking pots. Of these, two samples were rejected at the demagnetisation stage as being unsuitable for archaeointensity analysis; one because it did not demagnetise towards the origin whilst the other was rejected because it did not demagnetise even when exposed to high power. The two other samples of cooking pots which were subject to an archaeointensity experiment gave very poor results, typically with high CDRATs implying significant alteration occurred during the experiment.

6.6.3. Consistency of Archaeointensity Values

Repeat archaeointensity experiments were conducted on sister sub-samples for three samples to check for within sherd consistency. The subsamples were cut from within 10mm of the first subsample (see table 6.5). The three samples which were studied were MPEC4 and MPEC9 from Philia Early Cypriot and ECMC5 from Early Cypriot III/ Middle Cypriot I. The five accepted samples from Philia Early Cypriot have a large range of 25µT. The samples MPEC4 and MPEC9 represent the maximum and minimum values from this time period. Sample ECMC5 gave the highest intensity value for the time period Early Cypriot III/ Middle Cypriot I. The aim of these within sherd consistency tests was to determine to what extent this range in values was accurate.

Using the two archaeointensity values measured in the experiments on the subsamples, the mean archaeointensity value is calculated at the sherd level. The criteria applied by other authors e.g. Gallet et al. (2006) when considering three subsamples from a sherd is

that the mean intensity value for a sherd must have a standard deviation of the mean value of less than 5 μT or <10% of the mean. In this instance we only considered 2 subsamples per sherd, and each of the three samples had a standard deviation >5(μT) of the mean archaeointensity value. However, two of the samples (MPEC4 and ECMC5I) had percentage of the error of the mean of less than 10% (7.4% and 9.8% respectively). The average intensity value for each sherd is used in the calculations of the average archaeointensity value for each time period. Rejecting these three values because they had mean values greater than 5 μT did not change the intensity value determined for the Philia Early Cypriot Phase (56.8 ± 8.8 without the values and 56.0±11 with them) and changed the value for Early Cypriot III/ Middle Cypriot I by 1.5 μT (from 43.43 ±2.3 without sample ECMC5I to 43.9±3.2 with ECMC5I). As a consequence of this and because an average of two results is too small a sample set to give a true average, all results which passed the modified SELCRIT criteria were used in the determination of the average field value over this time.

Table 6.5

Sample	**F1(μT)**	**F2(μT)**	**Mean F (μT)**	**% of the mean**
MPEC4	75.3	83.7	79.5±5.9	7.4%
MPEC9I	47.7	57.5	52.6±6.9	13.1%
ECMC5I	65.4	56.9	61.2±6.0	9.8%

F1, archaeointensity calculated in the initial archaeointensity experiment; F2, archaeointensity calculated for a sister sample from the same sherd; Mean F, average intensity value for the sherd reported with one standard deviation; % of the mean, standard deviation of the mean intensity expressed as a percentage of the mean.

6.7. Discussion

Considering their use in antiquity the low success rate for pot sherds from cookery pots is perhaps unsurprising. Cooking pots are subject to considerable physical stress from repeated handling, as well as thermal stress caused by the effects of expansion and contraction during use on the cooking fire (Webb and Frankel, 2004). Therefore it is not thought that these samples were capable of stably recording the geomagnetic field. It has not been possible to determine how the other samples were used in antiquity but it is theoretically possible that the use of a pot in antiquity would dictate its potential success rate during archaeomagnetic experiments. It would have been interesting to explore to what extent the use of a pot in antiquity influences it ability to reliably record the magnetic field with a particular focus on cooking pots, unfortunately time did not permit such a study.

It is unclear why there is a difference in the calculated cooling rate corrections when the samples were from the same time period, archaeological site and composed of the same pottery typology. However, it may represent normal variation as the difference between the two cooling rate values is 0.14 which is a difference of 16%. As only a restricted number of samples were analysed to give a cooling rate correction it is difficult to know what the normal distribution of cooling rate values would be for this sample set. However, we saw in the hypocaust samples in Chapter 4 differences in the cooling rate of 16.4% between the largest correction applied (16.9%) and the smallest correction (0.5). It would be expected that depending on the relative position of the samples within a kiln they would cool at slightly different rates so a certain amount of variability is to be expected.

Alternatively if the differences in the calculated corrections are not due to natural variation in cooling rate the observed difference could be due to differences in the pottery. It was common for local craftsmen to imitate the style of fashionable imports. For example, at Tell Atchana there were a number of black and white sherds found and identified as Nuzi Ware. Nuzi Ware is named after its location of origin: Nuzi, a Mesopotamian city in modern day Iraq. However, a study by Erb-Satullo et al. (2011) on the chemistry and mineralogy of the Nuzi Ware discovered at Tell Atchana revealed that it was not imported from Nuzi but was actually made locally. Whilst no Nuzi Ware was studied as part of this thesis it does provide an interesting example of the difficulty faced when identifying pottery. Pottery may look the same but be chemically distinct.

The average intensity decreased over the time period from 56.0±11.0μT between 2400 BC and 2250 BC to 43.9±3.2μT between 2100 BC and 1900 BC (figure 6.5). This 13 μT intensity decrease over a 200 year period is consistent with previously published data (Genevey et al., 2003, Gallet and Butterlin, 2014, Gallet and Le Goff, 2006, Gallet et al., 2014, Gallet et al., 2008) gathered from archaeological sites across Syria, Turkey and Iran (figure 6.6) and with the data gathered for this thesis from Tell Atchana and Kilise Tepe, and is well within the limits calculated by Livermore et al(2014) for maximum core flow. The calculated virtual axial dipole moments (VADMs) are consistent with data from GEOMAGIA50v2 (Donadini et al., 2006, Korhonen et al., 2008) based on data from Turkey and Greece.

Figure 6.5

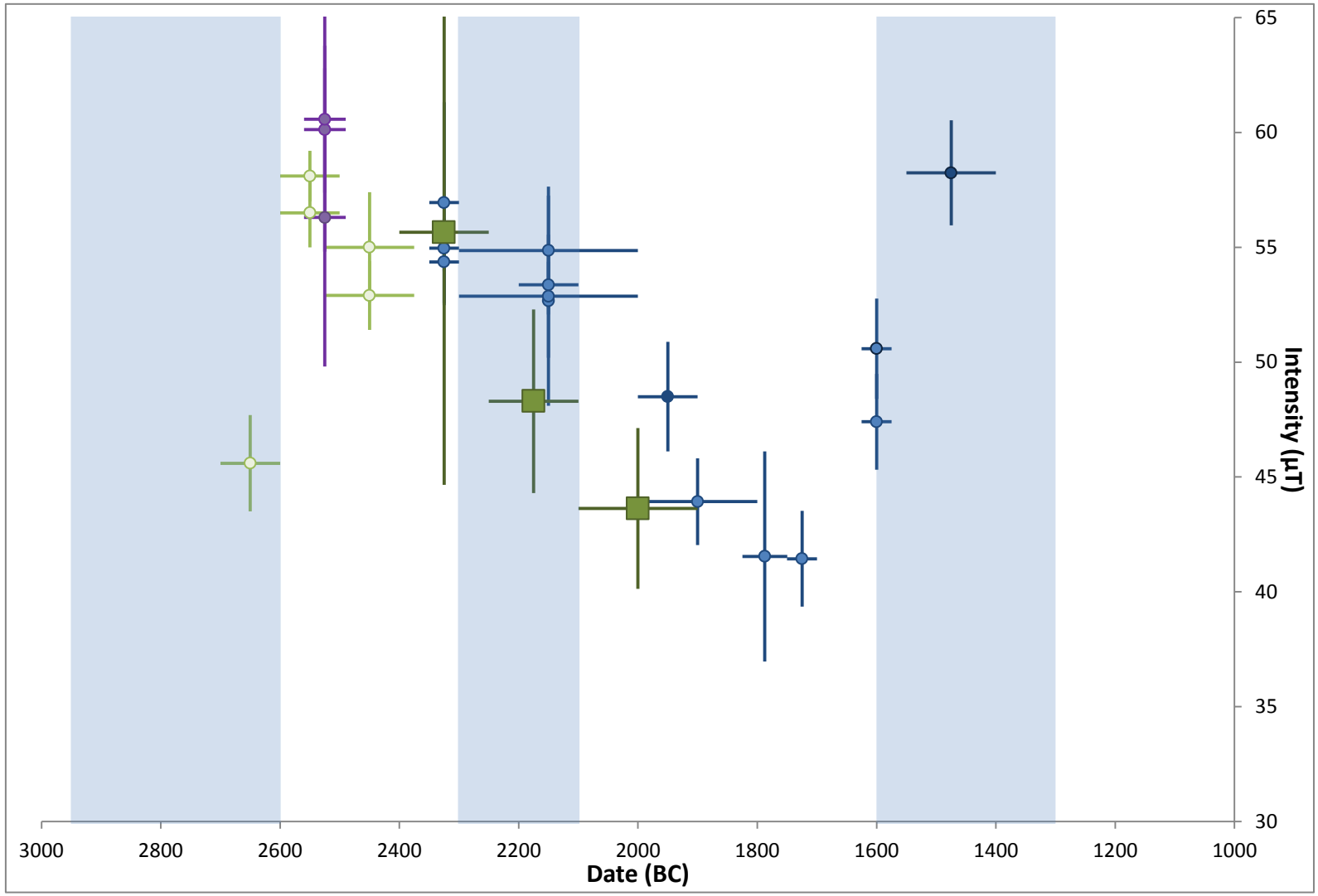
65
60
55
50
45
40
35
30
Intensity (µT)
3000
2800
2600
2400
2200
2000
1800
1600
1400
1200
1000
Date (BC)

Figure 6.6

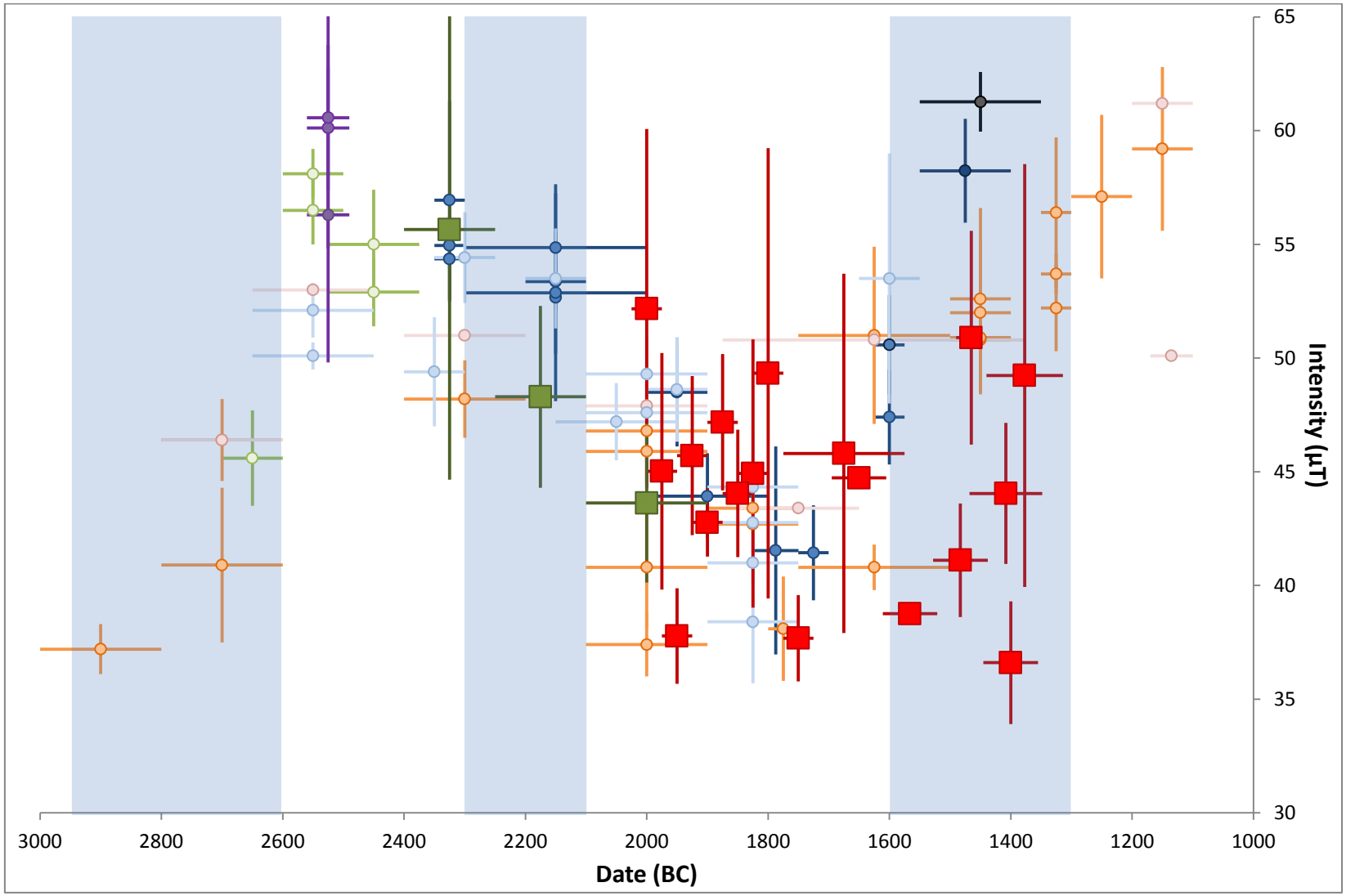
65
60
55
50
45
40
35
30
Intensity (µT)
3000
2800
2600
2400
2200
2000
1800
1600
1400
1200
1000
Date (BC)

Figure 6.5: Archaeointensity data obtained from Cyprus (this study, dark green squares) and Syria, Ebla blue circles (Gallet et al 2014) and Mari, pale green circles, (Gallet and Butterlin, 2014).. All results have been relocated to Mari in Syria. For this study the vertical error bars are one standard deviation plus and minus the mean of the age estimate. The values themselves have been plotted in the middle of the age estimate so the horizontal error bars indicate the range of the age estimate. The blue vertical bars represent cooling periods in the North Atlantic as discussed in Gallet et al. (2003).

Figure 6.6: Archaeointensity data from this study and recent data from Syria, Iran and Turkey. All results have been relocated to Mari, Syria. The dark green squares is data from Marki Alonia, dark blue circles, (Gallet et al,. 2014), pale green circles, (Gallet and Butterlin, 2014), orange circles, (Gallet et al., 2006), pale blue circles, Gallet et al (2008), black circe, Gallet and Al-Maqdissi (2010), pink circles, Genevey et al (2003), purple circles, Ertepinar et al (2012), red squares, Tell Atchana (as reported in chapter 5). Horizontal error bars are errors associated with the age estimate whilst the vertical error bars are one standard deviation plus and minus the mean of the intensity estimate. The blue vertical bars represent cooling periods in the North Atlantic as discussed in Gallet et al. (2003).

Gallet and Butterlin (2014) state that there were two relative intensity maxima during the Early Bronze Age of the near east. The first was during the 26th Century BC which had a magnitude comparable to that obtained at Arslantepe in Turkey by Ertepinar et al (2012). The second maximum was between 2300 and 2000 BC and is documented by archaeomagnetic data obtained at Ebla/ Tell Mardikh (Gallet et al., 2014, Gallet et al., 2008). The samples studied here cover the same time period as this second maximum and do not show evidence of an intensity maximum. We suggest three possible explanations for this. Either the maximum was short lived thereby making the chances of sampling material which records this maxima small, the samples studied here are from a later time period then the relative maxima or the existence of a maxima was exaggerated. The second explanation is supported by figure 5 in Gallet and Butterlin (2014) which suggests that the intensity maxima occurred at the beginning of this time period (although this is not explicitly stated in the text).

Our data also do not support the theory that an archaeomagnetic jerk (defined as a period of intensity maxima coinciding with a sharp cusp in geomagnetic field direction (Gallet et al., 2003)) occurred between 2100-1900 BC (Gallet et al., 2006, Gallet and Le Goff, 2006) unless it was an exceptionally short lived event. We do not rule out the possibility that the archaeomagnetic jerk occurred earlier than this time, however, (prior to 2300 BC). We find this period to show an overall decreasing intensity and this is supported by the findings of Gallet and Butterlin (2014) and Gallet et al, (2014). This overall decreasing trend may potentially be punctuated by short lived relative intensity increases. Other work in the Middle East (e.g. Ben-Yosef et al., 2009, Shaar et al., 2011) has proposed very short lived extreme intensity changes on the order of 20-30 years which may explain why this study does not see the intensity maxima as it would be exceptionally lucky to sample potsherds which recorded such a short lived event.

6.8. Conclusions

The results presented here are very consistent with previously published data for the period ~2400 -~1900 BC from neighbouring countries; Greece, Turkey, Syria and Iran. Although previous interpretations of the behaviour of the field over this time period have suggested there was a period of relative intensity maxima between ~2300-1900 BC, this was not found in this data set. The overall trend over this time period was one of decreasing field intensity.

Whilst only a small sample set was considered the poor quality of the results from cooking pots suggests that cooking pots may not be suitable for archaeointensity analysis. This would benefit from further, detailed study.

6.9. Appendix 1: Details of Pottery Wares

For photographs of the different pottery wares see Appendix 2

Red Polished Philia Ware (Marki *Alonia*)

Fine medium-soft yellowish brown fabric, usually with a thick dark grey core and few to medium small to medium-sized black, white and occasionally red inclusions and vegetable filler. For example, sample CPEC1

Red Polished Philia Coarse Ware (Marki *Alonia*)

Medium to coarse brown to strong brown fabric, medium-hard to hard with a dark core and a large number of small and medium white inclusions. For example, sample CPEC3

Early Cypriot I–II Red Polished Ware (Marki *Alonia*)

Medium-textured, hard or very hard brown or reddish brown fabric with many small and medium or small, medium and large black, brown and, in lesser numbers, white inclusions. For example, sample CEC4

Early Cypriot I–II Red Polished Ware (Bellapais *Vounous*)

Fine, medium-soft light brown to buff fabric with few to medium small and medium-sized inclusions and organics. For example, sample BVEC1

Early Cypriot III/Middle Cypriot I Red Polished Ware (Marki *Alonia*)

Fine, medium-hard light brown to buff fabric with few to medium small and medium-sized inclusions and organics. For example, sample ECMC5

Early Cypriot III/Middle Cypriot I Red Polished Coarse Ware (Marki *Alonia*)

A relatively coarse hard variety of Red Polished ware with a larger number of inclusions and a grey-black or black core. For example, sample ECMC7

Early Cypriot III/Middle Cypriot I Drab Polished Ware (Marki *Alonia*)

A fine, dense, medium-hard or hard fabric with medium to many quartz and calcareous inclusions. Fabric colour is typically yellowish-red frequently with a blue-grey core. For example, sample CDPW9

6.9. Appendix 2: Photographs of samples

Marki *Alonia* Samples

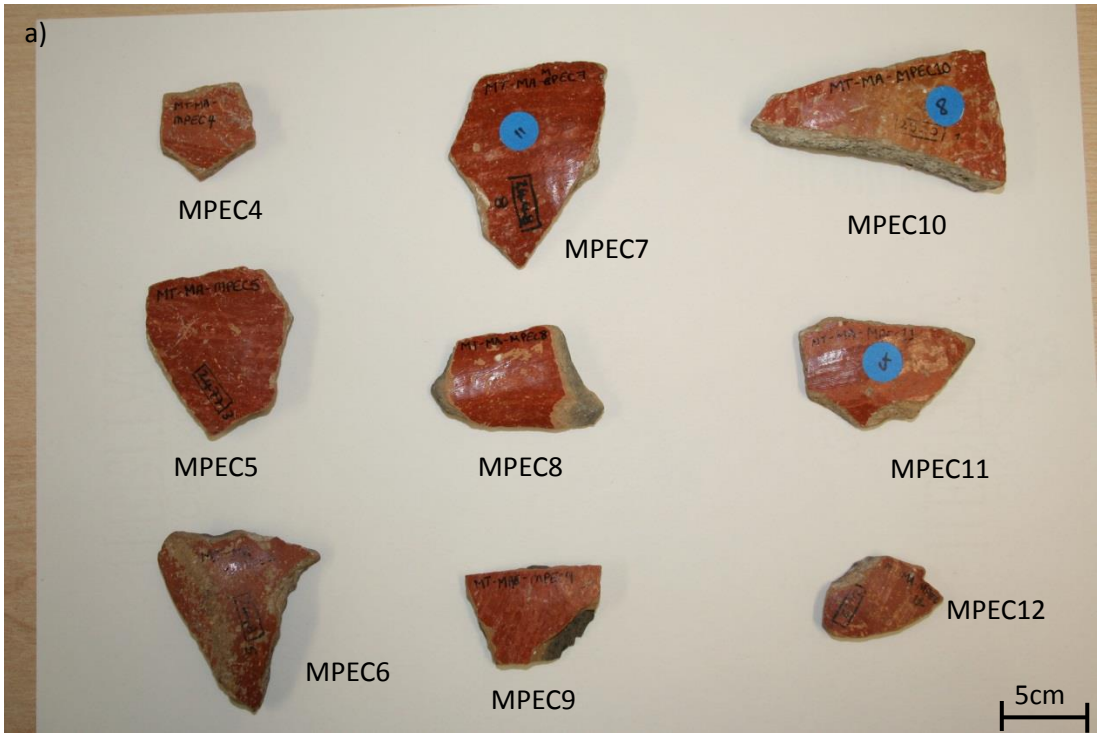

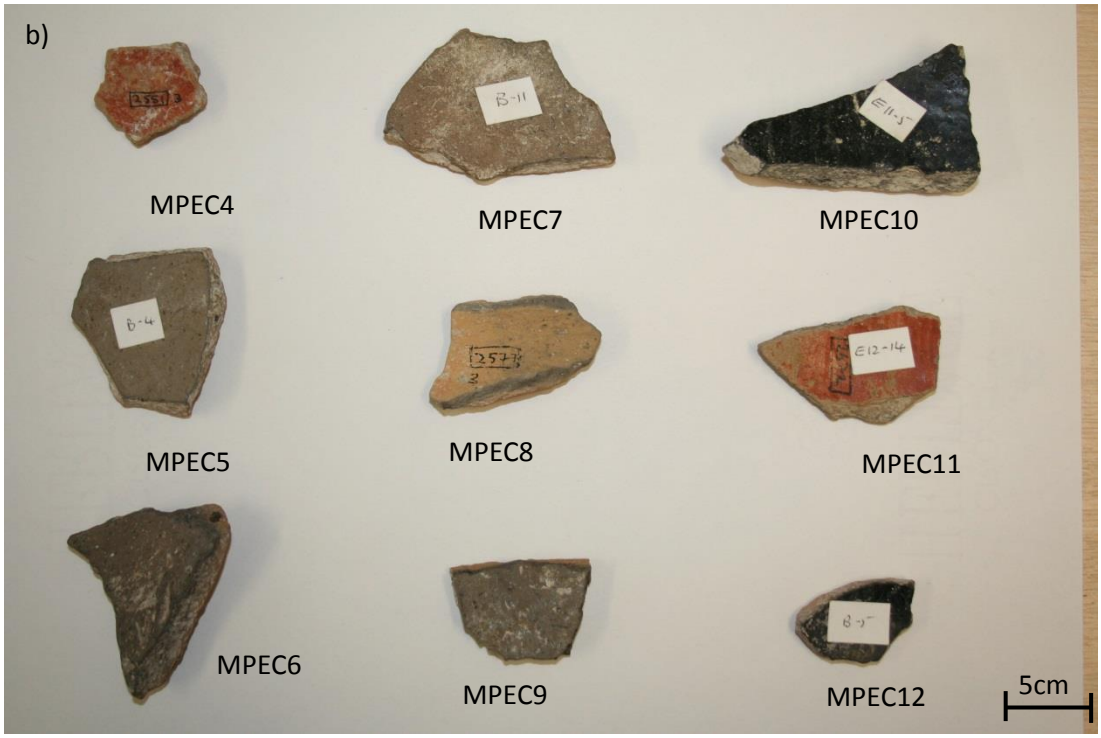

Bellapais *Vounous* Samples

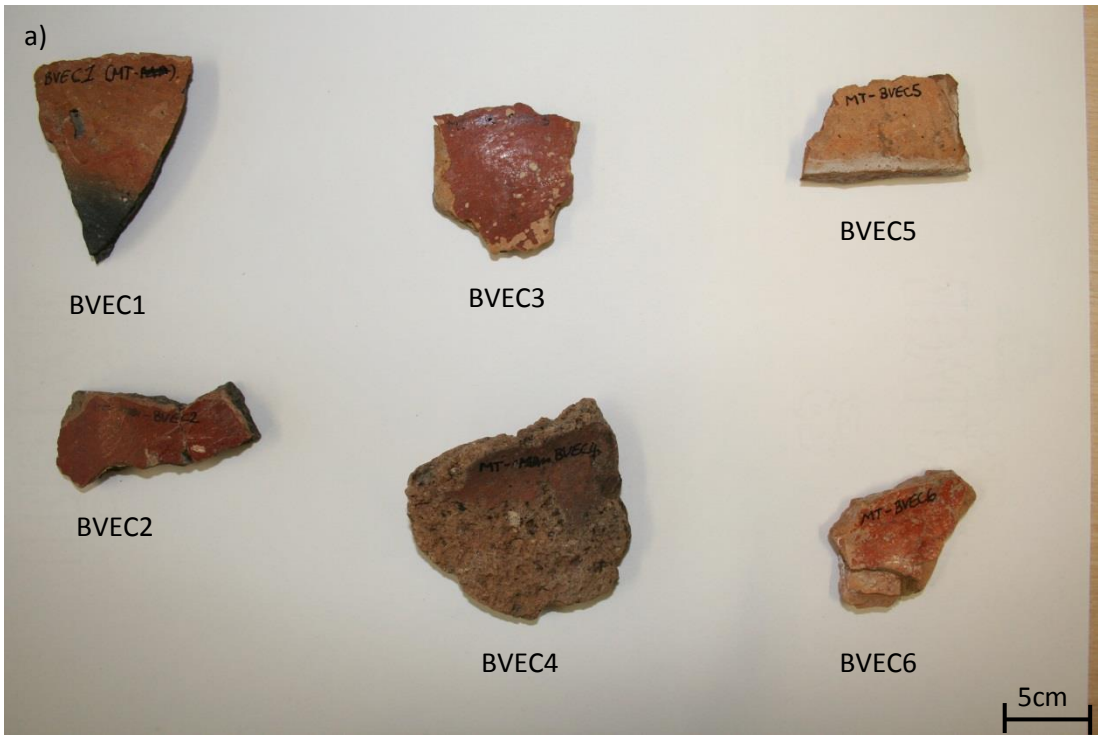

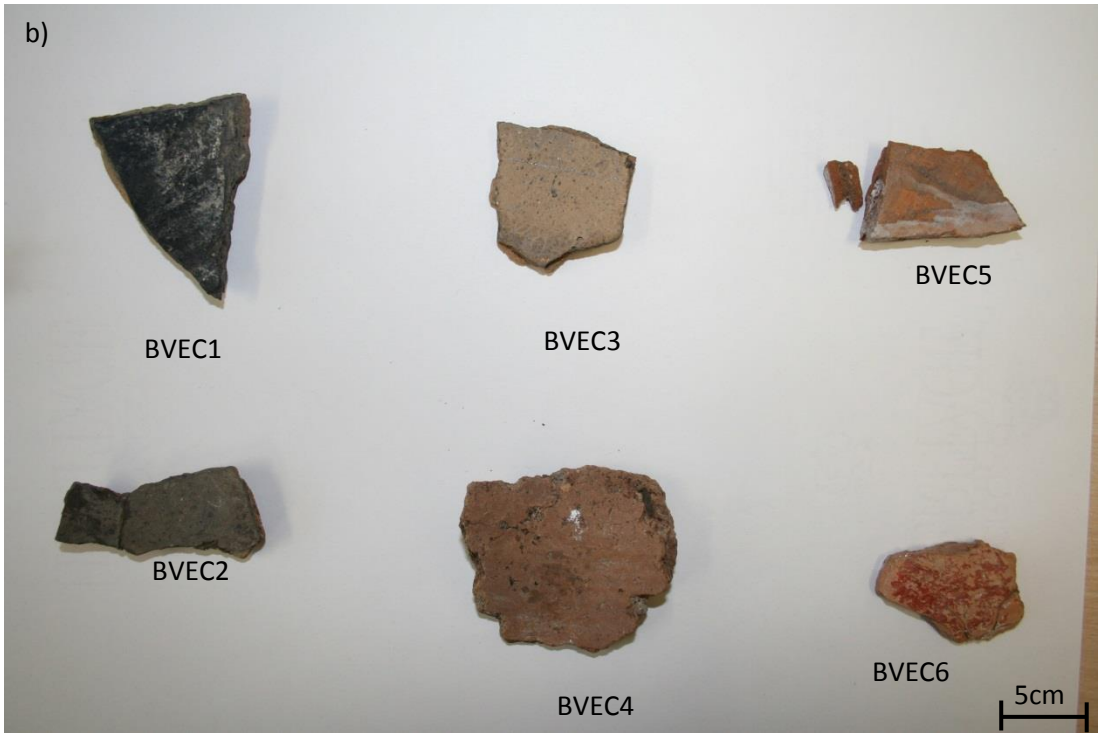

Marki *Alonia* Samples

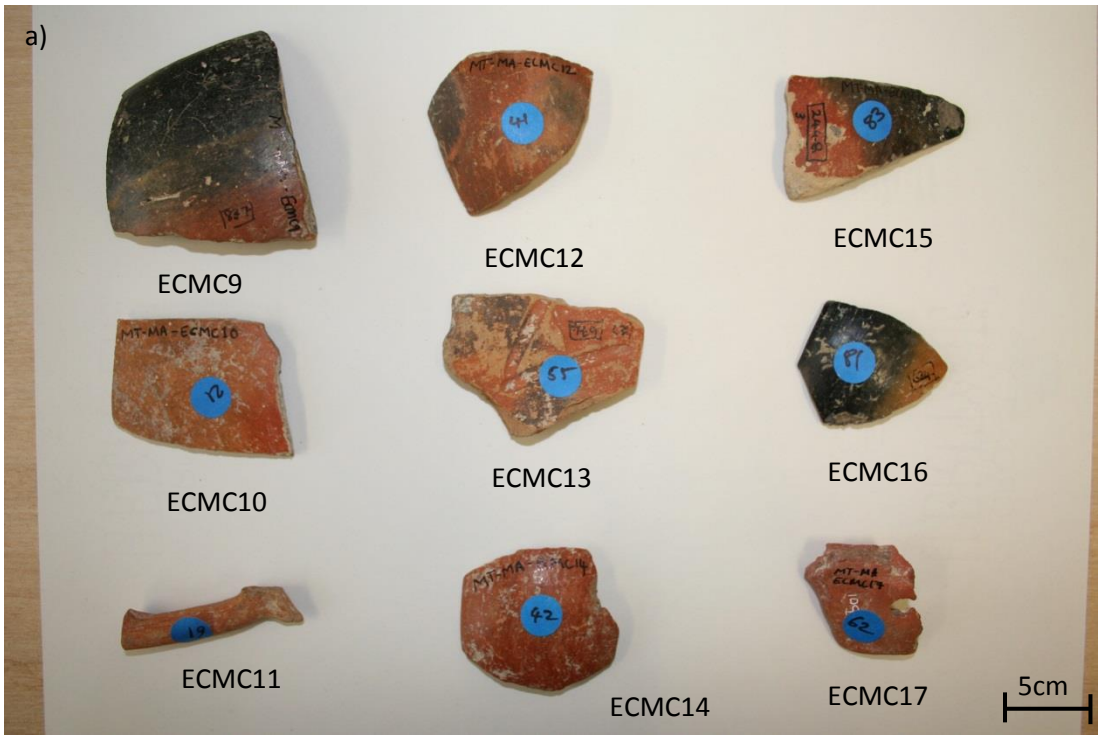

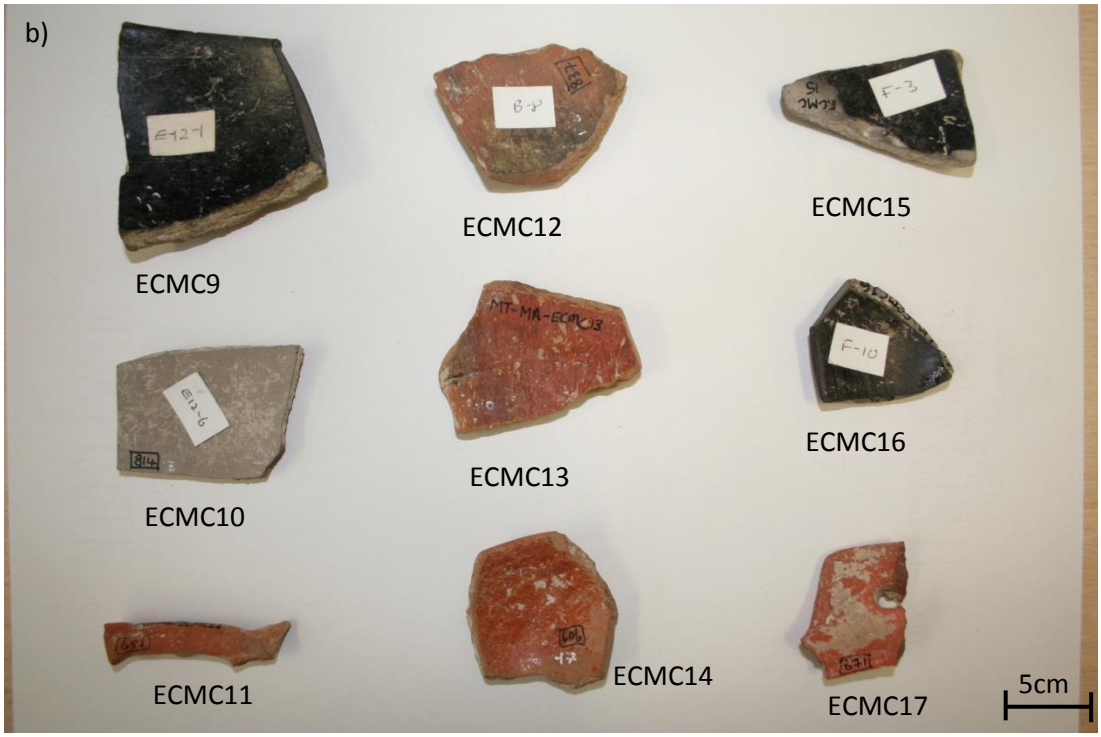

Photographs show the majority of the Marki Alonia and Bellapais Vounous potsherds with the sample names indicated next to the sample. Photographs labelled a) show one side of the sherds whilst b) shows the reverse of the same sample. Note the differences in decoration and thickness of the sherds analysed. Each photograph shows the sherds lying on a sheet of A4 paper

7. Discussion and Further Work

Archaeomagnetism can, and has been, used to answer a wide variety of geomagnetic and archaeomagnetic questions. This thesis aimed to demonstrate some of the variety of potential applications of archaeomagnetism through three discrete aims:

1. To use the magnetic signature recorded in samples from an unidentified burnt feature (most likely a kiln) from the Oylum Höyük archaeological site in Turkey to determine the temperature this feature reached in antiquity and, therefore, establish what materials the kiln was producing.
2. To use archaeomagnetism to date construction events at the St Jean Poutge archaeological site.
3. To determine to what extent the magnetic record contained within pottery samples from Turkey and Cyprus confirms or refutes the occurrence of archaeomagnetic jerks and geomagnetic spikes.

7.1. Archaeological Applications of Archaeomagnetism

In chapter 3, archaeomagnetism was used to establish the maximum temperature reached at the base of a kiln at the Oylum Höyük archaeological site. The objectives of the study at Oylum Höyük were to determine the maximum temperature reached in this kiln using thermal demagnetisation experiments in association with an analysis of the samples' rock magnetic properties and the temperature at which alterations of these properties occurred. This was necessary because the baking oven, the lime kiln, the glass furnace and the bath furnace all technologically resemble a ceramic kiln and/ or leave similar archaeological traces, making it very difficult to distinguish between them. However, the different kilns would have reached different maximum temperatures. A bread oven would have routinely been heated to between 300-500°C (Hasaki, 2002 and references therein) whilst a lime kiln would have been heated to 900°C (Zuideveld and van den Berg, 1971). It chapter 3 it was confirmed that the samples had previously been heated to between 600 and 700 °C and, therefore, the feature was not used as a bread oven. The temperature determined is a minimum temperature because of the following: a) the distance between the blocks and the heat source is unknown and b) the topmost surface of the blocks, which

would have been exposed to the most heat, was removed during the field sampling. It is not, therefore, possible to reject the hypothesis that the feature was a lime kiln.

A further objective of this work was to determine how many components of magnetisation were recorded in the samples using thermal demagnetisation experiments. Whilst we were able to confirm that Block 2 contained only a single component of magnetisation, we were not able to unambiguously confirm that the samples from Block 1 contained two components of magnetisation. The most significant difficulty associated with this work was the quality of the samples analysed. The mud bricks studied were generally poorly consolidated and very dry and required consolidation prior to experiment.

In chapter 4 it was demonstrated how archaeomagnetism can be used to corroborate (or dispute) the archaeological understanding of the evolution of a site. Based on the archaeointensity record it was possible to tentatively confirm the archaeological interpretation that the hypocaust and gutter, CAN4, from the Roman aged archaeological Site de la Molère in Southern France were constructed at a different time to other gutters found on the site, CANs 3 and 5. A maximum date for CAN4 (2nd century AD) and CANs 3 and 5 (3rd Century AD) was assigned to these features based on the archaeological interpretation. This *terminus anti quem* was indicated by the stratigraphic relationships on site. The average intensity determined for the hypocaust was 56±7 μT whilst for CAN4 it was 58±8 μT. In comparison, the average intensity for CAN3 was 68±6 μT and for CAN5 it was also 68±7 μT thereby confirming the different relative ages of the two construction events.

The results for this chapter demonstrated both the importance and difficulty of using corrections for anisotropy and cooling rate. In this chapter it was demonstrated how applying these corrections improved the consistency between results from different contexts e.g. prior to the application of corrections the average intensity for the hypocaust was 63±10 μT and for CAN4 it was 70±4 μT whilst after the corrections were applied the results were 56±7 μT and 58±8 μT respectively. However, at a context level, application of the cooling and anisotropy corrections did not necessarily reduce the spread of the data. For CAN4 applying anisotropy and cooling rate corrections increased the standard deviation of the mean for the data from ±4 μT to ±8 μT. The tiles used in CAN's3, 4 and 5 were originally designed to be used as roofing tiles so it is highly likely they were recycled for use in the gutters. It is possible that the tiles were fired in a variety of kilns at different times. Consequently, it is highly likely that individual samples contain non-identical intensity

values. Therefore, it is unsurprising that the application of corrections does not lead to a significant reduction in the spread of the data. It is noted, however, that the tiles are not thought to contain significantly different field values as there is no evidence to suggest they were fired far apart geographically or temporally. It is highly unlikely the bricks in the hypocaust were recycled, however, as here the bricks were square (rather than the more common rectangular shape) and therefore fired for a specific use in the hypocaust and highly likely to have been fired together. In the case of the hypocaust the application of an anisotropy correction reduced one standard deviation of the mean from 10 μT to 8 μT whilst the application of the cooling rate correction reduced this deviation further to 7 μT. Due to the relatively small number of successful samples from the hypocaust (4/26) it is not altogether surprising that the standard deviation of the mean for this context is still relatively high even after the corrections have been applied.

Difficulties were encountered in chapters 3 and 4 associated with the material studied. In chapter 3 the difficulty of using very dry, unconsolidated mud bricks was faced whilst in chapter 4 the praefurnium samples contained relatively few magnetic minerals making it difficult to distinguish the signal from noise. The difficulty of sampling kiln material in comparison with other archaeological material has been studied by previous authors e.g. Kovacheva et al. (1998). During the manufacture of pottery and bricks in ancient times the raw material was pre-selected (Kovacheva et al., 1998) . Consequently, bricks and pottery are, in general, more homogeneous and finer-grained than material taken from ovens and kilns with burnt soil layers containing the widest grain-size and mineralogical spectra of all studied archaeomagnetic material. In addition to this, kilns experience variable firing conditions which can produce heterogeneity in archaeomagnetic results (Spassov and Hus, 2006, Hrouda et al., 2003). The large difference in maximum heating temperatures and in the amount of secondary phases produced by hydration during burial within a particular feature are the major causes of non-uniformity in magnetic behaviour between individual specimens from kilns (Jordanova et al., 2003).

7.2. Experimental Success Rates

A common problem with determining archaeointensities and palaeointensities is low experimental success rates. A number of authors have tried a variety of techniques to increase success rates:

- Applying rigorous rock magnetism criteria prior to conducting archaeointensity experiments e.g. Thomas (1993)
- Applying demanding quality criteria to the final results (most recently reviewed in Paterson et al., 2014).
- Using different archaeointensity methods to reduce the potential for alteration during the experiment e.g.Hill et al. (2007), Le Goff and Gallet (2004) de Groot et al. (2013).

In this thesis, the microwave system was used (where possible) instead of conducting thermal experiments. The microwave system was utilised because sample alteration should theoretically be less in the microwave method than in thermal methods. During the microwave experiments the time the samples were exposed to microwaves was increased rather than the power of the microwaves, again to try to reduce alteration.

The consequence on data quality of applying stringent or more lenient criteria was also considered. It was found that the more lenient criteria gave very similar results to the stringent criteria whilst accepting a greater number of values. The more lenient criteria was, therefore, preferred. The Cumulative Difference Ratio (CDRAT) was found to be the most useful criterion for providing a quantitative basis to reject results where systematic alteration had occurred during the course of the experiment. The DRAT ratio was found to be less useful because all checks could pass this criterion and yet the checks could all fail in one direction indicating systematic alteration (and therefore the sample would fail the CDRAT criterion). Consequently, the Arai plot would be an overestimate or underestimate of the intensity. The criterion f was also useful at ensuring that a representative proportion of the magnetic signature in the sample was used to calculate the intensity. From the remaining criteria utilised, β was also found to a useful indicator of the quality of the result. There is a plethora of criteria used by palaeo- and archaeomagnetists, however, in the experiments conducted here it was found that the criteria CDRAT, f and β were most frequently used to reject a sample. In other words, if the sample passed the CDRAT, f and β criteria then in the vast majority of cases the sample passed all the other criteria as well.

There is also a debate about the cut-off values for each criterion and Paterson et al. (2014) has very usefully addressed this issue. The cut-off values recommended in Paterson et al. (2014) should be followed unless doing so rejects results which give values consistent with other accepted results and which only just fail the criteria. In such cases a certain amount of common sense can be used as in chapter 5 where a higher cut off value for CDRAT was applied. This was only done because doing so meant more data were accepted, improving the confidence in the result without significantly changing the average values calculated.

Another potential way to evaluate the data, which was not done due to time restrictions, would be to use the Thellier GUI program proposed by Shaar et al. (2013). This program takes the raw data and processes a number of potential manifestations of the Arai plot (by varying which points on the plot are included in the calculations of intensity) and determines the most consistent result for each context by looking at all the results for that context. Theillier GUI has the advantage of being subjective and removes human error or bias. It also enables fast processing of large datasets so would be ideal for the analysis of the Tell Atchana potsherds. It would be particularly interesting to compare the Tell Atchana data set processed manually with the Tell Atchana data set processed using Theillier GUI. Ideally there would be no differences between the two but as this is highly unlikely it would be very interesting to study where they differ and why.

Whilst rigorous rock magnetism criteria are valuable in reducing the number of inaccurate archaeointensity experiments which are accepted, there is such a variety in the natural world that the likelihood of rejecting potentially successful samples is significant. Using the multiple-specimen method (Hoffman and Biggin, 2005) it is possible to analyse samples with a variety of grain sizes. This is in stark contrast to the Thellier-Thellier (Thellier and Thellier, 1959) technique and its variants (e.g. Coe Method (Coe et al., 1978), Microwaves (Shaw and Share, 2007)) which are based on single domain theory. The multiple-specimen method can therefore be applied to a much greater variety of samples than the more traditional Thellier-Thellier techniques. This method removes the need for rigorous pre-archaeointensity experiment rock magnetism criteria. It also reduces alteration by minimising the number of heating steps to which each sample is subject to. An additional benefit is that only samples with internal consistency are accepted, thereby increasing confidence in the reliability of the sample and the result. The only drawback is the amount of material required for analysis (at least five subsamples). The samples from Kilise Tepe were exceptionally small and the maximum number of microwave subsamples cut from the

smallest sample was three. If time and sample size had permitted we would have tried the multiple-specimen method on the Tell Atchana, Kilise Tepe and the Cypriot potsherds because alteration towards the end of experiments was a common problem despite using the Microwave system to reduce alteration. Additionally, time prevented many within-sherd consistency tests from being carried out, therefore, using this method would enable us to confirm if the intensity values contained within a sample were internally consistent. This would increase our confidence in the existing data set. It is acknowledged that generally we did not find evidence of multidomain grains in our samples so the other advantage of this method is redundant here.

The quality of the data produced by the Triaxe system is also exceptionally high (Le Goff and Gallet, 2004) as is the within sample consistency reported by authors using the Triaxe system e.g. Gallet et al. (2014). In order to increase our confidence in our results from Turkey (and again to try to carry out experiments with minimal alteration) we would like to use the Triaxe system on the Tell Atchana Kilise Tepe, Marki *Alonia* and Bellapais *Vounous* pot sherds. It would also be advantageous to carry out more within sherd consistency tests as this may eliminate some of the results which have caused such a large spread in the data.

7.3. Geomagnetic Applications of Archaeomagnetism

In chapters 5 and 6 we considered results from a geomagnetic perspective and reflected on the evidence for dramatic, almost unprecedented changes in the strength of the geomagnetic field and what this might mean about the processes occurring within the Earth. The most striking of these changes is the 1000 BC event.

7.3.1. Discovery of the 1000 BC Event

In Gallet et al. (2003) the concept of "archaeomagnetic jerks" was introduced to the archaeomagnetic and geomagnetic community. These authors proposed that there were certain periods over archaeological time where geomagnetic field intensity maxima coincided with sharp cusps in geomagnetic field direction which they dubbed "archaeomagnetic jerks". Archaeomagnetic jerks have time characteristics intermediate between 'geomagnetic jerks' and 'magnetic excursions'. In this initial paper four jerks were proposed at ~800 BC, 200 AD, 800 AD and 1400 AD based on Western European and Eastern Mediterranean data. In Gallet et al. (2006) the apparent time coincidence between archaeomagnetic jerks and periods of cooling in the North Atlantic along with episodes of enhanced aridity in the Middle East and abrupt societal changes in the eastern

Mediterranean and Mesopotamia was noted. A mechanism proposed to link the magnetic field and climate involved the modulation of cosmic ray flux interacting with the atmosphere (Gallet et al., 2006). Also in Gallet et al. (2006) three additional, earlier, archaeomagnetic jerks at ~2800-2600 BC, ~2100-1900 BC, ~1750-1500 BC were proposed and further evidence of a jerk at ~1100-800 BC was presented. These archaeomagnetic jerks were found in data from Iran, Syria and Mesopotamia. It is noted that this second set of archaeoemagnetic jerks were identified based on intensity data from the Middle East and directional data from Swedish lake varves.

This was followed by Shaar et al. (2011) who recorded two short-lived double-peak "geomagnetic spikes" where (according to their chronology) the field changed rapidly from a Virtual Axial Dipole Moment (VADM) of 127±4 ZAm^2 to 204±12 ZAm^2 (104 μT) between 910 and 890 BC (coincident with the 1100-750 BC archaeomagnetic jerk proposed by Gallet et al., (2003, 2006)). The second peak proposed by Shaar et al. (2011) from 980-960 BC was marked by a peak in VADM from144±3 ZAm^2 to 189±3 ZAm^2 (possibly as high as 250 ZAm^2 (115μT) before dropping to 133±7 ZAm^2.

These three papers have sparked a number of big questions. Are archaeomagnetic jerks and geomagnetic spikes genuine features of the magnetic field and if so what mechanism is causing them? What is the geographic extent of these features? Is the magnetic field linked to climate and if so, by what mechanism? A flurry of work centred in the Middle East and in particular focused 1000 BC followed.

7.3.2. The 1000 BC Event and This Thesis

This thesis adds to this discussion by presenting evidence of high geomagnetic field strength (84.7 ± 6.2 μT/ 153 ZAm^2) in the Middle East between 800-600 BC, significantly later than has been found by other authors in the Middle East (Gallet et al., 2006, Ben-Yosef et al., 2009, Shaar et al., 2011, Ertepinar et al., 2012). In this thesis we have presented values of between 72 ZAm^2 (38.5 ±1.9 μT) and 153 ZAm^2 (84.7 ± 6.2 μT) for the field strength between ~2400 BC and ~600 BC gathered from mud bricks and potsherds from the Cypriot and Turkish archaeological sites Marki Alonia, Bellapais *Vounous*, Tell Atchana and Kilise Tepe (figure 7.1). A VADM of 153 ZAm^2 is nearly twice as large as the present field in Turkey of 81 ZAm^2 (47 μT). It is noted that the samples measured here did not cover the time period over which Shaar et al. (2011) observed the highest field intensity. The high field value reported is from sherds up to 300 years younger than the

geomagnetic spike (Shaar et al., 2011). This discrepancy can be explained in two ways. Either there was another, more recent high field intensity event, or the geomagnetic spike lasted longer than has been proposed by Shaar et al. (2011). A third hybrid solution is that the geomagnetic spike was felt at different times in different locations. There is additional evidence that the strength of the magnetic field in Turkey was high at 1050 ± 150 BC provided by Ertepinar et al. (2012). We need more data from Turkey for before and after the event before we can confirm how long the field remained elevated. The high field value we measured does overlap the end of the period proposed by Gallet et al. (2006) for an archaeomagnetic jerk at 1100-750 BC.

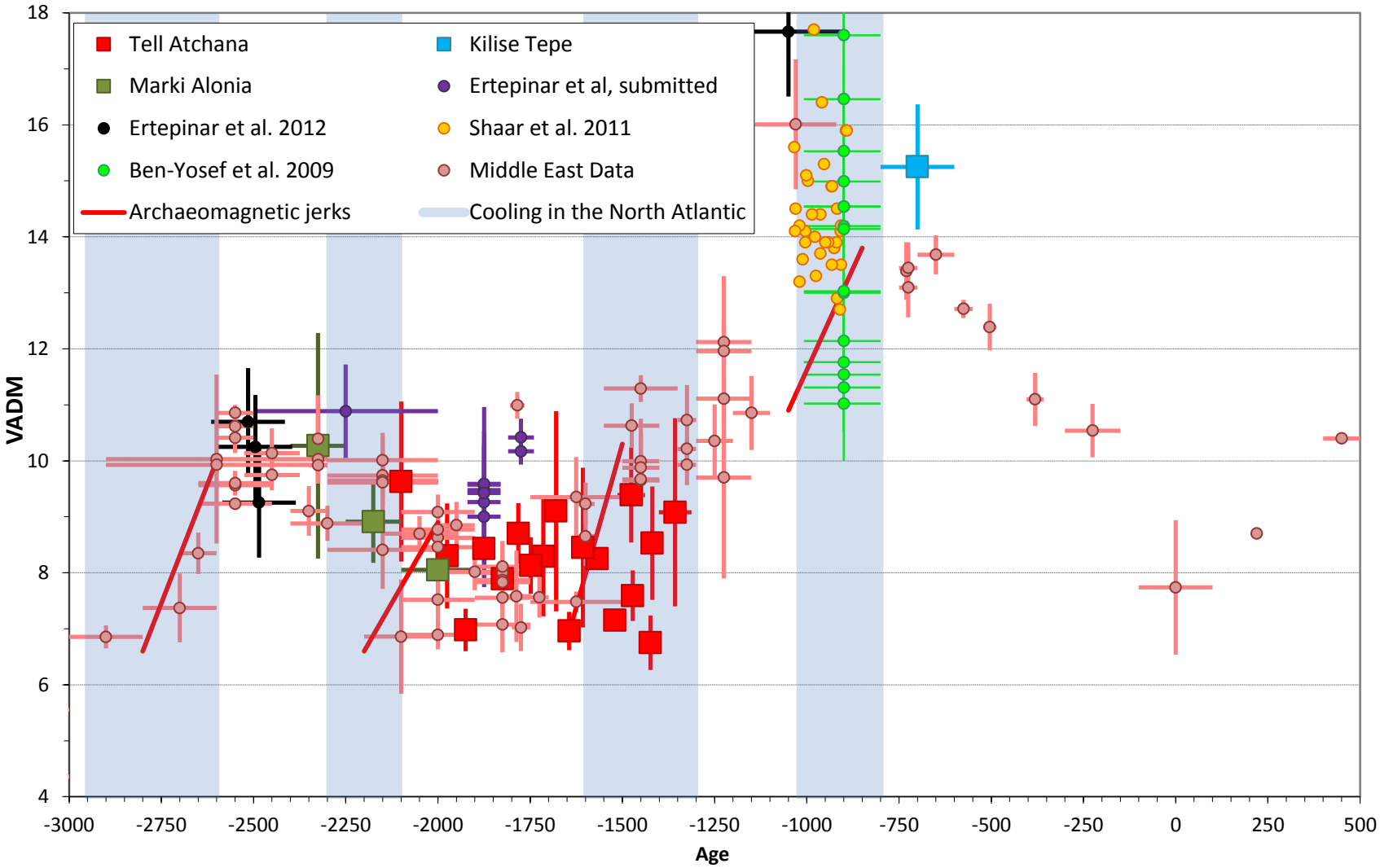
Tell Atchana
Kilise Tepe
Marki Alonia
Ertepinar et al, submitted
Ertepinar et al. 2012
Shaar et al. 2011
Ben-Yosef et al. 2009
Middle East Data
Archaeomagnetic jerks
Cooling in the North Atlantic
VADM
Age
18
16
14
12
10
8
6
4
-3000
-2750
-2500
-2250
-2000
-1750
-1500
-1250
-1000
-750
-500
-250
0
250
500

Figure 7.1: This figure is a redrawing of figure 4 from Gallet et al(2006) where the pink circles are data from Gallet et al. (2006), Gallet et al. (2008), Gallet et al. (2014) Gallet and Le Goff (2006) and Genevey et al(2003). The original figure only contained data from the latter two papers. The red squares are from Tell Atchana, the blue square is Kilise Tepe data and the green squares are from Marki Alonia (as reported in this thesis). Also plotted (Shaar et al., 2011) (yellow circles); (Ertepinar et al., 2012) (black circles); Ertepinar et al. (submitted to EPSL) (purple data) and (Ben-Yosef et al., 2009) (green data). Four proposed archaeomagnetic jerks from Iran, Syria and Mesopotamia (Gallet et al., 2006) are plotted as red lines. The blue columns indicate periods of cooling in the North Atlantic (originally reported in Gallet et al (2006)). Horizontal error bars represent errors associated with the age estimate whilst the vertical error bars are errors associated with the intensity estimate.

It is physically impossible to model the geomagnetic spikes proposed by Shaar et al. (2011) based on our current understanding of the generation of the geomagnetic field (Livermore et al., 2014). Our present limited understanding of the duration and geographic extent of geomagnetic spikes/ archaeomagnetic jerks must be resolved before we can fully understand the processes that generate them. If they are as rapid in duration as indicated by the temporal constraints of the copper slag heap measured by Shaar et al. (2011) then we have to invoke a field that behaves significantly differently from how we understand it behaves at present (Livermore et al., 2014). This itself raises a number of interesting questions: if the field has evolved significantly since 1000 BC, is it still evolving? How much has it evolved over geological time? How much can we trust the key pillar of geological theory that 'the present is the key to the past'? A much less controversial suggestion is that the field did not change as rapidly as suggested by Shaar et al. (2011). This conclusion involves either casting doubt on copper slag as a geomagnetic field recorder (the results from which have met strict quality criteria (Ben-Yosef et al., 2008b, Ben-Yosef et al., 2008a)) or we cast doubt on the archaeological dating of the copper slag.

7.3.3. Duration of the 1000 BC Event

The two key findings of this thesis are 1) the field experienced in Turkey and Cyprus between 2400 BC and 1200 BC varied between ~37 µT and ~53 µT and 2) the field in Turkey between ~800-600 BC was nearly double this at ~84 µT. This period of relative geomagnetic stability prior to the high is in contrast to the findings of Gallet et al. (2006). Gallet et al. (2006) proposed that the field increased by a factor of two in an irregular fashion over this time period, beginning with a strong increase between ~1750 and 1500 BC followed by a moderate increase between 1500 and 1200-1100 BC and finally another strong increase up to 750 BC. Whilst we do not find unambiguous evidence for the strong

increase in field strength between ~1750 and 1500 BC or evidence for a moderate increase between 1500 and 1200-1100 BC we do see a strong increase up to 750 BC.

We have identified two questions about the duration of this event that need to be answered. First, how quickly was this field high reached? Second, how quickly did it decay back to pre-elevated field strength values? Based on the timescales proposed by Gallet et al. (2006) and Shaar et al. (2011) the cartoon seen in figure 7.2 was plotted.

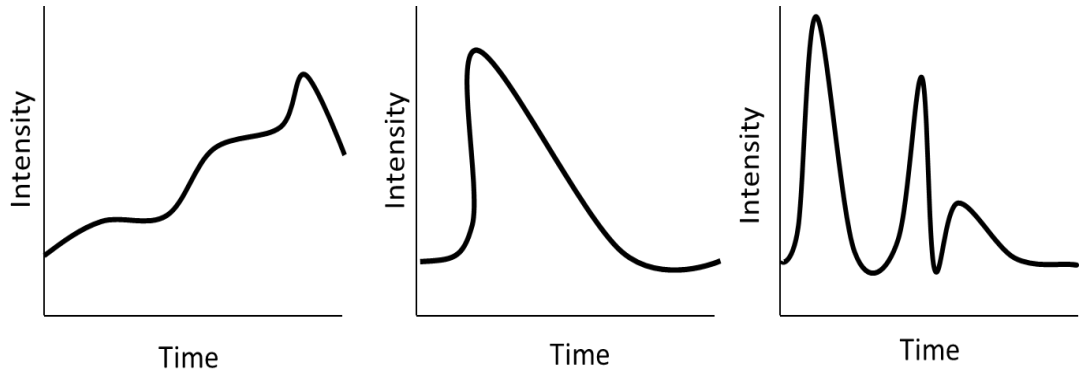

Figure 7.2: Possible pattern in field strength changes experienced in the Middle East around 1000 BC. a) was proposed (Gallet et al., 2006) and shows a staggered increase b) shows the trend favoured here which is for a relatively sudden increase in intensity followed by a long decline. c) is a redrawing of figure 5a from (Shaar et al., 2011) who proposed a double peak in intensity, both peaks increased and declined rapidly.

Did the field strength increase in a staccato fashion as proposed by Gallet et al. (2006) (figure 7.2a) or did it increase quickly and decay slowly as in figure 7.2b? Alternatively did it increase and decay twice quickly as proposed by Shaar et al. (2011) (figure 7.2c). Based on the results presented in this thesis, the curve proposed in b is preferred as no evidence of an increasing field prior to 1200 BC was found here. As evidence of high (although not as high as reported by Shaar et al. (2011) for 1000 BC) geomagnetic field strength at ~700 BC is also reported here, we therefore believe the feature endures for at least 300 years or decays over 300 years as this is more consistent with our current understanding of geomagnetic field behaviour.

These three possible scenarios invoke different mechanism within the core. Before the mechanism which generated this feature can be established, it is essential that the geographic extent of the event is determined. Was it confined to the Middle East or was it

felt throughout Europe? If it was global in extent then different core processes must have been occurring in the Earth than if it was a localised feature centred on the Middle East.

7.3.4. Determining the Geographic Extent of the 1000 BC Event

There is evidence of high field intensity from Turkey (Ertepinar et al., 2012) Syria and Iran (Gallet et al., 2006) Israel (Shaar et al., 2011) and Jordan (Ben-Yosef et al., 2009). Some authors have proposed that there was a globally strong geomagnetic field circa 3000 years ago. For example Hong et al. (2013) report intensity values from South Korea 40% larger than the present value. Additionally a high of 130ZAm^2 is reported from Eastern China (Cai et al., 2014) at 1300 BC following a low of 20 ZAm^2 at 2250 BC. This again implies rapid changes in archaeointensity (a 6 fold change over 1000 years).

However, there is no evidence for exceptionally high field strength found in the extremely well studied neighbouring Bulgaria. Such an exceptional level of study is primarily due to the prolific work of Mary Kovacheva. The highest field intensity recorded in Bulgaria was at 0 BC (Kovacheva et al., 2014). It is striking that whilst the field strength in Bulgaria was increasing towards 1000 BC, it actually peaked at 0 BC. This lack of evidence from Bulgaria is difficult to explain. Either the 1000 BC event was a localised feature centred in the Middle East, with its effects diminishing with distance from its source. This may explain why the results from Ertepinar et al. (2012) and the results from Kilise Tepe are lower than recorded for Israel and Jordan (Ben-Yosef et al., 2009, Shaar et al., 2011). However, this does not explain the evidence from China and South Korea. We suggest two alternatives: either the event migrated rapidly eastwards or there were two simultaneous, localised, events occurring in the Middle East and East Asia. It is not yet possible to know if the high field strength was experienced in Cyprus as there is no intensity data gathered from this time period.

7.3.5. Mechanisms to Explain the 1000 BC Event

Potential mechanisms which have been invoked to explain the occurrence of archeomagnetic jerks include episodes of maximum geomagnetic field hemispheric asymmetry. During such episodes the evolution of the centre of the eccentric dipole reflects the production and gathering of flux patches at the core-mantle boundary within preferential hemispheres (Gallet et al., 2009). Dumberry and Finlay (2007) proposed they are a result of rapid changes in the direction of underlying azimuthal core flow near the surface corresponding to motion of the two high latitude flux lobes. This conclusion was

reached following an analysis of the CALs7k.2 model (Korte and Constable, 2005). Another potential mechanism to explain archaeomagnetic jerks is dipole tilt. Nilsson et al. (2011) noted that the timing of archaeomagnetic jerks appears to correlate with dipole tilt peaks and troughs. Nilsson et al. (2011) proposed that the dipole tilt and eccentricity of the dipole originate from common processes in the core. What is not clear and warrants further investigation is whether every episode of dipole tilt correlates with an archaeomagnetic jerk. Livermore et al. (2014) tried to model the extreme intensity changes observed by Ben-Yosef et al. (2009) and Shaar et al. (2011) using purely toroidal core surface flow and unrestricted core surface flow. Unfortunately neither of these end members flows can explain such rapid changes in field intensity.

7.3.6. Potential Climatic Consequences of the 1000 BC Event

The potential consequences of a sudden change in the magnetic field is an area of heated debate. Not least of all because the relationship between the magnetic field and climate is not fully understood. Some authors believe the correlation in time between archaeomagnetic jerks and periods of cooling in the North Atlantic (Gallet and Le Goff, 2006) is evidence of causation. Other authors have pointed out the good temporal concordance between geomagnetic field intensity maxima and fluctuations in length of Swiss glaciers (Genevey et al., 2013). Dergachev et al. (2012) proposed that geomagnetic field variations modulate the cosmic ray flux which would influence climate. However, Lockwood (2012) argues that a modulation of low-altitude clouds by galactic cosmic rays is an inadequate explanation of observations. Knudsen and Riisager (2009) observed a good correlation between speleotherm $\delta^{18}O$ records and the dipole moment, suggesting that Earth's magnetic field to some degree influences low-latitude precipitation. Some of the difficulty in finding a realistic mechanism to link the geomagnetic field and climate lies in the fact that the magnetic field and climate are both exceptionally complex systems, however, it is my sincere belief that correlation does not imply causation and that this issue needs to be thoroughly investigated by a climate scientist.

7.4. Other Periods of Exceptionally High Geomagnetic Field Strength

In Gallet and Le Goff (2006) an archaeomagnetic jerk was proposed for the time period ~2100-1900 BC based on data from baked brick fragments from the archaeological site Mari, which is locate in Syria. This data implied the occurrence of rapid intensity variations between ~2100-1900 BC but could not be resolved due to insufficient dating precision. It is for this reason that this particular 'archaeomagnetic jerk' in the Gallet et al. (2006) paper has a question mark next to it. It now appears that the field was decreasing over this time period and this has been collaborated by the Cypriot data presented in this thesis but also by additional Syrian data from Gallet and Butterlin (2014) (see figure 7.3). The timing of the archaeomagnetic jerk has been revised to between 2300 and 2000 BC (Gallet and Butterlin, 2014) as these authors believe there was a period of intensity maxima over this time period. Again, this is not supported by the data presented in this thesis.

Evidence for other potential archaeomagnetic jerks has been presented from across the globe. De Groot (2013) found a short period of high intensity occurring ~1000 years ago in Hawaii, Snowball and Sandgren (2004) report cusps in directional data at 6400 BC, 4400 BC, 1900 BC and 800BC in Swedish lake sequences. In South Korea, Yu et al. (2010) believe they found evidence of sharp and dull [sic] cusps in magnetic field direction at ~745 BC, ~AD 300, and ~AD1400-1700 from kilns and hearths. A peak in field strength of 163.5ZAm^2 with an estimated age of around 600 BC was also found in lava flows in the Azores (Di Chiara et al., 2014). Evidence from the Azores and Sweden overlaps in time with the evidence presented here from Kilise Tepe which has been interpreted here to be correlated with the 1000 BC event. If the data are recording the same event, this represents further evidence that the 1000 BC event was a global phenomenon with a duration of ~400 years.

The data presented in this thesis from Turkey and Cyprus casts doubt on the occurrence of two of Gallet's proposed archaeomagnetic jerks between 2300-2000 BC and 1750-1500 BC as proposed in Gallet et al. (2006) and revised in Gallet and Butterlin (2014). For the earlier of the two jerks (2300-2000 BC), the data from Marki Alonia is for decreasing field intensity over this time period whilst for the later jerk (1750 and 1500 BC), the evidence from Tell Atchana is for a slowly increasing field (which is in contrast to the definition of an archaeomagnetic jerk as a sudden increase in geomagnetic field strength).

Out of the seven jerks proposed by Gallet et al.(2003, 2006) only two have accompanying directional data from the same region (200 AD and 1400 AD). Of the remaining five jerks,

the evidence found in this thesis discredits the occurrence of two of them (2300-200 BC and 1750-1500 BC) and neither confirms nor refutes the occurrence of the 200 AD event. This brings into question the validity of the theory. Certainly linking jerks with climate change and population collapse undermined archaeomagnetic jerk theory in the eyes of many within the geomagnetic and archaeomagnetic community. Additionally, the wealth of evidence from a number of authors that the field behaved exceptionally at approximately 1000 BC complicates the issue of determining the legitimacy of archaeomagnetic jerks. However, as yet there is very little directional data for this time period so it is not clear if it was accompanied by a change in geomagnetic field direction.

Whilst it is tempting to completely dismiss archaeomagnetic jerks as being a result of zealous over-interpretation of a small amount of data, the work of Gallet et al. (2006) has had the consequence of stimulating debate and research (if only by authors trying to discredit the original papers). It also emphasised the need to study the field on all timescales beginning with days to weeks and extending to millions of years.

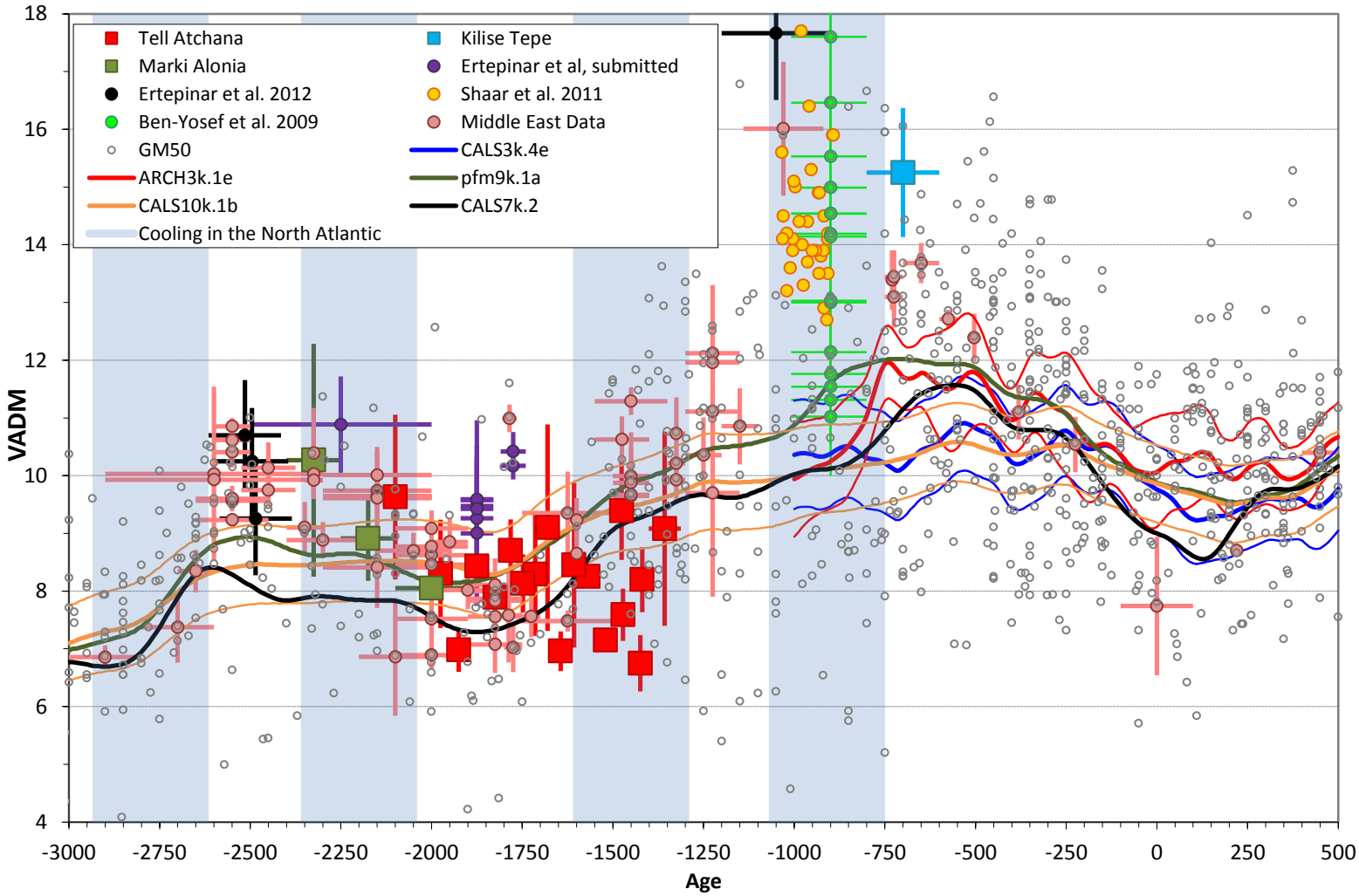
Tell Atchana
Kilise Tepe
Marki Alonia
Ertepinar et al, submitted
Ertepinar et al. 2012
Shaar et al. 2011
Ben-Yosef et al. 2009
Middle East Data
GM50
CALS3k.4e
ARCH3k.1e
pfm9k.1a
CALS10k.1b
CALS7k.2
Cooling in the North Atlantic
VADM
Age
18
16
14
12
10
8
6
4
-3000
-2750
-2500
-2250
-2000
-1750
-1500
-1250
-1000
-750
-500
-250
0
250
500

Figure7.3. This figure shows all the data gathered in this thesis for the Middle East (red, dark green and bright blue squares) plotted with all the data published by other authors working in the region: (Shaar et al., 2011) (yellow circles); (Ertepinar et al., 2012) (black circles); Ertepinar et al. (submitted to EPSL) (purple data) and (Ben-Yosef et al., 2009) (green data) the remaining Middle East data are plotted in pink (Genevey et al., 2003, Gallet et al., 2006, Gallet et al., 2008, Gallet et al., 2014, Gallet and Le Goff, 2006) with GEOMAGIA50 data plotted as grey open circles. Model predictions for Turkey from CALS7k.2 (Korte and Constable, 2005), CALS3k.4e (Korte and Constable, 2011), CALS10k.1b (Korte et al., 2011) ARCH3k_CST.1 (Korte et al., 2009) and pfm9k.1a (Nilsson et al., 2014). In addition to this data, colder periods in the North Atlantic are indicated by blue columns as first discussed in Gallet et al. (2006).

7.5. Definitions

A consensus could usefully be reached on the name and definition of features of the geomagnetic field so that events can be correlated around the globe. With respect to the 1000 BC event the term adopted by Shaar et al. (2011) of "geomagnetic spike" is preferred here to the term "archaeomagnetic jerks".

Leaving aside questions about the validity of archaeomagnetic jerk theory, if authors continue to talk about it, it should be more clearly defined. Archaeomagnetic jerks were defined in Gallet et al. (2003) as sharp cusps in geomagnetic field direction coincident with intensity maxima with time characteristics intermediate between 'geomagnetic jerks' and 'magnetic excursions' which leaves a degree of ambiguity in terms of which part of the feature it refers to. However, in Gallet et al. (2006) archaeomagnetic jerks were described as being 'marked by strong intensity increases'. In this thesis the original definition has been used. However, both definitions imply that any decrease back to pre-jerk values after the intensity high is not part of the event whereas it could be argued it is an integral part as the rate of decay will be a reflection of the core processes causing the feature. It is for this reason that the exact duration of archaeomagnetic jerks needs to be more closely defined. To address this, the following definition is proposed: *'a sudden increase in geomagnetic field intensity coinciding with a sharp cusp in geomagnetic field direction following which the field returns to pre jerk values. The whole feature can last for between 300 - 500 years.'* This definition was devised following a study of the average duration of features identified in Gallet et al. (2003,) Gallet et al (2006) and Gallet and Butterlin (2014) as archaeomagnetic jerks. It is also crucial, in order to ensure a clear debate, that it is established if the rate of change and maximum field strength during the occurrence of a jerk has to be of a certain magnitude before it can be classified as an archaeomagnetic jerk. Or is it used to describe any period of relative intensity high? E.g. Gallet and Butterlin

(2014) describe an archaeomagnetic jerk where the field only reaches a maximum of ~60μT which is significantly lower than field values measured elsewhere.

Note whilst no counter name for the features is proposed here, the term "archaeomagnetic jerk" is felt to be unfit for purpose for the following reasons:

1. Use of the word archaeomagnetic suggests it is confined to archaeomagnetic results/ archaeological material when there is no reason for this to be the case.
2. Jerk has a strict definition in physics as the rate of change of acceleration which is not how it is applied in this term.

Now that more data have been gathered it seems increasingly unlikely that there was an archaeomagnetic jerk between 2100-1900 BC as the intensity in the Middle East during the time period was actually decreasing. It is, therefore, proposed that the term archaeomagnetic jerk be confined (until we have more directional data for the other proposed archaeomagnetic jerks) to the originally proposed events at AD 200 and 1400 where there is also directly associated directional data.

The term archaeomagnetic jerk has been used to describe many events and despite its definition involving field direction, a number of archaeomagnetic jerks have been identified based on intensity data alone. More directional data are needed for the Middle East between ~2500 and ~500 BC to aid the interpretation and characterisation of archaeomagnetic jerks (if such features exist) and geomagnetic spikes. Data from the Middle East during this time period are unique in having such a strong bias towards intensity results when it is far more common to see a directional bias in archaeomagnetism data sets.

There is an increasing body of evidence that the 1000 BC event was a period of exceptionally high field strength felt over a large area of the Middle East. The maximum field strength experienced at this time was much greater than in any of the other proposed archaeomagnetic jerks and potentially was much shorter lived. The terminology of Shaar et al (2011) is, therefore, preferred and this event should be called a geomagnetic spike.

7.6. Archaeomagnetists and Archaeologists

As has been demonstrated in this thesis, archaeomagnetic investigations can benefit both the archaeologist and the archaeomagnetist. In order for this relationship to be successful it is crucial that regular communication occurs between the archaeomagnetist and the archaeologist to ensure any changes in dating, site and material interpretation is communicated quickly and effectively. The accurate dating of a site is particularly crucial to the archaeomagnetist and it not uncommon for this to be frequently refined by the archaeologist. When this happens, it is important that the archaeomagnetist is aware of the changes as it can heavily influence the interpretation of the data. There is, additionally, a responsibility on the archaeomagnetist to communicate this uncertainty to their audience in papers targeted at geomagnetists who may be unaware of the relative and sometimes subjective nature of archaeological dating. Conveying this uncertainty needs to be done with care, however, so as not to devalue the archaeomagnetic investigations.

The archaeomagnetist could also usefully revisit work as and when new dating becomes available. In the future, it could be very useful to revisit the results from Tell Atchana as the excavation of this site is on-going and the dating likely to be revised (although it is not expected that this revision will be substantial and will likely only affect the lower levels).

7.7 Potential future avenues of work

The most significant dataset in support of the 1000 BC geomagnetic spike is that gathered from slag deposits by Shaar et al (2011) and Ben Yosef et al. (2009). Copper slag deposits are abundant througout the world and so their potential as a recorder of the archaeomagnetic field is significant. Currently only one group of researchers based at SCRIPPS (or working with SCRIPPS researchers) has explored this research avenue with mixed success (compare the qaulity of the data produced in Shaar et al (2011) with that in Shaar et al. (2015)). Future work on slag deposits could usefully consider the quality of the dating as well as the quality of the data. Potentially there may be a correlation between the composition of the slag and its quality as a geomagnetic recorder and/ or a correlation between production techniques and the reliability of the material for palaeomagnetism studies.

8. Conclusions

Archaeomagnetic samples from two locations in Turkey and two locations in Cyprus yielded high quality archaeomagnetic field strength values using the microwave and thermal Thellier techniques. One archaeological site in France yielded high quality archaeomagnetic field strength values and directional results using thermal Thellier techniques. Using demagnetisation and rock magnetisation experiments it was confirmed that the kiln of unknown use found on the Oylum Höyük archaeological site was heated to between 600-700°C. This eliminated the possibility that it was used as a bread oven.

The very good quality data measured from Southern France strengthen the archaeological interpretation of at least two discreet construction phases of the bath area of the Roman-aged archaeological site, Site de la Molère. It was possible to tentatively confirm the archaeological interpretation that the hypocaust and a gutter (CAN4) were constructed at a different time to gutters CAN3 and CAN5. Archaeointensity results were accepted for 85 samples out of a sample set of 137 giving an overall success rate of 62%. The average intensity determined for the hypocaust was 56±7 µT whilst for CAN4 it was 58±8 µT. In comparison, the average intensity for CAN3 was 68±6 µT and for CAN5 it was also 68±7 µT implying that two construction events had different relative ages. The values determined for the early 2nd Century AD (56 ±7 and 58 ±8) appear to potentially confirm that the field was slightly lower at 100 AD before returning to former, higher, levels by 200 AD. If there was a decrease in field strength during this time period then the intensity measured here reflects a period of increasing field strength, back to pre-100 AD values. Significantly more data is needed from 100 AD before this interpretation can be confirmed.

It is acknowledged that whilst the intensities measured from features of the same age appear to group together (CAN4 and the Hypocaust for example) all five average intensity values are within the error envelopes of each other. This is a difficult time period to study due to the lack of variability in the intensity of the field and so this study would have been strengthen by the addition of directional data. Where directional data was available, for the praefurnium, four potential calendar dates were proposed by the ChronoModel 1.1 dating software. Combing archaeological information with the archaeomagnetic dating suggests that the final heating of the praefurnium most likely occurred at 399 AD ± 96.

The potsherds from Turkey yielded 58 successful results from 136 potsherds, giving a success rate of 41% whilst 17 successful archaeointensity values were recorded from mud brick samples giving a success rate of 94%. Ten Cypriot potsherds from a sample set of 34 gave successful results, producing a success rate of 29%.

The majority of samples studied as part of this thesis were suitable for archaeointensity experiments but frequently failed to meet archaeointensity selection criteria. The criterion which most samples failed on was the Cumulative DRAT with the majority of samples having values greater than 15% implying consistent alteration during the experiment. The bulk of samples contained a viscous component of magnetisation which was removed at low power/ temperature. Once this was removed almost all the samples had a single component of magnetisation which headed towards the origin. The main magnetic carrier was almost exclusively observed to be Titanomagnetite with varying Titanium concentrations. Technical difficulties associated with sampling were generally restricted to burnt soil samples taken from Oylum and St Jean Poutge.

A higher success rate was recorded for the small number of thermal experiments conducted in this thesis than for the microwave experiments with microwave success rates ranging from 25% to 41% and thermal success rates ranging between 15% and 94%. We utilised the Thellier-Thellier (Thellier and Thellier, 1959), Coe (Coe et al., 1978) and IZZI (Yu et al., 2004) methods when carrying out both microwave and thermal experiments. Comparison experiments on samples using both microwave and thermal techniques were not carried out. Consequently it was not possible to confirm to what degree this varying success rate was due to the material or to the technique.

This thesis adds to the debate about archaeomagnetic jerks/ geomagnetic spikes. It provides more data on the strength of the magnetic field in the Middle East during the Bronze Age. A maximum intensity of 84 μT between 800-600 BC was measured for Southern Turkey. This is a very robust result which was measured on two discreet potsherds. Within sherd consistency was also measured for these sherds. Prior to 800 BC, the field in Cyprus and Turkey was comparatively stable over the time period 2400 - 1200 BC and only varied between ~35 μT and ~58 μT. This finding casts doubt on the occurrence of a staccato archaeomagnetic jerk proposed by Gallet et al. (2006). In Gallet et al. (2006) it was proposed that the field increased by a factor of two in an irregular fashion, beginning with a strong increase between ~1750 and 1500 BC, followed by a moderate increase between 1500 and 1200-1100 BC and finally followed by another strong increase up to 750

BC. Whilst unambiguous evidence for the strong increase in field strength between ~1750 and 1500 BC or evidence for a moderate increase between 1500 and 1200-1100 BC was not observed here, evidence of a strong increase up to 750 BC was.

This thesis presents evidence that the intensity of the geomagnetic field in Cyprus between 2400-1900BC was decreasing. This is in contrast to the prediction by Gallet et al. (2006) that the field would increase, based on the occurrence of cooling in the North Atlantic over this time period. It is in agreement with the results of Gallet and Butterlin (2014) from Syrian archaeological samples.

Key future research should be focused on collecting continuous intensity and directional data sequences spanning the 1000BC event from the Middle East, surrounding countries and more distant locations. Lake sediment sequences most clearly fit these criteria but lava sequences might also be useful. This will enable archaeomagnetists to accurately characterise the 1000 BC event and therefore potentially link it with core processes. Effort should be focused on distinguishing/ more completely characterising archaeomagnetic jerks and geomagnetic spikes so that a more thorough discussion of their global extent, significance and potential consequences (e.g. on climate) can be conducted.

References

AITKEN, M. J., ALLSOP, A. L., BUSSELL, G. D. & WINTER, M. B. 1984. GEOMAGNETIC INTENSITY IN EGYPT AND WESTERN ASIA DURING THE 2ND MILLENNIUM BC. *Nature,* 310**,** 305-306.

AITKEN, M. J., ALLSOP, A. L., BUSSELL, G. D. & WINTER, M. B. 1988. Determination of the intensity of the Earth's magnetic-field during archaeological times - reliability of the Thellier technique *Reviews of Geophysics,* 26**,** 3-12.

AKAR, M. 2013. *The Late Bronze Age II City of Alalakh and Its Social Context in the Northern Levant: A Re-Examination of the post-Level IV Stratigraphic Sequence (I-III) based on New Excavation Results (2003-2010).* PhD Thesis, Universita' Degli Studi di Firenze.

BAKER, H. D., COLLON, D., HAWKINS, J. D., POLLARD, T., POSTGATE, J. N., SYMINGTON, D. & THOMAS, D. 1995. Kilise Tepe 1994. *Anatolian Studies,* 45**,** 139-191.

BAMMER 1964. Die gebrannten Mauerziegel von Ephesos und ihre Datierung. *Jahrbuch der Österreichen Archäologische Institut* 47**,** 290-299.

BARD, E. & DELAYGUE, G. 2008. Comment on - "Are there connections between the Earth's magnetic field and climate?". *Earth and Planetary Science Letters,* 265**,** 302-307.

BEN-YOSEF, E., RON, H., TAUXE, L., AGNON, A., GENEVEY, A., LEVY, T. E., AVNER, U. & NAJJAR, M. 2008a. Application of copper slag in geomagnetic archaeointensity research. *Journal of Geophysical Research,* 113.

BEN-YOSEF, E., SHAAR, R., TAUXE, L., LEVY, T. E. & KASSIANIDOU, V. 2011. Cyprus Archaeomagnetic Project (CAMP): targeting the slag deposits of Cyprus and the eastern Mediterranean. *Antiquity,* 85.

BEN-YOSEF, E., TAUXE, L., LEVY, T. E., SHAAR, R., RON, H. & NAJJAR, M. 2009. Geomagnetic intensity spike recorded in high resolution slag deposit in Southern Jordan. *Earth and Planetary Science Letters,* 287**,** 529-539.

BEN-YOSEF, E., TAUXE, L., RON, H., AGNON, A., AVNER, U., NAJJAR, M. & LEVY, T. E. 2008b. A new approach for geomagnetic archaeointensity research: insights on ancient metallurgy in the Southern Levant. *Journal of Archaeological Science,* 35**,** 2863-2879.

BIETAK, M. & CZERNY, E. (eds.) 2003. *The Synchronisation of Civilisations in the Eastern Mediterranean in the Second Millennium B.C. III,* Vienna: Verlang der Österreichlischen Akademie der Wissenschaften.

BIGGIN, A. J. 2010. Are systematic differences between thermal and microwave Thellier-type palaeointensity estimates a consequence of multidomain bias in the thermal results? *Physics of the Earth and Planetary Interiors,* 180**,** 16-40.

BIGGIN, A. J., BADEJO, S., HODGSON, E., MUXWORTHY, A. R., SHAW, J. & DEKKERS, M. J. 2013. The effect of cooling rate on the intensity of thermoremanent magnetization (TRM) acquired by assemblages of pseudo-single domain, multidomain and interacting single-domain grains. *Geophysical Journal International,* 193**,** 1239-1249.

BIGGIN, A. J., PERRIN, M. & DEKKERS, M. J. 2007. A reliable absolute palaeointensity determination obtained from a non-ideal recorder. *Earth and Planetary Science Letters,* 257**,** 545-563.

BOLGER, D. & WEBB, J. M. 2013. Ceramics. *In:* PELTENBURG, E. (ed.) *Associated Regional Chronologies for the Ancient Near East and the Eastern Mediterranean. Volume II. Cyprus.* Turnhout: Brepols.

BOND, G., KROMER, B., BEER, J., MUSCHELER, R., EVANS, M. N., SHOWERS, W., HOFFMAN, S., LOTTI-BOND, R., HAJDAS, I. & BONANI, G. 2001. Persistent solar influence on North Atlantic climate during the Holocene. *Science,* 294**,** 2130-2136.

BRAIDWOOD, R. J. & BRAIDWOOD, L. S. 1960. *Excavations in the plain of Anticoch: The earlier assesmblages phases A-J,* Chicago, The University of Chicago Press.

BUCHA, V. & MELLAART, J. 1967. Archaeomagnetic intensity measurements on some neolithic samples from Catal Huyuk (Anatolia) *Archaeometry,* 10**,** 23-25.

BUCUR, I. 1994. The direction of the terrestrial magnetic field in France, during the last 21 centuries. Recent progress. *Physics of the Earth and Planetary Interiors,* 87**,** 95-109.

BUTLER, R. F. 1992. *Paleomagnetism: Magnetic Domains to Geologic Terranes*, Blackwell Scientific Publications.

CAI, S., TAUXE, L., DENG, C., PAN, Y. X., JIN, G., ZHENG, J., XIE, F., QIN, H. & ZHU, R. X. 2014. Geomagnetic intensity variations for the past 8 kyr: New archaeointensity results from Eastern China. *Earth and Planetary Science Letters,* 392**,** 217-229.

CARRANCHO, A., MORALES, J., GOGUICHAICHVILI, A., ALONSO, R. & TERRADILLOS, M. 2014. Thermomagnetic monitoring of lithic clasts burned under controlled temperature and field conditions. Implications for archaeomagnetism. *Geofisica Internacional,* 53**,** 473-490.

CARRANCHO, A. & VILLALAIN, J. J. 2011. Different mechanisms of magnetisation recorded in experimental fires: Archaeomagnetic implications. *Earth and Planetary Science Letters,* 312**,** 176-187.

CASAS, L., RAMÍREZ, J., NAVARRO, A., FOUZAI, B., ESTOP, E. & ROSELL, J. R. 2013. Archaeometric dating of two limekilns in an industrial heritage site in Calders (Catalonia, NE Spain). *Journal of Cultural Heritage*.

CHAUVIN, A., GARCIA, Y., LANOS, P. & LAUBENHEIMER, F. 2000. Paleointensity of the geomagnetic field recovered on archaeomagnetic sites from France. *Physics of the Earth and Planetary Interiors,* 120**,** 111-136.

CHAUVIN, A., ROPERCH, P. & LEVI, S. 2005. Reliability of geomagnetic paleointensity data: the effects of the NRM fraction and concave-up behaviour on paleointensity determinations by the Thellier method. *Physics of the Earth and Planetary Interiors,* 150**,** 265-286.

CHURCH, M. J., PETERS, C. & BATT, C. M. 2007. Sourcing fire ash on archaeologicla sites in the Western and Northern Isles of Scotland, using minearl magnetism. *Geoarchaeology - An International Journal,* 22**,** 747-774.

COE, R. S. 1967. Paleo-intensities of Earths magnetic field determined from Tertiary and Quaternary rocks *Journal of Geophysical Research,* 72**,** 3247-&.

COE, R. S., GROMME, S. & MANKINEN, E. A. 1978. GEOMAGNETIC PALEOINTENSITIES FROM RADIOCARBON-DATED LAVA FLOWS ON HAWAII AND QUESTION OF PACIFIC NONDIPOLE LOW. *Journal of Geophysical Research,* 83**,** 1740-1756.

COLLEONI, F. 2012. La station routière antique de *Vanesia*: les fouilles du site de La Molère à Saint-Jean-Poutge (Gers). *L'Archéologue, Archéologie nouvelle***,** 64-68.

COURTILLOT, V., GALLET, Y., LE MOUEL, J. L., FLUTEAU, F. & GENEVEY, A. 2007. Are there connections between the Earth's magnetic field and climate? *Earth and Planetary Science Letters,* 253**,** 328-339.

COURTILLOT, V., GALLET, Y., LE MOUEL, J. L., FLUTEAU, F. & GENEVEY, A. 2008. Response to comment on - "Are there connections between Earth's magnetic field and climate? *Earth and Planetary Science Letters,* 265**,** 308-311.

DAY, R., FULLER, M. & SCHMIDT, V. A. 1977. HYSTERESIS PROPERTIES OF TITANOMAGNETITES - GRAIN-SIZE AND COMPOSITIONAL DEPENDENCE. *Physics of the Earth and Planetary Interiors,* 13**,** 260-267.

DE GROOT, L. V., BIGGIN, A. J., DEKKERS, M. J., LANGEREIS, C. G. & HERRERO-BERVERA, E. 2013. Rapid regional perturbations to the recent global geomagnetic decay revealed by a new Hawaiian record. *Nature Communications,* 4.

DEKKERS, M. J. & BÖHNEL, H. N. 2006. Reliable absolute palaeointensities independent of magnetic domain state. *Earth and Planetary Science Letters,* 248**,** 508-517.

DERGACHEV, V. A., VASILIEV, S. S., RASPOPOV, O. M. & JUNGNER, H. 2012. Impact of the geomagnetic field and solar radiation on climate change. *Geomagnetism and Aeronomy,* 52**,** 959-976.

DI CHIARA, A., TAUXE, L. & SPERANZA, F. 2014. Paleointensity determination from São Miguel (Azores Archipelago) over the last 3 ka. *Physics of the Earth and Planetary Interiors,* 234**,** 1-13.

DIKAIOS, P. 1940. *The Excavations at Vounous-Bellapais in Cyprus, 1931-2,* London, The Society of Antiquaries of London.

DODSON, M. H. & MCCLELLANDBROWN, E. 1980. MAGNETIC BLOCKING TEMPERATURES OF SINGLE-DOMAIN GRAINS DURING SLOW COOLING. *Journal of Geophysical Research,* 85**,** 2625-2637.

DONADINI, F., KORHONEN, K., RIISAGER, P. & PESONEN, L. 2006. Database for Holocene geomagnetic intensity information. *EOS, Transactions, American Geophysical Union,* 87**,** 137.

DONADINI, F., KORTE, M. & CONSTABLE, C. G. 2009. Geomagnetic field for 0-3 ka: 1. New data sets for global modeling. *Geochemistry Geophysics Geosystems,* 10.

DUMBERRY, M. & FINLAY, C. C. 2007. Eastward and westward drift of the Earth's magnetic field for the last three millennia. *Earth and Planetary Science Letters,* 254**,** 146-157.

DUNLOP, D. J. 2002a. Theory and application of the Day plot (M-rs/M-s versus H-cr/H-c) 1. Theoretical curves and tests using titanomagnetite data. *Journal of Geophysical Research-Solid Earth,* 107.

DUNLOP, D. J. 2002b. Theory and application of the Day plot (M-rs/M-s versus H-cr/H-c) 2. Application to data for rocks, sediments, and soils. *Journal of Geophysical Research-Solid Earth,* 107.

DUNLOP, D. J. & ÖZDEMIR, O. 1997. *Rock Magnetism: Fundamentals and Frontiers,* Cambridge, Cambridge University Press.

DUNN-VATURI, A.-E. 2003. *Vounous. C.F.A. Schaeffer's Excavations in 1933. Tombs 49–79, ,* Jonsered, Paul Astroms Forlag.

ECH-CHAKROUNI, S., HUS, J. & SPASSOV, S. 2013. Constraints of archaeomagnetic dating and field intensity determinations in three ancient tile kilns in Belgium. *Studia Geophysica Et Geodaetica,* 57**,** 585-604.

ERB-SATULLO, N., SHORTLAND, A.J. & EREMIN, K. 2011. Chemical and mineralogical approaches to the organization of Late Bronze Age Nuzi Ware production. *Archaeometr,.* 53, 1171-1192

ERTEPINAR, P., LANGEREIS, C. G., BIGGIN, A. J., FRANGIPANE, M., MATNEY, T., ÖKSE, T. & ENGIN, A. 2012. Archaeomagnetic study of five mounds from Upper Mesopotamia between 2500 and 700 BCE: Further evidence for an extremely strong geomagnetic field ca. 3000 years ago. *Earth and Planetary Science Letters,* 357–358**,** 84-98.

ERTEPINAR, P., LANGEREIS, C.G., BIGGIN, A.J., DE GROOT. L., KULAKOGLU, F., OMURA, S., SUEL, A. (Submitted) Full vector archaeomagnetic records from Anatolia between 2000 and 1400 BCE: implications for geomagnetic field models and the dating of fires in antiquity. *Earth and Planetary Science Letters.*

FERK, A., LEONHARDT, R., HESS, K. U., KOCH, S., EGLIS, R., KRÁSA, D. & DINGWELL, D. B. 2014. Influence of cooling rate on thermoremanence of magnetite grains: Identifying the role of different magnetic domain states. *Journal of Geophysical Research,* 119**,** 1599-1606.

FISHER, R. 1953. DISPERSION ON A SPHERE. *Proceedings of the Royal Society of London Series a-Mathematical and Physical Sciences,* 217**,** 295-305.
FOX, J. M. W. & AITKEN, M. J. 1980. COOLING-RATE DEPENDENCE OF THERMOREMANENT MAGNETIZATION. *Nature,* 283**,** 462-463.
FRANKEL, D. 2014. Cyprus during the Middle Bronze Age. *In:* STEINER, M. L. & KILLEBREW, A. E. (eds.) *The Oxford Handbook of the Archaeology of the Levant (c. 8000–332 BCE),.* Oxford: Oxford University Press.
FRANKEL, D. & WEBB, J. 2000. Marki Alonia: a prehistoric Bronze Age settlement in Cyprus. *Antiquity,* 286**,** 763 -64.
FRANKEL, D. & WEBB, J. M. 2006. *Marki Alonia. An Early and Middle Bronze Age Settlement in Cyprus. Excavations 1995–2000.,* Sävedalen, Paul Astroms Forlag.
GALLET, Y. & BUTTERLIN, P. 2014. Archaeological and Geomagnetic Implications of New Archaeomagnetic Intensity Data from the Early Bronze High Terrace 'Massif Rouge' at Mari (Tell Hariri, Syria). *Archaeometry***,** n/a-n/a.
GALLET, Y., D'ANDREA, M., GENEVEY, A., PINNOCK, F., LE GOFF, M. & MATTHIAE, P. 2014. Archaeomagnetism at Ebla (Tell Mardikh, Syria). New data on geomagnetic field intensity variations in the Near East during the Bronze Age. *Journal of Archaeological Science,* 42**,** 295-304.
GALLET, Y., GENEVEY, A. & COURTILLOT, V. 2003. On the possible occurrence of 'archaeomagnetic jerks' in the geomagnetic field over the past three millennia. *Earth and Planetary Science Letters,* 214**,** 237-242.
GALLET, Y., GENEVEY, A., LE GOFF, M., FLUTEAU, F. & ESHRAGHI, S. A. 2006. Possible impact of the Earth's magnetic field on the history of ancient civilizations. *Earth and Planetary Science Letters,* 246**,** 17-26.
GALLET, Y., HULOT, G., CHULLIAT, A. & GENEVEY, A. 2009. Geomagnetic field hemispheric asymmetry and archeomagnetic jerks. *Earth and Planetary Science Letters,* 284**,** 179-186.
GALLET, Y. & LE GOFF, M. 2006. High-temperature archeointensity measurements from Mesopotamia. *Earth and Planetary Science Letters,* 241**,** 159-173.
GALLET, Y., LE GOFF, M., GENEVEY, A., MARGUERON, J. & MATTHIAE, P. 2008. Geomagnetic field intensity behavior in the Middle East between similar to 3000 BC and similar to 1500 BC. *Geophysical Research Letters,* 35.
GENEVEY, A. & GALLET, Y. 2002. Intensity of the geomagnetic field in western Europe over the past 2000 years: New data from ancient French pottery. *Journal of Geophysical Research-Solid Earth,* 107.
GENEVEY, A., GALLET, Y., THÉBAULT, E., JESSET, S. & LE GOFF, M. 2013. Geomagnetic field intensity variations in Western Europe over the past 1100 years. *Geochemistry, Geophysics, Geosystems,* 14**,** 2858-2872.
GENEVEY, A. S., GALLET, Y. & MARGUERON, J. C. 2003. Eight thousand years of geomagnetic field intensity variations in the eastern Mediterranean. *Journal of Geophysical Research-Solid Earth,* 108.
GOGUITCHAICHVILI, A., LOPONTE, D., MORALES, J. & ACOSTA, A. 2012. THE ARCHAEOINTENSITY OF THE EARTH'S MAGNETIC FIELD RETRIEVED FROM PAMPEAN CERAMICS (SOUTH AMERICA). *Archaeometry,* 54**,** 388-400.
GÓMEZ-PACCARD, M., CHAUVIN, A., LANOS, P., DUFRESNE, P., KOVACHEVA, M., HILL, M. J., BEAMUD, E., BLAIN, S., BOUVIER, A. & GUIBERT, P. 2012. Improving our knowledge of rapid geomagnetic field intensity changes observed in Europe between 200 and 1400 AD. *Earth and Planetary Science Letters,* 355–356**,** 131-143.
GOMEZ-PACCARD, M., CHAUVIN, A., LANOS, P., THIRIOT, J. & JIMENEZ-CASTILLO, P. 2006. Archeomagnetic study of seven contemporaneous kilns from Murcia (Spain). *Physics of the Earth and Planetary Interiors,* 157**,** 16-32.

GOULPEAU, L. 1994. Analyse archaeomagnetique de structures en hypocauste. *Revue de archeometrie,* 18**,** 43-51.
GREAVES, A. M. 2002. The Oylum Hoyuk project 2002. *Anatolian Archaeology,* 8**,** 4.
GROMMÉ, C. S., WRIGHT, T. L. & PECK, D. L. 1969. Magnetic properties and oxidation of iron-titanium oxide minerals in Alae and Makaopuhi Lava Lakes, Hawaii. *Journal of Geophysical Research,* 74**,** 5277-5293.
HALGEDAHL, S. L., DAY, R. & FULLER, M. 1980. THE EFFECT OF COOLING RATE ON THE INTENSITY OF WEAK-FIELD TRM IN SINGLE-DOMAIN MAGNETITE. *Journal of Geophysical Research,* 85**,** 3690-3698.
HANSEN, C. K. & POSTGATE, J. N. 1999. The Bronze to Iron Age Transition at Kilise Tepe. *Anatolian Studies,* 49**,** 111-121.
HASAKI, E. 2002. *Ceramic kilns in Ancient Greece: Technology and Organization of ceramic workshops.* Doctorate of Philosophy (Ph.D.), University of Cincinnati.
HENRY, B., JORDANOVA, D., JORDANOA, N. & LE GOFF, M. 2005. Transformations of magnetic mineralogy in rocks revealed by difference of hysteresis loops measured after stepwise heating: theory and case studies *Geophysics Journal International***,** 64-78.
HERRIES, A. I. R. & FISHER, E. C. 2010. Multidimensional GIS modeling of magnetic mineralogy as a proxy for fire use and spatial patterning: Evidence from the Middle Stone Age bearing sea cave of PInnacle Point 13B (Western Cape, South Africa). *Journal of Human Evolution,* 59**,** 306-320.
HERRIES, A. I. R., KOVACHEVA, M., KOSTADINOVA, M. & SHAW, J. 2007. Archaeo-directional and -intensity data from burnt structures at the Thracian site of Halka Bunar (Bulgaria): The effect of magnetic mineralogy, temperature and atmosphere of heating in antiquity. *Physics of the Earth and Planetary Interiors,* 162**,** 199-216.
HERVE, G., CHAUVIN, A. & LANOS, P. 2013a. Geomagnetic field variations in Western Europe from 1500 BC to 200 AD. Part II: New intensity secular variation curve. *Physics of the Earth and Planetary Interiors,* 218**,** 51-65.
HERVE, G., CHAUVIN, A. & LANOS, P. 2013b. Geomagnetic field variations in Western Europe from 1500BC to 200AD. Part I: Directional secular variation curve. *Physics of the Earth and Planetary Interiors,* 218**,** 1-13.
HERVÉ, G., CHAUVIN, A. & LANOS, P. 2013. Geomagnetic field variations in Western Europe from 1500BC to 200AD. Part I: Directional secular variation curve. *Physics of the Earth and Planetary Interiors,* 218**,** 1-13.
HILL, M. J. 2000. *The microwave palaeointensity technique and its application to lava.* Ph.D., University of Liverpool.
HILL, M. J., GRATTON, M. N. & SHAW, J. 2002. A comparison of thermal and microwave palaeomagnetic techniques using lava containing laboratory induced remanence. *Geophysical Journal International,* 151**,** 157-163.
HILL, M. J., LANOS, P., CHAUVIN, A., VITALI, D. & LAUBENHEIMER, F. 2007. An archaeomagnetic investigation of a Roman amphorae workshop in Albinia (Italy). *Geophysical Journal International,* 169**,** 471-482.
HILL, M. J., LANOS, P., DENTI, M. & DUFRESNE, P. 2008. Archaeomagnetic investigation of bricks from the VIIIth-VIIth century BC Greek-indigenous site of Incoronata (Metaponto, Italy). *Physics and Chemistry of the Earth,* 33**,** 523-533.
HILL, M. J., SHAW, J. & HERRERO-BERVERA, E. 2005. Paleointensity record through the Lower Mammoth reversal from the Waianae volcano, Hawaii. *Earth and Planetary Science Letters,* 230**,** 255-272.
HOFFMAN, K. A. & BIGGIN, A. J. 2005. A rapid multiple-sample approach to the determination of absolute paleointensity. *Journal of Geophysical Research,* 110.

HONG, H., YU, Y., LEE, C. H., H., K. R., PARK, J., DOH, S.-J., KIM, W. & SUNG, H. 2013. Global strong geomagnetic field intensity circa 3000 years ago. *Earth and Planetary Science Letters,* 383**,** 142-152.

HROUDA, F., MULLER, P. & HANAK, J. 2003. Repeated progressive heating in susceptibility vs. temperature investigation: a new palaeotemperature indicator? *Physics and Chemistry of the Earth,* 28**,** 653-657.

JORDANOVA, N., KOVACHEVA, M., HEDLEY, I. & KOSTADINOVA, M. 2003. On the suitability of baked clay for archaeomagnetic studies as deduced from detailed rock-magnetic studies. *Geophysical Journal International,* 153**,** 146-158.

KIRSCHVINK, J. L. 1980. THE LEAST-SQUARES LINE AND PLANE AND THE ANALYSIS OF PALEOMAGNETIC DATA. *Geophysical Journal of the Royal Astronomical Society,* 62**,** 699-718.

KISSEL, C. & LAJ, C. 2004. Improvements in procedure and paleointensity selection criteria (PICRIT 03) for Thellier and Thellier determinations: application to Hawaiian basaltic long cores. *Physics of the Earth and Planetary Interiors,* 147**,** 155-169.

KNAPP, A. B. 2013. *The Archaeology of Cyprus: From Earliest Prehistory Through the Bronze Age,* Cambridge, Cambridge University Press.

KNUDSEN, M. F. & RIISAGER, P. 2009. Is there a link between Earth's magnetic field and low-latitude precipitation? *Geology,* 37**,** 71-74.

KORHONEN, K., DONADINI, F., RIISAGER, P. & PESONEN, L. 2008. GEOMAGIA50: an archeointensity database with PHP and MySQL. *Geochemistry Geophysics Geosystems,* 9.

KORTE, M. & CONSTABLE, C. 2011. Improving geomagnetic field reconstructions for 0–3ka. *Physics of the Earth and Planetary Interiors,* 188**,** 247-259.

KORTE, M. & CONSTABLE, C. G. 2005. Continuous geomagnetic field models for the past 7 millennia: 2. CALS7K. *Geochemistry Geophysics Geosystems,* 6.

KORTE, M., CONSTABLE, C. G., DONADINI, F. & HOLME, R. 2011. Reconstructing the Holocene Geomagnetic Field. *Earth and Planetary Science Letters,* 312**,** 235-246.

KORTE, M., DONADINI, F. & CONSTABLE, C. G. 2009. Geomagnetic field for 0-3 ka: 2. A new series of time-varying global models. *Geochemistry Geophysics Geosystems,* 10.

KOSTADINOVA-AVRAMOVA, M., KOVACHEVA, M. & BOYADZHIEV, Y. 2014. Contribution of stratigraphic constraints of Bulgarian prehistoric multilevel tells and a comparison with archaeomagnetic observations. *Journal of Archaeological Science***,** 227-238.

KOSTADINOVA, M., JORDANOVA, N., JORDANOVA, D. & KOVACHEVA, M. 2004. Preliminary study on the effect of water glass impregnation on the rock-magnetic properties of baked clay. *Studia Geophysica Et Geodaetica,* 48**,** 637-646.

KOVACHEVA, M., BOYADZIEV, Y., KOSTADINOVA-AVRAMOVA, M., JORDANOVA, N. & DONADINI, F. 2009. Updated archeomagnetic data set of the past 8 millennia from the Sofia laboratory, Bulgaria. *Geochemistry Geophysics Geosystems,* 10.

KOVACHEVA, M., HEDLEY, I., JORDANOVA, N., KOSTADINOVA, M. & GIGOV, V. 2004. Archaeomagnetic dating of archaeological sites from Switzerland and Bulgaria. *Journal of Archaeological Science,* 31**,** 1463-1479.

KOVACHEVA, M. & JORDANOVA, N. 2001. Bulgarian archaeomagnetic studies: A review of methodological progress and applications in archaeology. *Journal of Radioanalytical and Nuclear Chemistry,* 247**,** 685-696.

KOVACHEVA, M., JORDANOVA, N. & KARLOUKOVSKI, V. 1998. Geomagnetic field variations as determined from Bulgarian archaeomagnetic data. Part II: The last 8000 years. *Surveys in Geophysics,* 19**,** 431-460.

KOVACHEVA, M., KOSTADINOVA-AVRAMOVA, M., JORDANOA, N., LANOS, P. & BOYADZHIEV, Y. 2014. Extended and revised archaeomagnetic database and

secular variation curves form Bulgaria for the last eight millennia. *Physics of the Earth and Planetary Interiors*.

LANOS, P. 1987. THE EFFECTS OF DEMAGNETIZING FIELDS ON THERMOREMANENT MAGNETIZATION ACQUIRED BY PARALLEL-SIDED BAKED CLAY BLOCKS. *Geophysical Journal of the Royal Astronomical Society,* 91**,** 985-1012.

LANOS, P. 1998. L'archéomagnétisme. *In:* EVIN, J., LAMBERT, G.-N., LANGOUËT, L., LANOS, P. & OBERLIN, C. (eds.) *La datation en laboratoire.* Paris: Errance.

LANOS, P., KOVACHEVA, M. & CHAUVIN, A. 1999. Archaeomagnetism, methodology and applications: Implentation and practice of the archeomagnetic method in France and Bulgaria. *European Journal of Archaeology,* 2**,** 365-392.

LANOS, P., PHILIPPE, A., VIBET, M.A. & DUFRESNE, P. (2015) User's manual of ChronoModel (version 1.1)0 [Online] Available from: http://www.chronomodel.fr [Accessed: 3rd May 2015]

LE GOFF, M. & GALLET, Y. 2004. A new three-axis vibrating sample magnetometer for continuous high-temperature magnetization measurements: applications to paleo- and archeo-intensity determinations. *Earth and Planetary Science Letters,* 229**,** 31-43.

LE GOFF, M., GALLET, Y., GENEVEY, A. & WARME, N. 2002. On archeomagnetic secular variation curves and archeomagnetic dating. *Physics of the Earth and Planetary Interiors,* 134**,** 203-211.

LEONHARDT, R., HEUNEMANN, C. & KRASA, D. 2004. Analyzing absolute paleointensity determinations: Acceptance criteria and the software ThellierTool4.0. *Geochemistry Geophysics Geosystems,* 5.

LIVERMORE, P. W., FOURNIER, A. & GALLET, Y. 2014. Core-flow constraints on extreme archeomagnetic intensity changes. *Earth and Planetary Science Letters,* 387**,** 145-156.

LOCKWOOD, M. 2012. Solar Influence on Global and Regional Climates. *Surveys in Geophysics,* 33**,** 503-534.

MANNING, S. W. 2013a. Appendix: a new radiocarbon chronology for Prehistoric and Protohistoric Cyprus, ca. 11,000–1050 Cal BC,. *In:* KNAPP, A. B. (ed.) *The Archaeology of Cyprus: From Earliest Prehistory Through the Bronze Age.* Cambridge: Cambridge University Press.

MANNING, S. W. 2013b. Cyprus at 2200 BC: rethinking the chronology of the Cypriot Early Bronze Age. *In:* KNAPP, A. B., WEBB, J. M. & MCCARTHY, A. (eds.) *J.R.B. Stewart: An Archaeological Legacy, Studies in Mediterranean Archaeology* Uppsala: Paul Astroms Forlag.

MCCLELLANDBROWN, E. 1984. Experiments on TRM intensity dependence on cooling rate. *Geophysical Research Letters,* 11**,** 205-208.

MCINTOSH, G., KOVACHEVA, M., CATANZARITI, G., DONADINI, F. & LOPEZ, M. L. O. 2011. High coercivity remanence in baked clay materials used in archeomagnetism. *Geochemistry Geophysics Geosystems,* 12.

MCINTOSH, G., KOVACHEVA, M., CATANZARITI, G., OSETE, M. L. & CASAS, L. 2007. Widespread occurrence of a novel high coercivity, thermally stable, low unblocking temperature magnetic phase in heated archeological material. *Geophysical Research Letters,* 34.

MERRILL, R. T. & MCELHINNY, M. W. 1983. *The Earth's Magnetic Field,* London, Academic Press.

MERRILL, R. T., MCELHINNY, M. W. & MCFADDEN, P. L. 1996. *The magnetic field of the earth: paleomagnetism, the core and the deep mantle,* San Diego, Academic Press, San Diego.

MUXWORTHY, A. R. & HESLOP, D. 2011. A Preisach method for estimating absolute paleofield intensity under the constraint of using only isothermal measurements: 1. Theoretical framework. *Journal of Geophysical Research: Solid Earth,* 116**,** B04102.
NAGATA, T., MOMOSE, K. & ARAI, Y. 1963. SECULAR VARIATION OF GEOMAGNETIC TOTAL FORCE DURING LAST 5000 YEARS. *Journal of Geophysical Research,* 68**,** 5277-&.
NÉEL, L. 1949. Théorie du trainage magnétique des ferromagnétiques en grains fines avec appications aux terres cuites. *Annals of Geophysics,* 5**,** 99-136.
NÉEL, L. 1955. Some theoretical aspects of rock-magnetism. *Advances in Physics,* 4**,** 191-243.
NILSSON, A., HOLME, R., KORTE, M., SUTTIE, N. & HILL, M. J. 2014. Reconstructing Holocene geomagnetic field variation: New methods, modles and implications. *Geophysical Journal International*.
NILSSON, A., MUSCHELER, R. & SNOWBALL, I. 2011. Millennial scale cyclicity in the geodynamo inferred from a dipole tilt reconstruction. *Earth and Planetary Science Letters,* 311**,** 299-305.
ÖZGEN, E. & HELWING, B. 2003. On the Shifting Border Between Mesopotamia and the West: Seven Seasons of Joint Turkish-German Excavations at Olyum Höyük *Anatolica,* 29**,** 61-85.

PAPUSOI, C. 1972. Effet de la vitesse de refroidissement sur l'intensité de l'animantation thermorémanente d'un ensemble de grains monodomaines. *An. Stiint. Univ. Al. I. Cuza lasi Sect 1b. Tomul,* 18**,** 31-47.PATERSON, G. A., BIGGIN, A. J., YAMAMOTO, Y. & PAN, Y. 2012. Towards the robust selection of Thellier-type paleointensity data: The influence of experimental noise. *Geochemistry, Geophysics, Geosystems,* 13**,** 05.

PATERSON, G. A., TAUXE, L., BIGGIN, A. J., SHAAR, R. & JONESTRASK, L. C. 2014. On improving the selection of Thellier-type paleointensity data. *Geochemistry, Geophysics, Geosystems,* 15**,** 1180-1192.
PELTENBURG, E. (ed.) 2013. *Associated Regional Chronologies for the Ancient Near East and the Eastern Mediterranean. Volume II. Cyprus,* Turnhout: Brepols.
PÉTRONILLE, M., GOGUITCHAICHVILI, A., MORALES, J., CARVALLO, C. & HUEDA-TANABE, Y. 2012. Absolute geomagnetic intensity determinations on Formative potsherds (1400–700 BC) from the Oaxaca Valley, Southwestern Mexico. *Quaternary Research,* 78**,** 442-453.
PICK, T. & TAUXE, L. 1994. Characteristics of magnetite in submarine basaltic glass. *Geophysical Journal International,* 119**,** 116-128.
POLETTI, W., HARTMANN, G. A., HILL, M. J., BIGGIN, A. J. & TRINDADE, R. I. F. 2013. The cooling-rate effect on microwave archeointensity estimates. *Geophysical Research Letters***,** n/a-n/a.
POSTGATE, J. N. & THOMAS, D. C. (eds.) 2011. *Excavations at Kilise Tepe, 1994-1998: From Bronze Age to Byzantine in Western Cilicia*: McDonald Institute/ British Institue at Ankara.
RIISAGER, P. & RIISAGER, J. 2001. Detecting multidomain magnetic grains in Thellier palaeointensity experiments. *Physics of the Earth and Planetary Interiors,* 125**,** 111-117.
ROGERS, J., FOX, J. M. W. & AITKEN, M. J. 1979. MAGNETIC-ANISOTROPY IN ANCIENT-POTTERY. *Nature,* 277**,** 644-646.
SARIBUDAK, M. & TARLING, D. H. 1993. Archaeomagnetic studies of the Urartian Civilization, Eastern Turkey. *Antiquity,* 67**,** 620-628.

SAYIN, N. & ORBAY, N. 2003. Investigation of secular variations of geomagnetic field using archaeomagnetic samples obtained from central anatolia. *Turkish Journal of Earth Sciences,* 16**,** 33-43.

SCHNEPP, E., PUCHER, R., GOEDICKE, C., MANZANO, A., MULLER, U. & LANOS, P. 2003. Paleomagnetic directions and thermoluminescence dating from a bread oven-floor sequence in Lubeck (Germany): A record of 450 years of geomagnetic secular variation. *Journal of Geophysical Research-Solid Earth,* 108.

SELKIN, P. A. & TAUXE, L. 2000. Long-term variations in palaeointensity. *Philosophical Transactions of the Royal Society of London Series a-Mathematical Physical and Engineering Sciences,* 358**,** 1065-1088.

SHAAR, R., BEN-YOSEF, E., RON, H., TAUXE, L., AGNON, A. & KESSEL, R. 2011. Geomagnetic field intensity: How high can it get? How fast can it change? Constraints from Iron Age copper slag. *Earth and Planetary Science Letters,* 301**,** 297-306.

SHAAR, R. & TAUXE, L. 2013. Thellier GUI: An integrated tool for analyzing paleointensity data from Thellier-type experiments. *Geochemistry Geophysics Geosystems,* 14**,** 677-692.

SHAAR, R., TAUXE, L., BEN-YOSEF, E., KASSIANIDOU, V., LORENTZEN, B., FEINBERG, J. M., LEVY, T. E. 2015. Decadal-scale variations in geomagnetic field intensity from ancient Cypriot slag mounds *Geochemistry, Geophysics, Geosystems, 16, 195-214.*

SHAW, J. 1974. A new method of determining the magnitude of the paleomagnetic field application to five historic lavas and five archaeological samples. *Geophysical Journal of the Royal Astronomical Society,* 39**,** 133-141.

SHAW, J. & SHARE, J. A. 2007. A new automated microwave demagnetiser/ remagnetiser system for palaeointensity studies. *Fall Meet. Suppl., Eos Trans. AGU* 88.

SNOWBALL, I. & SANDGREN, P. 2004. Geomagnetic field intensity changes in Sweden between 9000 and 450 cal BP: extending the record of "archaeomagnetic jerks" by means of lake sediments and the pseudo-Thellier technique. *Earth and Planetary Science Letters,* 227**,** 361-376.

SPASSOV, S. & HUS, J. 2006. Estimating baking temperatures in a Roman pottery kiln by rock magnetic properties: implications of thermochemical alteration on archaeointensity determinations. *Geophysical Journal International,* 167**,** 592-604.

STEIN, D. (ed.) 1997. *Alalakh,* Oxford: Oxford University Press.

STEWART, E. & STEWART, J. R. 1950. Vounous 1937–38. Field Report of the Excavations Sponsored by the British School at Athens. Lund: Acta Instituti Romani Regni Sueciae XIV.

STEWART, J. R. 1962. The Early Cypriote Bronze Age. *In:* DIKAIOS, P. & STEWART, J. R. (eds.) *Swedish Cyprus Expedition Volume IV, Part IA. The Stone Age and the Early Bronze Age in Cyprus,.* Lund.

SUTTIE, N., SHAW, J. & HILL, M. J. 2010. Direct demonstration of microwave demagnetization of a whole rock sample with minimal heating. *Earth and Planetary Science Letters,* 292**,** 357-362.

SUTTIE, N, HOLME, R. HILL, M. J. & SHAW, J. (2011) Consistent treatment of errors in archaeointensity implies rapid decay of the dipole. *Earth and Planetary Science Letters*, 304. 13-21.

TAUXE, L. 2010. *Essentials of Paleomagnetism: Web Edition 1.0,* California, University of California Press.

TAUXE, L., MULLENDER, T. A. T. & PICK, T. 1996. Potbellies, wasp-waists, and superparamagnetism in magnetic hysteresis. *Journal of Geophysical Research-Solid Earth,* 101**,** 571-583.

TAUXE, L. & STAUDIGEL, H. 2004. Strength of the geomagnetic field in the Cretaceous Normal Superchron: New data from submarine basaltic glass of the Troodos Ophiolite. *Geochemistry Geophysics Geosystems,* 5.

TAUXE, L. & YAMAZAKI, T. 2007. Paleointensities. *In:* KONO, M. (ed.) *Geomagnetism.*

TEMA, E., GOMEZ-PACCARD, M., KONDOPOULOU, D. & ALMAR, Y. 2012. Intensity of the Earth's magnetic field in Greece during the last five millennia: New data from Greek pottery. *Physics of the Earth and Planetary Interiors,* 202**,** 14-26.

THELLIER, E. 1981. Sur la direction du champ magnetique terrestre en France durant les deux derniersmillhaires. *Physics of the Earth and Planetary Interiors,* 24**,** 89-132.

THELLIER, E. & THELLIER, O. 1959. Sur l'intensité du champ magnétique terrestre dans le passé historique et geologique. *Annales Geophysicae,* 15**,** 285-378.

THOMAS, N. 1993. An integrated rock magnetic approach to the selection or rejection of ancient basalt samples for palaeointensity experiments. *Physics of the Earth and Planetary Interiors,* 75**,** 329-342.

VEITCH, R. J., HEDLEY, I. G. & WAGNER, J. J. 1984. An investigtaion of the intensity of the geomagnetic field during Roman times using magnetically anisotropic bricks and tiles. *Archeological Sciences, Geneve,* 37**,** 359.

WEBB, J. 1994. Techniques of pottery manufacture at Marki, Cyprus. *Τόμος III (Archaeologia Cypria, Volume III)*.

WEBB, J. & FRANKEL, D. 2004. Prehistoric Cooking Pots from Cyprus. *Ceramics Technical***,** 91-96.

WEBB, J. M. 2014. Cyprus during the Early Bronze Age. *In:* STEINER, M. L. & KILLEBREW, A. E. (eds.) *The Oxford Handbook of the Archaeology of the Levant (c. 8000–332 BCE).* Oxford: Oxford University Press.

WEBB, J. M. & FRANKEL, D. 1999. Characterizing the Philia Facies: Material Culture, Chronology, and the Origin of the Bronze Age in Cyprus. *American Journal of Archaeology,* 103**,** 3-43.

WINKLHOFER, M., FABIAN, K. & HEIDER, F. 1997. Magnetic blocking temperatures of magnetite calculated with a three-dimensional micromagnetic model. *Journal of Geophysical Research: Solid Earth,* 102**,** 22695-22709.

WOOLLEY, L. 1955. *Reports of the Research Committee of the Society of Antiquaries of London No.XVIII: Alalakh: An Account of the Excavations at Tell Atchana in the Hatay, 1937-1949,* Oxford, Oxford University Press.

YANG, S., SHAW, J. & ROLPH, T. 1993. ARCHAEOINTENSITY STUDIES OF PERUVIAN POTTERY - FROM 1200-BC TO 1800-AD. *Journal of Geomagnetism and Geoelectricity,* 45**,** 1193-1207.

YENER, K. A. 2013. New excavations at Alalakh: the 14th - 12th Centuries BC. *In:* YENER, K. A. (ed.) *Across the border: Late Bronze-Iron Age relations between Syria and Anatolia: Proceedings of a Symposium held at the research Center of Anatolian Studies, Koç University, Istanbul, May 31-June 1, 2010.* Peeters.

YENER, K. A., EDENS, C., HARRISON, T. P., VERSTRAETE, J. & WILKINSON, T. J. 2000. The Amuq Valley Regional Project, 1995-1998. *American Journal of Archaeology,* 104**,** 163-220.

YU, Y. 2011. Importance of cooling rate dependence of thermoremanence in paleointensity determination. *Journal of Geophysical Research: Solid Earth,* 116**,** B09101.

YU, Y., DOH, S.-J., KIM, W., PARK, Y.-H., LEE, H.-J., YIM, Y., CHO, S.-G., OH, Y.-S., LEE, D.-S., LEE, H.-H., GONG, M.-G., HYUN, D.-H., CHO, J.-K., SIN, Y.-S. & DO, M.-S. 2010. Archeomagnetic secular variation from Korea: Implication for the occurrence of global archeomagnetic jerks. *Earth and Planetary Science Letters,* 294**,** 173-181.

YU, Y., TAUXE, L. & GENEVEY, A. 2004. Toward an optimal geomagnetic field intensity determination technique. *Geochemistry, Geophysics, Geosystems,* 5**,** Q02H07.

YU, Y. J. & DUNLOP, D. J. 2003. On partial thermoremanent magnetization tail checks in Thellier paleointensity determination. *Journal of Geophysical Research-Solid Earth,* 108.

ZANANIRI, I., BATT, C. M., LANOS, P., TARLING, D. H. & LINFORD, P. 2007. Archaeomagnetic secular variation in the UK during the past 4000 years and its application to archaeomagnetic dating. *Physics of the Earth and Planetary Interiors,* 160**,** 97-107.

ZIJDERVELD, J. D. A. 1967. Demagnetization of rocks: Analysis of results. *In:* COLLINSON, D. W., CREER, K. M. & RUNCORN, S. K. (eds.) *Methods in Paleomagnetism.* Amsterdam: Elsevier.

ZUIDEVELD, P. L. & VAN DEN BERG, P. J. 1971. Design of lime shaft kilns. *Chemical Engineering Science,* 26**,** 875-883.